

**NUMERICAL SIMULATION OF WATER FLOW THROUGH
UNSATURATED SOIL IN VERTICAL AND INCLINED LAYERED
SYSTEMS**

by

Jorge Luis Rodriguez

A thesis submitted in partial fulfillment of the requirements for the degree of

Master in Science

In

Geotechnical Engineering

Department of Civil and Environmental Engineering
University of Alberta

© Jorge Luis Rodriguez, 2016

Abstract

In past decades, there were discussions explaining the mechanisms and factors that influence water flow through soil in unsaturated conditions. This phenomenon is of major importance to the mining industry as water is one of the trigger mechanisms for Acid Rock Generation (ARD) generation. In 1999, Newman evaluated water flow in unsaturated conditions for two column experiments using a vertical layer system of sandy materials and waste rock from the Golden Sunlight mine. Later in 2009, Andrina analyzed water flow using waste rock from the Grasberg Mine in three Meso-scale experiments to understand flow mechanisms for incline layers of waste rock. The current study focuses on modeling the two column experiments by Newman and the three Meso-scale panels by Andrina to analyze the mechanisms controlling water flow in unsaturated soils. Additionally, one of the models is evaluated under three additional materials to compare the effect of different hydraulic properties in an incline layering system.

With finite element methods, the experiments are modeled and calculated under equal boundary conditions. The use of climate boundaries recreates the precipitation flux and head pressure boundary to generate the suction from the discharge points. The models are run using SvFlux software, which runs an automatic mesh refinement algorithm and solves the Partial Differential Equations (PDEs) using FlexPDE.

The models are validated based on the correlation of the discharge volume from each experiment. The results from the models describe the profile changes of head pressure (h_p), flux, flow paths, and matric suction to describe the mechanism of flow in the unsaturated conditions. The validation of the models was achieved through back analyzing the different tests in the experiments, due to the low correlation of the model using the laboratory properties and the experimental results. The back analysis of the material is focused on the air entry value, and the saturated hydraulic conductivity as a means to change the unsaturated flow.

The result from the research displays similarities and disagreements between the models and experiments. The models showed that the measured discharge from a particular material does not represent the preferential flow path of water, as a small gradient in the pressure distribution can generate breakthrough at the base of the system.

Acknowledgements

I start to thank my parents for the enormous effort to help me achieve my dreams, giving me their unconditional support in every step of way. They always believe in me and push me to higher goals.

I would also like to thank my wife Diana, the most special woman I've ever met, helping me in every day of my Masters, giving me the company, affection, and support. Despite the distance during all this time our love grew unimaginably. Thank you for always giving company and helping me in the darkest days.

I also want to give a special acknowledgement to my supervisor Dr. Ward Wilson without whom this project would not have been possible, a great mentor who taught me great things. Thank you very much for giving me the unique opportunity to work under your wing, Thank you very much for believing and trusting me.

A very special appreciation to Dr. Macciotta for helping me, even though he did not have any obligation, but gave me guidance nonetheless to proceed with my research in the different stages of the investigation, and also helped me evaluate the early edition of the thesis.

Thank you Dr. Andrina for taking the time to clarify the procedures and giving more detailed information from the experiment that she conducted in her PhD.

Thank you to Vivian Giang for all the grammatical tips and quick revisions you provided me.

Sally and Lorene, thank you very much for everything you did for me, helping me with all department procedures and letters in the department.

I want to thank all the people who were part of my academic process, all the friends I made that in one way or another gave me their advice, particularly Ahlam Abdulnabi for all the talk about unsaturated flow mechanics.

Finally, I would like to thank the University of Alberta and the Department of Civil & Environmental Engineering. I feel an honor to become a former student at this prestigious institution.

TABLE OF CONTENTS

ABSTRACT	II
ACKNOWLEDGEMENTS	III
CHAPTER 1 INTRODUCTION	1
1.1. BACKGROUND	1
1.2. RESEARCH OBJECTIVES	3
CHAPTER 2 LITERATURE REVIEW	4
2.1. WATER IN MINE WASTE ROCK	4
2.2. WASTE ROCK EMBANKMENT IN GOLDEN SUNLIGHT MINE	6
2.3. FLOW PATH OF WATER INFILTRATION FROM THE SURFACE	10
2.4. LATERAL FLOW IN A VERTICAL COLUMN	12
2.4.1. LABORATORY TEST PROGRAM	12
2.4.1. EXPERIMENT CONDITIONS	15
2.4.2. MATERIAL PROPERTIES	16
2.4.3. EXPERIMENT RESULTS	20
2.5. WATER FLOW MODEL IN WASTE ROCK EMBANKMENTS	23
2.6. FLOW IN INCLINE LAYERING SYSTEM	28
2.6.1. SINGLE LAYER SYSTEM	28
2.6.2. DOUBLE LAYER SYSTEM	30
2.6.3. MULTIPLE LAYER SYSTEM	32
2.7. SUMMARY	45
CHAPTER 3 THEORY AND UNSATURATED FLOW	47
3.1. UNSATURATED SOILS	47

3.1.1. SOIL WATER CHARACTERISTIC CURVE	49
3.1.1. ESTIMATION OF THE HYDRAULIC CONDUCTIVITY CURVE	53
3.2. WATER FLOW IN UNSATURATED CONDITION	55
3.3. NUMERICAL MODELING FOR WATER FLOW IN UNSATURATED SOILS	57
3.3.1. FLOW LAWS	59
3.3.2. MASS BALANCE	60
3.3.3. PDE FOR UNSATURATED STEADY STATE WATER FLOW	61
3.4. SUMMARY	62

CHAPTER 4 NUMERICAL MODEL OF WATER FLOW IN UNSATURATED COLUMN LAYERED

SYSTEM	64
4.1. INTRODUCTION	64
4.2. OBJECTIVES	64
4.3. LABORATORY COLUMN EXPERIMENT	65
4.3.1. MATERIAL CHARACTERISTICS	68
4.3.2. EXPERIMENT RESULTS	74
4.3.1. SEEP/W SIMULATION RESULTS	76
4.4. NUMERICAL MODEL	79
4.4.1. MODELLING METHODOLOGY	80
4.4.2. MODELING ASSUMPTIONS	84
4.4.3. THEORY ADOPTED BY THE NUMERICAL INTEGRATION FOR A COLUMN LAYERED SYSTEM	84
4.4.4. MODEL BOUNDARY CONDITIONS	87
4.5. WATER FLOW SIMULATION RESULTS	88
4.5.1. WATER FLOW IN SANDY MATERIAL	88
4.5.2. WATER FLOW IN WASTE ROCK MATERIAL	103
4.5.3. INTERNAL RESPONDS FOR SENSITIVITY MODELS	107
4.5.4. HIGHEST CORRELATION CONDITIONS FOR THE COLUMN EXPERIMENT	113
4.6. ANALYSIS AND DISCUSSION	115
4.7. CONCLUSIONS	118

CHAPTER 5 NUMERICAL MODEL OF WATER FLOW MODEL IN INCLINE LAYERED SYSTEM **120**

5.1. INTRODUCTION	120
5.2. OBJECTIVES	120
5.3. MESO-SCALE PANEL EXPERIMENT	121
5.3.1. MATERIAL PROPERTIES	126
5.3.2. EXPERIMENT RESULTS	128
5.4. NUMERICAL MODEL	131
5.4.1. MODEL METHODOLOGY	132
5.4.2. MODEL ASSUMPTION	135
5.4.3. THEORY ADOPTED FOR THE NUMERICAL INTEGRATION FOR A COLUMN LAYERED SYSTEM	135
5.4.4. MODEL BOUNDARY CONDITIONS	138
5.5. SIMULATION OF PANEL-1	140
5.5.1. SIMULATION APPLYING EXPERIMENTAL CONDITIONS AND MEASURE PROPERTIES	140
5.5.2. SIMULATION OF PANEL-1 WITH CALIBRATED PROPERTIES	144
5.6. SIMULATION OF PANEL-2	152
5.7. SIMULATION OF PANEL-3	157
5.8. ANALYSIS AND DISCUSSION	167
5.8.1. MODELLING OF MESO-SCALE PANELS	168
5.8.2. NUMERICAL MODEL COMPARISON	175
5.9. CONCLUSIONS	177
 CHAPTER 6 CONCLUSIONS	 180
 6.1. FURTHER RESEARCH	 181
 APPENDIX	 183
 A. Back Analysis of k_{sat} for BCS in Column-1	 183
B. Back Analysis of K_{sat} for SS in Column-1	186
C. Back Analysis of AEV for BCS in Column-1	188
D. Back Analysis of K_{sat} For WR in Column-2	190
E. Water Flow Transfer in Sandy Soil	192
F. Water Flow Transfer in Waste rock	198

G. Pressure Profiles In Column-1 Using Sandy Soils	200
H. Pressure Profiles In Column-2 Using Waste Rock	203
I. Profile Results from Simulation in Column-1	204
J. Profile Results from Simulation in Column-2	208
K. Calibration of Acid Rock in Panel-1	209
L. Simulation Profiles in Panel-1	218
M. Simulation Profiles in Panel-2	221
N. Simulation Profiles in Panel-3	223
O. Simulation of Panel-1 Under Different Material Properties	226
REFERENCES	246

LIST OF FIGURES

Figure 2.1 ARD Trigger Mechanisms (INAP, 2009, p. Chapter 4)	4
Figure 2.2 Types of Hydrostratigraphy in Rock Pile Embankments	5
Figure 2.3 Waste Rock Benches (Wilson, 2003)	7
Figure 2.4 Waste Rock Embankment Structure (Wilson, 2001)	8
Figure 2.5 Water Cycle in a Waste Rock Embankment (Herasymuik, 1996)	9
Figure 2.6 Column Design Experiment for Horton and Hawkins (1965)	11
Figure 2.7 Scheme of Laboratory Column 1 after Newman (1999)	14
Figure 2.8 Scheme of Laboratory Column 2 after Newman (1999)	14
Figure 2.9 Soil Water Characteristic Curve for Materials in Column-1 Wilson (1990), Swanson (1991), Newman (1999)	17
Figure 2.10 Hydraulic Conductivity Curve for Material in Column-1 (Newman, 1999)	18
Figure 2.11 Soil Water Characteristic Curve for Materials in Column-2 (Herasymuik, 1996)	19
Figure 2.12 Hydraulic Conductivity Curve for Material in Column-1 (Herasymuik, 1996)	20
Figure 2.13 Total Discharge of the Fine Material for Column-1, after Newman (1999)	21
Figure 2.14 Total Discharge of the Coarse Material for Column-1, after Newman (1999)	21
Figure 2.15 Total Discharge for Column-2, after Newman (1999)	23
Figure 2.16 Model Results for EPM and TPROGS at T=65 Days A) Material Zone; B) Pressure Head; C) Saturation (Broda, et al., 2013)	26
Figure 2.17 Saturation Distribution in 5 Days (a) and Change in Time of Total Flow Entering the Base Compacted Layer (b) In X=35 M (Broda, et al., 2013)	27
Figure 2.18 General Characteristics of Soil Tank (Lv, et al., 2013)	29
Figure 2.19 Profile of Vector Flow at 100 Hr for a Tank Inclination of 9° and 19° (Lv, et al., 2013, p. 325 Fig.9.)	30
Figure 2.20 Geometry of the Incline Capillary Barrier (Tami, et al., 2004)	30
Figure 2.21 Vertical Hp Profiles At 5% of Ksat (Tami, et al., 2004)	31
Figure 2.22 Meso-Scale Experiment for Panel-3 (Andrina, 2009)	33
Figure 2.23 Meso-scale Experiment for Panel-1 (Based on Andrina, 2009)	34
Figure 2.24 Meso-scale Experiment for Panel-2 (Based on Andrina, 2009)	35
Figure 2.25 Meso-scale Experiment for Panel-3 (Based on Andrina, 2009)	36
Figure 2.26 Boundary Conditions for the Meso-scale Experiment	37

Figure 2.27 Sieve Analysis from Waste Rock Material (Andrina, 2009)	38
Figure 2.28 Soil-Water Characteristic Curves for Waste Rock, after Andrina (2009)	40
Figure 2.29 Hydraulic-Conductivity-Curve (Right) for Waste Rock, after Andrina (2009)	40
Figure 2.30 Measured Matric Suction from Panel-1 and Panel-3 at 0.5 m and 1.0 m Elevation for 2 mm/Day and 10 mm/Day (Andrina, 2009)	45
Figure 3.1 Unsaturated Flow in Hydrologic Cycle	47
Figure 3.2 Unsaturated Soil Phases (Fredlund, et al., 2012)	48
Figure 3.3 Example of A SWCC for A Sandy Soil, Silty Soil, and Silty Clay (Fredlund & Xing, 1994 A)	49
Figure 3.4 Hysteresis in the Soil Water Characteristic Curve for A Silty Soil (Fredlund & Xing, 1994 A)	51
Figure 3.5 Void Ratio Constitutive Surface for Beaver Creek Sand, Fredlund et al. (2006)	52
Figure 3.6 Gravimetric Water Content Constitutive Surface for Beaver Creek Sand, Fredlund et al. (2006)	52
Figure 3.7 Saturation Constitutive Surface for Beaver Creek Sand, Fredlund et al. (2006)	52
Figure 3.8 Hydraulic Conductivity Function for Fine and Coarse Sand	54
Figure 3.9 Element Generation Used By SvFlux (SoilVision Systems Ltd., 2012)	58
Figure 3.10 Referential Elemental Volume (REV) For Conservation Of Mass (SoilVision Systems Ltd., 2012)	61
Figure 4.1 Column Test Characteristics Using Sandy Materials (a) and Waste Rock (b), after Newman (1999)	67
Figure 4.2 SWCC (a) and Hydraulic Conductivity Curve (b) for Materials in Column-1 (Newman, 1999)	70
Figure 4.3 Grainsize Distribution Curve (Herasymuik, 1996)	71
Figure 4.4 SWCC (a) and Hydraulic Conductivity Curve (b) for Materials in Column-2 (Herasymuik, 1996)	73
Figure 4.5 Discharge Flow of the Fine (a) And Coarse (b) Material in Column-1 after Newman (1999)	75
Figure 4.6 Total Discharge for Column-2 after Newman (1999)	76
Figure 4.7 Model Mesh with Seep/W Ver. 2.0 by Newman (1999)	77
Figure 4.8 Discharge Flow from Fine Material from Seep/W Simulation (Newman, 1999)	78
Figure 4.9 Model Proposed By Herasymuik (Herasymuik, 1996)	79
Figure 4.10 Methodology for Column-1	82
Figure 4.11 Methodology for Column-2	83
Figure 4.12 Model Mesh with SvFlux Ver. 7.0	86
Figure 4.13 Discharge Flow from Fine Material Using the Laboratory k_{sat}	89
Figure 4.14 Matric Suction and Flux Vectors for Test 2 and 4 Under 450 mm/day (Flux c) Using A Base Suction of 0.8 kPa on the Coarse and 2.5 kPa on the Fine	91
Figure 4.15 Corrected Discharge Flow from Fine Material Using the Laboratory k_{sat} for Test 3 and Test 4	92
Figure 4.16 Discharge Flow from Fine Material Using k_{sat} From Calibrated Newman Simulation	93
Figure 4.17 Discharge Flow from Fine Material by Calibrating k_{sat} on the Fine Sand	95

Figure 4.18 Change in k_{sat} with the Precipitation from Fine Sand Calibration to give a discharge within 10% difference using a Base Suction in the coarse of 0.1, 0.8, and 2.5 kPa	96
Figure 4.19 Change in Discharge from BCS Vs k_{sat} for Test 1 and Test 4	97
Figure 4.20 Discharge Flow from Fine Material by Calibrating k_{sat} on the Coarse Sand	98
Figure 4.21 Change in k_{sat} with the Precipitation from Coarse Sand Calibration to give a discharge within 10% difference using a Base Suction in the coarse of 0.1, 0.8, and 2.5 kPa	99
Figure 4.22 Change in Discharge from SS vs k_{sat} for Test 1 and Test 4	100
Figure 4.23 Discharge Flow from Fine Material by Calibrating AEV on the BCS	101
Figure 4.24 Average AEV per Flux from Fine Sand Calibration to give a discharge within 10% difference using a Base Suction in the coarse of 0.1, 0.8, and 2.5 kPa	102
Figure 4.25 Discharge Flow from Fine-waste-rock using the Laboratory k_{sat}	103
Figure 4.26 Discharge Flow from Fine-waste-rock by Calibrating k_{sat} on the Fine-waste-rock and on the Coarse-waste-rock	105
Figure 4.27 Calibrated k_{sat} for F-WR (a) and For C-WR (b)	106
Figure 4.28 Change in Precipitation for Test 1 with a Base Suction of 2.5 kPa in the Fine Material and 0.8 kPa in the Coarse Material	108
Figure 4.29 Comparison on the Change in Contact Length for a Precipitation of 800 mm/day with a Base Suction of 2.5 kPa in the Fine Material and 0.8 kPa in the Coarse Material	110
Figure 4.30 Change in Contact Length for a Precipitation of 1120 mm/day with a Base Suction of 2.5 kPa in the Fine Material and 0.8 kPa in the Coarse Material	111
Figure 4.31 Comparison of Pressure Profiles for Column-2 at Different Precipitation Rates	112
Figure 5.1 Meso-Scale Experiment for Panel-3 (Andrina, 2009)	122
Figure 5.2 Physical Characteristics of Panel 1 Geometry, Material, Instrumentation, Drainage Points (Andrina, 2009)	123
Figure 5.3 Physical Characteristics of Panel-2 Geometry, Material, Instrumentation, Drainage Points (Andrina, 2009)	124
Figure 5.4 Physical Characteristics of Panel-3 Geometry, Material, Instrumentation, Drainage Points (Andrina, 2009)	124
Figure 5.5 Grainsize Distribution Curve for Waste Rock in Meso-scale Panels	126
Figure 5.6 SWCC for Waste Rock in Meso-scale Experiment	127
Figure 5.7 Hydraulic-Conductivity-Curves for the Meso-scale Experiment Estimations Using Fredlund & Xing (1994)	128
Figure 5.8 Discharge Flow of the Fine (a) and Coarse (b) Waste Rock in Panel-1 after Andrina (2009)	129
Figure 5.9 Discharge Flow of the Fine (a) and Coarse (b) Waste Rock in Panel-2 after Andrina (2009)	129
Figure 5.10 Discharge Flow of the Fine (a) and Coarse (b) Waste Rock in Panel-3 after Andrina (2009)	130

<i>Figure 5.11 Measured Matric Suction from Panel-1 and Panel-3 at 0.5 m and 1.0 m Elevation for 2 mm/Day and 10 mm/Day (Andrina, 2009)</i>	131
<i>Figure 5.12 Mesh Geometry for Panel-1</i>	137
<i>Figure 5.13 Boundary Conditions and Geometry of Panel-1</i>	139
<i>Figure 5.14 Simulation of Total Outflow for Panel-1 under Laboratory Conditions for the Fine Layers (a) and Coarse Layers (b)</i>	140
<i>Figure 5.15 Head Pressure, Streamtraces and Flux Vector for Panel-1 for 10 mm/Day and 4 kPa of Suction</i>	142
<i>Figure 5.16 Simulation of Total Outflow for Panel-1 Using Calibrated Parameters in the Acid Rock for the Fine Layers (a) and Coarse Layers (b)</i>	144
<i>Figure 5.17 Simulated Matric Suction at 0.5 m (a) and 1.0 m (b) Elevations Applying a Base Suction of 4.0 kPa</i>	145
<i>Figure 5.18 Contrast Discharge at Three Precipitation Rates in Panel-1 Applying a Base Suction of 4.0 kPa</i>	146
<i>Figure 5.19 Simulation of Panel-1 using Calibrated Parameters under a Precipitation of 2 mm/day and a Base Suction of 2.0 kPa</i>	148
<i>Figure 5.20 Simulation of Panel-1 using Calibrated Parameters under a Precipitation of 10 mm/day and a Base Suction of 2.0 kPa</i>	149
<i>Figure 5.21 Profile Simulation of Panel-1 using Calibrated Parameters under Base Suction of 0.0 kPa and a Precipitation of 10 mm/Day</i>	150
<i>Figure 5.22 Profile Simulation of Panel-1 using Calibrated Parameters under a Base Suction of 4.0 kPa and a Precipitation of 10 mm/Day</i>	151
<i>Figure 5.23 Water Flow in the Discharge Points at a Precipitation of 10 mm/Day</i>	152
<i>Figure 5.24 Simulation of Total Outflow for Panel-2 under a Base Suction of 4.0 kPa for the Fine Layers (a) and Coarse Layers (b)</i>	153
<i>Figure 5.25 Simulation in Panel-2 at a Precipitation of 2 mm/day and 4 kPa of Base Suction for Case 3</i>	155
<i>Figure 5.26 Simulation in Panel-2 at a Precipitation of 10 mm/day and 4 kPa of Base Suction for Case 3</i>	156
<i>Figure 5.27 Total Outflow for Panel-3 for a Precipitation of 2 mm/Day in the Experiment Results and the Three Simulation Cases</i>	158
<i>Figure 5.28 Simulation of Panel-3 under at a Base Suction of 2 kPa and a Precipitation of 2 mm/Day for Case 3</i>	161
<i>Figure 5.29 Simulation of Panel-3 under at a Base Suction of 4 kPa and a Precipitation of 2 mm/Day for Case 3</i>	162
<i>Figure 5.30 Water Flow from the Discharge Points for a Suction of 2.0 kPa and 4.0 kPa at a Precipitation of 2 mm/Day in Case 3, Panel 3</i>	163
<i>Figure 5.31 Total Outflow for Panel-3 for Base Suction of 4.0 kPa in the Experiment Results (a) and the third Simulation Cases (b)</i>	164

Figure 5.32 Simulation of Panel-3 under a Precipitation of 2 mm/day and a Base Suction of 4.0 kPa For Case 3	165
Figure 5.33 Simulation of Panel-3 under a Precipitation of 10 mm/day and a Base Suction of 4.0 kPa For Case 3	166
Figure 5.34 Correlation between Simulation and Experiment in Panel-1	169
Figure 5.35 Correlation between Simulation and Experiment at 4.0 kPa of Suction in Panel-2	171
Figure 5.36 Correlation between Simulation and Experiment with Respect to the Change in Precipitation (a) and Change in Suction (b) for Panel-3	172
Figure 5.37 Contrast Discharge from Four Material Sets in Panel-1 under Three Precipitation Rates and Applying a Base Suction of 4.0 kPa	173
Figure 5.38 Contrast Discharge from Four Material Sets in Panel-1 under Three a Base Suction and at a Precipitation of 10 mm/Day	174
Figure A.1 Back Analysis Results from BCS in Column-1 for a Suction of at the Coarse Base of 0.1, 0.8, and 2.5 kPa; and a Precipitation of 1120 mm/day (a), 800 mm/day (b), 440 mm/day (c) and 330 mm/day (d)	183
Figure A.2 Calibrated Saturated Hydraulic Conductivity for Fine Sand	184
Figure B.1 Back Analysis Results from SS in Column-1 for a Suction of at the Coarse Base of 0.1, 0.8, and 2.5 kPa; and a Precipitation of 1120 mm/day (a), 800 mm/day (b), 440 mm/day (c) and 330 mm/day (d)	186
Figure B.2 Calibrated Saturated Hydraulic Conductivity for Coarse Sand	187
Figure C.1 Back Analysis of AEV for the BCS in Column-1 for a Suction of at the Coarse Base of 0.1, 0.8, and 2.5 kPa; and a Precipitation of 1120 mm/day (a), 800 mm/day (b), 440 mm/day (c) and 330 mm/day (d)	188
Figure D.1 Back Analysis of F-WR k_{sat} (a) and C-WR k_{sat} (b) for Waste Rock in Column-2 for a Suction of at the Base of 0.0 kPa; and a Precipitation of 445 mm/day (a), 12 mm/day (b), and 5 mm/day (c)	190
Figure D.2 Total Discharge from the Back Analysis of F-WR and C-WR in Column-2	191
Figure E.1 Sensitivity Curves for Lateral Flow with Changes k_{sat} from BCS for a Suction of at the Coarse Base 0.1, 0.8, and 2.5 kPa; and a Precipitation of 1120 mm/day (a), 800 mm/day (b), 440 mm/day (c) and 330 mm/day (d)	193
Figure E.2 Lateral Flow in Column-1, Comparison between Laboratory Results, and Model Calibration of k_{sat} from BCS	194
Figure E.3 Sensitivity Curves for Lateral Flow with Changes k_{sat} from SS for a Suction of at the Coarse Base of 0.1, 0.8, and 2.5 kPa; and a Precipitation of 1120 mm/day (a), 800 mm/day (b), 440 mm/day (c) and 330 mm/day (d)	195
Figure E.4 Lateral Flow in Column-1, Comparison between Laboratory Results, and Model Calibration of k_{sat} from SS	196
Figure F.1 Water Transfer between Coarse Sand and Fine Sand from Iteration of k_{sat} for the Fine-waste-rock and Coarse-waste-rock	198

<i>Figure F.2 Lateral Flow in Column-2, Comparison Between Laboratory Results, Model with Laboratory Properties and Model Calibration of k_{sat} from F-WR, C-WR</i>	199
<i>Figure G.1 Change in Suction at Calibration of k_{sat} in BCS-Test 1, 2, 3, And 4 for a Suction of at the Coarse Base of 0.8 kPa; and a Precipitation of 1120 mm/day (a), 800 mm/day (b), 440 mm/day (c) and 330 mm/day (d)</i>	200
<i>Figure H.1 Change In Suction at Calibration Of k_{sat} In C-WR for a Suction of at the Base of 0.0 kPa; and a Precipitation of 445 mm/day (a), 12 mm/day (b), and 5 mm/day (c)</i>	203
<i>Figure I.1 Results from Test-1 with A Contact Length of 550 mm for for a Suction of at the Base of 0.8 kPa and a Precipitation of 1120 mm/day (a), 800 mm/day (b), 440 mm/day (c) and 330 mm/day (d)</i>	204
<i>Figure I.2 Results from Test-2 with A Contact Length of 750 mm for for a Suction of at the Base of 0.8 kPa and for Precipitation of 1120 mm/day (a), 800 mm/day (b), 440 mm/day (c) and 330 mm/day (d)</i>	205
<i>Figure I.3 Results from Test-3 with A Contact Length of 1000 mm for for a Suction of at the Base of 0.8 kPa and for Precipitation of 1120 mm/day (a), 800 mm/day (b), 440 mm/day (c) and 330 mm/day (d)</i>	206
<i>Figure I.4 Results from Test-4 with A Contact Length of 1100 mm for for a Suction of at the Base of 0.8 kPa and for Precipitation of 1120 mm/day (a), 800 mm/day (b), 440 mm/day (c) and 330 mm/day (d)</i>	207
<i>Figure J.1 Results from Column-2 with A Contact Length of 1000 mm for a Suction of at the Base of 0.0 kPa; and a Precipitation of 445 mm/day (a), 12 mm/day (b), and 5 mm/day (c)</i>	208
<i>Figure K.1 Calibration of The AEV from the F-AR in Test VI (10 mm/Day and A Suction of 2.0 kPa)</i>	210
<i>Figure K.2 Calibration of The AEV from the C-AR in Test VI (10 mm/Day and A Suction of 2.0 kPa)</i>	211
<i>Figure K.3 Panel-1 Correlations for 10 mm/Day and 2.0 kPa Suction</i>	212
<i>Figure K.4 Calibration Of The k_{sat} from the F-AR in Test VI - 10 mm/Day and a Suction of 2.0 kPa</i>	214
<i>Figure K.5 Calibration Of The k_{sat} From the C-AR in Test VI - 10 mm/Day and a Suction of 2.0 kPa</i>	215
<i>Figure K.6 HCCs after Calibration of the Acid Rock in Panel-1</i>	217
<i>Figure L.1 Simulation of Panel-1 Under A Base Suction of 0.0 kPa and a Precipitation of 10 mm/Day</i>	218
<i>Figure L.2 Simulation of Panel-1 under a Base Suction of 2.0 kPa and a Precipitation of 2 mm/Day</i>	218
<i>Figure L.3 Simulation of Panel-1 under a Base Suction of 2.0 kPa and a Precipitation of 10 mm/Day</i>	219
<i>Figure L.4 Simulation of Panel-1 under a Base Suction of 4.0 kPa and a Precipitation of 2 mm/Day</i>	219
<i>Figure L.5 Simulation of Panel-1 under a Base Suction of 4.0 kPa and a Precipitation of 5 mm/Day</i>	220
<i>Figure L.6 Simulation of Panel-1 under a Base Suction of 4.0 kPa and a Precipitation of 10 mm/Day</i>	220
<i>Figure L.7 Change in Matric Suction at 0.5 m and 1.0 m Elevations</i>	220
<i>Figure M.1 Simulation of Panel-2 under a Base Suction of 4.0 kPa and a Precipitation of 2 mm/Day</i>	221
<i>Figure M.2 Simulation of Panel-2 under a Base Suction of 4.0 kPa and a Precipitation of 5 mm/Day</i>	221
<i>Figure M.3 Simulation of Panel-2 under a Base Suction of 4.0 kPa and a Precipitation of 10 mm/Day</i>	222
<i>Figure M.4 Change in Matric Suction at 0.5 m, 1.0 m, and 1.5 m Elevations for a Base Suction of 4.0 kPa in Panel-2</i>	222

Figure N.1 Simulation of Panel-3 under a Base Suction of 2.0 kPa And a Precipitation of 2 mm/Day _____	223
Figure N.2 Simulation of Panel-3 under a Base Suction of 4.0 kPa And a Precipitation of 2 mm/Day _____	223
Figure N.3 Simulation of Panel-3 under a Base Suction of 4.0 kPa And a Precipitation of 5 mm/Day _____	224
Figure N.4 Simulation of Panel-3 under a Base Suction of 4.0 kPa And a Precipitation of 10 mm/Day _____	224
Figure N.5 Change In Matric Suction At 0.5 m, And 1.0 m Elevations For A Base Suction Of 2.0 kPa And 4.0 kPa In Panel-3 _____	225
Figure O.1 HCCs from the Four Tests Applied To the Fine and Coarse Layers in Panel-1 _____	226
Figure O.2 Simulation Discharge from the Coarse Material (Right) and Fine Material (Left) Using the Calibrated Properties of Sandy Soils from Column-1 _____	227
Figure O.3 Contrast Profile from Changes in Precipitation in Test 2 Applying a Base Suction of 4.0 kPa _____	228
Figure O.4 Contrast Discharge at Three Precipitation Rates in Test 2 Applying a Base Suction of 4.0 kPa _____	229
Figure O.5 Contrast Profile from Changes in Base Suction in Test 2 at a Precipitation of 10 mm/Day _____	230
Figure O.6 Contrast Discharge from Changes in Base Suction in Test 2 at a Precipitation of 10 mm/Day _____	231
Figure O.7 Change In Matric Suction in Test 2 at 0.5 m and 1.0 m Elevations _____	232
Figure O.8 Simulation Discharge from the Coarse Material (a) and Fine Material (b) Using the Calibrated Properties of Waste Rock From Column-2 _____	233
Figure O.9 Contrast Profile from Changes in Precipitation in Test 3 Applying a Base Suction of 4.0 kPa _____	234
Figure O.10 Contrast Discharge at Three Precipitation Rates in Test 3 Applying a Base Suction of 4.0 kPa _____	235
Figure O.11 Contrast Profile from Changes in Base Suction in Test 3 at a Precipitation of 10 mm/Day _____	236
Figure O.12 Contrast Discharge from Changes in Base Suction in Test 3 at a Precipitation of 10 mm/Day _____	237
Figure O.13 Change in Matric Suction at 0.5 m and 1.0 m Elevations _____	238
Figure O.14 SWCC for TBS and Devon Silt _____	239
Figure O.15 Simulation Discharge from the Coarse Material (Right) and Fine Material (Left) Using the Calibrated Properties of Waste Rock From Column-2 _____	240
Figure O.16 Contrast Profile from Changes in Precipitation in Test 4 Applying a Base Suction of 4.0 kPa _____	241
Figure O.17 Contrast Discharge at Three Precipitation Rates in Test 4 Applying a Base Suction of 4.0 kPa _____	242
Figure O.18 Contrast Profile from Changes in Base Suction in Test 4 at a Precipitation of 10 mm/Day _____	243
Figure O.19 Contrast Discharge from Changes in Base Suction in Test 4 at A Precipitation of 10 mm/Day _____	244
Figure O.20 Change In Matric Suction at 0.5 M And 1.0 M Elevations _____	244

LIST OF TABLES

<i>Table 2.1 Experimental Conditions for Column Test (Newman, 1999)</i>	15
<i>Table 2.2 Sand Properties for Column-1</i>	16
<i>Table 2.3 Waste Rock Properties for Column-2 (Herasymuik, 1996, pp. 103,124)</i>	18
<i>Table 2.4 Porosity and Hydraulic Conductivity for EPM and TPROGS Model</i>	24
<i>Table 2.5 Testing Conditions for Each Panel</i>	37
<i>Table 2.6 Waste rock Properties (Andrina, 2009)</i>	39
<i>Table 2.7 Drainage Point Outflow from Meso-scale Experiments</i>	41
<i>Table 2.8 Discharge Results from the Three Panels Grouped By Material</i>	42
<i>Table 2.9 Discharge Results from Panel-3 Grouped By Grain Size</i>	43
<i>Table 4.1 Experimental Conditions for Column Test</i>	66
<i>Table 4.2 Material Properties for Column-1</i>	68
<i>Table 4.3 Material Properties for Column-2 (Herasymuik, 1996)</i>	71
<i>Table 4.4 Simulation Results and Comparison to the Laboratory Test for Column-1</i>	113
<i>Table 4.5 Simulation Results and Comparison to the Laboratory Test for Column-2</i>	114
<i>Table 5.1 Testing Conditions for Each Panel</i>	125
<i>Table 5.2 Material Properties for Simulation</i>	127
<i>Table 5.3 Simulation Cases for Back Analysis of the AEV</i>	133
<i>Table 5.4 Simulation Cases for Back Analysis of the k_{sat}</i>	133
<i>Table G.1 Longitude of Equilibrium Suction for Colum-1 (m)</i>	201
<i>Table K.1 Calibration Results for AEV of the F-AR</i>	212
<i>Table K.2 Calibration Results for AEV of the C-AR</i>	213
<i>Table O.1 Material Characteristics for TBS and Devon Silt</i>	239

LIST OF SYMBOLS

ARD: Acid Rock Drainage	LAB: Laboratory
AEV: Air entry value	m_v : Coefficient of Compressibility
BCS: Beaver Creek Sand	n : Porosity
C-WR: Coarse Waste Rock	nm: Not Measured
C-AR: Coarse Acid Rock	PDE: Partial differential Equation
C_c : coefficient of curvature	PPMCC: Pearson Product Moment Correlation Coefficient
C_u : coefficient of uniformity	q : flow
EPM: Equivalent Porous Media	WR: Waste Rock
F-AR: Fine Acid Rock	SS: Silica Sand
F-WR: Fine Waste Rock	SWCC: Soil Water Characteristic Curve
G_s : Specific Gravity	TPROGS: Transition Probability Geo-Statistical Software
h : total head	u_a = air pressure
HCC: Hydraulic conductivity Curve	u_w = pore water pressure (PWP)
h_p : Head Pressure	VWC: Volumetric water content
k : Hydraulic conductivity	WRE: Waste rock Embankments
k_{sat} : Saturated Hydraulic Conductivity	

CHAPTER 1 INTRODUCTION

1.1. BACKGROUND

Understanding the mechanisms controlling water flow in unsaturated soil is of great importance, particularly in waste rock embankments. In open pit or underground mining operations, the extraction of the ore is usually accomplished by large excavations that produce high volumes of waste rock with no economic value. Most mining companies are aware of the importance for the proper treatment of these large structures. Barrick Gold Corp. are the owners of Golden Sunlight Mine in the United States. Operating since 1975, this mine has produced over 100 million tons of waste rock; just in the year 2014 Freeport-McMoRan, the owners of Grasberg mine in Indonesia, produced 380 million tons of waste rock from different sites (Freeport-McMoran, 2015). Excavations on the waste rock embankments of the Golden Sunlight and Grasberg mines exposed the stratification of a dipping layer at the angle of repose of fine and Coarse-waste-rock (Wilson, 1995; Andrina, 2009). This by-product is stored temporally or permanently (according to the mining plan) usually in large embankments. Most of these structures are a large environmental hazards due to the potential generation of acid rock drainage (ARD). The exposure of sulphide minerals within the embankment to air and water is the main component to the generation of ARD. Once the reaction starts to produce leachate, it can take decades to stop. Waste rock embankments are massive structures with an enormous area of exposure to precipitation and air circulation. The water that flows through the embankment can drive the ARD to nearby stream, aquifers, or any other water sources. This situation highlights the importance of understanding water flow mechanism in waste rock embankments.

Water flows under specific regimes, and it becomes a function of the type of soil, the water content and the degree of saturation. Geotechnical practice has ignored the importance of understanding unsaturated soil mechanics, probably because most of the soil mechanics courses have been focused on the saturated world of soils. However, this is not generally the case, especially in waste rock embankments. Soils are a discontinuous system of particles. In unsaturated soils, this system is made up of four phases (air, water, soil and air-water interface) that allows generating negative

pore water pressure due to the air trap between grains. "Nowadays it has well accepted and tested that water will flow in unsaturated media only through pores with a continuous liquid phase, neglecting vapor phase transport" (Lu & Likos, 2004).

In the past two decades there have been major investigations involving unsaturated water flow in waste rock embankments. These investigations initiated the early understanding of the high complexity of the structure formed within waste rock embankments. These studies showed that the various construction processes controlled the embankment's internal structure.

In 1994, an excavation at Golden Sunlight Mine exposed the physical structure of the waste rock embankment. This profile was studied to characterize the properties and hydraulic behavior of the material (Herasymuik, 1996). The investigation showed that the structure is a function of the method used to place the material. The most commonly used method in the mining industry is named end-dumping and generates a segregation in the material that forms a layering system. Despite understanding the general structure of this kind of waste embankments, current models still lack the degree of precision required to properly assess the mechanism of flow in unsaturated conditions. Due to the high complexity of these structure, generalizations have been proposed to make the first approach using more simplistic models that describe the mechanism of water flow. In 1999, Newman constructed two column experiments to examine the relationship between precipitation and contact length with the lateral flow, and describe the mechanism that drives water flow in sandy material and in waste rock from Golden Sunlight. Later on, in 2009 Andrina constructed three Meso-scale experiments of incline layers of waste rock from Grasberg Mine to identify the flow mechanisms in incline coarse and fine layers of waste rock, under unsaturated conditions.

This research presents the numerical simulation associated with the two laboratory programs (Newman, 1999; Andrina, 2009) of unsaturated water flow. The thesis is divided in four main sections. The first section consists of contextual information that states the relevance of this investigation, followed by background information from the studies that are the bases of the numerical models. The second section consists of the base theory that the numerical model must satisfy. The third and four sections present the numerical analysis for the two column experiments and three Meso-scale (intermediate size) panels, respectively. The model simulations are validated by comparing the result to the experimental data.

1.2. RESEARCH OBJECTIVES

The objectives of this thesis are to evaluate the water flow mechanism in an unsaturated system, focusing on flow through waste rock material. The accomplishment of this objective is through numerical methods involving modeling using finite element methods of different laboratory experiments. The specific objectives are as follows:

1. Simulate unsaturated water flow from a vertical layer system of sandy material under steady state conditions for different precipitation rates and compare with the laboratory results.
2. Simulate unsaturated water flow from a vertical layer system of waste rock material under steady state conditions for different precipitation rates and compare with the laboratory results.
3. Simulate unsaturated water flow from three different configurations of incline layer systems of waste rock material under steady state conditions for different precipitation rates. and compare with the laboratory results
4. Calibrate the soil water characteristic curve and the hydraulic conductivity curve through a sensitivity analysis of the Air Entry Value and the Saturated Hydraulic Conductivity to verify the experimental results and validate the numerical models.

The research focuses on assessing the effect of precipitation rates and matric suction on the flow mechanism. The study will advance on the previous work conducted by Newman (1999) and Andrina (2009). These two studies involved experimental modelling of water flow in unsaturated soil conditions. The comparison between the results from these numerical models and the experimental data is limited by the available information from their theses. Nonetheless, the numerical models have reasonable conditions and information, which result in acceptable theoretical implications from the patterns and relationships.

CHAPTER 2 LITERATURE REVIEW

2.1. WATER IN MINE WASTE ROCK

Mineral oxidation can become a significant environmental issue to deal with, and most mines are not exempt from this concern. The oxidation is the sum of water and oxygen reactions with minerals containing sulphide. These reactions trigger Acid Rock Drainage or ARD (INAP, 2009). As such water flow within the structure of the embankment becomes an important issue to take into account, and therefore it is important to know the sources that contribute to this problem, such as the precipitation and evaporation. In waste rock embankments it is essential to characterize the transport of water (Wilson, 2001).

Figure 2.1 from the GARD guide shows the process in which ARD is generated in a waste rock embankment. Air would flow in through the bottom of the embankment due to advection process; the big openings and spaces formed from the construction process allow airflow through the whole embankment bed. Likewise, at the top of the embankment, the infiltration process occurs from precipitations. If the infiltration process is higher than the actual evaporation, seepage could have contact with the oxygen flowing in at the bottom, resulting in the oxidation process of the minerals in the embankment.

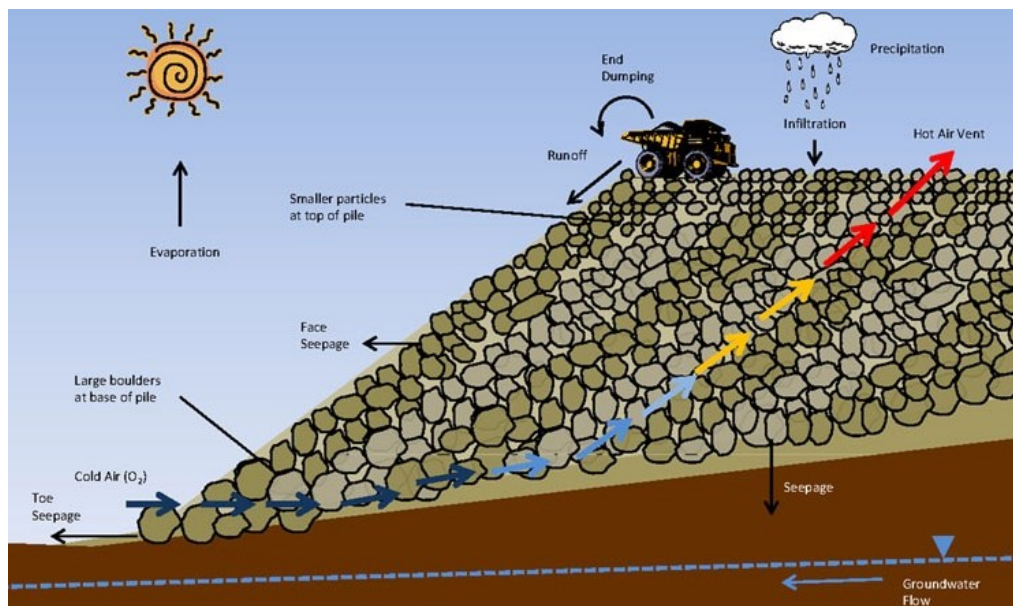


Figure 2.1 ARD Trigger Mechanisms (INAP, 2009, p. Chapter 4)

A waste rock embankment (WRE) has additional factors that also change water movement through the soil. These factors can alter the internal structure or material properties of the soil, such as: blasting, ore extraction, water chemistry, construction techniques, climate and local groundwater regime.

In order to make a proper analysis of water transport in WRE, it is fundamental to understand the internal structure that develops during the construction, as well as the hydraulic properties of the materials.

The type of material and the method of construction have a high influence in the hydrology that will govern in the waste rock dump (Smith, et al., 1995). There are four types of waste rock deposition (Broda, et al., 2013):

- I. End-dumping: the top zone has a finer particle concentration, while coarser material accumulates at the foot, as shown in Figure 2.1;
- II. Push-dumping from dozers: less segregation occurs; nonetheless, coarser material is located at the foot and near top;
- III. Free-dumping in small heaps: little segregation occurs by creating denser waste rock layers;
- IV. Drag-line: little segregation occurs as the Free-dumping process but with less dense layers.

Each type of deposition of waste rock material would influence in different degrees the amount and arrangement of the segregation that would occur. Figure 2.2 presents a general relationship of the stratigraphy and hydrogeology occurring in a WRE.

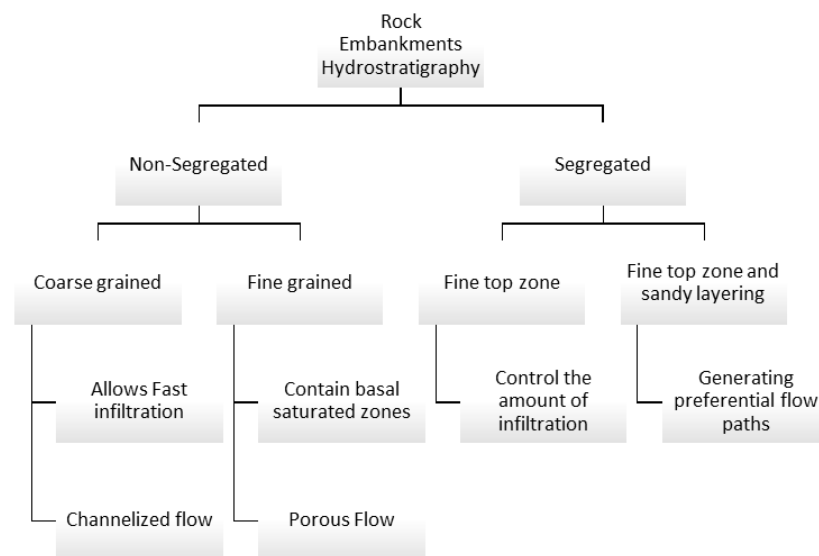


Figure 2.2 Types of Hydrostratigraphy in Rock Pile Embankments

The importance of water flow characteristics in this large structure is due to the high relation between the time at which a pile starts to generate ARD and the time in which the pile releases concentrations of metals to the water (Smith, et al., 1995).

According to the GARD (INAP, 2009) guide, “the hydraulic characteristics of a mine or process waste/facility may determine the contact time between solid and solution (e.g. rapid preferential flow vs. gradual matrix flow) or the proportion of mine waste being flushed”. Therefore the importance of understanding unsaturated water flows.

The generation of ARD in the WRE has led to numerous investigations that aim to improve our understanding of the behavior of water flow through unsaturated media. This chapter summarizes examples of some of the research directly related to the work presented in this thesis.

2.2. WASTE ROCK EMBANKMENT IN GOLDEN SUNLIGHT MINE

One of the most detailed works on the description and characterization of waste rock embankment was done at Golden Sunlight Mine. In 1994 at the Golden Sunlight Mine in Montana, United States, an excavation was studied to evaluate the reduction of drainage through the structure and to block oxygen transport using soil covers systems. The waste rock materials from this mine were used in a laboratory testing by Newman (1999), involving a column experiment. This experiment became the basis of the initial numerical simulations for this thesis.

The study of the drainage behavior and oxygen flow investigated the prevention or reduction of the oxidation of sulphide minerals. The climate conditions in the mine have high potential for evaporation. The mine is located in an arid region where the annual precipitation is around 240 mm/year, with a potential evaporation of 750 mm/year (Wilson, 1995).

The excavation of a waste rock embankment exposed a 100 m vertical section (see Figure 2.3); the section revealed a defined structure with respect to particle size distribution, or segregated stratigraphy (Wilson, 1995).

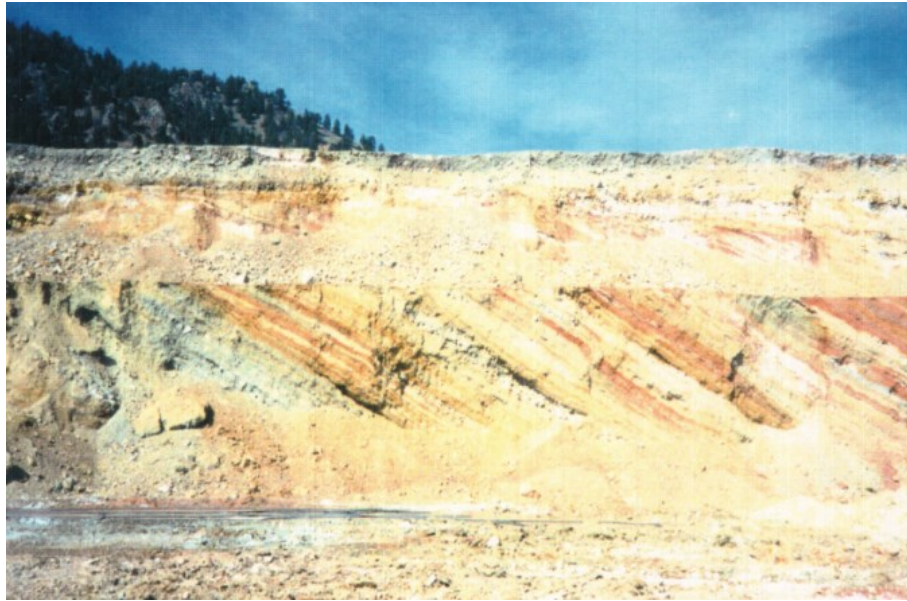


Figure 2.3 Waste Rock Benches (Wilson, 2003)

The waste rock dump was composed mainly of shale with a high potential for generating Acid Rock Drainage (ARD) due to the high concentrations of sulphite. The highest traces of oxidation were found at the top layers with temperatures exceeding 65°C. At the base, the seepage did not appear present in the layers, leaving the material dry and with no traces of ARD (Wilson, 1995).

Figure 2.3 shows the structure found at the excavation of the embankment; composed by incline layers at 38°, the dipping occurred due to the angle of repose of the material and the process of construction of the waste rock, in which the material is dumped from the top of the embankment, a process named end-dumping (Wilson, 2001). The materials within the layers had relatively uniform grain size and color (Wilson, 1995). During the construction process, segregation occurs as the material rolls downslope, leaving the coarsest material at the base of the dump and a layering structure of fine and coarse material at the face of the slope (see Figure 2.4).

At Golden Sunlight Mine, Herasymuik (Herasymuik, 1996) describes these dipping layers appearing “interfingered” and not continuous, as in some areas the layers become coarse rubble at the base of the pile. These variations in grain size distribution create random layering changes both horizontally and vertically. The grain size can also be affected by the heavy traffic at the top of the platform. The equipment compacts the waste rock during the construction the material, increasing the density.

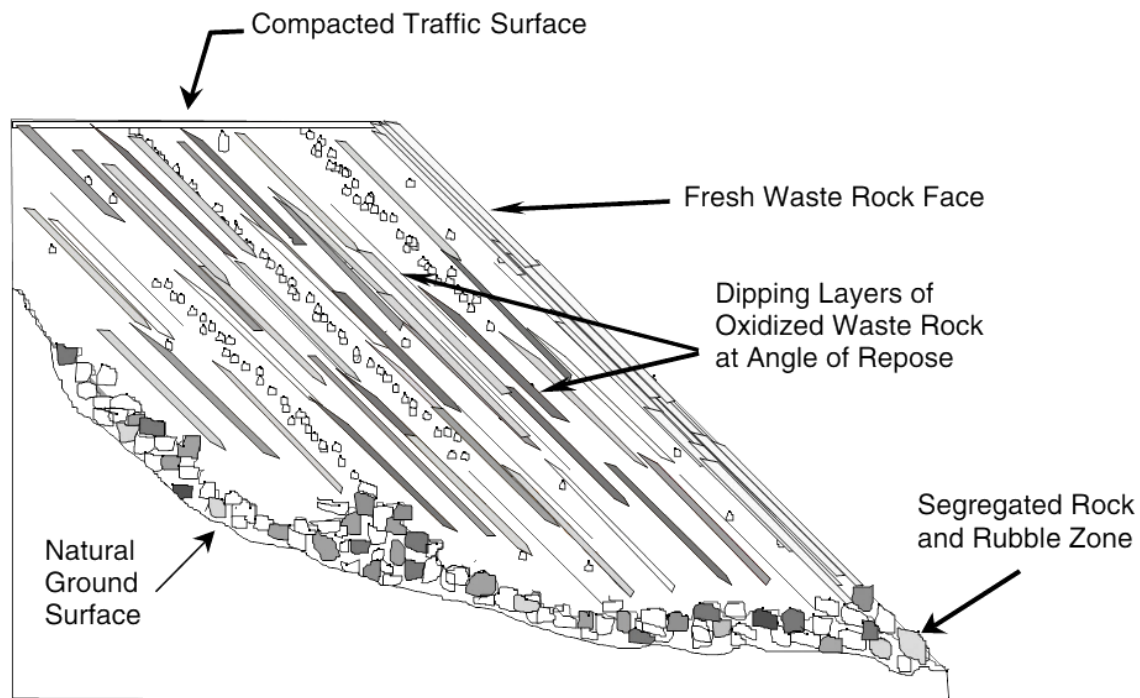


Figure 2.4 Waste Rock Embankment Structure (Wilson, 2001)

As segregation has a big influence for the grain distribution and structure, weathering also plays an important role, creating major changes. The material that is recently deposited at the top of the waste rock embankment only shows changes in grain size distribution with respect to the previously place that was exposed to physical and chemical degradation (Herasymuik, 1996).

The material was found to be in unsaturated conditions in the excavation. The coarse layers were almost entirely drained, with volumetric water content below 5%, contrary to the fine layers at the top 20 m where the volumetric water content ranges from 9% to 23% and saturation from 30% to 75%.

Wilson (1995) concluded in the site investigation that the embankment was under unsaturated conditions, with no presence of water at the bottom of the dump. The lower 80 m of the dump were dry and the upper 20 m were moist. That could have been related to the recently placed material that had a high water content due to the ore extraction process.

In the water cycle of a waste rock dump, water from precipitation may infiltrate, runoff, or evaporates at the surface. The water that infiltrates the top surface would travel through formed fissures and the interbedded layering. To overcome the water infiltration on top of the waste rock dump, a cover system might be placed on top,

allowing to “store and release” water through evaporation. Additionally due to segregation, the coarse fraction at the base and within the embankment creates a conduit for gas flow, and through diffusion and advection process water vapor and oxygen flow within the embankment. Herasymuik (1996) describes the water cycle in the waste rock in Figure 2.5.

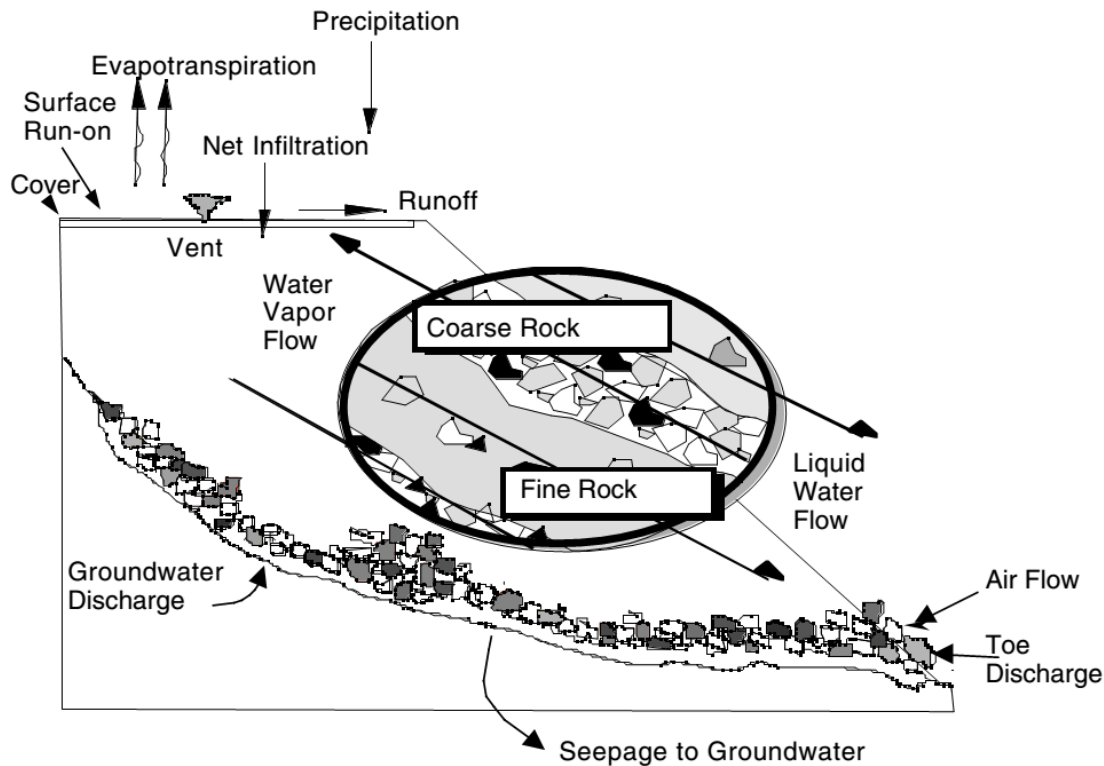


Figure 2.5 Water Cycle in a Waste Rock Embankment (Herasymuik, 1996)

Once water has infiltrated the top of the cover system, it may flow to the groundwater. As water will flow downward through gravity, it would be discharging at the toe of the embankment. As a specific stratified system (i.e. heterogeneous soil, with two or more types of soil with contrasting Soil Water Characteristic Curves) is formed within the embankment, a preferential flow path is developed (Herasymuik, 1996). The changes in negative head pressure (i.e. suction) conditions influence the paths that channel the water to flow from high pressure to low pressure.

2.3. FLOW PATH OF WATER INFILTRATION FROM THE SURFACE

In 1897 Briggs (Horton & Hawkins, 1965) found that soils can retain water due to capillary forces, but such forces would be directly related to the size of the pores. Once these forces are reached, then downward movement of water would occur.

In the early 19th-century, it was common belief that water flow under gravitational force was only related to the empty spaces found within the structure of the soil, i.e. flow paths made by continuous pores filled with air; this way water would not find any resistance and would flow downward to the empty channels.

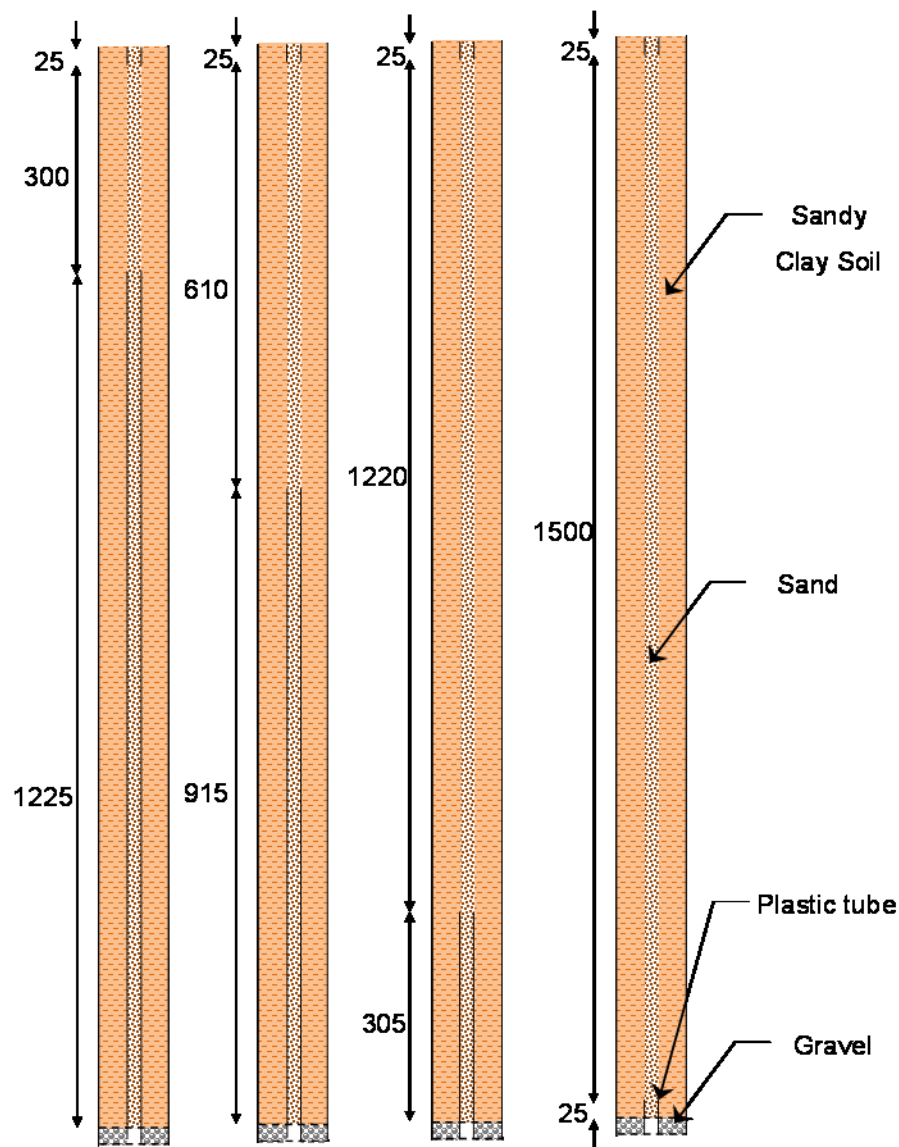
In 1956, however, Baver explained that water flow in the soil due to gravitational force was related to the amount and continuity of the pores (structure of the soil), but also to the texture, volume change, and biological channels (Horton & Hawkins, 1965).

Horton and Hawkins (1965) developed two experiments to evaluate more precisely water flow through soil, the results revealing that water infiltration is accomplished by downward displacement of water previously held by the soil, and that empty pores did not have any impact.

The first experiment was intended to demonstrate that most of the water that infiltrates into large pores of a sand soil would flow through smaller pores of sandy clay soil at shallow depths. To evaluate this premise, they used four column configurations of 1500 mm in height and 50 mm in diameter (See Figure 2.6). The column consisted in a central core ($\Phi=16$ mm) of sand surrounded by a sandy clay soil with an air entry value (AEV) sufficient enough to support water for the entire column (Horton & Hawkins, 1965). Each column had a plastic tube of different length to measure lateral flow at different depths. Simulated rainwater was added in the sand core at three different rates to each column, 2.5 cm/hr, 5 cm/hr, and 7.6 cm/hr, and seepage at the bottom from both materials were measured separately.

The results showed that water flowed from the sand core to the sandy clay soil at shallow depths, and at high rates of in flow. In addition, it was observed that in time there was a decrement in the capacity to absorb water in sandy clay. The column with the longest contact length (1500 mm) displayed contradictory results as all collected water was within the core. Horton and Hawkins concluded that water flowed from the core to the outside material at a shallow depth and flowed back into the core at a depth in which the water held by the surface tension of the sand was in contact with the water in the sandy clay soil (Horton & Hawkins, 1965).

The second experiment conducted by Horton and Hawkins (Horton & Hawkins, 1965) was intended to show that water flow would occur through the pores filled with water (displacement of water previously retained) and not through large pores filled with air. This experiment was conducted using one column 1220 mm in height and 50 mm in diameter, filled with 25 mm of gravel at the bottom and the rest comprised of sandy clay soil. The column was initially saturated and let to drain. Then to evaluate water flow displacement, a simulation rain with tritium was added at the top of the column. Afterward a simulation rain with no tritium was run. During this experiment the effluent coming out of the column was measured for tritium concentration.



Note: Not to Scale - All values are in mm.

Figure 2.6 Column Design Experiment for Horton and Hawkins (1965)

The results showed that while rain with tritium was added, the effluent coming out of the column had less than 2% of tritium concentration. Horton and Hawkins (1965) concluded that the rain simulation was displacing the initial water even though there were air filled pores.

The experiment presented by Horton & Hawkins allows a clear visualization of the effect of water flow in unsaturated soil and its relation with the permeability curve. The fine material becomes the preferential flow path of water as the coarse material under high suction has a lower hydraulic conductivity.

2.4. LATERAL FLOW IN A VERTICAL COLUMN

Horton and Hawkins showed the behavior of water flow when two materials of different grain size came into contact and water was applied to the coarse one; this demonstration came to be the first approach to the understanding of the hydrology within the structure in a waste rock dump. Newman (1999) presented in her thesis a laboratory test program that improved our understanding of this hydrology; a vertical layer system showed the significance of the mechanism of preferential flow path in a waste rock dump. This section describes the main procedures, results, and conclusions from the column experiments that are part of the modelling program in this thesis.

2.4.1. Laboratory Test Program

The laboratory test program conducted by Newman was based on research conducted by Horton and Hawkins (Newman, 1999). Her research consisted of two experiments (see Figure 2.7 and Figure 2.8) conducted using an acrylic column; the first experiment consisted in testing fine grained material and coarse grain material using Beaver Creek Sand and Medium Silica Sand, respectively; a material that was used by many other researchers and whose range of properties was well known. The second experiment was undertaken to verify if the same preferential flow path could be found using a Fine-waste-rock and Coarse-waste-rock material taken from the Gold Sunlight Mine.

The first column of 1400 mm in height was assembled with a cut-off in the middle that was adjusted for four different heights: 590 mm (Test 1), 390 mm (Test 2), 140 mm (Test 3), and 40 mm (Test 4), while the second column had the cut-off fixed to 360 mm. The total placement height of material in the first column was up to 1140 mm and 1360 mm for the second column.

Outlet tubes were installed in order to measure the amount of flux coming out of each column. For the first column, the tubes were placed 250 mm below the base of the materials, creating a boundary condition of 2.5 kPa of suction; in contrast with the second column, the outlet tubes were placed at the same height of the base of the waste material, creating a boundary condition of 0 kPa of suction. Additionally, each side of the column had a base of gravel up to a height of 100 mm to avoid clogging of the drainage tubes.

The suction created at the base of the first column became an issue during the tests, but was solved through numerical modeling by performing a sensitivity analysis. This difficulty occurred due to the difference between the air entry value of the silica sand (equal to 0.8 kPa) and the applied suction at the base. The low AEV of the silica sand with respect to the boundary condition causes desaturation of the material. This boundary condition allowed the suction at the bottom of the Silica sand to be controlled by the residual suction of the gravel material (the SWCC was not measured for this material), as it was the maximum suction that the gravel could exert on the coarse side of the column (Newman, 1999). In contrast, the fine material did not have any problems as the Beaver Creek sand had an air entry value of 3 to 4 kPa (Newman, 1999).

The material inside the first column was placed in 100 mm lifts for both sides. The materials were compacted uniformly to a total compactive effort of approximately 130 kN-m/m³. The material in the second column was placed with a much lower compactive energy. The waste material was placed in 200 mm lifts with a lighter compaction than Column-1. The total compactive effort for Column-2 was approximately 67 kN-m/m³.

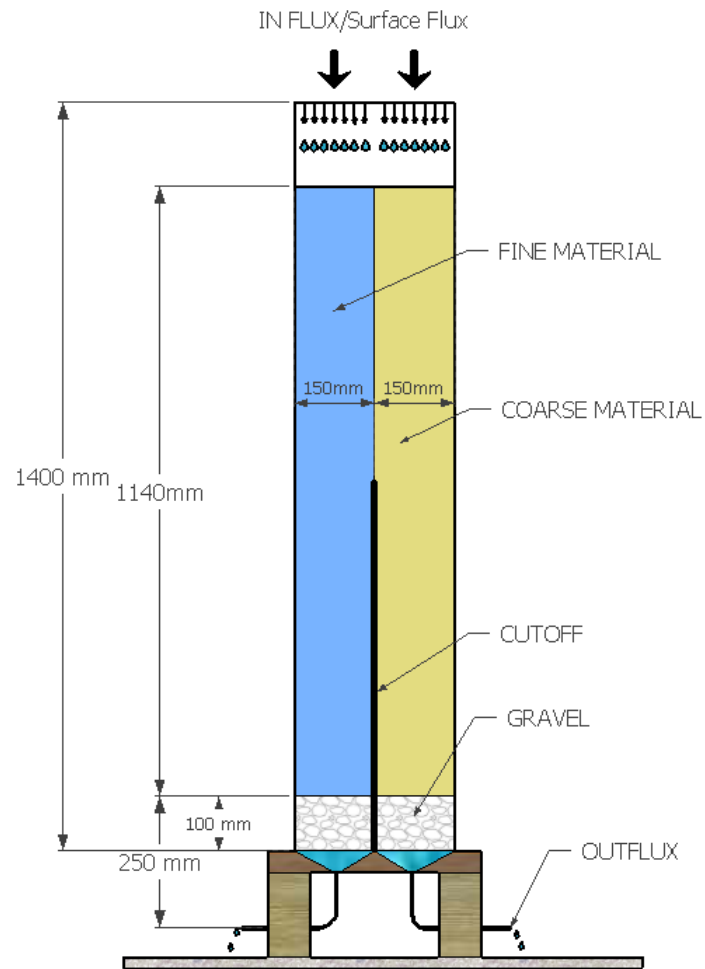


Figure 2.7 Scheme of Laboratory Column 1 after Newman (1999)

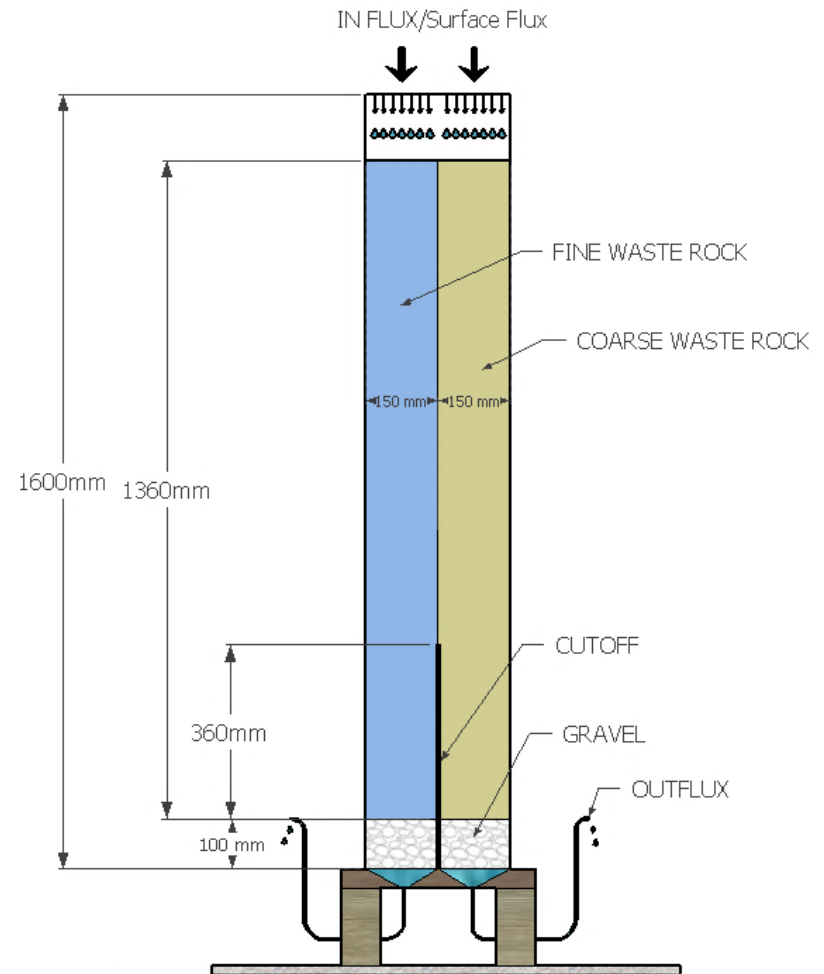


Figure 2.8 Scheme of Laboratory Column 2 after Newman (1999)

2.4.1. Experiment Conditions

In order to evaluate the preferential flow path for both columns, different precipitation rates were applied at the top of the materials. The application system was designed to apply a constant rate, in a raindrop way. Each column was initially saturated and allowed to drain until the soil was at a suction of the respective AEV, i.e. unsaturated conditions. Once the initial conditions were established, each test started by adjusting the cut-off and applying one-half of the total flux to each material until a steady state condition was established.

Table 2.1 shows the experimental conditions used in both column tests. The evaluation of water flow through the first column using sandy soil applied four different precipitations rates at the top of each material. The change in cut-off height allowed changes in the contact between the coarse and fine grain materials in the column. In each case, a slight variability of applied flux occurred in the experimentation. Contrary to the second column, the waste rock material had a single cut-off height and three flux rates.

Table 2.1 Experimental Conditions for Column Test (Newman, 1999)

Column	1				2
Material	Sandy Soil				Waste rock
Test	1	2	3	4	1
Cut-off Height (mm)	590	390	140	40	360
Contact length (mm)	550	750	1000	1100	1000
Precipitation Flux (mm/day)					
Flux (a)	1123	1123	1123	1123	445
Flux (b)	804	804	752	821	12
Flux (c)	449	432	406	475	5
Flux (d)	337	320	320	337	-

In Column-1, the highest precipitation rate created a thin free water surface; with the second highest, the water surface disappeared but indentations with water formed on the fine material. The other two precipitation rates were chosen to be less than the first two. In Column-2, the highest precipitation rate was applied to create a free water surface at the top of the column, and the other two were less than the first precipitation rate.

2.4.2. Material Properties

The fine material used for the first experiment (Column-1) was taken from a pit close to the South Saskatchewan River; this material had been studied and characterized for various research projects; Wilson (1990), Swanson (1996) and Newman (1999). Wilson (1990) described the Beaver Creek Sand to be a fine to medium Aeolian Clean Sand, poorly sorted, oxidized, and calcareous. This material has a texture 98% Sand and 2% Silt & Clay. The material used as coarse for the first experiment (Column-1) was a commercialized medium Silica Sand. For the coarse material, the soil water characteristic curve was measured.

The characterized hydraulic properties for the Beaver Creek Sand and Silica Sand are summarize in Table 2.2.

Table 2.2 Sand Properties for Column-1

Properties\Material	Silica Sand (SS)	Beaver Creek Sand (BCS)
Porosity	-nm-	0.43
AEV (kPa)	0.7	3 to 5
Sat. VWC	0.37	0.4
Specific Gravity	2.6	2.67

The SWCCs shown in Figure 2.9 are for the BCS and the SS. The BCS was measured by Wilson (1990), Swanson (1991), and Newman (1999). During the laboratory test program for the BCS made by Newman (1999) a falling head permeameter test measured k_{sat} equal to 6.2×10^{-5} m/s. The SWCC for the SS was measured as part of the laboratory program, the results revealed an AEV equal to 0.7 kPa; and k_{sat} of 1.5×10^{-2} m/s from a constant head permeameter test.

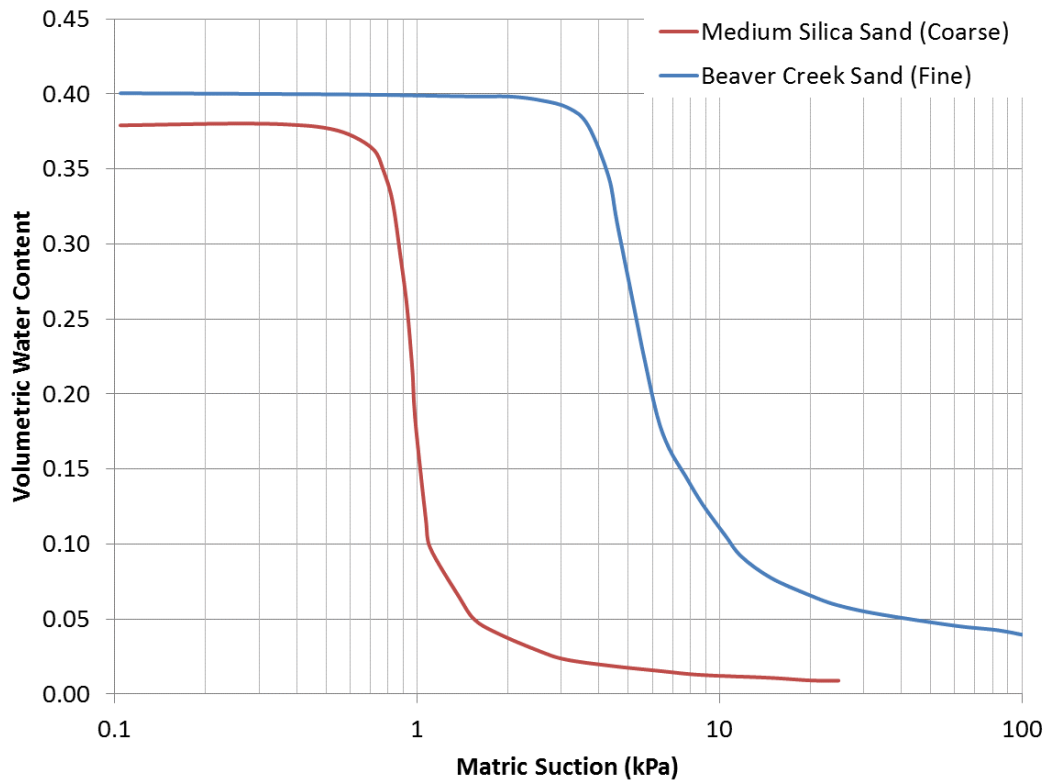


Figure 2.9 Soil Water Characteristic Curve for Materials in Column-1
Wilson (1990), Swanson (1991), Newman (1999)

To take into account the effect of the precipitation rate in preferential flow, the first two fluxes (Flux “a” and Flux “b”) were greater than the saturated permeability of the fine material; and the last two (Flux “c” and Flux “d”) were less than the saturated permeability of the fine material. Nonetheless, all precipitation rates were below the saturated hydraulic conductivity of the coarse material 1.5×10^{-2} m/s.

The hydraulic conductivity curves for the materials in Column-1 shown in Figure 2.10 were obtained using the estimation equation using the SWCC developed by Fredlund & Xing (1994). The gray shaded area in the Beaver Creek Sand represents the range of values reported by Wilson (1990)¹.

¹ Even though Newman doesn’t report a possibly variance with respect to the saturated hydraulic conductivity for the Silica sand, it should be kept in mind that variances can occur, as will be discussed further in the thesis.

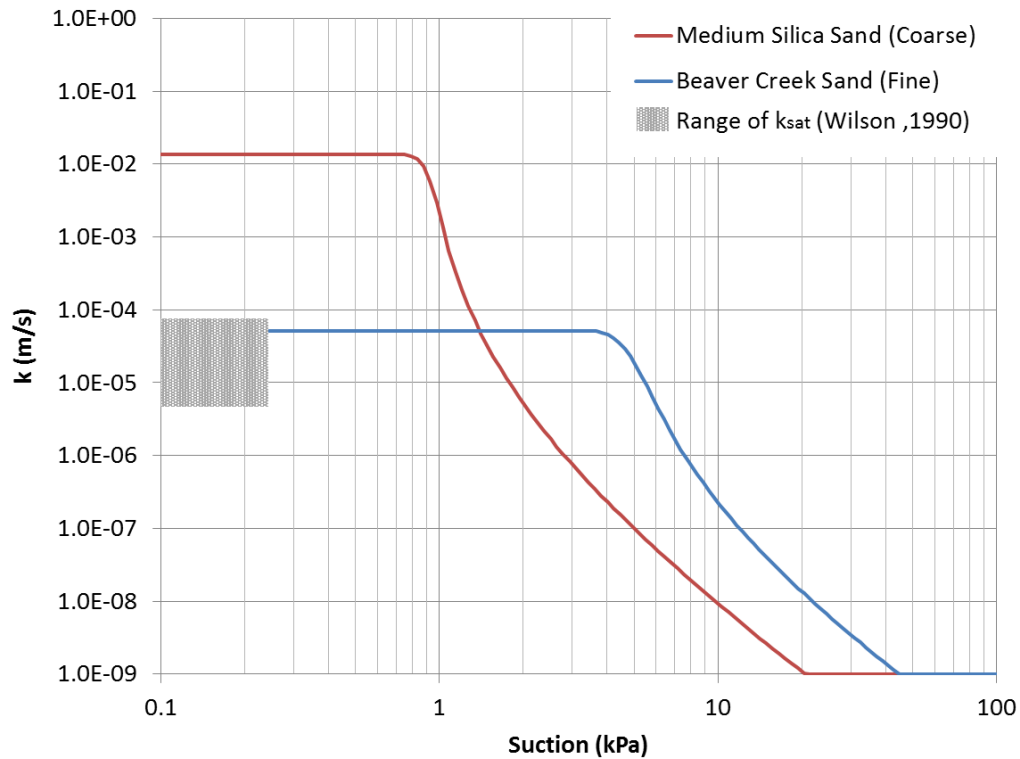


Figure 2.10 Hydraulic Conductivity Curve for Material in Column-1 (Newman, 1999)

Herasymuik (1996) characterized the waste rock from Golden Sunlight Mine, materials used in analysis of Column-2. The Coarse-waste-rock material (name TP6GS5, test pit 6) had a range of particles passing the #4 sieve between 30% and 39%. The Fine-waste-rock material (name TP5GS1, test pit 5) had more than 50% of particles passing the #4 sieve. Table 2.3 presents the material properties for the materials used in Column-2.

Table 2.3 Waste Rock Properties for Column-2 (Herasymuik, 1996, pp. 103,124)

Properties\Material	Coarse-waste-rock (C-WR)	Fine-waste-rock (F-WR)
Gravimetric water content	0.37%	0.56%
Porosity	29.4	31.2
Void ratio	0.42	0.45
Dry density (g/cm³)	1.95	2.03
AEV (kPa)	-	3.5
Sat. VWC	0.29	0.31
Specific Gravity	2.78	2.63

The SWCC's were determined using large pressure plate tests that allowed for the testing of a more representative sample that included the coarse fraction. The points for suction vs volumetric water content shown in Figure 2.11 were plotted using the software CVIEW for best fitting; this software uses a nonlinear least-squares regression (Herasymuik, 1996, p. 93). The residual part of the curve was not calculated.

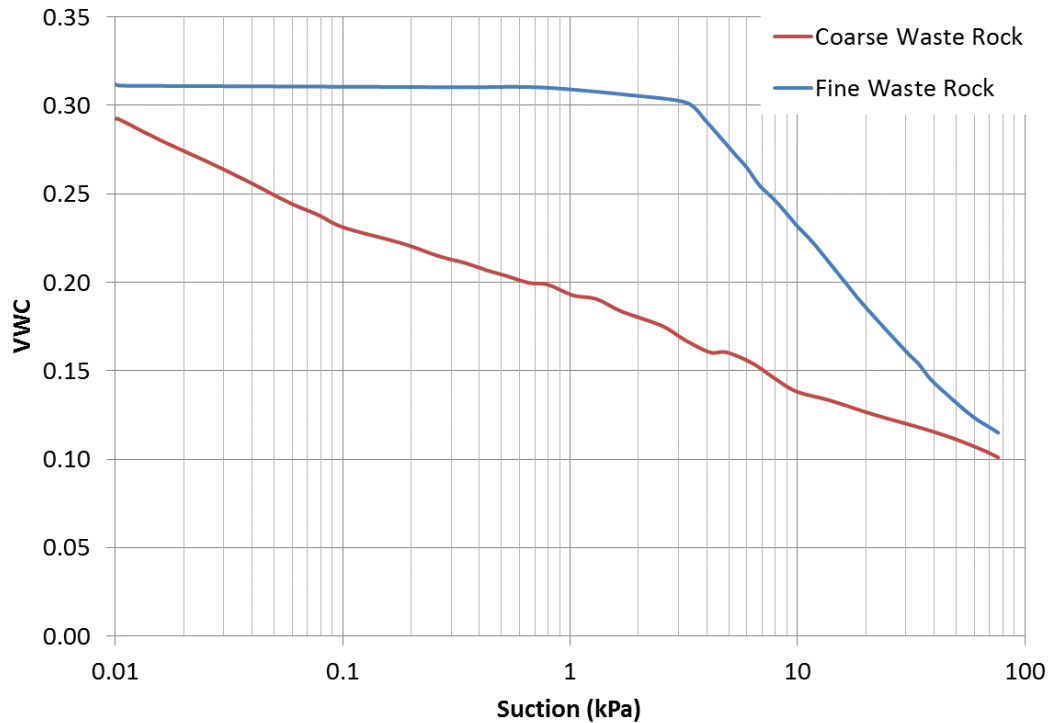


Figure 2.11 Soil Water Characteristic Curve for Materials in Column-2 (Herasymuik, 1996)

The hydraulic conductivity functions were estimated from the SWCC and the curve fitting software CVIEW as shown in Figure 2.12. For the fine waste rock, the saturated hydraulic conductivity was measured to be $3.4 \times 10^{-3} \text{ m/s}$; through constant head permeability tests. For the Coarse-waste-rock, the saturated hydraulic conductivity was assumed to be $1.0 \times 10^{-5} \text{ m/s}$; the selected value was consistent with previous models made at Golden Sunlight Mine. No permeability test was performed due to the lack of laboratory equipment for large size samples (Herasymuik, 1996, pp. 125-130).

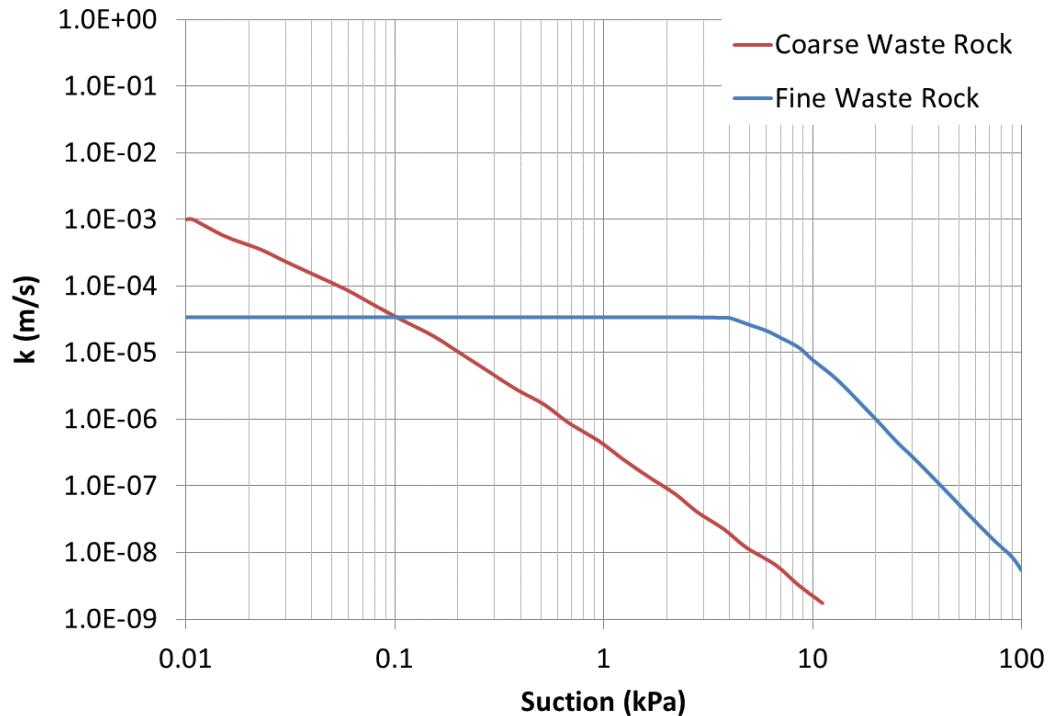


Figure 2.12 Hydraulic Conductivity Curve for Material in Column-1 (Herasymuik, 1996)

2.4.3. Experiment Results

The measured volumes of water discharge from the fine and coarse sand are shown in Figure 2.13 and Figure 2.14 from the laboratory experiments from Column-1 (i.e. Beaver Creek Sand and Silica Sand). The discharge from Column-2 (i.e. Golden Sunlight Mine rock waste material) are shown in Figure 2.15. The discharge measurements were taken out of each material individually and computed as a percentage of the total applied in-flux rate at the top of each column.

Despite the variances of total precipitation applied in Column-1, Column-1 showed similarities in the water infiltrating the top of the column. Newman observed that applying 1120 mm/day (*Flux a*) allowed a thin free water surface to form on the fine material; this result showed that there was more water than the material could allow to infiltrate. Reducing the precipitation from 1120 mm/day (*Flux a*) to 800 mm/day (*Flux b*) caused the thin water film to disappear, but water remained in the small indentations. As precipitation decreases from 800 mm/day (*Flux b*) to 440 mm/day (*Flux c*) and from 440 mm/day (*Flux c*) to 330 mm/day (*Flux d*), there was no more water at the surface. According to Newman, the surface at 330 mm/day (*Flux d*) appeared to be the driest case in the experiment.

The column experiment (Newman, 1999, pp. 47-48) shows a preferential flow path formed in the fine material for an applied in-flux rate below 440 mm/day (*Flux c*) with a discharge over 50%.

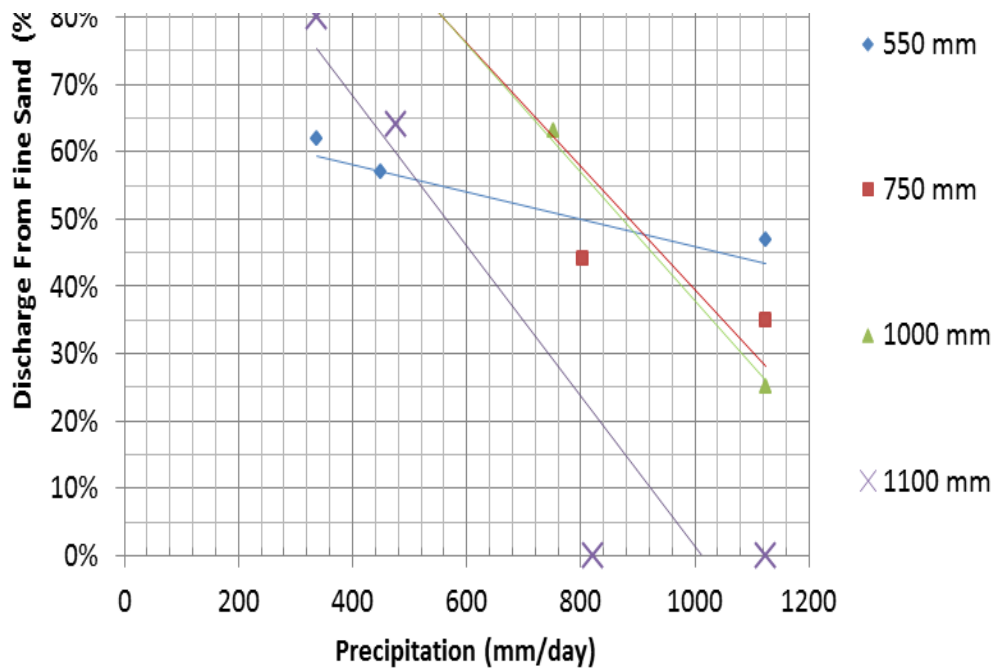


Figure 2.13 Total Discharge of the Fine Material for Column-1, after Newman (1999)

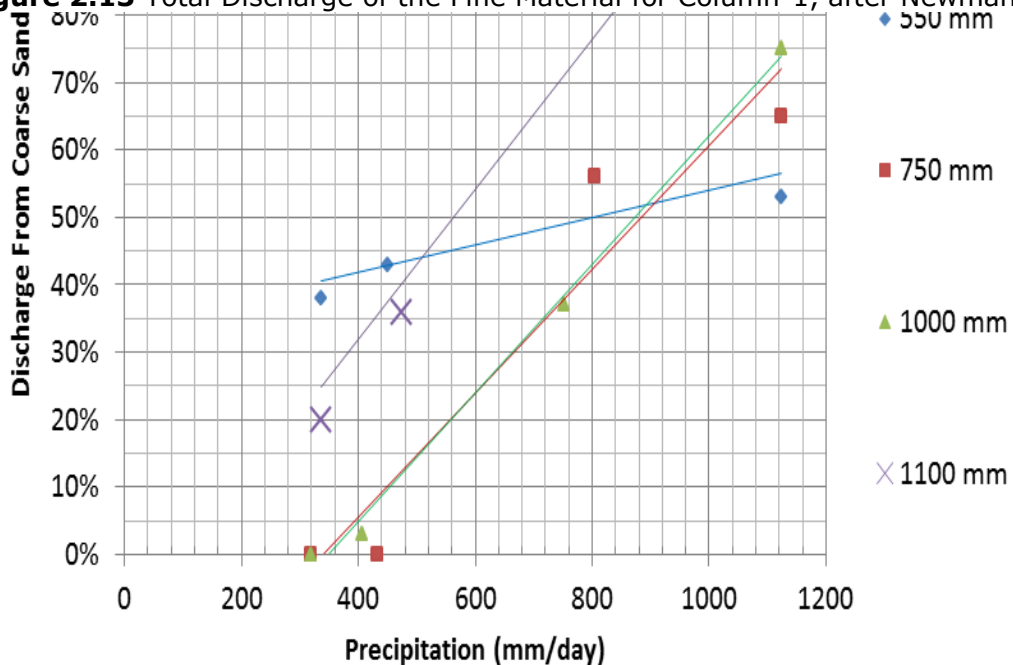


Figure 2.14 Total Discharge of the Coarse Material for Column-1, after Newman (1999)

For Column-1 in the coarse material, the results (Newman, 1999, pp. 47-48) showed a preferential flow path formed for an applied precipitation higher than 440 mm/day (*Flux c*) with a discharge over 50%. Newman concluded that if the precipitation rate is less than the saturated hydraulic conductivity of the fine, then it resulted in the drainage through the coarse pores.

Decreasing the cut-off height establishes an increment of contact length between the two materials, consequently allowing a longer length of lateral transfer flow from one material to the other. The experimental result (Newman, 1999, pp. 49-52) shows that increasing the contact length between the materials in Column-1 resulted in the following:

- Increments in lateral transfer over 50% to the *Coarse* material for 1120 mm/day (*Flux a*) and 800 mm/day (*Flux b*). Nevertheless *Flux (b)* did not show the same trend on Test 3 (i.e. 1000 mm of contact length). Newman used numerical modeling (Seep/W-V2.0 software) to establish that the exception on Test 3 occurred due to a gradient change, formed at the tip of the cut-off, due to the difference in suction generated at the base of both materials.
- Water flow increases over 50% through the *Fine* material for 440 mm/day (*Flux c*) and 330 mm/day (*Flux d*). Still, increasing the contact length above 1000 mm (Test 3) generated a gradient, allowing water transfer back to the coarse material; the percentage of water flowing out of the fine material reduced between 20% to 33% for *Flux (c)* and *Flux (d)*, respectively. The reason for this reduction was that the suction near the base of the Column-1 was lower than the suction at the intersection of the hydraulic conductivity curve of both materials.

Some errors occurred during Newman's experiment that could have contributed to not establishing a clear trend on the effect on contact length between the materials. One problem that occurred was the densification of the coarse material due to the movement of the cut-off barrier, resulting in a change of the hydraulic properties. Secondly, the boundary condition at the base of the coarse material altered the h_p pressure distribution due to the change in suction generated by the filter gravel at the bottom. However, it was clear that the relation of the in-flux rate and the saturated hydraulic conductivity had a strong influence on the preferential path of water.

Column-2 had applied three precipitation rates with a 1000 mm contact length, resulting in the following discharges through each material. Figure 2.15 shows that decreasing the amount of in-flux at the top of the column resulted in an increment of

discharge on the Fine-waste-rock. Likewise, the contrary happened: as the in-flux water decreased, the discharge from the Coarse-waste-rock decreased. Newman concluded that conditions exist for preferential flow paths in Golden Sunlight Mine; these preferential paths through the Fine-waste-rock can result in a source of potential slope instability (Newman, 1999, pp. 119-120).

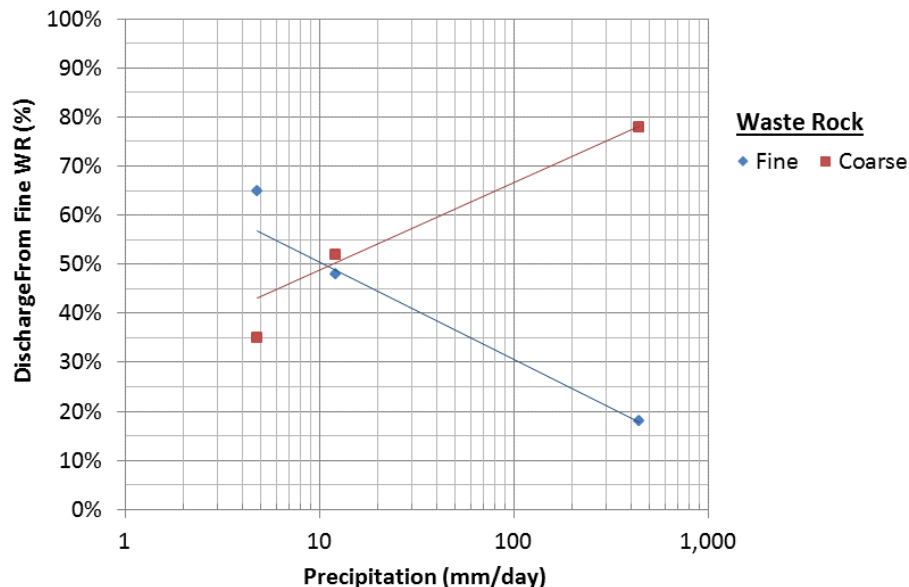


Figure 2.15 Total Discharge for Column-2, after Newman (1999)

The experiment (Newman, 1999, pp. 119-120) displayed that the saturated conductivity measure by Herasymuik should be lower, because in order to make the fine waste the preferential flow path, the flow rate was required to be less than 10 mm/day.

2.5. WATER FLOW MODEL IN WASTE ROCK EMBANKMENTS

At the 23rd World Mining Congress in Montreal, Broda et al. (2013) presented a comparison between two modeling techniques for water flow. The first technique is often used; it considers the waste rock as an Equivalent Porous Media (EPM); i.e. the waste rock as a continuum with homogeneous properties. The second methodology considers the waste rock as a massive fracture rock media for preferential flow paths, applying modeling techniques to simulate flow process in macro-pores. The authors employed *Transition Probability Geo-statistical software* (TPROGS) in order to define the stochastic zones; i.e., random zones of fractures and macro-pores, and the hydrogeological properties in the model.

The simulation created for the analysis was a three-dimensional model using HydroGeoSphere, which allows integration of the effects of flow between the surface and subsurface of the WRE. The model fulfills the mass balance equations applying discretization through a finite element method, and used the Van Genuchten equation to describe water flow in unsaturated conditions. Additionally, the model was run in a transient state in order to simulate the change in time of water flow within the waste rock.

The conditions used for the simulation of water flow through the WRE correspond to three cycles of 30 days; each cycle corresponds to 5 days of rain simulation at $2.31 \times 10^{-7} \text{ m/s}$ at the top boundary, and 25 days of free drainage through the downward slope. In the simulation the authors considered that in order to obtain the worst case scenario, the effect of evapotranspiration and runoff had to be neglected.

The input properties of the models were from large scale laboratory tests and field tests to characterize the hydraulic properties and Van Genuchten parameters of the waste rock material from an ilmenite mine. The material properties for the EPM and TPROGS model are presented in Table 2.4.

Table 2.4 Porosity and Hydraulic Conductivity for EPM and TPROGS Model

EPM			TPROGS		
Grain Size Class ²	n	K _{sat} (m/s)	#	n	K _{sat} (m/s)
P50	0.3	4.30E-03	1	0.3	4.30E-03
P28	0.24	1.40E-03	2	0.26	1.20E-03
P19	0.27	1.20E-03			
P10	0.28	1.10E-03			
P5	0.31	2.70E-04	3	0.33	1.50E-04
P2	0.34	3.60E-05			

For the EPM model, the material P2 grain size class represents the properties for the top and bottom zones of waste rock, while the core is the average of the classes P50 to P2 grain size. For the TPROGS model, the properties used for the top and bottom are also homogeneous materials P2, while the main core volume is composed of 10% P50, 50% P28, and 40% P5.

² P# corresponds to classification passing 50, 28, 19, 10, 5, and 2 mm sieves.

The geometry of the model used by the authors corresponded to that of a field experiment planned at 7.0 m height and approximately 70 m long. The mesh size was between 0.1 m and 0.2 m for the element in the plane x-y, while the z component was of 1.0 m in length. The Figure 2.16 (Broda, et al., 2013) shows the contours (material distribution, total head (h), and degree of saturation) of the EPM and TPROGS models.

The authors explained that the results in Figure 2.16 for the EPM model did not represent the behavior found in the field for WRE; because, the EPM model showed a uniform infiltration and downslope seepage that caused a homogenous head and saturation through the WRE. Contrary to the TPROGS model, due to the stochastic distribution of the material in the core, the results showed a higher correlation with observation in the field. The TPROGS model showed a smaller maximum head with localize points of zero pressure head and saturation.

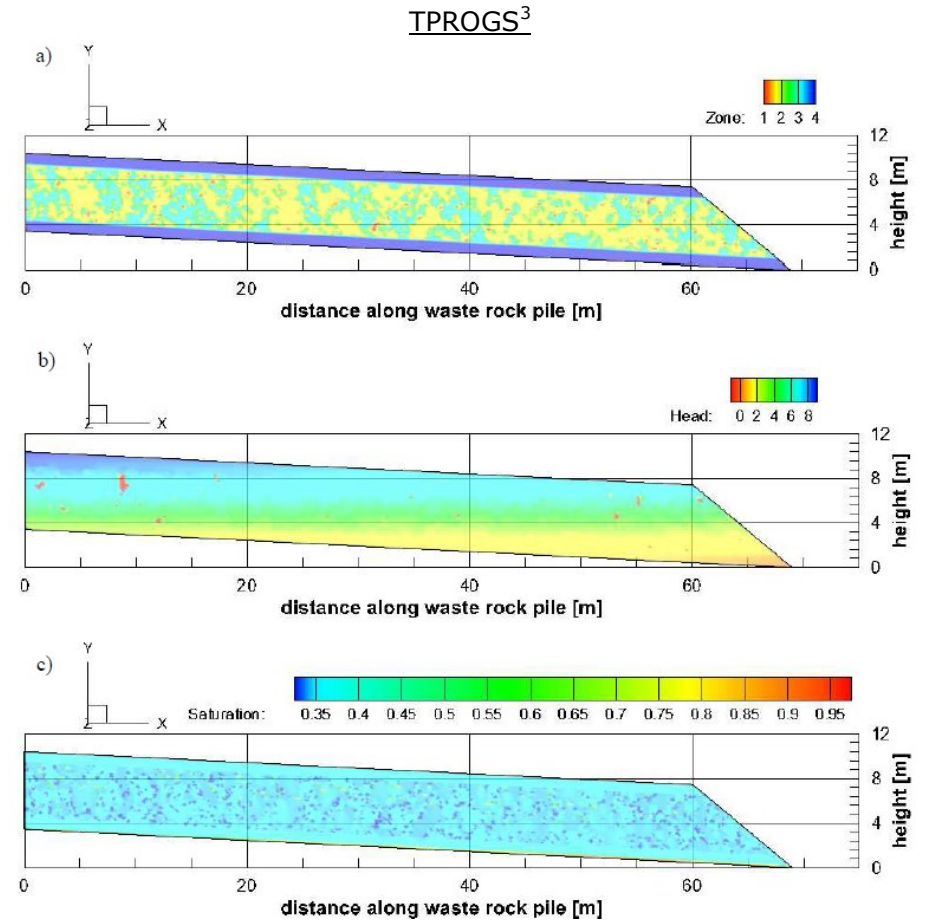
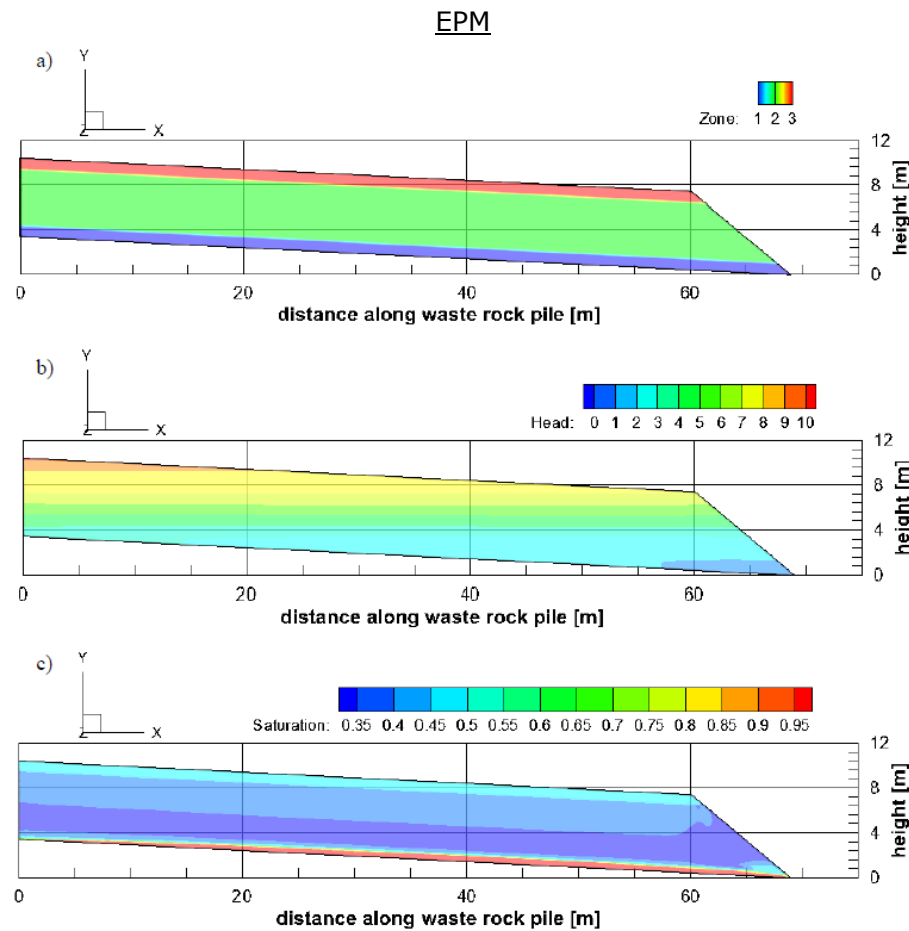


Figure 2.16 Model Results for EPM and TPROGS at T=65 Days
A) Material Zone; B) Pressure Head; C) Saturation (Broda, et al., 2013)

³ The figures presented in the paper by Broda (et al., 2013) representing the results for the TPROGS have contrary color distribution for a) and b).

A vertical flux section in the analysis (Broda, et al., 2013), located at a distance of 35 m along the WRE, showed the change in saturation on both models with elevation (Figure 2.17, a). The section showed high variability (presence of fractures and macro-pores) for the TPROGS along the core of the WRE. This variability causes the seepage to reach the base of the WRE faster as shown in Figure 2.17, b, but with less amount of water. This outcome is contrary to the EPM model where slower but a higher infiltration occurs at the top of the WRE due to the homogeneity of the layer, allowing a uniform infiltration.

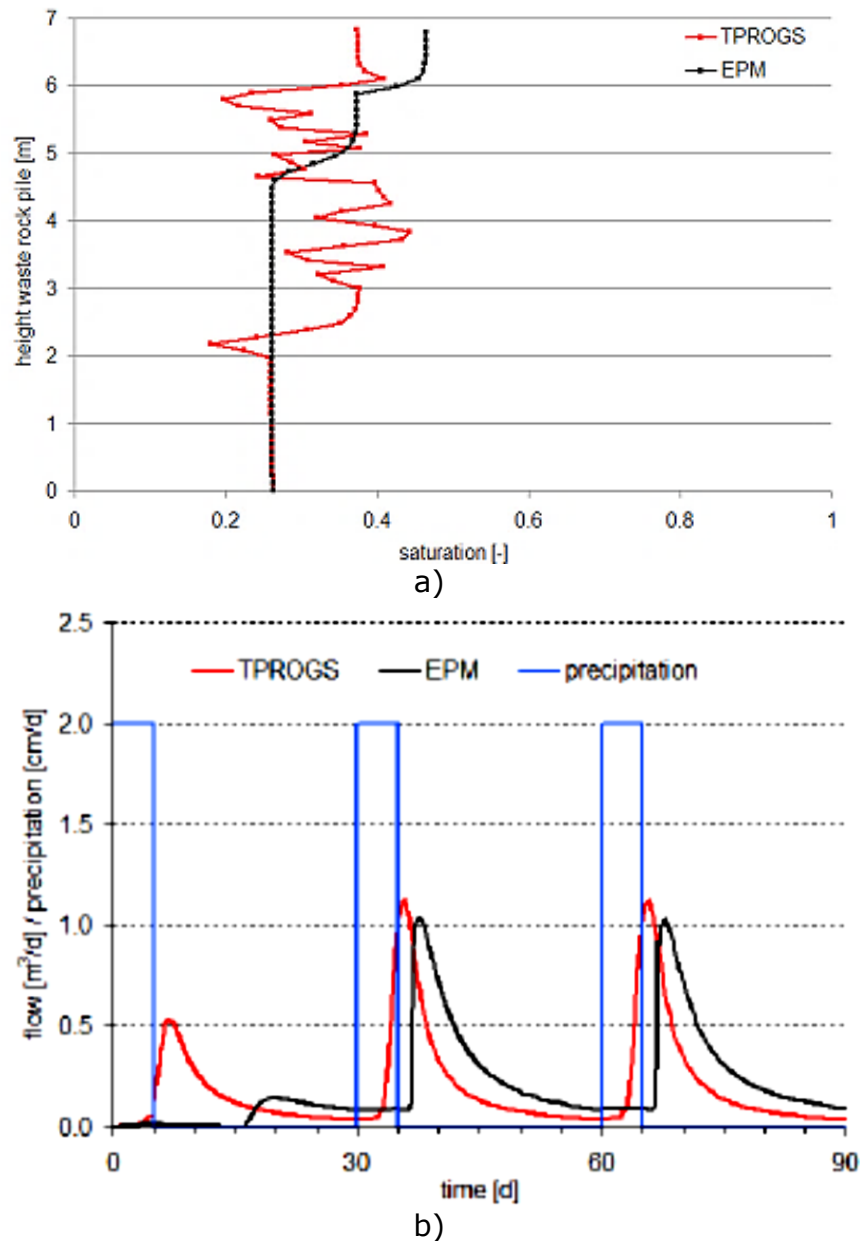


Figure 2.17 Saturation Distribution in 5 Days (a) and Change in Time of Total Flow Entering the Base Compacted Layer (b) In X=35 M (Broda, et al., 2013)

It should be noticed that even though at the beginning the TPROGS model shows a faster infiltration response, the EPM model would start having similar response of infiltration as the time passes. For long-term analysis, EPM models could be optional for global analysis and cost.

The changes of head and saturation relate to the hydrological, geochemical and geotechnical behaviors. The authors concluded that the changes in the TPROGS model are critical for WRE designs. The effect of including fractures and macro pores in the modelling of WRE shows a faster and “higher flow in looser waste rock zones, as it causes weak or absent capillary barriers and a preferential flow paths” (Broda, et al., 2013). This analysis show a significant change in the techniques used to improve the analysis and design of WRE.

2.6. FLOW IN INCLINE LAYERING SYSTEM

Different studies had been made to understand different conditions in unsaturated water flow in an incline system. The following sections give a brief review of three studies in inclined layer soils. The first study evaluates the effect of different inclinations in the drainage of an incline tank; the second study shows an experiment carried in a two-layer system to study the capillary barrier effect. The last study relates to the experiment of three Meso-scale panels that will be the primary focus in modelling for this thesis.

2.6.1. Single Layer System

In 2013, a study evaluated the conditions for lateral downslope flow in unsaturated soil in hillslopes. Lv et al. (2013) focused their research on the influence of the slope angle in moisture content. From a hydrology standpoint Lv et al. (2013) states that changes in moisture can be triggered by factors such as “water-routing processes, solar radiation, precipitation, topography, and heterogeneity in soil and vegetation characteristics”. The analysis presented in their investigation, however, only considered the water-routing processes. Water routing is the process of changes of flow over time along the channel.

The experiment used a large rectangular tank at three different slope angles (9°, 19°, and 28°) as shown in Figure 2.18. The tank had two layers of soil; the top layer was 1.42 m thick sandy loam overlaying a filter of 5.0 cm of thick quartz sand. The materials were initially saturated and let to drain for the testing (i.e. it is a drying state process). Tensiometers were installed at different depths to measure change in moisture in the sandy

loam. Additionally to the experiment, a numerical model was developed using HYDRUS-2D to analyze changes of moisture near the surface.

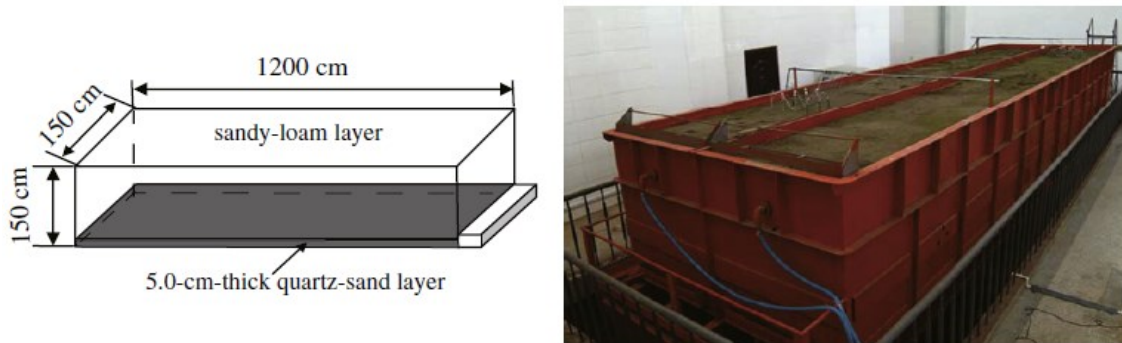


Figure 2.18 General Characteristics of Soil Tank (Lv, et al., 2013)

The study intended to differentiate the mechanism of water flow. Water particles move from a high energy (Total Head) to low energy, and their direction is controlled by the gradient in moisture content (matric potential). However, the results showed that “matric potential did not completely control the direction of water particles”. The results from the experiment show that the change in inclination had an effect on the matric potential. The total head (H) changed with the inclination of the tank, increasing with the inclination.

The change in matric potential normal to the surface has a high fluctuation, while the measure of the vertical component to the surface indicates that the change is constant. This fluctuation was found to increase towards the surface of the slope. The results from the experiment and simulation showed that near the surface water particles move parallel to the slope. Then the particles are redirected in a vertical direction flow and as it gets closer to the bottom of the impermeable boundary it starts to flow parallel to the base.

The change in inclination showed that increasing the angle of the slope would decrease the verticality of flow in between the tank; i.e., water particles would move parallel to the surface as shown in Figure 2.19. The study showed that drainage occurred faster at the surface and bottom of the layer. However, the middle layer was closer to the drainage velocity at the surface. The experiment also showed that in a drying state, the VWC in the tank decreased faster in the upper slope than in the downslope with a higher accumulation at the base.

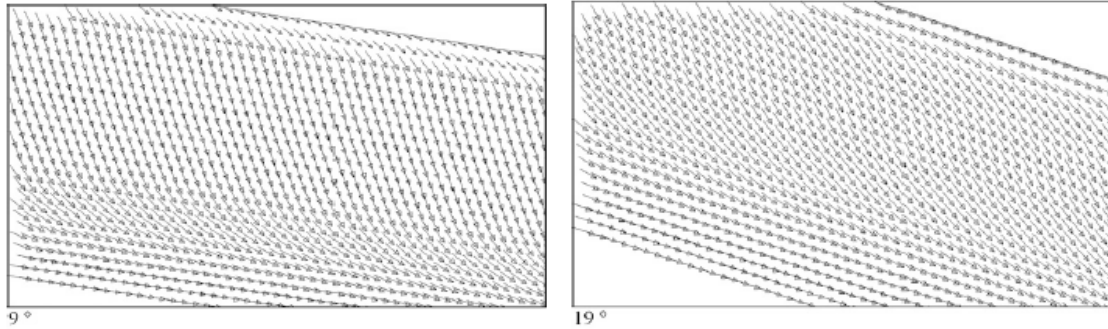


Figure 2.19 Profile of Vector Flow at 100 Hr for a Tank Inclination of 9° and 19° (Lv, et al., 2013, p. 325 Fig.9.)

2.6.2. Double Layer System

In 2004, a study was carried out by Tami et al. (2004) to investigate the mechanism associated with capillary barriers in slopes. In the study, a physical model shown in Figure 2.20 was constructed and compared to the numerical simulation. The model consisted of a two-layer panel inclined at 30°. The top layer was fine-grained soil of fine sand overlaying a coarse-grained layer of gravelly sand. The selection of the material was related to the large range of properties that these material have as a capillary barrier. The side and bottom of the panel had impervious boundaries. At the top, a precipitation was simulated with a flux rate that varied between 2% and 100% of the saturated hydraulic conductivity of the fine grain.

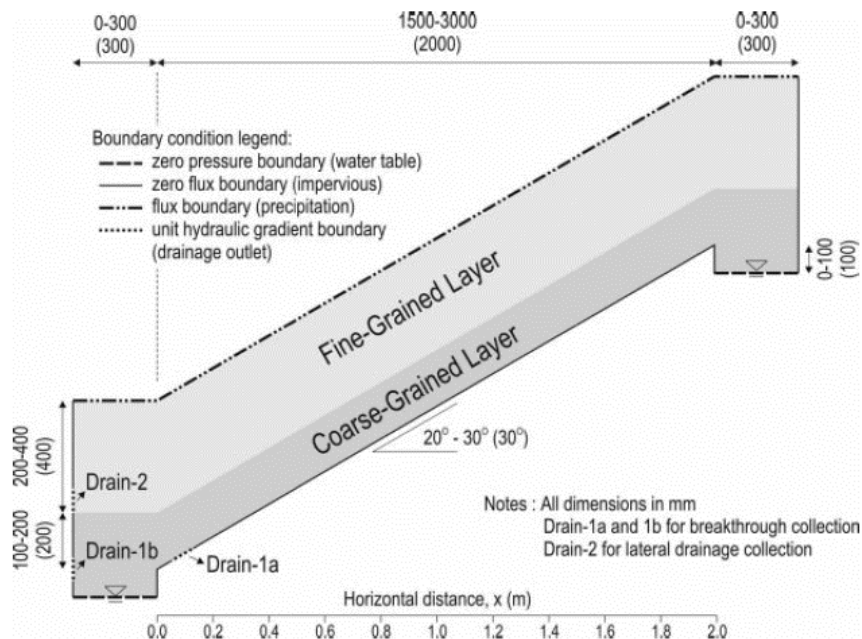


Figure 2.20 Geometry of the Incline Capillary Barrier (Tami, et al., 2004)

The experiment showed that head pressure (h_p) was affected by the precipitation rates. At low precipitation rates, h_p was close to the hydrostatic pressure. Once the precipitation was increased, the h_p in the fine sand increased while in the pea gravel the h_p did not change. Tami et al. (2004) concluded that increments of infiltration at high precipitation rates, did not generated changes in h_p are related to into the coarse layer.

Figure 2.21 shows the comparison of the h_p profiles at different vertical locations. The figure showed that the minimum distance of influence of the sidewalls was located at 20 cm from each end, while the distance of influence of the upper and lower boundary was controlled by the precipitation rate, soil thickness, slope angle, and hydraulic properties. Tami et al. stated that as the capillary barrier decreased in the inclination and thickness, the distance of influence also decreased. This resulted in extending by 20 cm the geometry to each side to avoid boundary influences.

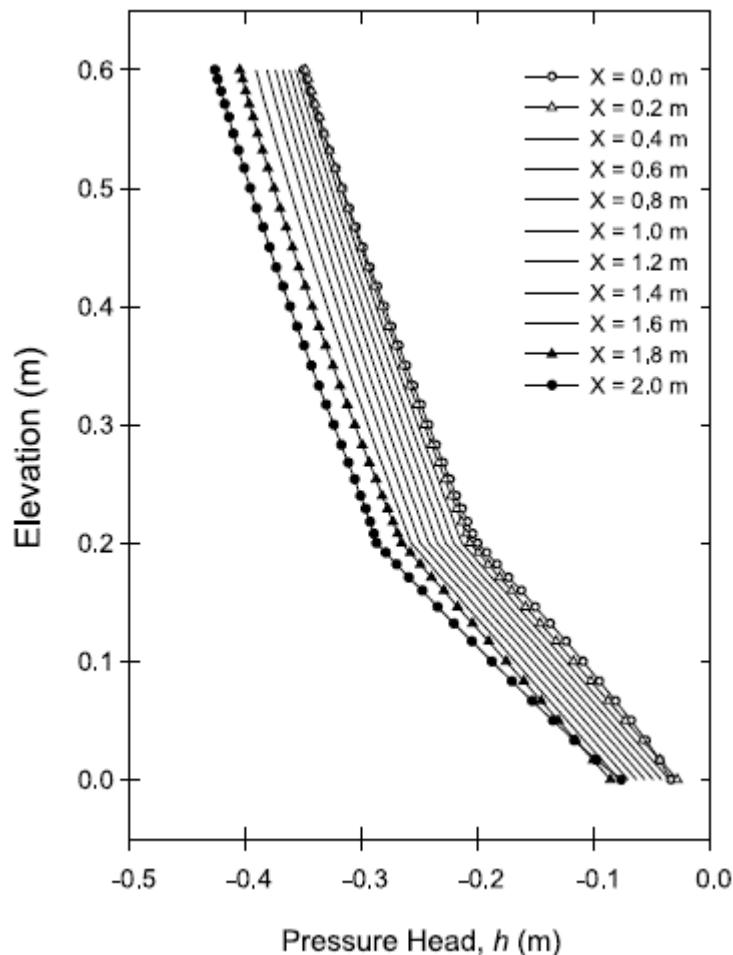


Figure 2.21 Vertical H_p Profiles At 5% of K_{sat} (Tami, et al., 2004)

The numerical model was run in steady state and transient state conditions. The analysis for the panel was made using the wetting and drying curves from the SWCC to accounting for a low and a high storage capacity. The model showed that water flows in the fine material at the contact interface and that during the infiltration (absorption), the matric suction decreased while the VWC increased. The comparison revealed that the model correlates better to the laboratory experiment by using the wetting curve of the SWCC. When the drying curve was used in the model, the matric suction was overestimated. The authors related these result to the different increments of VWC in the material, as equal VWCs would have a higher suction in the drying curve. In contrast, during the discharge (desorption) of the model, the results showed a better correlation of matric suction using the drying curve.

Tami et al. (2004) concluded that the model behaved better using the wetting properties to describe the infiltration process, while using the drying process to describe the discharge as the material dries. Tami et al. (2004) suspect that the discrepancy was related to the inaccuracy of the instrumentation of the experiment or the high non-linearity of the SWCC. Nonetheless, the authors concluded that the drying or wetting process (i.e. hysteresis behaviour) has less effects on the changes of VWC than on the PWP and matric suction. The VWC had better correlation to the experiment using the drying curve in the infiltration and draining process.

The comparison between the model and the laboratory experiment show that changes in VWC and matric suction were similar. Furthermore, the result showed that numerical models should be run with the wetting curve of the SWCC if the materials are in an infiltration process or with the drying curve if it is in a draining process.

2.6.3. Multiple Layer System

The main objective of this thesis is the focus on the simulation of three Meso-scale experiments using waste rock from Grasberg Mine in Indonesia. Andrina (2009) at the University of British Columbia conducted this experiment to identify the flow mechanism in incline coarse and fine layers of waste rock. The study evaluated water flow in unsaturated conditions from three different panel configurations. Each panel was composed of alternating layers of waste rock inclined at the angle of repose from the waste rock embankments from Grasberg Mine.

2.6.3.1. LABORATORY TEST PROGRAM

The laboratory test program by Andrina (2009) consisted of three panels filled with interbedded layers of waste rock, placed at 37° , corresponding to the angle of repose as

shown in Figure 2.22. This geometry represents a common inclination for waste rock embankments worldwide using end-dumping techniques. The material used to evaluate water flow consisted of acid rock and limestone. The grain size distribution for these materials was adjusted to the scale of the experiment in order to have a correlation to the in-situ conditions. The materials were classified into two categories according to the grain size: Fine-Acid-Rock (F-AR) and Coarse-Acid-Rock (C-AR), and Fine-Limestone (F-L) and Coarse-Limestone (C-L).



Figure 2.22 Meso-Scale Experiment for Panel-3 (Andrina, 2009)

The three panels were built using 10 mm-thick acrylic with a height between 1.5 m and 2.0 m; the width for the three panels was 0.25 m. The panels had alternating layers of waste rock; each layer was 0.25 m width. A filter material between 3.0 cm and 5.0 cm height was placed at the base of each layer. Underneath the filter material a drainage system was installed to collect the leachate from each layer; the system consisted on suction lysimeters. The change in the elevation of the collector containers generated a negative pressure varying between 0.0 kPa, 2.0 kPa, and 4.0 kPa.

Drainage pipes were placed at the internal slope of the first layer; three for Panel-1 and Panel-3, and four for Panel-2. At the base of the Panel, Acrylic strips of 25cm × 11cm × 1cm were installed between layers to prevent water transferring at the collection points. The internal slope of the first layer also had acrylic strips to drive the collected water to the center and into the drainage points. Additionally, each panel had installed a set of instrumentation of tensiometers, thermocouples, and gas tubing. Panel-1 and Panel-3 had the instrumentations located in each layer at a height of 50 cm and 100 cm measured from the base. Panel-2 had the same instrumentation as the other two panels adding an additional instrumentation at 150 cm height.

The first panel used seven layers; the layers alternated between F-AR and C-AR as shown in Figure 2.23.

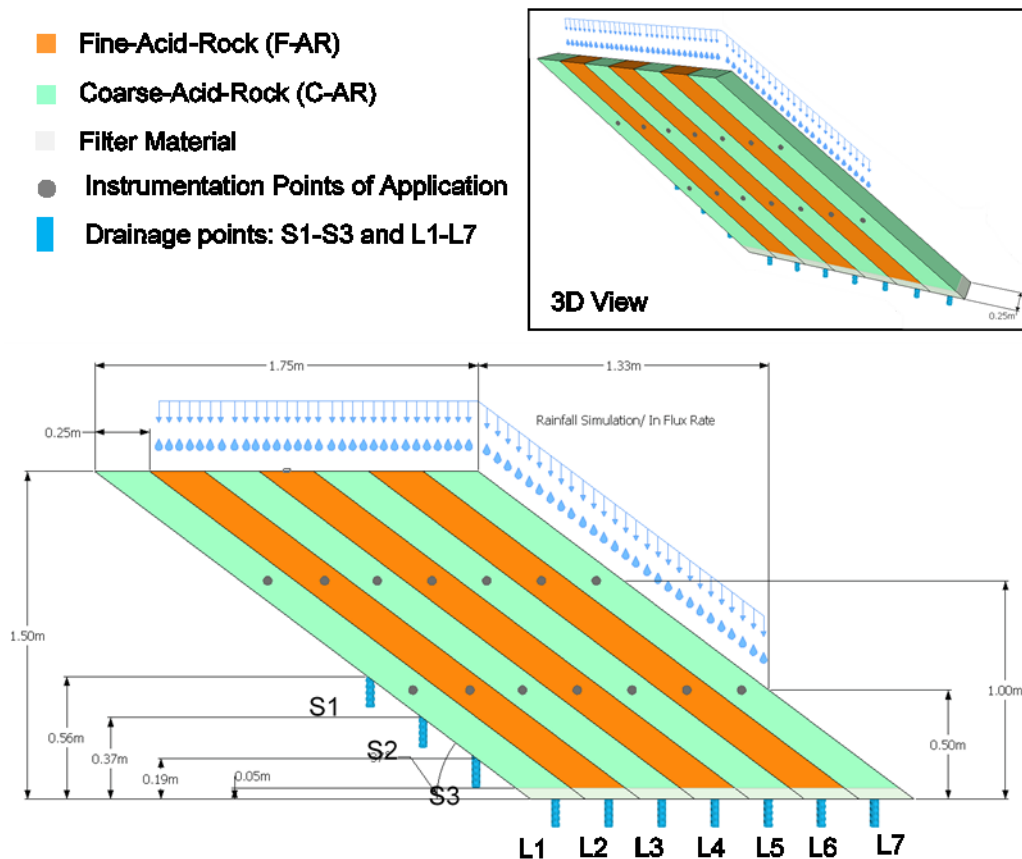


Figure 2.23 Meso-scale Experiment for Panel-1 (Based on Andrina, 2009)

The second panel had the same distribution of layers as the first panel plus an addition of a 50 cm horizontal layer at the top of C-L as shown in Figure 2.24. The objective for this panel was to assess the effect of the alkaline solution (solution with a PH>7) from

the C-L on the leachate quality. Also the second panel had the additional instrumentation placed at the interface between the Acid Rock and the Limestone.

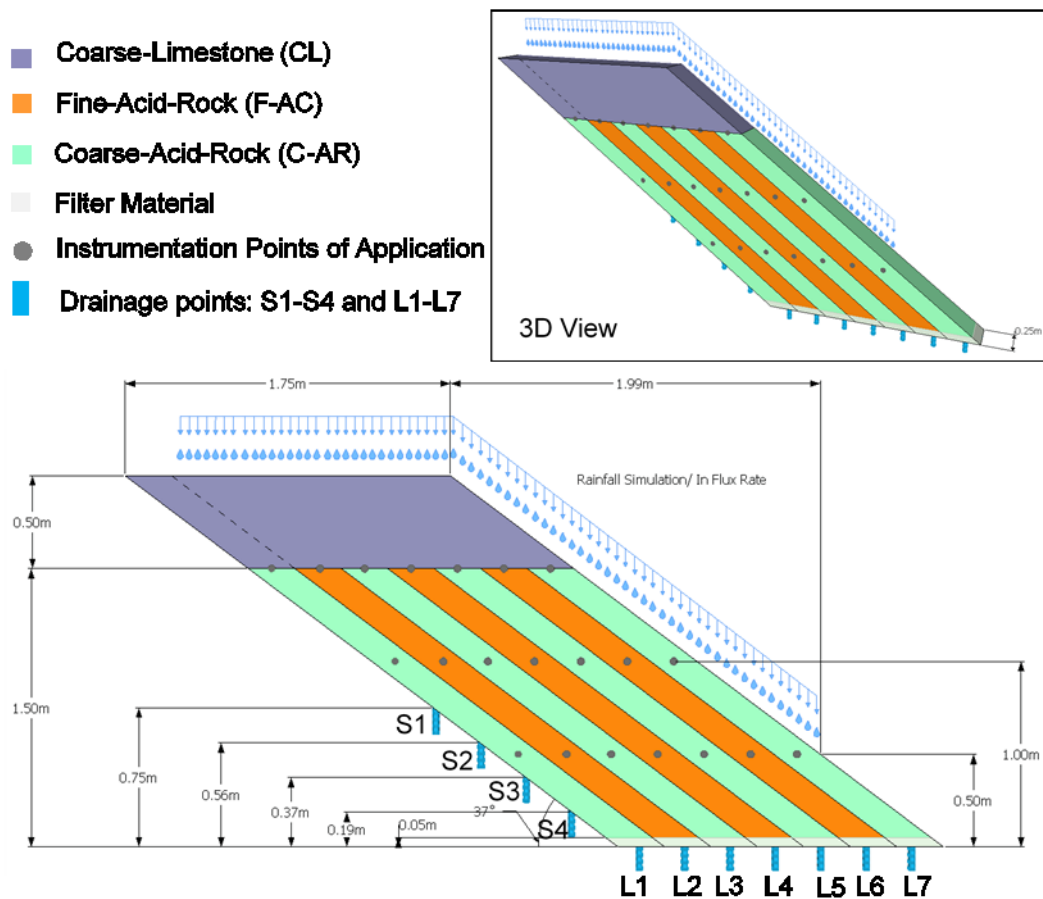


Figure 2.24 Meso-scale Experiment for Panel-2 (Based on Andrina, 2009)

A waste rock trial-dump was constructed at Grasberg Mine to investigate the leaching behavior of waste rock and evaluation of appropriate treatments to reduce the long-term generation of ARD, Andrina (2009). The main material for the third panel was C-L as it was the dominant internal structure found within the trial-dump. The layering system for this panel had a different arrangement with respect to the other panels as shown in Figure 2.25, increasing the number of layers to nine. The materials for the panel included F-AR, C-AR, C-L, and F-L.

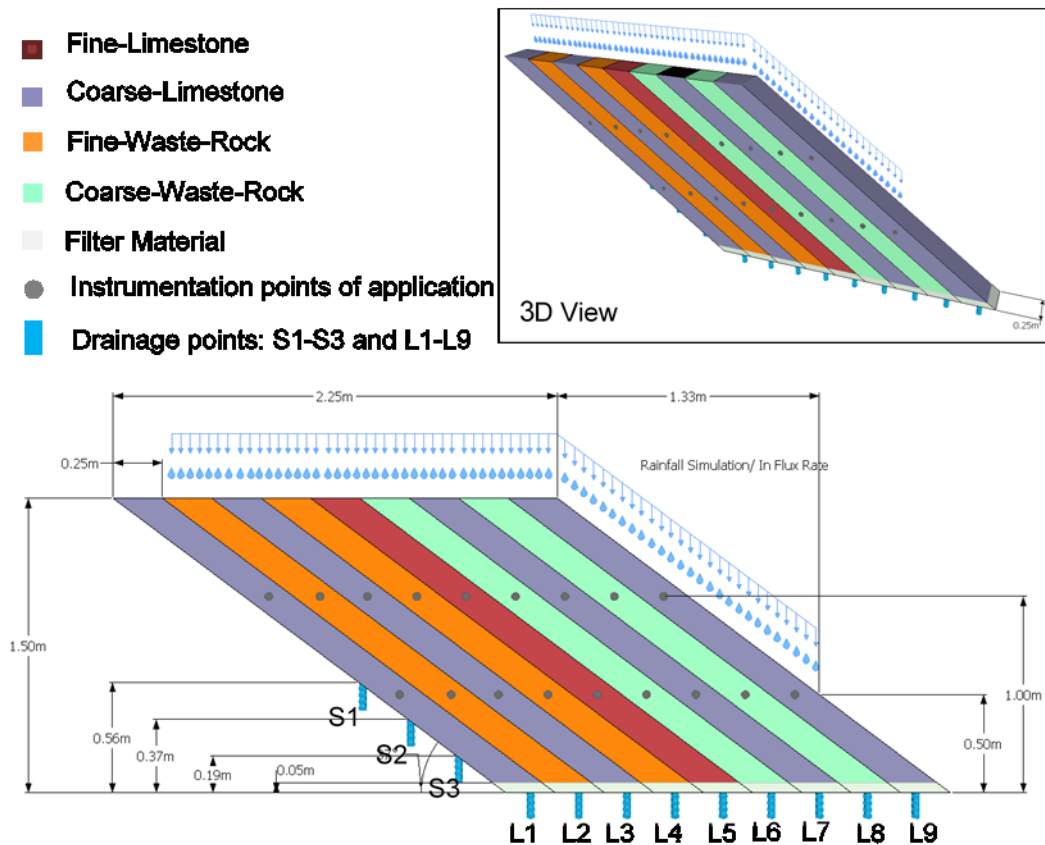


Figure 2.25 Meso-scale Experiment for Panel-3 (Based on Andrina, 2009)

The evaluation of water flow in waste rock using the Meso-scale experiment was conducted using the infiltration tests. The infiltration tests were applied through a simulated rainfall system representing three climate types.

2.6.3.2. EXPERIMENT CONDITIONS

The simulated rainfall rate changed between 2 mm/day, 5 mm/day, and 10 mm/day. The water was applied at the top of each panel, from the second layer to the outer slope in the last layer; no precipitation was applied to the lower 50 cm of the outer slope. Each layer received the same amount of flux rate. The coefficient of uniformity using the Christiansen Formula varied between 97% and 99%; it confirmed that all layers in the panels received the same rainfall rate, Andrina (2009). The water distribution system applied a uniform and constant flux rate through the entire experiment; the measure of the outflow from the drainage points was made once steady state conditions were reached.

The structure for the Meso-scale experiment in each panel allowed nine possible configurations for the boundary condition as shown in Figure 2.26. However, Andrina (2009)

only tested five configurations for Panel-1, three for Panel-2, and three for Panel-3. **Table 2.5** summarizes the tested conditions for the Meso-Scale experiments.

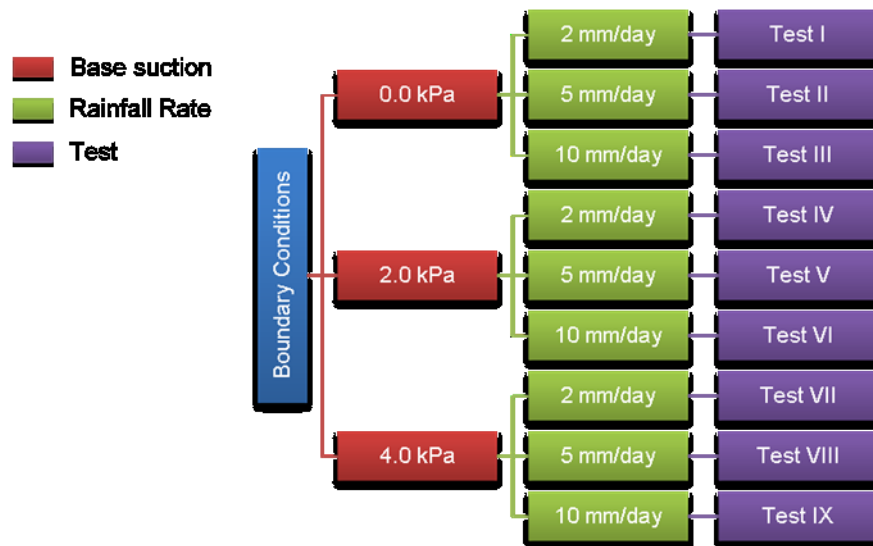


Figure 2.26 Boundary Conditions for the Meso-scale Experiment

The evaluation of water flow in the Meso-scale experiments had changes in the boundary conditions for the top and bottom of each panel (Table 2.5). The top boundary corresponds to the precipitation simulation with a constant flux rate due to the steady state conditions of the experiment. The flux rate for the panels was 2 mm/day, 5 mm/day, and 10 mm/day. The base boundary corresponds to the suction lysimeters; the panels had a constant suction applied in each layer at the drainage points L1 to L9.

Table 2.5 Testing Conditions for Each Panel

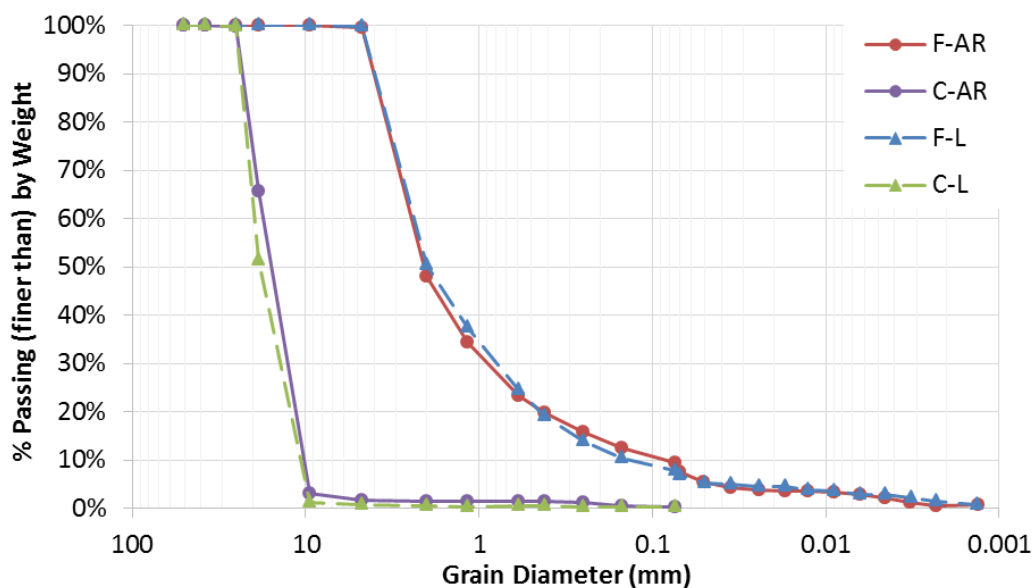
Panel	Test	Suction (kPa)	Precipitation (mm/day)
1	III	0	10
	IV	2	2
	VI	2	10
	VII	4	2
	VIII	4	5
	IX	4	10
2	VII	4	2
	VIII	4	5
	IX	4	10

Table 2.5 (Continue) Testing Conditions for Each Panel

Panel	Test	Suction (kPa)	Precipitation (mm/day)
3	IV	2	2
	VII	4	2
	VIII	4	5
	IX	4	10

2.6.3.3. MATERIAL PROPERTIES

The materials used in the Meso-scale experiment came from a Waste rock Deposit on Grasberg Mine in Indonesia. The Waste rock is classified in two categories; one consisted in Acid-Rock due to the 5% sulfur content; the second is limestone from a limestone quarry. The waste rock material was crushed and sieved to achieve the grain size distribution of the Acid-Rock and Limestone for the panels. The particle size distribution fitted the scaling of the experiment with respect to the condition in the mine (Andrina, 2009). It resulted in a fine fraction similar to the fine portion of the run-of-mine with a diameter less than 10 mm. The coarse particles had a 10:1 ratio between the layer thickness and the maximum particle size; this dimension resulted in a grain particle with a diameter between 10 mm and 25 mm (Andrina, 2009). The sieve analysis showed a uniform gradation for the Coarse-waste-rock, and non-uniformity for the Fine-waste-rock Figure 2.27 shows the grain size classification for the coarse and fine particles.

**Figure 2.27** Sieve Analysis from Waste Rock Material (Andrina, 2009)

The coarse grain particles for the Acid-Rock and Limestone have the same gravel content, but with a larger particle size in the Limestone (42% of coarse gravel). This distribution with such a low percentage of sand particles generates large voids within the matrix causing low desaturation suction (difficult to detect even through laboratory experimentation). Furthermore, the difference in the AEV is expected to be insignificant between the C-AR and C-L, with the C-AR having a larger AEV.

The classification of the fine particles shows a 14% higher content of fine gravel for the F-L and 8% higher content of sand in the F-AR. The difference in the sand between the F-AR and F-L related to the coarse and fine fraction with a 10% difference and a similar content in medium sand size. The higher content of finer particles in the F-AR gives an indication to expect a higher AEV than the F-L.

In the Meso-scale experiment, Andrina (2009) assumed that both types of coarse and fine grain materials had similar unsaturated properties as shown in Table 2.6. i.e., the material unsaturated properties of the F-AR and F-L are the same, as well as the C-AR and the C-L.

Table 2.6 Waste rock Properties (Andrina, 2009)

Properties\Material	Coarse-Waste-Rock (C-AR and C-L)	Fine-Waste-Rock (F-AR and F-L)
k_{sat} (m/s)	$1.0 \times 10^{-2} \leftrightarrow 1.5 \times 10^{-2}$	$3.9 \times 10^{-4} \leftrightarrow 8.0 \times 10^{-4}$
AEV (kPa)	0.025	1.42
Sat. VWC	0.37	0.44
Sat Suction (kPa)	0.01	0.01

The measurement of the Saturated-Hydraulic-Conductivity (k_{sat}) was made using constant head and falling head test for C-AR, F-AR, C-L, and F-L. The results showed that the Fine-waste-rock and Coarse-waste-rock vary within the same range. The Soil Water Characteristic Curve (SWCC) for the Fine-waste-rock was measured using Tempe Cells test and is shown in Figure 2.28; however, the SWCC for the Coarse-waste-rock was estimated using Fredlund and Xing equation (Andrina, 2009).

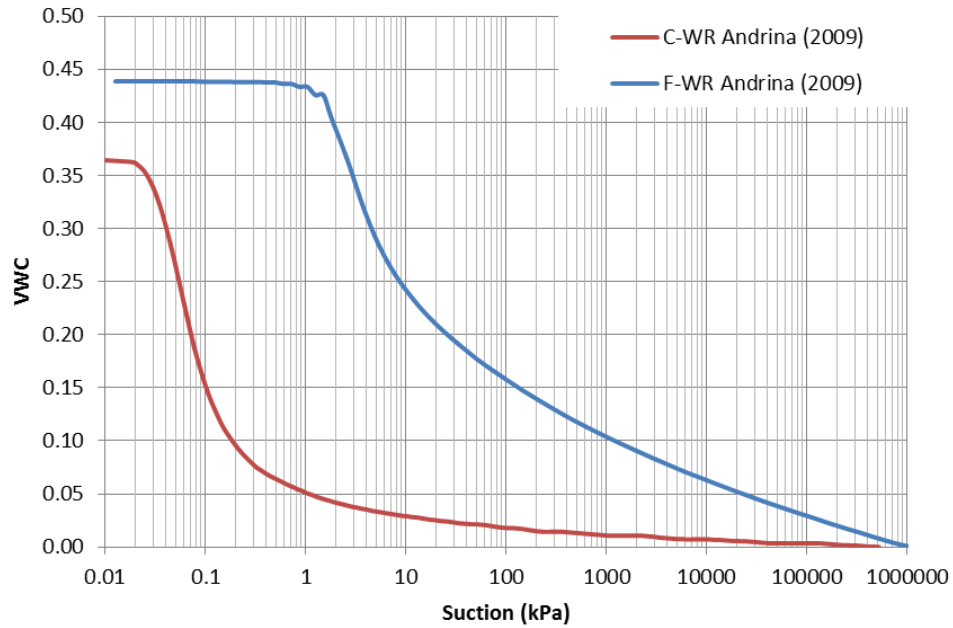


Figure 2.28 Soil-Water Characteristic Curves for Waste Rock, after Andrina (2009)

The reported hydraulic conductivity curves are estimated from the SWCC, k_{sat} , and Fredlund & Xing equation as shown in Figure 2.29. The Fine-waste-rock had a k_{sat} equal to $3.0 \times 10^{-4} \text{ m/s}$ and the Coarse-waste-rock a k_{sat} of 0.01 m/s . Once the suction exceeded the AEV for the Fine-waste-rock (0.03 kPa) and Coarse-waste-rock (1.0 kPa), the materials desaturated quickly with a small changes in suction (Andrina, 2009).

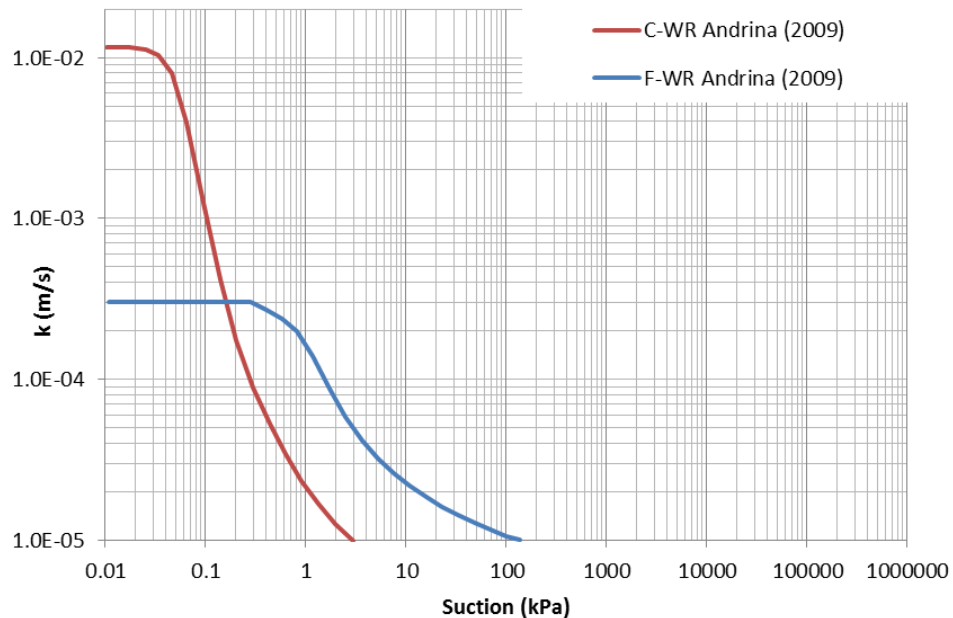


Figure 2.29 Hydraulic-Conductivity-Curve (Right) for Waste Rock, after Andrina (2009)

2.6.3.4. EXPERIMENT RESULTS

The results from the Meso-scale panels are presented from each drainage point as a percentage of the total flux rate applied at the top of each panel. Table 2.7 summarizes the results from the tests run for the three Panels with respect to the nine possible boundary configurations (Figure 2.26). The contour color is set to visualize the Low Outflow (GREEN) and High Outflow (RED) from each layer with respect to a particular test and panel.

Table 2.7 Drainage Point Outflow from Meso-scale Experiments

Panel	Test		I	II	III	IV	V	VI	VII	VIII	IX
	Suction (kPa)		0			2			4		
	Precipitation (mm/day)		2	5	10	2	5	10	2	5	10
	Drainage Point	Material	Outflow (%)								
1	S1	C-AR			6%	0%		5%	1%	4%	5%
	S2	C-AR			7%	0%		4%	0%	3%	7%
	S3	C-AR			4%	2%		4%	3%	5%	15%
	L1	C-AR			17%	11%		26%	6%	19%	25%
	L2	F-AR			19%	13%		24%	31%	21%	18%
	L3	C-AR			19%	19%		13%	22%	15%	13%
	L4	F-AR			11%	26%		12%	16%	16%	7%
	L5	C-AR			15%	28%		10%	20%	17%	9%
	L6	F-AR			2%	1%		3%	1%	1%	1%
	L7	C-AR			0%	0%		0%	0%	0%	0%
2	S1	C-AR							2%	1%	0%
	S2	C-AR							0%	3%	0%
	S3	C-AR							4%	9%	5%
	S4	C-AR							5%	2%	30%
	L1	C-AR							18%	37%	21%
	L2	F-AR							14%	16%	13%
	L3	C-AR							16%	11%	7%
	L4	F-AR							7%	3%	4%
	L5	C-AR							25%	13%	17%
	L6	F-AR							8%	6%	2%
	L7	C-AR							0%	0%	0%
3	S1	C-L				0%			0%	0%	0%
	S2	C-L				0%			0%	0%	0%
	S3	C-L				0%			0%	0%	0%
	L1	C-L				1%			4%	12%	19%
	L2	F-AR				14%			15%	30%	21%
	L3	C-L				18%			15%	17%	23%
	L4	F-AR				31%			54%	17%	8%
	L5	F-L				26%			0%	8%	13%
	L6	C-AR				5%			7%	11%	9%
	L7	C-L				5%			5%	5%	8%
	L8	C-AR				0%			0%	0%	0%
	L9	C-L				0%			0%	0%	0%

Note. The color scale is defined for each test, for specific precipitation and suction conditions. C-AR= Coarse-Acid-Rock; F-AR=Fine-Acid-Rock; C-L=Coarse-Limestone; F-L= Fine-Limestone.

The Meso-Scale experiments by Andrina (2009) showed that 70% of the outflow was collected from the drainage points underneath the precipitation simulators in Panel-1. For Panel-1 the coefficient of variability with respect to the drainage point in each test decreases when the rainfall rate increases from 2 mm/day to 10 mm/day (Andrina, 2009). This relationship meant that increments in rainfall rate generate less water moving according to the profile of the layers. The results from the tests in Panel-2 showed that the coefficient of variation had the contrary result as in Panel-1; as the rainfall rate increased, more water moved according to the profile of the layers. Also Andrina observed that the difference in water flow between Panel-1 and Panel-2 was related to the change in geometry from the top layer of C-L. Since most of the rainfall simulation was applied directly above the slope in the first layer, the location of rainfall resulted in Panel-2 having a higher outflow from L1 and L2 than in Panel-1. Despite Panel-1 and Panel-2 having relatively high difference in the outflow distribution, the outer layer in both Panels showed similar low outflow values in all tests. Panel-3 at 2 mm/day had concentrated outflow in the middle as in Panel-1 and Panel-2, with no outflow from the slope in the first layer and from L8 and L9. Panel-3 behaved as Panel-1 where the coefficient of variation decreases as rainfall rate increases. Andrina observed that vertical flow exhibited more in Panel-1 and Panel-2 than in Panel-3. In addition, the wider geometry and arrangement of layers of Panel-3 affected the flow path.

The discharge from the three Meso-scale experiments shown in Table 2.7 are grouped with respect to the material type as shown Table 2.8. In Panels 1 and 2, the total outflow from the layers with F-AR includes drainage points L2, L4, and L6; for the layers with C-AR the drainage points are S1, S2, S3, L1, L3, L5, and L7. In Panel-3 the results are grouped in four materials (F-AR, C-AR, F-L, and C-L).

Table 2.8 Discharge Results from the Three Panels Grouped By Material

Panel	Test	I	II	III	IV	V	VI	VII	VIII	IX
	Suction (kPa)	0			2			4		
	Precipitation (mm/day)	2	5	10	2	5	10	2	5	10
	Material	Discharge (%)								
1	F-AR	32%			41%	39%		48%	37%	26%
	C-AR	68%			59%	61%		52%	63%	74%

Note. C-AR= Coarse-Acid-Rock; F-AR=Fine-Acid-Rock; C-L=Coarse-Limestone; F-L= Fine-Limestone.

Table 2.8 (continue) Discharge Results from the Three Panels Grouped By Material

Panel	Test	I	II	III	IV	V	VI	VII	VIII	IX
	Suction (kPa)	0			2			4		
	Precipitation (mm/day)	2	5	10	2	5	10	2	5	10
	Material	Discharge (%)								
2	F-AR							29%	26%	19%
	C-AR							71%	74%	81%
3	F-AR				45%			69%	47%	28%
	C-AR				5%			7%	11%	9%
	F-L				26%			0%	8%	13%
	C-L				24%			24%	42%	50%

Note. C-AR= Coarse-Acid-Rock; F-AR=Fine-Acid-Rock; C-L=Coarse-Limestone; F-L= Fine-Limestone.

The discharge from the three Meso-scale experiments shown in Table 2.7 are grouped with respect to the grain size as shown Table 2.9. The similarities in the grain size distribution between the C-L and the C-AR; as well the similarities between the F-C and the F-AR allows to group the discharge results with respect to the grain size.

Table 2.9 Discharge Results from Panel-3 Grouped By Grain Size

Panel	Test	I	II	III	IV	V	VI	VII	VIII	IX
	Suction (kPa)	0			2			4		
	Precipitation (mm/day)	2	5	10	2	5	10	2	5	10
	Grain Size	Discharge (%)								
3	Fine (F-AR + F-L)				71%			69%	55%	41%
	Coarse (C-AR + C-L)				29%			31%	53%	59%

Andrina (2009) observed that increasing the rainfall rate generated a lower outflow from the Fine-waste-rock; these decreases ranged between 9% and 29%. The minimum decrease was from Panel-2 and the maximum decrease from Panel-3. With respect to the changes in outflow from the Coarse-waste-rock, the results showed increments as rainfall rate increased. The maximum increase was approximately 30% from Panel-3. The result

from the different tests lead Andrina to conclude that gravitational flow was the dominant flow mechanism as rainfall rate increased.

The experimental results show that the flow path was affected by the precipitation, where lateral flow occurred at low precipitation rates. This lateral flow allowed water to reach the fine layers, making the fine layers the preferential discharge points. The discharge increased with precipitation, but with different proportions in each layer. Once the precipitation was increased, breakthrough occurred in the coarse layers making it the preferential discharge point. Andrina explains that the increasing the precipitation change the flow mechanism to gravitational.

The installed instrumentation allowed the measurement of the change in matric suction at the different heights. Figure 2.30 shows the measured matric suction before installing the lysimeters at the base (Andrina, 2009, pp. 279-280). The experimental results showed matric suction between 0.1 kPa and 0.2 kPa in layer 6 for Panel-1. In Panel-2, the matric suction increased from 0.3 kPa to 0.6 kPa. The matric suction increased toward the outer layer (L7 for Panel-1 and Panel-2, and L9 for Panel-3). Andrina explains that increasing the matric suction in the outer layers makes the permeability of the material drop, changing the flow mechanism to film flow.

The result from the experiment contradicted the study conducted by Tami (et al. 2004) where a correlation was found between matric suction and precipitation. This correlation showed that higher precipitation rates did not always lower the matric suction (Andrina, 2009).

The effect from applying suction at the base of the panel resulted in a decrease of the total discharge from the coarse layers and increase in the fine layers. However, the effect was not similar for all layers, the change in suction showed that the increment in discharge was more pronounced in the inner layer (towards L1). The increment in preferential flow from the fine layers was determined from the increase of VWC. In Panel-3 the increment was observed in L4 and L5 where a thicker zone of Fine-waste-rock was located. These two layers, despite being Acid Rock and Limestone, acted as a single layer, thereby performing as a barrier for the inner layers.

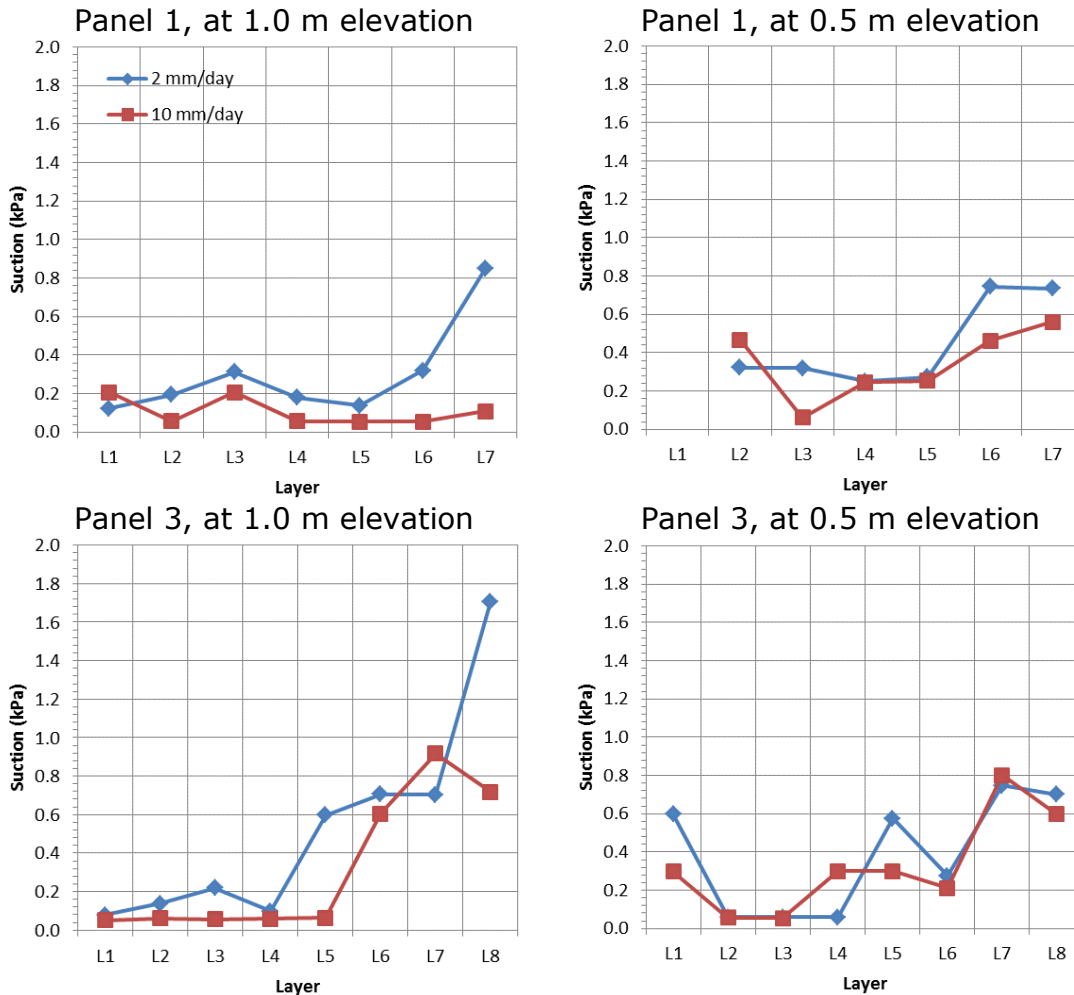


Figure 2.30 Measured Matric Suction from Panel-1 and Panel-3 at 0.5 m and 1.0 m Elevation for 2 mm/Day and 10 mm/Day (Andrina, 2009)

2.7. SUMMARY

The results of the laboratory testing completed by Newman (1999) and Andrina (2009) illustrate the importance in understanding the mechanism that controls water flow in unsaturated conditions, particularly on waste rock embankments. Previous investigation had been made to understand this mechanism from different perspectives and methodologies. The studies presented in this chapter form the base understanding for the development of this thesis.

One of the most currently complex models considering water flow in an unsaturated conditions was found to be the TPROGS models. The analysis presented by Broda (et al., 2013) exhibits the variability and uncertainty that may be found in the water flow simulation in WRE's. The models allowed the viewing of the behavior of vertical water transfer on a

quasi-horizontal layering system. Selecting an improper methodology of incorrect assumption would lead to the wrong conclusions. The results from their studies showed that the TPROGS model is a powerful tool to analyze the hydrology for these cases, and, given the heterogeneous configuration of the core waste rock, this hydrology resembles the water behavior on WRE found in the field. These complex models are not on the scope of the models presented in the investigation for this thesis. However, it is important to highlight the direction of the development of numerical modeling for water flow in unsaturated conditions.

The column experiments (Newman, 1999) and analysis highlight the effect of preferential flow in unsaturated soils, specifically for waste rock embankments. This experiment reflects the effect of contact length and precipitation on the mechanism controlling water flow in unsaturated conditions. The simulation of these two column experiments are the initial step to developing the model for the three Meso-scale Experiments conducted by Andrina (2009).

CHAPTER 3 THEORY AND UNSATURATED FLOW

3.1. UNSATURATED SOILS

Initially geotechnical science was mostly developed to analyze saturated soils leaving aside the unsaturated portion in which most stratigraphy is exposed. Even though unsaturated soils are extremely common in the world and are part of many of the engineering challenges, it was easier to measure the geotechnical properties in soils containing either air or water between the pores (Lu & Likos, 2004). Unsaturated soils are part of the environmental hydrologic cycle as shown in Figure 3.1, and it corresponds to the portion above the phreatic level where negative pressure takes place. This condition is also part of many industrial processes, especially in the mining industry where embankments and cover barriers may be partially saturated or dry.

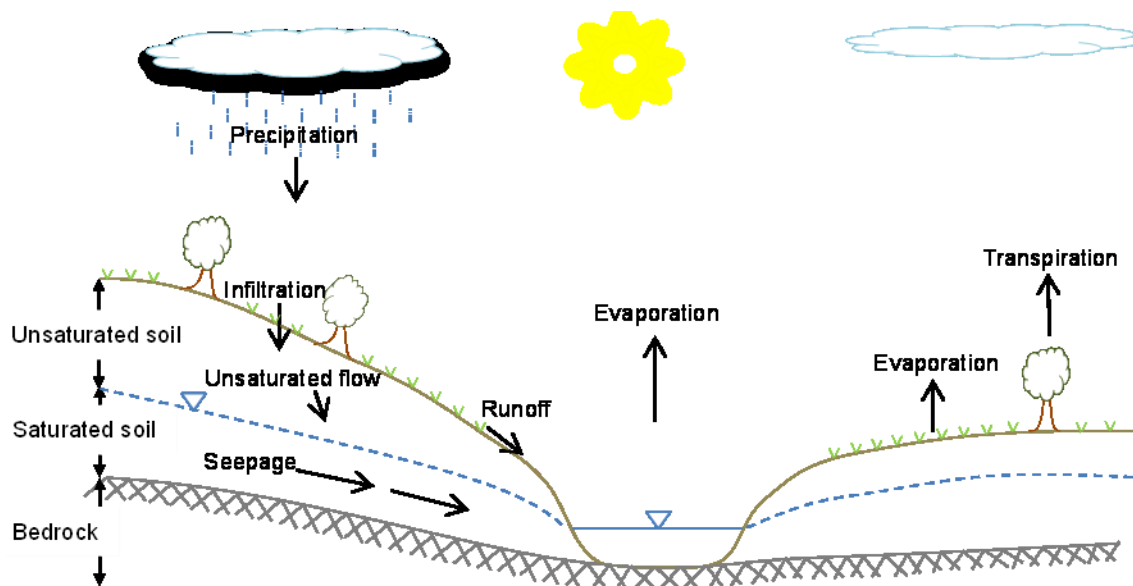


Figure 3.1 Unsaturated Flow in Hydrologic Cycle

Much of the earliest understanding of the unsaturated soil relates to agricultural disciplines, creating physical and hydraulic models. Many testing techniques and procedures were taken from this discipline and adjusted to the geotechnical science (Fredlund D.G, 2006). Soils are a discontinuous system of particles, and the phases that make up the soil establish the difference in response between saturated and unsaturated soils. Saturated soils have two phases; soil and water; this means that any pore in the matrix is filled with

water making the pore water pressure positive. Alterably Unsaturated soils have more than two phases (see Figure 3.2) and the pore pressure is negative.

Fredlund et al. (2012) proposed that in addition to analyzing an air-water-soil phase system, one must consider an air-water interface (contractile skin), as this can reflect changes in stress state analysis as the surface tension pulls the particles together generating a volume decrease and an increase in the shear strength of the soil. The contractile skin behaves as an elastic membrane under tension (surface tension) between particles. This air-water interface can be neglected in volume-mass relations, since the volume is small and the mass can be included in the mass of water.

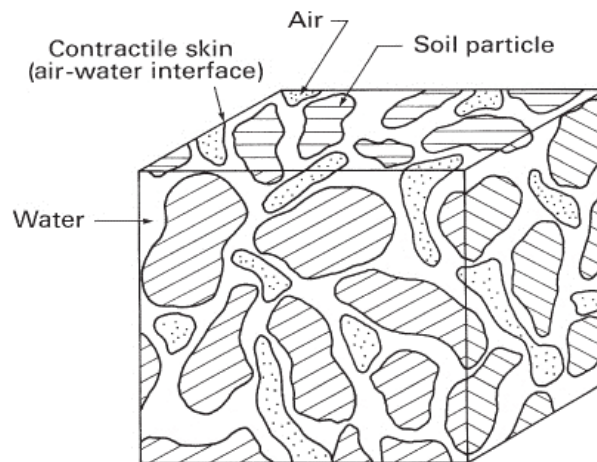


Figure 3.2 Unsaturated Soil Phases (Fredlund, et al., 2012)

In 1931 Richard's (1931) explained that surface tension or suction makes water particles concentrate in the corners of the pores or where the grains are close together; the size and thickness of the particles depends on saturation of the medium. The join between water particles creates channels of water that are in contact with the solid particles and the air-water interface, through which liquid in the unsaturated porous medium flows.

The contractile skin is subjected to a pressure difference from air and water phases called matric suction ($u_a - u_w$). This suction causes contractive skin to bend forming a meniscus at the space between soil particles. As the curvature of the meniscus decreases, the associated surface tension increases; when the matric suction is zero, the curvature disappears (Fredlund, et al., 2012). The decrease in particles size, increases the suction that the soil can withstand, without displacing the water within the pores. The maximum suction that a soil can withstand without letting air penetrate into the soil is referred as the air-entry value (AEV).

The suction in the soil becomes primarily a function of the pore size distribution and the AEV becomes a function of the largest pore space between particles. This behavior of unsaturated soil is described by the soil-water characteristic curve (SWCC).

3.1.1. Soil Water Characteristic Curve

The SWCC relates the amount of water contents and suction within a soil (Fredlund & Xing, 1994 A). The relation of water content and suction helps to understand the distribution of water in the voids. As revealed by Lu & Likos (2004), the SWCC gives an indication of material properties such as pore size distribution, grain size distribution, density, organic material content, clay content, and mineralogy on the pore-water retention behavior. Fredlund (2006) considers that the SWCC “becomes the key in unsaturated soil properties for unsaturated soil mechanics problems”. Figure 3.3 shows the general shape of the SWCC for different soils.

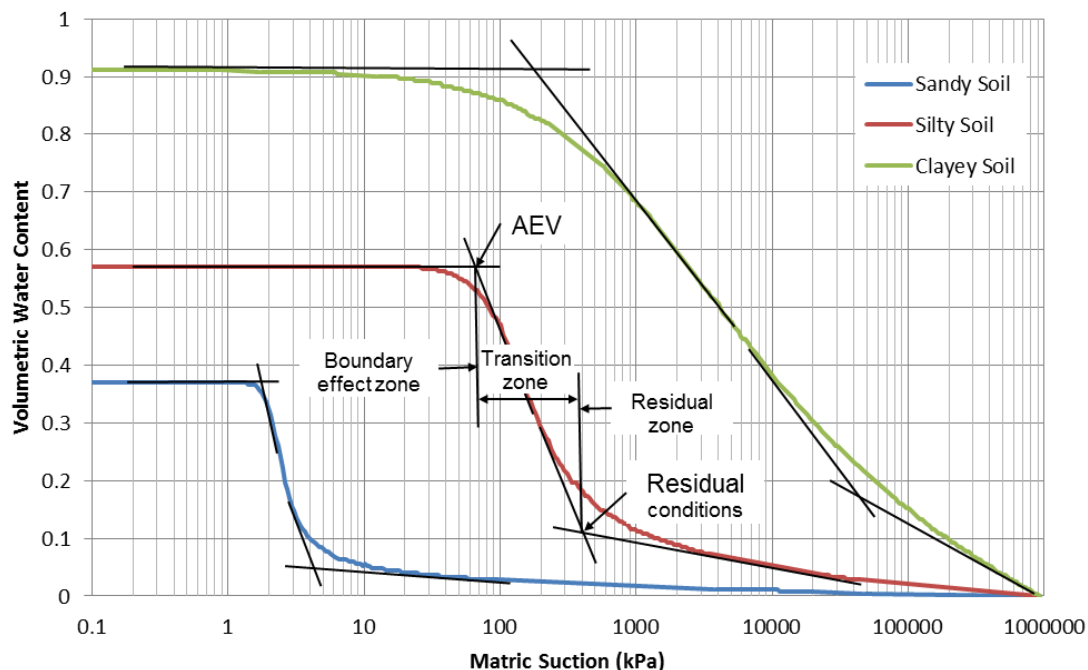


Figure 3.3 Example of A SWCC for A Sandy Soil, Silty Soil, and Silty Clay (Fredlund & Xing, 1994 A)

The SWCC is determined by measuring the change in moisture at different suctions using pressure cells. This test requires small increments in suction in order to obtain a precise AEV. The methods to measure unsaturated properties especially for the SWCC are complex, costly, and time-consuming (Fredlund D.G, 2006). Such estimation procedures have been developed over time; the most commonly used are Gardner (1958), Brooks and

Corey (1964), Brutsaert (1967), Van Genuchten (1980), Campbell (1974), Fredlund & Xing (1994), and Fredlund (2006).

Fredlund and Xing (1994 A) proposed a general equation for the SWCC to describe the volumetric water content (W_w) in a soil at a specific suction (Ψ). The equation fit experimental data for suction ranging from 0 kPa to 10^6 kPa.

$$W_w = W_s \left[1 - \frac{\ln \left(1 + \frac{\Psi}{h_r} \right)}{\ln \left(1 + \frac{10^6}{h_r} \right)} \right] \left[\frac{1}{\left[\ln \left[\exp(1) + \left(\frac{\Psi}{a_f} \right)^{n_f} \right] \right]^{m_f}} \right]$$

where:

W_s = saturated volumetric water content.

a_f = material parameter, function of the AEV.

n_f = material parameter, function of the rate of water extraction from the soil at the transition zone.

m_f = material parameter, function of the residual water content.

h_r = suction at the residual water content.

The Fredlund and Xing (1994) equation allows a better fit for high-suction values than other equations previously mentioned. The equation takes the SWCC to a suction of 10^6 kPa at zero water content by applying a correction factor, thereby avoiding the evaluation of the residual VWC in the prediction of the coefficient of permeability, Fredlund, et al. (1994 B).

The SWCCs are also dependent on the volumetric water content history or path of water flow through the soil; i.e., it has a hysteretic behavior as shown in Figure 3.4. When the material is going through a desorption process (i.e. drying), the material would generate higher suction; this increase makes it more difficult for the water to leave the pores as the surface tension is more difficult to overcome. The contrary happens when the material goes into an absorption process (i.e. wetting): the suction is lower for water to get into the pores. The measure of the SWCC through laboratory experiments is typically run for the drying curve; because, the desorption of the material is the easiest process to control (Fredlund, et al., 2012). The differences of the desorption and absorption curve for the volumetric water content and AEV of a single material is found to be larger in finer soils (Fredlund & Xing, 1994 A).

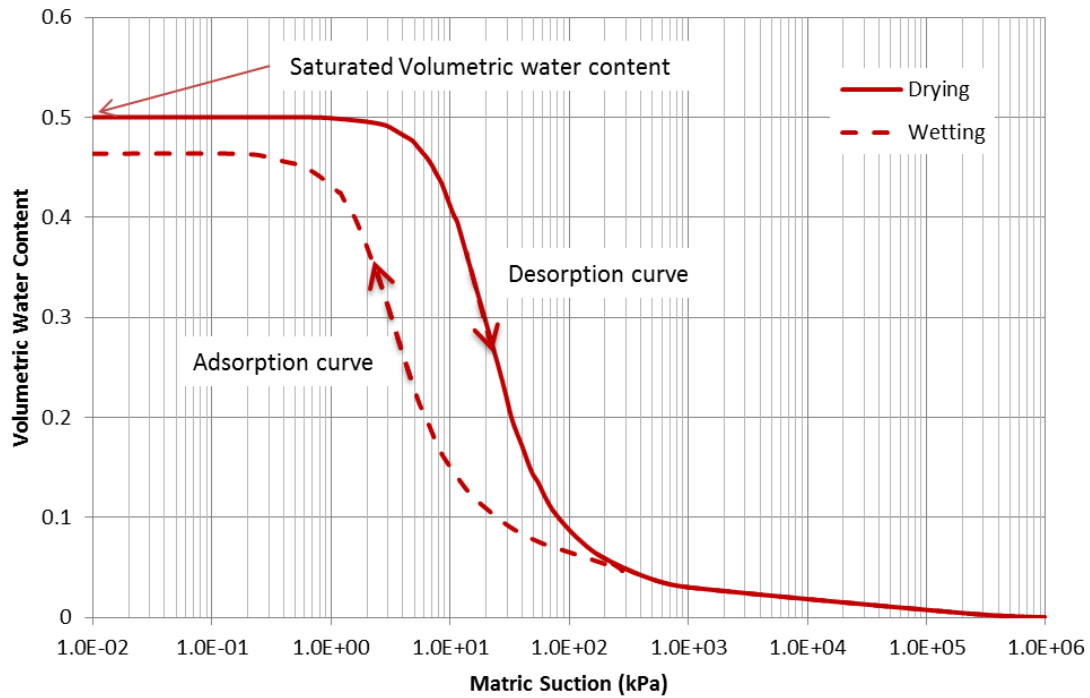


Figure 3.4 Hysteresis in the Soil Water Characteristic Curve for A Silty Soil (Fredlund & Xing, 1994 A)

The hysteresis in the absorption and desorption process reveals that there is no unique SWCC for a particular material Fredlund, et al. (2012); even stress history has been found to affect the SWCCs, Fredlund & Xing (1994 A). Volume mass relations such as the void ratio and degree of saturation are also part of the constitutive properties in an unsaturated soil. Researchers like Pham (2005) have used a constitutive surface that can describe the behavior of the material in the stress state. Figures 3.5, 3.6 and 3.7 show the constitutive surface for the Beaver Creek sand; this material will be explained in more detail in Chapter 4.

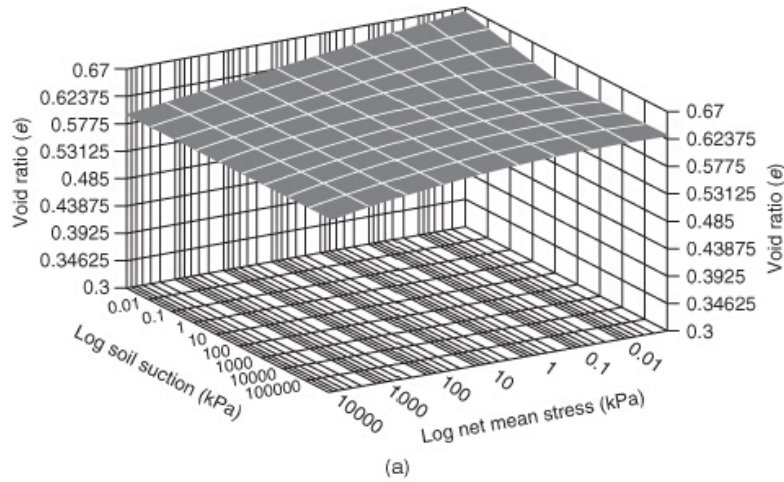


Figure 3.5 Void Ratio Constitutive Surface for Beaver Creek Sand, Fredlund et al. (2006)

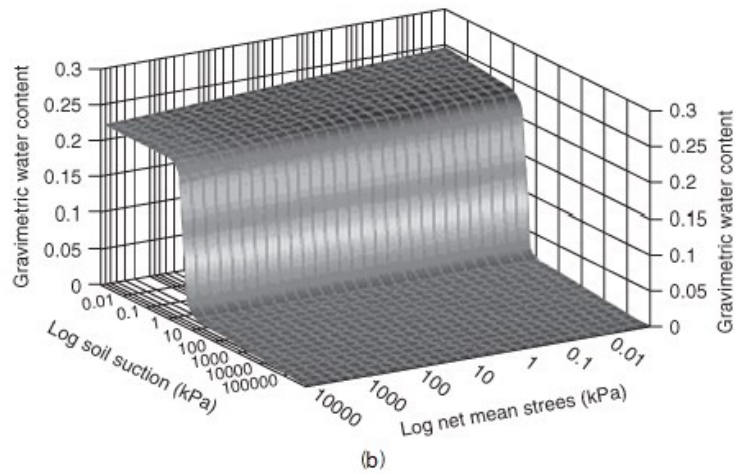


Figure 3.6 Gravimetric Water Content Constitutive Surface for Beaver Creek Sand, Fredlund et al. (2006)

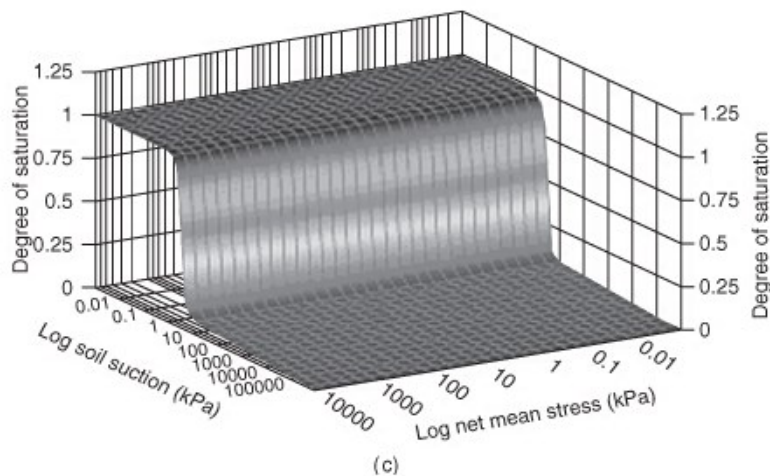


Figure 3.7 Saturation Constitutive Surface for Beaver Creek Sand, Fredlund et al. (2006)

The first constitutive surface (Figure 3.5) shows that changes in the stress state generate changes in the void ratio. The increment in the mean stress decreases the void ratio. In this material, the void ratio drops from 0.67 to 0.5775 for a stress state between 0.01 kPa and 10000 kPa. This drop in the void ratio allows the material to generate a higher suction; the rearrangement of the particles allows building more negative pore pressure. Nonetheless, the change is small and only at a low stress condition is there a higher relation between suction and the void ratio.

The second constitutive surface (Figure 3.6) shows that high increments in the mean stress would also have a slight impact in the gravimetric water content, due to the small reduction in the void ratio (Figure 3.5). The small influence of the stress results in a constant AEV between 1 kPa and 10 kPa for the Beaver Creek Sand. Nonetheless, the change in the mean stress affects the relation between the gravimetric water content and suction. The gravimetric-water-content is inversely proportional to suction, and as the stress state decreases, the relation increases.

The third constitutive surface (Figure 3.7) shows that the degree of saturation is constant for the same stress state in the same way that the rate of change in the void ratio is constant. In the Beaver Creek Sand, the saturation drops drastically at a soil suction between 1 kPa and 10 kPa, the same as the AEV in the SWCC. This drop to a small suction is caused by the rearrangement of sand particles due to increments in the mean stress. An increment in stress would generate a volume change either in coarse or fine materials (i.e. reducing the amount of voids); as a consequence, a smaller void ratio would increase the AEV within the material.

The SWCC also allows estimating of the parameters in unsaturated soil called Unsaturated Soil Property Functions (USPFs), Fredlund, et al. (2012), such as hydraulic conductivity function, storage function, shear strength function, and volume-mass change functions, Fredlund & Xing (1994 A). The better understanding and development of the SWCC also triggers the development of more precise equations for the coefficient of permeability, Fredlund, et al. (1994 B).

3.1.1. Estimation of the Hydraulic Conductivity Curve

The hydraulic conductivity is conditioned by the characteristics of the soil and the fluid. The characteristics affecting the hydraulic conductivity for soils are closely related. These characteristics are the soil structure, grain size, void ratio, saturation, and composition. In saturated soil mechanics it is assumed that the hydraulic conductivity remains constant for a particular type of soil (Lu & Likos, 2004, pp. 142-143). Contrary to

unsaturated conditions, the hydraulic conductivity changes with changes in saturation and pore water pressure. In unsaturated soils, pore water pressure becomes negative (i.e. suction), and as suction increases the hydraulic conductivity drops once the AEV is reached (Figure 3.8). Different estimation models have been developed to describe the unsaturated hydraulic conductivity functions. The Fredlund & Xing (Fredlund, et al., 1994 B) estimation method is one of the well-accepted models that uses curve fitting parameters from Fredlund & Xing (1994) SWCC. This model allows the integration from zero VWC to the saturated VWC.

Two of the key parameters that affect the unsaturated hydraulic conductivity curve are the Saturated Hydraulic Conductivity (k_{sat}) and the Air-Entry-Value (AEV). The k_{sat} accounts for the maximum hydraulic conductivity that the soil can obtain at the maximum saturation; it is also the starting point at which the hydraulic conductivity decreases due to the desaturation of the soil. On the other hand, the AEV indicates the suction that overcomes the surface tension between water and soil particles. The change in suction makes the air phase continuous as the water phase becomes discontinuous. In the desorption process (Figure 3.4), as the soil dries and surpasses the AEV, there is a large drop in the hydraulic conductivity due to the rapid loss of VWC.

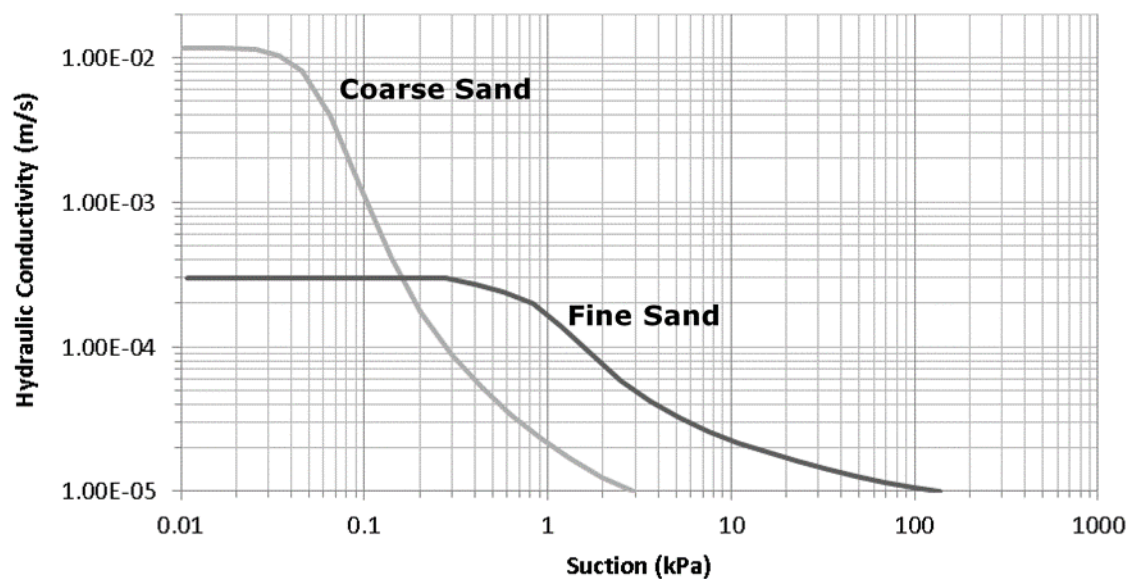


Figure 3.8 Hydraulic Conductivity Function for Fine and Coarse Sand

In theory, all soils have the same total suction for zero water content, but estimating the water content in which the hydraulic conductivity goes to zero is very complicated. It is known that even the driest soils may have a small volume of water content, and therefore can have high suction values, sometimes in nature exceeding 500 kPa (Wilson, et al.,

1997). For this reason, the hydraulic conductivity curve ignores the restriction of zero volumetric water content, Fredlund, et al. (2012).

The following hydraulic conductivity estimation method by Fredlund & Xing (Fredlund, et al., 1994 B) comes from a modification of the model proposed by Childs and Collis-George (1950), which in the integration form is:

$$k_r(\Psi) = \int_{\ln(\Psi)}^b \frac{\theta(e^y) - \theta(\Psi)}{e^y} \theta'(e^y) dy \bigg/ \int_{\ln(\Psi_{aev})}^b \frac{\theta(e^y) - \theta_s}{e^y} \theta'(e^y) dy$$

where:

Ψ_{aev} =suction at the AEV.

$b = \ln(10^6)$ = upper limit of the integration.

y = dummy variable representing suction.

θ' = derivative of the SWCC equation.

θ_s = volumetric water content at saturation.

e = natural number.

According to thermodynamic consideration, all soils would reach zero water content at the same total suction; this value is equal to the upper limit (10^6 kPa) of the integration proposed by Fredlund & Xing (Fredlund, et al., 2012). This assumption makes a closed solution for any integration model within the SWCC. The integration has a closed-form solution along the SWCC, making it very complex for a manual solution. The model assumes no volume change in the structure of the soil while the suction changes.

This equation is used in the software SvFlux (SoilVision Systems Ltd., 2012) for the modelling process (see section 3.2). On the other hand, it is important to mention that the equation works best for sandy soils in contrast with fine-grained soils (Fredlund, et al., 1994 B).

3.2. WATER FLOW IN UNSATURATED CONDITION

In past decades the movement of water through the soil in unsaturated conditions has been discussed in order to determine the mechanisms and factors that influence this process. Initially it was thought that only gravitational forces and air voids were the reason for the downward movement; by the 1960s, Gardner discovered some active absorption forces, and factors such as the moisture content, porosity, heterogeneity, and rate of water added all changed the water flow through the soil, Newman (1999). Later on in 1965, Horton and Hawkins (1965) conducted an experiment in which they concluded that water flow

occurs through the material with lower saturated permeability, and water will flow where water was previously held. These transport methods can be divided into different flow types with respect to the three-dimensional process, Newman (1999):

- Finger Flow: occurs when the wetting front is transferred from a fine to a coarse layer and water concentrates at certain locations.
- Funnel Flow: occurs on incline coarse layers embedded in fine layers and water flows along the slope of the interface to the end of the coarse layer.
- Macropore Flow: occurs when water infiltrates the soil through a large opening, either anthropic or natural.
- Macro/Micropore Flow: occurs when water flows under gravitational or capillary forces.

Researchers have asserted different mechanisms to explain water flow through waste rock. Pantelis et al, (1991) stated that water flow through a porous medium; Herries et al, (1983) stated that flow occurs through discrete channels. Others have said that water flow was the combination of both mechanisms, Newman (1999). Nowadays it is well accepted and tested that water will flow in unsaturated media only through pores with a continuous liquid phase, neglecting vapor phase transport (Lu & Likos, 2004). Therefore water flows under a specific regime, and it becomes a function of the type of soil, the water content, and the degree of saturation.

The total head or total energy of pore water from thermodynamic principles governs water flow. In a closed channel and under ideal conditions, Bernoulli's Principle describes water flow. The gradient in total energy will move the water particles from one place to another. However, Childs and Collis (1950) explained that such a principle also applies for soils in saturated and unsaturated conditions, Fredlund, et al. (2006). This energy can be expressed in terms of total head $h_T(m)$:

$$u_t = gh_T$$

where:

u_t = total pore water potential

g = gravitational acceleration, m/s^2

The total energy has four components: kinetic energy or velocity head (h_k), gravitational energy or elevation head (h_e), pressure energy or pressure head (h_p), and Osmotic suction head (h_o). The total energy is expressed by the following equation:

$$h_T = h_p + h_k + h_e + h_o$$

where:

$$h_p = u_w / \gamma_w, \text{ m}$$

$$h_k = v^2 / 2g, \text{ m}$$

$$h_e = \text{Length, m}$$

$$u_w = \text{pore water pressure, kN/m}^2$$

$$\gamma_w = \text{density of water, kN/m}^3$$

$$v = \text{velocity, m/s}$$

As soils are a porous medium, the velocity component (h_k) is negligible. Lu & Likos (2004) state that for most practical seepage problems occurring on a macroscopic scale, the total energy is sufficiently defined by the other three components to describe pore water pressure and flow. In a continuous liquid phase, the difference in total energy between two points create a hydraulic gradient that moves the water from one point to the other (see section 3.3.1).

Head energy is a state variable that describes flow in saturated or unsaturated soils. It becomes intrinsically associated with the equations used in the numerical model for water flow.

3.3. NUMERICAL MODELING FOR WATER FLOW IN UNSATURATED SOILS

Numerical modelling has become a common practice among engineers due to the fast development of computer capability that allow for the creation of larger and more complex models (SoilVision Systems Ltd., 2012). This numerical modelling allows for fast predictions with reasonable results, within the limits still found in most of our understanding in soil mechanic problems. One of the most complex problems that engineering has tried to solve for a long time, and every time more accurately, is water flow through a porous media in unsaturated conditions.

The solution of these problems involves the complex calculation of "Fluxional Equations" named Partial differential equations or PDE. These equations contain partial derivatives with two or more independent variables. PDEs allow the description of physical phenomena like fluid flow, heat, sound, electric charges, etc. In the case of water flow under unsaturated conditions, the PDE and soil properties are in a nonlinear form, making it more difficult to find the solution.

Models for water flow analysis can be simplistic or very complex depending on the type of problem or necessity of precision. Increments in the precision of a model may be

achieved by increasing the detail, or by having spatial variability of properties. Increments in precision also add a higher complexity in the definition and solution of the problem.

There are different ways to add precision into a model, starting from the characteristic of the mesh: changing the element size, the shape or even the number of nodes within the element as shown in Figure 3.9. Another way to add detail is to increase the dimensions of the model from 1D, to 2D, or 3D; however, not all dimensions apply to every situation and instead of helping to find a better solution may just add unnecessary complexity. Usually one-dimensional analyses are made to analyze large planes (e.g. cover system). Two-dimensional models are used for cross-sections (e.g. dams, slopes, retaining wall, etc.) and are not as complex as three-dimensional models.




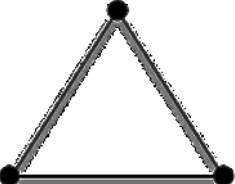
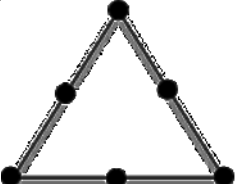
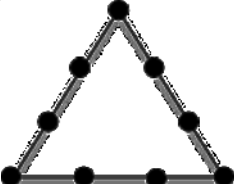
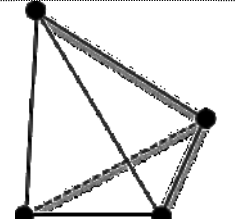
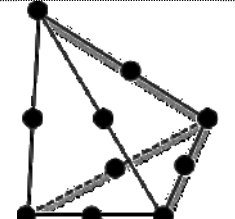
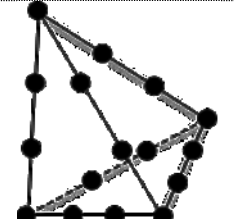
Analysis	Element Geometry		
	Linear	Quadratic	Cubic
1D			
2D			
3D			

Figure 3.9 Element Generation Used By SvFlux (SoilVision Systems Ltd., 2012)

Additionally numerical models for water flow can be either transient state models or steady state models. Transient state models are time dependent and can be spatially variable. The three PDE functions, the hydraulic conductivity function, the vapor conductivity function, and the soil water characteristic curve, describe water regimen and storage capacity through the soil. For steady state models, the variables are not time dependent, becoming a function of hydraulic conductivity function.

The analysis in this research focuses on steady state conditions for a two-dimensional space. The numerical models mimic two experimental conditions to evaluate water flow in an unsaturated system (see section 2.4 and 2.5). SvFlux Version 7.0 is used

to simulate water flow in unsaturated conditions. This package is developed by SoilVision Systems Ltd.

This software is used for groundwater flow analysis on soils in saturated or unsaturated conditions. SvFlux uses the solver FlexPDE to solve the linear and nonlinear PDEs. The solver implements an automatic mathematically designed mesh generation, with an additionally automatic mesh refinement, allowing a closer solution, especially in the critical zones of the model (SoilVision Systems Ltd., 2012). FlexPDE solves the nonlinear system using Newton-Raphson iteration process, Gui, et al., 2011.

3.3.1. Flow Laws

The flow laws relate the measure flow and the driving force (SoilVision Systems Ltd., 2012). Darcy's Law describes the movement of flow for liquid water; the driving force is the change or the gradient in the Hydraulic Head (h), contrary to Fick's Law that describes the movement of water vapor through diffusion. Still for unsaturated soil, the hydraulic conductivity related in Darcy's law cannot be assumed to be constant, as for this soil condition "pressure is controlled by capillary forces and the conductivity depends on the moisture content of the medium", Richards (1931).

- The generalized expression of Darcy's law for a saturated and unsaturated soil is expressed as (SoilVision Systems Ltd., 2012):

$$v_x^w = -k_x^w(\Psi) \frac{\partial h}{\partial x}; v_y^w = -k_y^w(\Psi) \frac{\partial h}{\partial y}; v_z^w = -k_z^w(\Psi) \frac{\partial h}{\partial z}$$

Where:

v_i^w = water flow rate in the i-direction.

$k_i^w(\Psi)$ = hydraulic conductivity in the i-direction as a function of the matric suction (Ψ).

h = hydraulic head, m.

The component for the hydraulic conductivity is obtained experimentally or estimated from the function of the Soil Water Characteristic Curve (SWCC), Fredlund, et al. (1994 B), which describes the change in the volumetric water content with the change in suction; as the soil dries the hydraulic conductivity increases.

As the model presented in the following analysis is made in a two-dimensional plane, the z component (v_z^w) becomes zero.

- Fick's law describes the movement of water vapor through the soil due to gradients in concentration; this movement takes place when the soil dries and the hydraulic conductivity becomes negligible and water movement happens in a gaseous state. This does not take place when the opposite happens; as the hydraulic conductivity increases, the volumetric water content increases and then vapor flow becomes negligible (SoilVision Systems Ltd., 2012).⁴ Vapor flow will not be taken into account in the following analysis as evaporation is negligible in the laboratory test made by Newman (1999).

3.3.2. Mass Balance

Mass balance or conservation of mass of water principle is used to derive the governing equation for saturated/unsaturated seepage. This principle states that the water coming into the material must be equal to the water coming out plus the storage water within the material at a specific rate. The conservation of mass is derived from a referential element volume (REV), describing the mass coming into the system and out of the system from each coordinate.

Figure 3.10 is the element that represents an infinitesimal volume of the body (a unit cell of a finite element mesh) in which the material is considered heterogeneous and continuous. The following differential equation is derived by taking the flow coming in and out of the REV for a three dimensional flow condition:

$$-\frac{\partial q_x^w}{\partial x} - \frac{\partial q_y^w}{\partial y} - \frac{\partial q_z^w}{\partial z} = \frac{1}{V_0} \frac{\partial M_w}{\partial t}$$

Where:

$\frac{\partial q_x^w}{\partial x}$ = change of total water flow rate in the i-direction.

$\frac{\partial M_w}{\partial t}$ = change of the water mass with time.

V_0 = reference volume.

⁴ Further information on Fick law for SvFlux can be found in the Theory Manual by SoilVision System Ltd (SoilVision Systems Ltd., 2012).

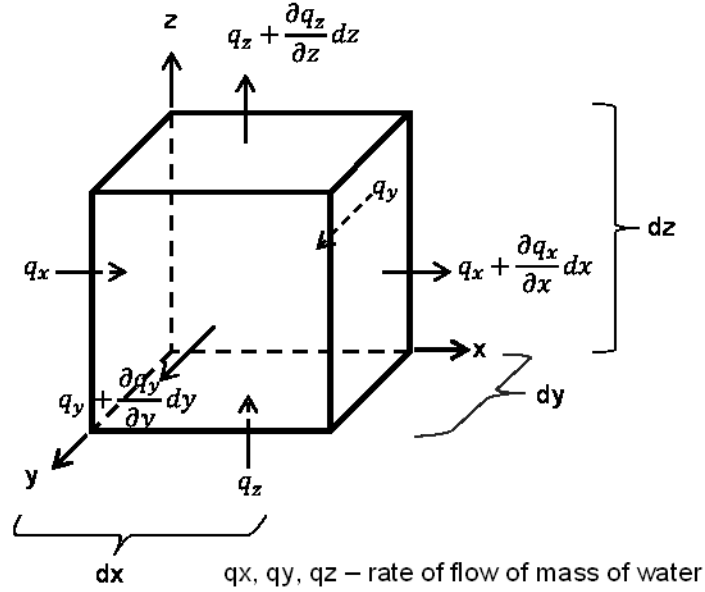


Figure 3.10 Referential Elemental Volume (REV) For Conservation Of Mass (SoilVision Systems Ltd., 2012)

As the experiment models were tested in steady state conditions, then no volume of stored water is taken into account, and the term at the right of the equation becomes zero. Additionally, as the models are in a two-dimensional space, the z component also becomes zero. The above equation becomes:

$$-\frac{\partial q_x^w}{\partial x} - \frac{\partial q_y^w}{\partial y} = 0$$

3.3.3. PDE for Unsaturated Steady State Water Flow

Unsaturated flow analysis requires solving linear and nonlinear PDEs, these equations involve Flow Laws and mass balance principles in order to describe the flow path of water through a material. Numerical analysis allows using Finite Element Methods to solve nonlinear PDE that governs water flow under unsaturated conditions within a soil. By replacing Darcy's law in the mass balance equation, the following generalized PDE for three-dimensional seepage is obtained (SoilVision Systems Ltd., 2012):

$$\frac{\partial}{\partial x} \left[(k_x^w + k^{vd}) \frac{\partial h}{\partial x} \right] + \frac{\partial}{\partial y} \left[(k_y^w + k^{vd}) \frac{\partial h}{\partial y} \right] + \frac{\partial}{\partial z} \left[(k_z^w + k^{vd}) \frac{\partial h}{\partial z} - k^{vd} \right] = -\gamma_w m_2^w \frac{\partial h}{\partial t}$$

Where:

x, y, z= components on the first horizontal direction, the second horizontal direction, and the vertical direction, respectively.

k_i^w = hydraulic conductivity in the i-direction, m/s.

k^{vd} = pore-water vapor conductivity, m/s.

γ_w = unit weight of water, kPa.

$m_2^w = \frac{d(V_w/V_o)}{d(u_a - u_w)} = \frac{\text{Volume water content}}{\text{matric suction}}$ = the slope of the SWCC passing the AEV.

h = hydraulic head, m.

t = time, s.

For Steady state conditions, the principal variable in the models is the coefficient of permeability as no changes in time are taken into account, Thieu, et al. (2001). This conditioning makes the right term of the equation become zero, and water storage is not considered. The conditions in which the experiments were conducted (see page 12) maintain an assumption that evaporation does not take place during the water infiltration. Finally, considering a two-dimensional space and the previous conditions, the generalized PDE for seepage is reduced, resulting in the following equation:

$$\frac{\partial}{\partial x} \left[k_x^w \frac{\partial h}{\partial x} \right] + \frac{\partial}{\partial y} \left[k_y^w \frac{\partial h}{\partial y} \right] = 0$$

The equation considers the flow in two directions, satisfying Darcy's law, and does not allow water storage in the system.

3.4. SUMMARY

The equation that describe water flow in an unsaturated system are highly complex to be solve, requiring the implementation of modeling techniques like Finite Element Methods, Fredlund, et al. (2012). These techniques have been developed to a point where engineers do not need to focus on the complexity of the equations, but rather focus on the problem to be solved. However, these tools should be used carefully as any input can easily generate a result that can be extremely far removed from the reality.

Defining the equation's parameters requires great care as unsaturated soil mechanics problems rely on a variety of parameters that are highly affected by the alterations or disturbance of the test's samples. One variation may or may not have a great impact on the solution, and by the use of numerical techniques this influence can be determined. In problems involving an unsaturated system, the solutions should be found for a range of

values in order to obtain a sensitivity of the potential problems with the parameters, while keeping in mind the implication of the assumption made in the model.

In modeling there is a strict relationship when considering the USPFs and SWCC. The use of back analysis methods or sensitivity methods should acknowledge the range of values in which the materials would need to be in order to satisfy the laboratory results. This relation must be maintained for any estimated function; altering any aspect of the USPF to improve convergence issues with nonlinear solving is equal to analyzing a different type of soil, Fredlund, et al. (2012).

For the purpose of this research, the unsaturated flow problems are solved through a series of back analysis that involved two main parameters of the PDEs, k_{sat} and AEV. The commercially available software SvFlux Ver. 7.0 from Soil Vision System Ltd was used to run multiple back analysis for the two parameters. SvFlux is a tool that allows the simulation of complex problems of water flow in a saturated or unsaturated system, and uses FEM to obtain detailed solutions. The following chapters describe and show the solutions from the simulations of a two column experiment and three incline panels that are tested for water flow in under unsaturated conditions.

CHAPTER 4 NUMERICAL MODEL OF WATER FLOW IN UNSATURATED COLUMN LAYERED SYSTEM

4.1. INTRODUCTION

Two column experiments were built at the University of Saskatchewan in 1999 to evaluate the effect of a preferential water flow path and column contact length under unsaturated conditions, Newman (1999). The laboratory test program was based on research conducted by Horton and Hawkins (1965) that evaluated the infiltration in porous media in a column experiment. The two experiments by Newman were conducted using an acrylic column. The first experiment consisted in testing fine-grain material and coarse-grain material using Beaver Creek Sand and Medium Silica sand, respectively. Both materials have been used by many other researchers and their range properties were well known. The second experiment was made to verify if the same preferential flow path could be found using a Fine-waste-rock and Coarse-waste-rock material taken from the Gold Sunlight Mine.

This chapter presents a numerical simulation of the two columns experiment by Newman using SvFlux. The data presented include the results of the following:

1. Simulation of Column with Beaver Creek Sand and Silica Sand
2. Simulation of Column with Waste Rock from Sunlight Mine
3. Calibration and comparison of the models to the laboratory results

4.2. OBJECTIVES

The objective of this study is to simulate water flow paths in an unsaturated system of a two layer vertical column under steady state condition in a two-dimensional space using numerical modelling with SvFlux Ver.7.0. The use of a numerical model allows the evaluation of the effect of precipitation and contact length in the preferential flow path under unsaturated conditions for sandy materials and waste rock. The simulations of water flow are made for two-column experiments, the first one using sandy materials and the second using waste rock material.

Initially, the simulations evaluate the numerical model using the same material properties measured in the laboratory. Then the simulations are run using the calibration

parameters from a Seep/W model made by Newman. As the first two simulations have high divergence, the model is back analyzed to improve the correlation between the model and the laboratory experiment.

Three main goals shape the general objective of this study:

- I. Evaluate the effect in controlling water flow in the numerical model by altering the saturated hydraulic conductivity.
- II. Calculate the internal response of the column experiments, considering the head pressure distribution, flow velocity, and movement of water particles.
- III. Compare the new model results to the simulation presented by Newman (Newman, 1999) by evaluating the influence of the saturated hydraulic conductivity of the materials in the preferential flow path, as well as the lateral transfer of flow.

4.3. LABORATORY COLUMN EXPERIMENT

In 1999, Newman at the University of Saskatchewan presented her results regarding two laboratory experiments and the numerical simulation of one of them. The objective of the research was to evaluate the preferential flow path through an unsaturated system, and the influence of the contact length between two materials. The study was carried measuring the discharge water at the base from a two vertical layer system in two column experiments. The first column test (Column-1) used sandy materials with a difference in saturated hydraulic conductivity (k_{sat}) of approximately three orders of magnitude. The materials in the second column test (Column-2) consisted of waste rock with an approximate difference in k_{sat} of two orders of magnitude.

The column is divided in two vertical halves, with each filled with a different material. Rain was simulated at the top of the columns and outlets placed at the bottom. The outlets were placed to measure the amount of flux coming out of each material. Additionally, each column had an impermeable barrier in the middle to control the contact length between the materials. The barrier was adjusted to four different heights for the Column-1 experiments, while for Column-2 the barrier was fixed for all tests. The total column height was 1400 mm and 1600 mm for the first and the second column, respectively. The total place materials in the first column were up to a height of 1140 mm and for the second Column-1360 mm. The materials in Column-1 were placed in 0.1 m lifts, while in Column-2 the waste rock was placed in 0.2 m lifts. The compaction was made using a 15 cm square plate, and the material was compacted by dropping six times a 5 kg weight.

Figure 4.1 shows the physical characteristics of the column experiments run by Newman (1999). The fine material used in Column-1 corresponds to Beaver Creek Sand, taken from a pit close to the South Saskatchewan River, while the coarse grain material corresponded to commercialized medium Silica sand. The materials in Column-2 consisted in Fine and Coarse waste rock from Golden Sunlight Mine in Montana, United States.

Additionally each side of the column had a base of gravel up to a height of 100 mm to avoid clogging of the drainage tubes. Newman (1999) found that the gravel material controlled the suction at the base of the coarse material, due to the difference between the air entry value of the Silica sand (equal to 0.8 kPa) and the applied suction at the base (i.e. the elevation of the outlets).

In order to evaluate the preferential flow path, two soils with contrasting hydraulic conductivity had to be placed in each column. Outlets were located at the base on each side to collect the discharge water from each material to evaluate the amount of water transferred at the contact zone. Table 4.1 presents the experiment conditions under which each column was tested. Column-1 was tested for four different cut-off heights and four precipitation rates (simulating precipitation conditions), while Column-2 had a constant height and three precipitation rates.

Table 4.1 Experimental Conditions for Column Test

Column	1				2
Material	Sandy Soil				Waste rock
Test	1	2	3	4	1
Cut-off Height (mm)	590	390	140	40	360
Contact Length (mm)	550	750	1000	1100	1000
Precipitation (mm/day)					
Flux (a)	1123	1123	1123	1123	445
Flux (b)	804	804	752	821	12
Flux (c)	449	432	406	475	5
Flux (d)	337	320	320	337	-

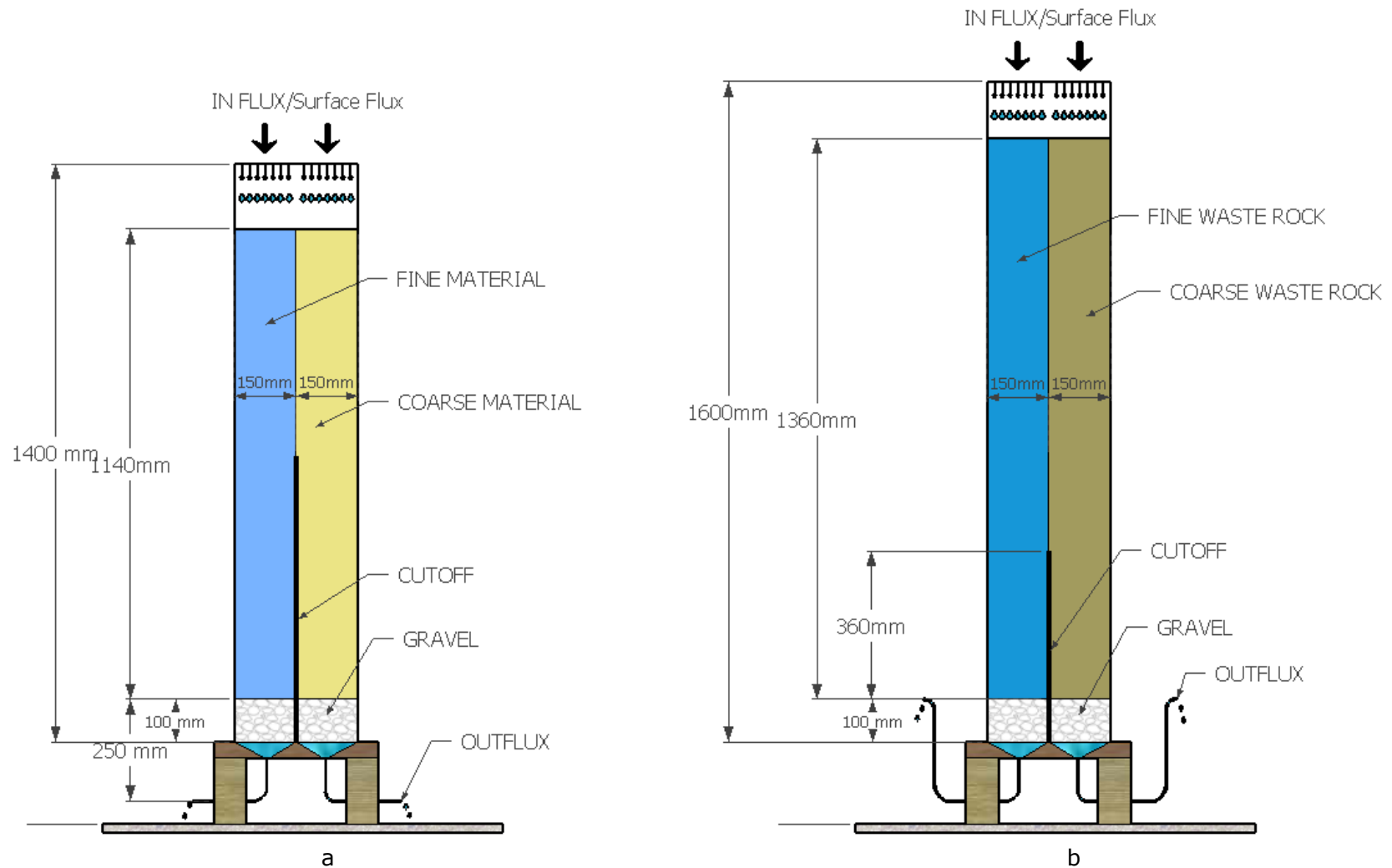


Figure 4.1 Column Test Characteristics Using Sandy Materials (a) and Waste Rock (b), after Newman (1999)

The applied precipitation allowed that each half of the column received half of the total applied flux. The simulated precipitations were intended to evaluate the effect of two flux rates to be above (Flux “a” and “b”) and below (Flux “c” and “d”) the Saturated-Hydraulic-Conductivity (k_{sat}) of the Fine Grain material in Column-1. The discussions in Column 1 will be made in round numbers due to the small variability in the precipitation flux in and for practical purposes; for Flux (a) the precipitations is 1120 mm/day, for Flux (b) is 800 mm/day, for Flux (c) is 440 mm/day, and for Flux (d) is 330 mm/day.

In the experiment of Column-2, the precipitations were calibrated for three different conditions. The highest flux at 445 mm/day (Flux “a”) resulted in the amount of water required to generate a thin film of water at the surface of the column. The other two flux rates (Flux “b” and “c”) were required to be approximately one and two orders of magnitude less than Flux “a”.

4.3.1. Material Characteristics

The two-column simulations use the material properties from the respective column experiment presented by Newman (1999). The characterization of the materials was made according to ASTM standards. From the four materials used in the two-column experiments, only the fine fraction of Column-1 had a long history of previous characterization studies. The characterization made by Wilson (1990) and Herasymuik (1996) served as the bases of Newman’s work for Columns 1 and 2, respectively, as well as the laboratory testing.

The model’s hydraulic properties, such as the soil water characteristic curves (SWCC), were measured using pressure cell tests, and the saturate hydraulic conductivities (k_{sat}) were measured using a constant head permeameter test. Table 4.2 shows the material properties of Column-1.

Table 4.2 Material Properties for Column-1

Property\Material	Medium Silica Sand (SS-Coarse)	Beaver Creek Sand (BCS-Fine)
Porosity	-nm-	0.43
GS	-nm-	2.67
AEV (kPa)	0.7	3.0 – 5.0
k_{sat} (m/s)	1.5×10^{-2}	6.2×10^{-5}
Sat. VWC	0.37	0.4

Table 4.2 (continue) Material Properties for Column-1

Property\Material	Medium Silica Sand (SS-Coarse)	Beaver Creek Sand (BCS-Fine)
mv (1/kPa)⁵	0.0027	0.0027

The model for Column-1 uses the Beaver Creek Sand (BCS) as the fine grain sand. The BCS is a fine to medium Aeolian Clean Sand, poorly sorted with 98% Sand and 2% Silt & Clay, oxidized, and calcareous (Wilson, 1990). The material for the coarse sand in the first column was medium silica sand (SS) poorly graded.

Wilson (1990) established that the k_{sat} for the BCS range is between 3.9×10^{-6} m/s and 8.1×10^{-5} m/s. The hydraulic conductivity curve is estimated using the Fredlund & Xing equation as a function of the Soil Water Characteristic Curve (SWCC) and the saturated hydraulic conductivity (k_{sat}) (Fredlund, et al., 1994 B). Figure 4.2 shows the SWCC and Hydraulic-Conductivity-Curve (HCC) for materials in Column-1. The gray shaded area in the BCS represents the range of variance of k_{sat} . Even though Newman does not report a possible variance with respect to k_{sat} for the SS, the variances can occur and will be discussed further in the thesis.

In the experiment of Column-1, the first two fluxes (Flux "a" and Flux "b") were above the k_{sat} of the fine material; and the last two (Flux "c" and Flux "d") were below the k_{sat} of the fine material to take into account the effect of flux rate in preferential flow. In either case, all flux rates were below the k_{sat} of the coarse material.

The AEV of the SS is 0.8 kPa, much lower than the boundary condition that causes desaturation on the material. This boundary condition enabled the suction at the bottom of the coarse material to predominate because of the residual suction of the gravel material (the SWCC was not measured for this material), as it was the maximum suction that the gravel could exert on the Silica sand, Newman (1999). The fine material, however, did not have any problems as the BCS had an air entry value of 3 to 4 kPa (Newman, 1999).

⁵ The coefficient of compressibility (mv) for positive pore water pressure is assume for the material used in the simulation; the assumption is based on the describe characteristics and typical values.

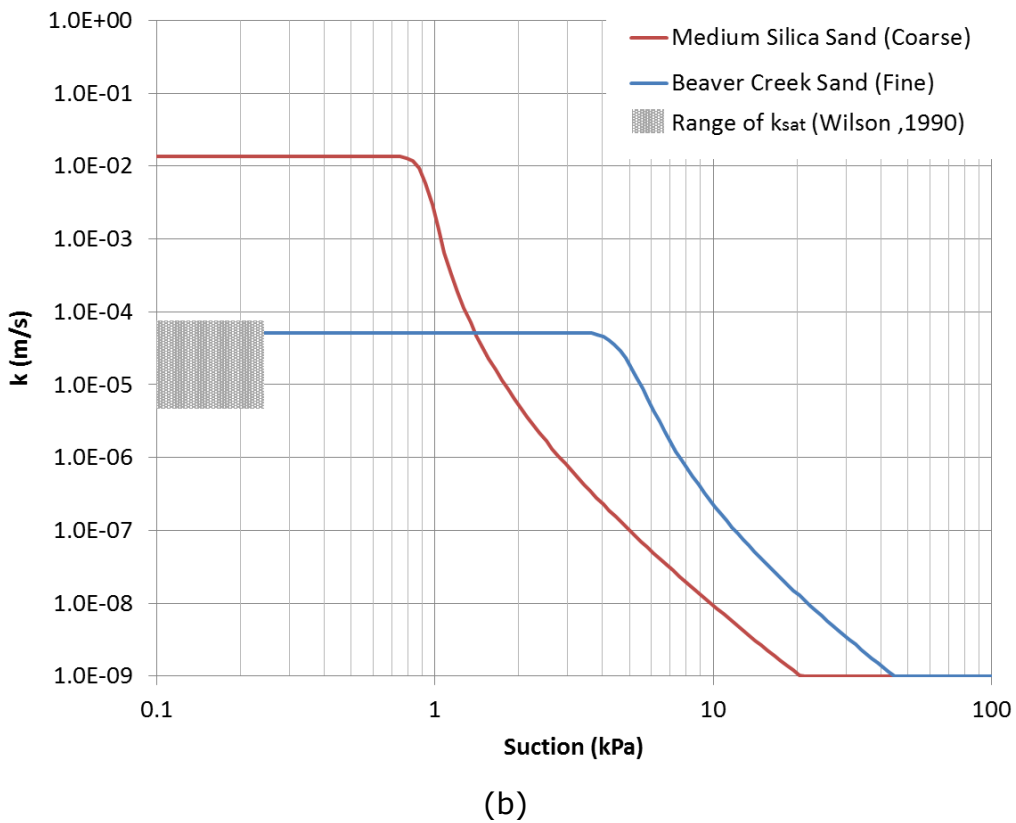
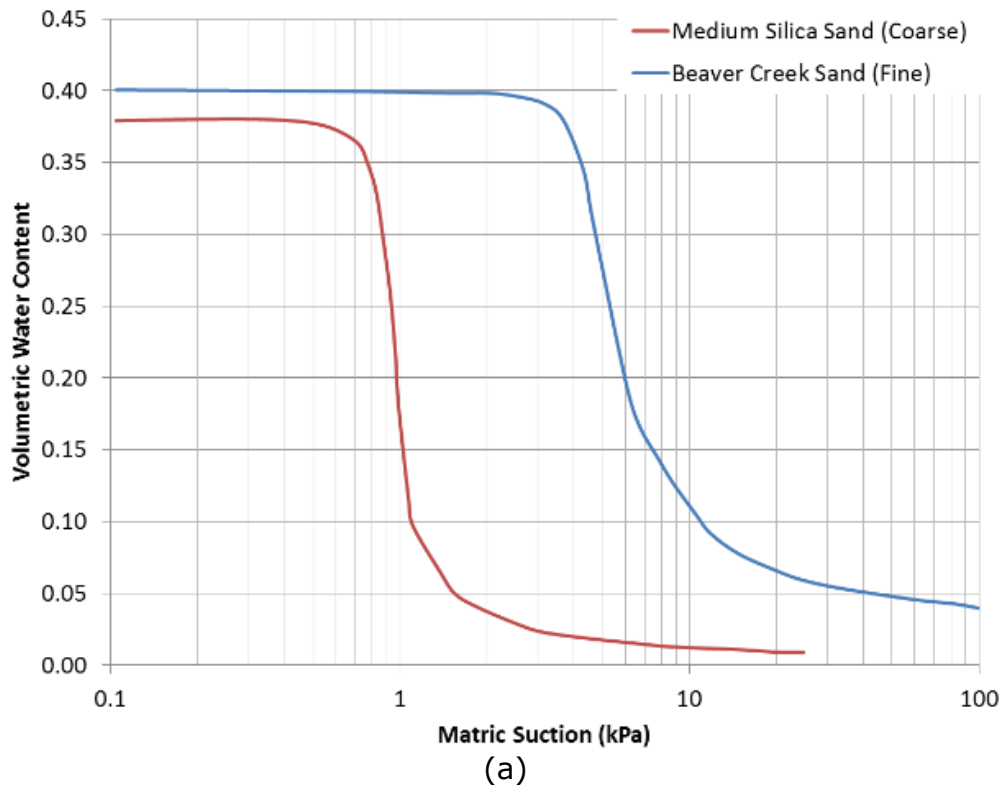


Figure 4.2 SWCC (a) and Hydraulic Conductivity Curve (b) for Materials in Column-1 (Newman, 1999)

In the model for Column-2, the left side corresponds to Fine-waste-rock material (F-WR; denoted TP5GS1 by Herasymuik to test pit 5 and layer 1 within the pit), having more than 50% of particles passing the #4 sieve. The right side of the column is Coarse-waste-rock material (C-WR; denoted TP6GS5 by Herasymuik to test pit 6 and layer 5); it had a range of particles passing the #4 sieve between 30% and 39%.

According to the Grainsize-Distribution-Curve shown in Figure 4.3, the F-WR has a coefficient of uniformity (C_u) equal to 39.3 and a coefficient of curvature (C_c) equal to 1.05, classifying the material as sand with silt (SW-SM) for the fine material in Column- 2. The C-WR has a C_u of 18.4 and a C_c of 1.84 classifying the coarse fraction from Column-2 as coarse gravel (GP). Both materials have a low fine content of less than 5%; for the F-WR the fine fraction has a LL of 17% a PL of 14% and an IP of 3%.

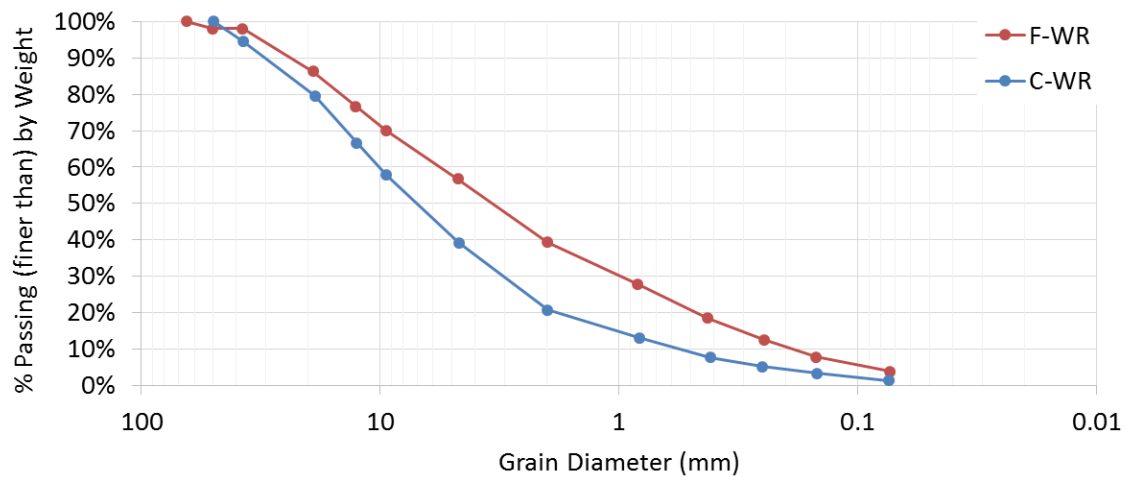


Figure 4.3 Grainsize Distribution Curve (Herasymuik, 1996)

Table 4.3 presents the material properties for the materials used for the second column model. The procedures for classifications were implemented according to ASTM; the saturated hydraulic conductivity was measured using a constant head permeability test.

Table 4.3 Material Properties for Column-2 (Herasymuik, 1996)

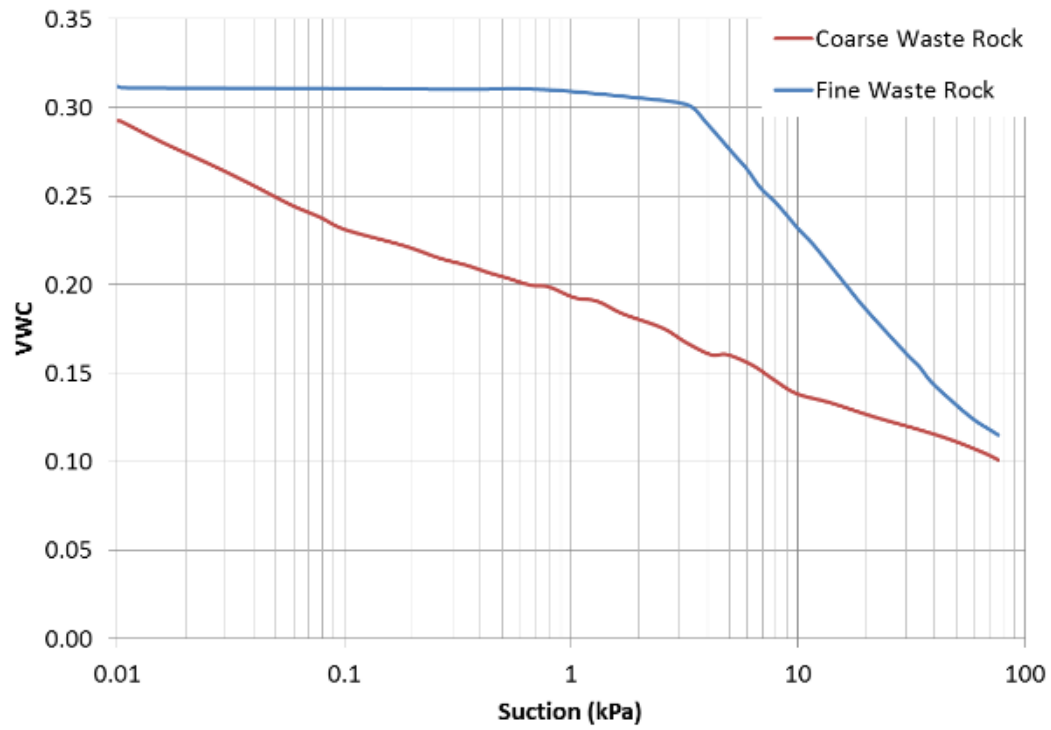
Property\Material	Coarse-waste-rock (C-WR)	Fine-waste-rock (F-WR)
Gravimetric water content	0.37%	0.56%
Porosity	29.4	31.2
Void ratio	0.42	0.45
Dry density (g/cm³)	1.95	2.03

Table 4.3 (continue) Material Properties for Column-2 (Herasymuik, 1996)

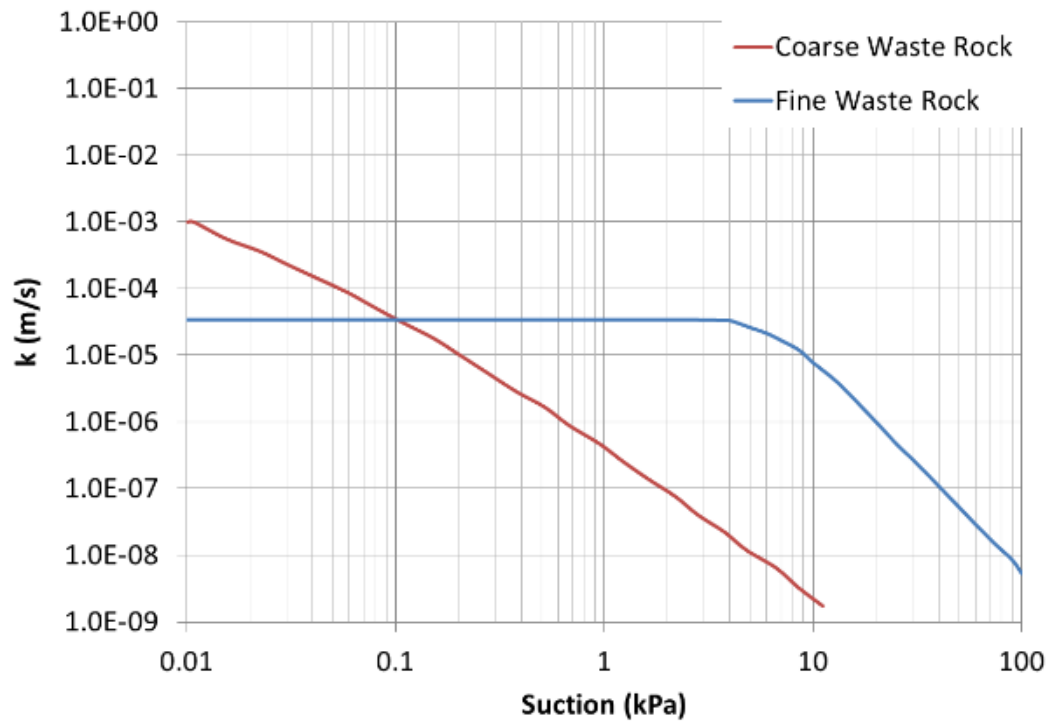
Property\Material	Coarse-waste-rock (C-WR)	Fine-waste-rock (F-WR)
Gs	2.78	2.63
AEV (kPa)	0.03	3.5
k_{sat} (m/s)	1.0x10 ⁻³	3.4x10 ⁻⁵
mv (1/kPa)⁶	2.7x10 ⁻³	9.1x10 ⁻⁶
Sat. VWC	0.29	0.31

The SWCCs were determined using large pressure plate tests that allowed testing a more representative sample that included the coarse fraction. The points for suction vs volumetric water content were plotted using the software CVIEW for best fitting as shown in Figure 4.4 (a); this software uses a nonlinear least-squares regression (Herasymuik, 1996, p. 93); the residual part of the curve was not calculated. Figure 4.4 (b) shows the hydraulic conductivity curve as a regression using Fredlund and Xing (1994 B) equations.

⁶ The coefficient of compressibility (mv) for positive pore water pressure is assumed for the material used in the simulation; the assumption is based on the described characteristics and typical values.



(a)



(b)

Figure 4.4 SWCC (a) and Hydraulic Conductivity Curve (b) for Materials in Column-2 (Herasymuik, 1996)

The simulations of Column-1 and Column-2 assume a minimum hydraulic conductivity (k_{\min}) for all materials of $1 \times 10^{-10} m/s$. This magnitude is reached at the residual suction. The magnitude for k_{\min} allows the simulation to reach suction values without a constant permeability for any of the simulated cases (i.e. the internal suction of the material during the steady state analysis was lower than the residual suction).

4.3.2. Experiment Results

The volumes of discharge from the laboratory experiments from Column-1 and Column-2 were measured for each material. The discharge is calculated as a percentage of the total applied in-flux rate at the top of each column as shown in Figure 4.5.

The measured discharge in Column-1 (Newman, 1999) shows a preferential flow path formed in the fine material for an applied precipitation rate below 450 mm/day (Flux c) with a discharge over 50%. Newman concluded that if the precipitation rate is less than the saturated hydraulic conductivity (k_{sat}) of the fine BCS, then it resulted in the drainage of pores through the coarse SS.

Test 2, Test 3, and Test 4 had a more accurate method than Test 1 to measure the discharge from the column (Newman, 1999). For each test, the water discharging was collected over one minute intervals using graduated cylinders to record the volume to determine the amount of water coming out of each material. The cylinders had a low precision, thus requiring a change of the method to determining the mass of water, Newman (1999).

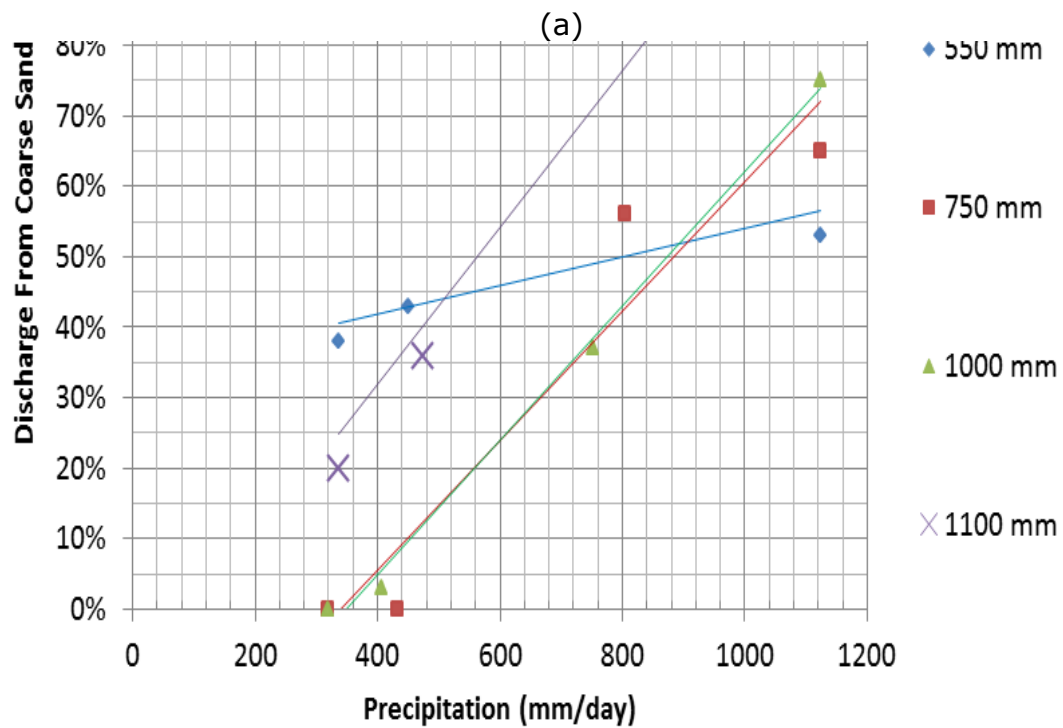
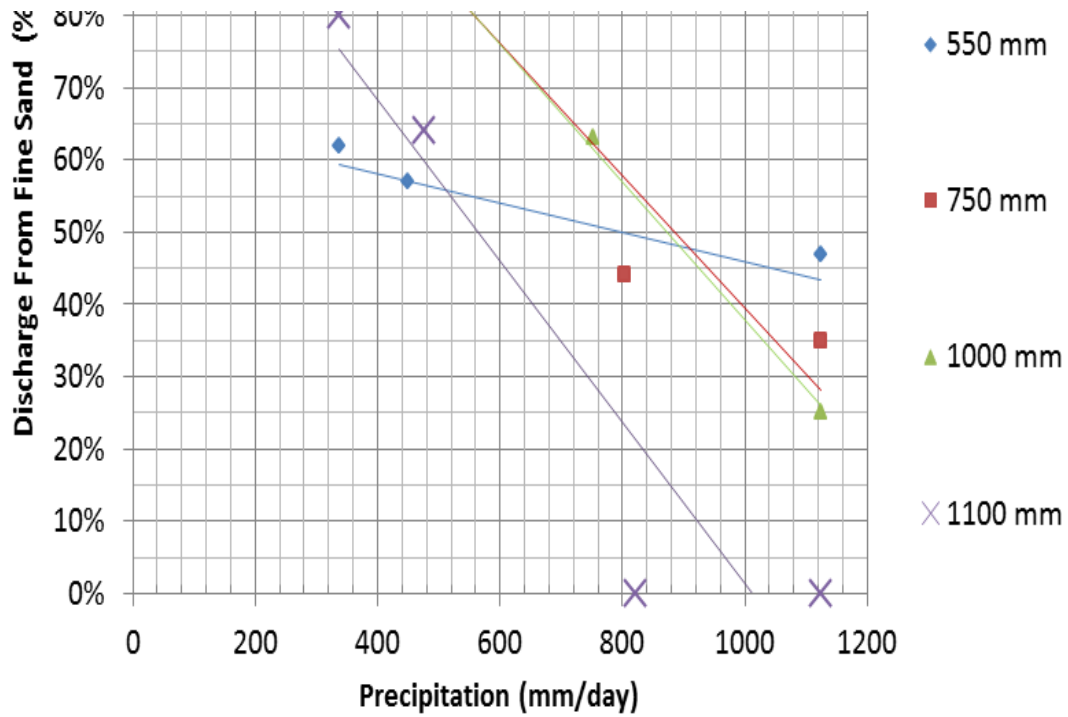


Figure 4.5 Discharge Flow of the Fine (a) And Coarse (b) Material in Column-1 after Newman (1999)

Evaluating waste rock materials, Column-2 resulted in increments of discharge in the fine and reduction in the coarse as the amount of precipitation decreases as

shown in Figure 4.6. Newman concluded that to make the F-WR the preferential flow path, the flow rate was required to be less than 20 mm/day Newman (1999).

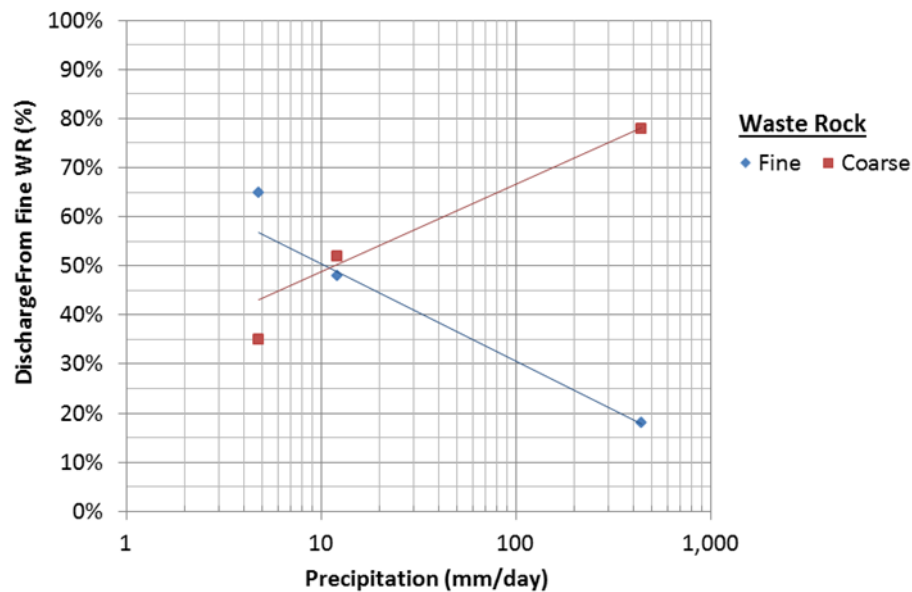


Figure 4.6 Total Discharge for Column-2 after Newman (1999)

4.3.1. Seep/W Simulation Results

Newman simulated Column-1 using a numerical model to identify parameters and mechanisms that governed water flow within the column (Newman, 1999). The model was created using Seep/w Ver. 2.0, while the mesh was composed by square elements with nodes space of 2.0 cm as shown in Figure 4.7. The cut-off was recreated by a one-millimeter gap between the materials for each test.

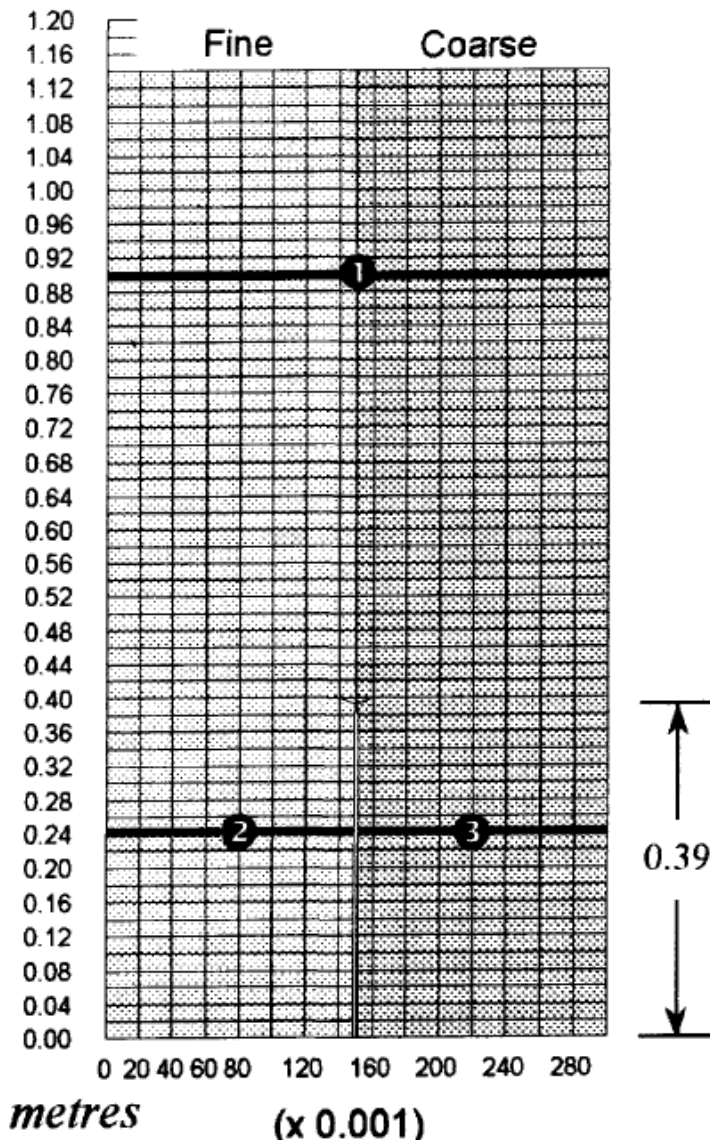


Figure 4.7 Model Mesh with Seep/W Ver. 2.0 by Newman (1999)

Figure 4.8 shows Newman's simulation results using a numerical simulation for a Column-1 with sandy material for a contact length of 550 mm (Test 1), 750 mm (Test 2), 1000 mm (Test 3) and 1100 mm (Test 4). With respect to the laboratory test, the results had variances up to 100% of the discharge at the bottom of the column. Additionally, the simulation required the calibration of k_{sat} , equal to $7.5 \times 10^{-6} \text{ m/s}$ for the fine material (BCS) and $1.48 \times 10^{-2} \text{ m/s}$ for the coarse material (SS). The results, despite being between the ranges established by Wilson (1990) for the BCS, show high contrasting value with respect to the laboratory measurement.

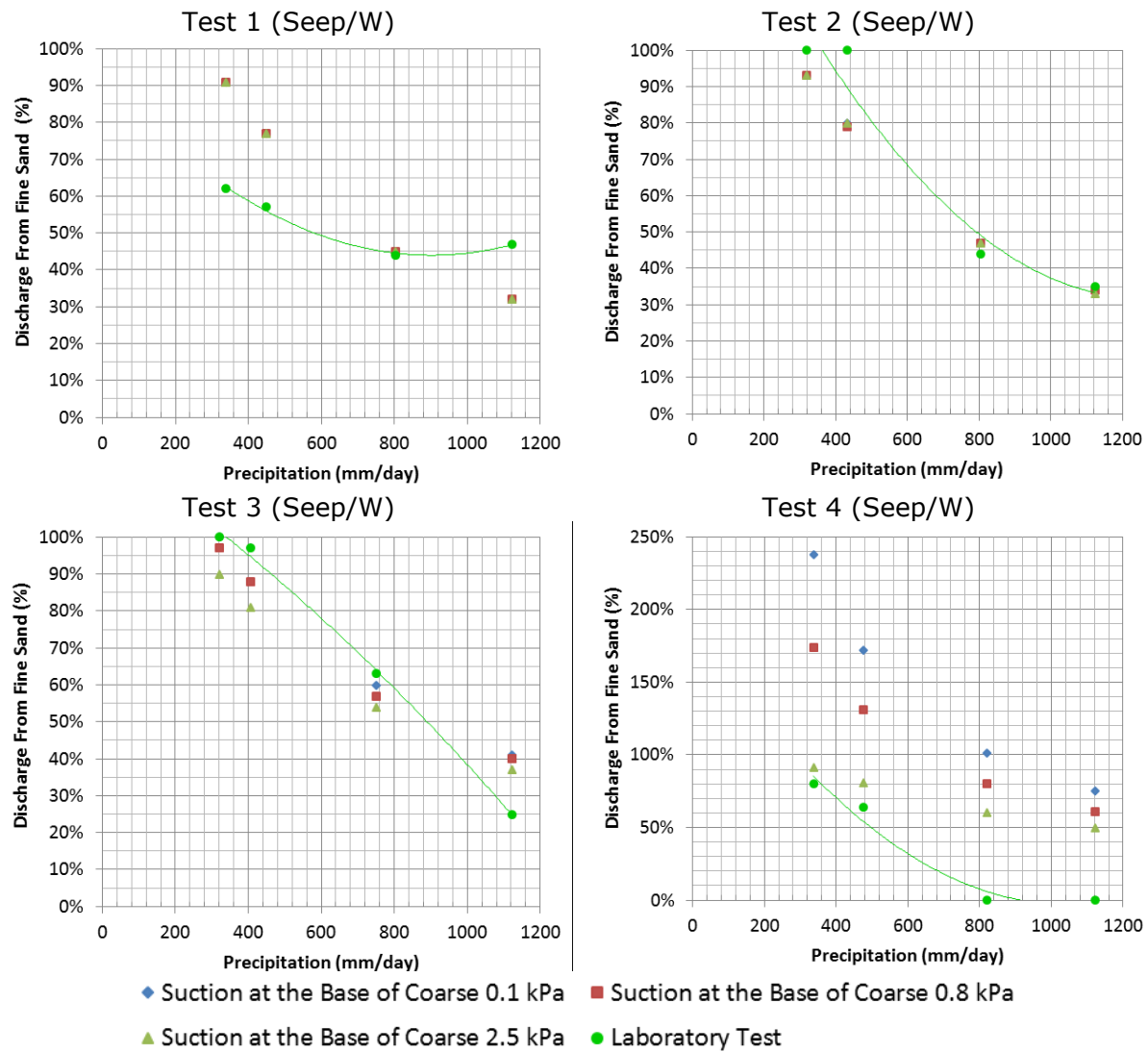


Figure 4.8 Discharge Flow from Fine Material from Seep/W Simulation (Newman, 1999)

Newman (1999) concluded that there is a difference in the stress state conditions between the numerical model and the column experiment. Since the SWCC is depended on the stress state of the material, the analysis through the numerical model only considered a uniform stress state for the entire length of the column. This condition assumes that the material at the base and top of the column has the same void ratio. On the other hand, Newman considered that the measure of the SWCC does not correspond to the same stress state as it was applied to the column, the stress being lower during the measurement of the SWCC. This condition affected the k_{sat} within the column, as the void ratio is sensitive to changes in the stress state and the

k_{sat} is sensitive to the void ratio; the column experiment had a different k_{sat} to that measured from the falling head test.

4.4. NUMERICAL MODEL

The simulation presented by Newman for Column-1 (using Beaver Creek sand and silica sand) had variances with respect to the laboratory test. For the second column using waste rock material, previous simulations were not found through the literature review. The first approached found to simulate waste rock from Golden Sunlight mine was made by Wilson (2003). He proposed to simulate water flow in a transient state using the 2-D Finite element method (FEM) of Seep/W Ver. 3.0 (1995) for a waste rock. Wilson (2003) used the proposed model and characterization of Golden Sunlight mine made by Herasymuik (1996) for the numerical model. The complexity in such a model lead him to simplify the Herasymuik model (Figure 4.9) using the information from the second column test (Newman, 1999).

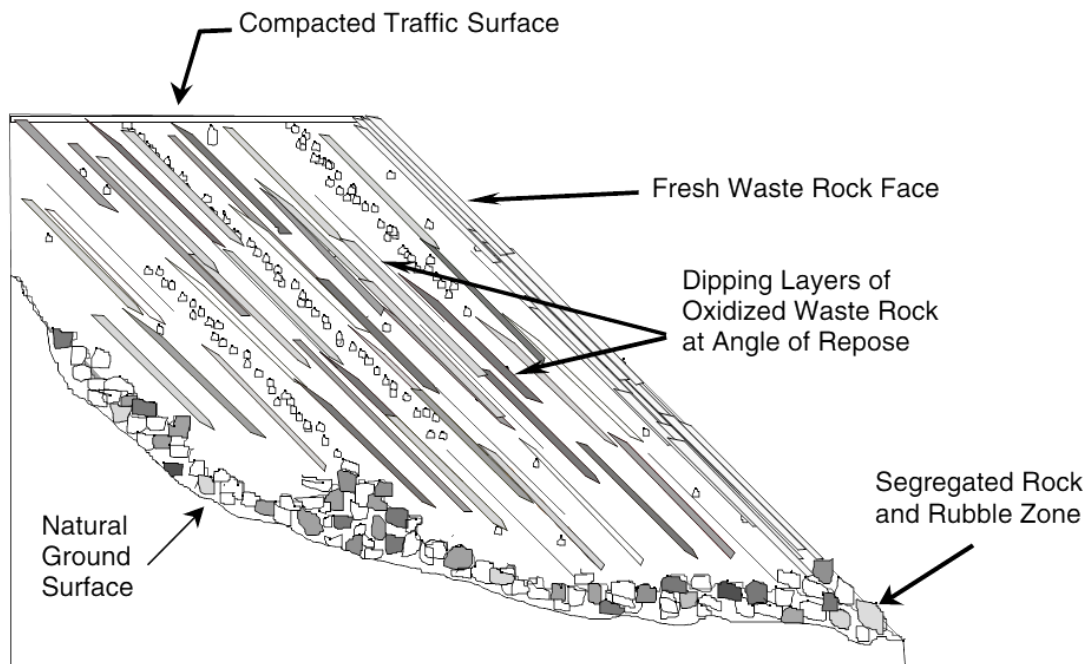


Figure 4.9 Model Proposed By Herasymuik (Herasymuik, 1996)

Finding the convergence of the previous model is a difficult task to achieve, as it requires high computing processing and extremely detailed information on the materials and geometry in order to have an exact convergence. Nonetheless, by considering several assumptions and generalizations, an acceptable convergence can

be found. The following section presents a description for modeling Newman columns using SvFlux.

4.4.1. Modelling Methodology

The simulation results obtained by Newman (Newman, 1999) by recreating the laboratory experiments of Column-1 showed a high divergence with respect to the measured discharge (ranging from 0% to 100%). She reported several difficulties in achieving convergence during the simulations. A methodology was established to overcome these issues.

To recreate the column experiments presented by Newman (1999), a model was created for each experiment. The models were made using the same dimensions from the experiments, as well for the reported properties and boundary conditions. The simulations were carried out using SvFlux Version 7 from Soil Vision Ltd. For each cut-off height in Column-1 a model was made.

The simulations presented in this chapter using SvFlux, initially consisted in recreating the column experiment made by Newman (1999) by applying the same conditions and properties measured in the laboratory. A second set of simulations were made using Newman's calibration for the saturated hydraulic conductivity to compare the Seep/w model to the SvFlux model. Finally, due to the difficulties in convergence of solution and high difference with the results compared to the laboratory measure, a third set of simulations using back analysis was made to improve the correlation between the numerical simulations and the laboratory experiment. As it was modeled by Newman, the simulations with SvFlux in Column-1 were made for suctions of 2.5 kPa, 0.8 kPa, and 0.1 kPa at the base of the coarse material as part of the uncertainty in the coarse boundary condition. Figure 4.10 shows a diagram for the methodology used in the calibration process of Column-1.

- The first set of simulations used a k_{sat} from the falling head tests in the laboratory equal to $6.2 \times 10^{-5} m/s$ for the fine sand (BCS) and $1.48 \times 10^{-2} m/s$ for the coarse sand (SS); the simulations are presented for each of the cases applied to the column test.
- The second set of simulations applied the calibrations presented by Newman using a k_{sat} equal to $7.5 \times 10^{-6} m/s$ for the fine sand and $1.48 \times 10^{-2} m/s$ for the coarse sand. The results showed high variability with respect to the laboratory results, and SvFlux did not correlate well with the simulation using Seep/W. For the second set of analysis,

numerical errors occurred at the lowest cut-off height of 40 mm (Test 4) where the discharge was greater than the precipitation.

- The third set of simulations consisted on back analysis for the k_{sat} of each material, and for the AEV of the fine fraction. The properties are calibrated individually for the four experimental tests using an iterations process by adjusting k_{sat} , and the AEV until the closest correlation with the laboratory results are achieved and before having convergence problems. The change of the k_{sat} and AEV is independent for each material, i.e. if k_{sat} of the fine material is varied, then the k_{sat} of the coarse is kept constant and equal to the value measured in the laboratory test. This iteration process is evaluated for all precipitation rates. The calibration of k_{sat} allows the determination of the sensitivity to small changes in k_{sat} of the simulations results.

To evaluate and compare the correlation between the simulations and the laboratory results, the discharge flow from each simulation is compared with its respective laboratory measure. Additionally, to corroborate any numerical error, a vertical flux line was located at the contact between both materials determining the amount of flow transfer between the materials. Furthermore, for the calibrated simulations, 2D pressure profiles with flux vectors are compared to evaluate the internal effect of change in precipitation and contact length.

The calibration allows the selection of the optimum characteristics (related to material properties and boundary conditions) that correlate best to the laboratory experiment. Finally, the model is run for the different tests to obtain the pressure profile and the discharge comparison.

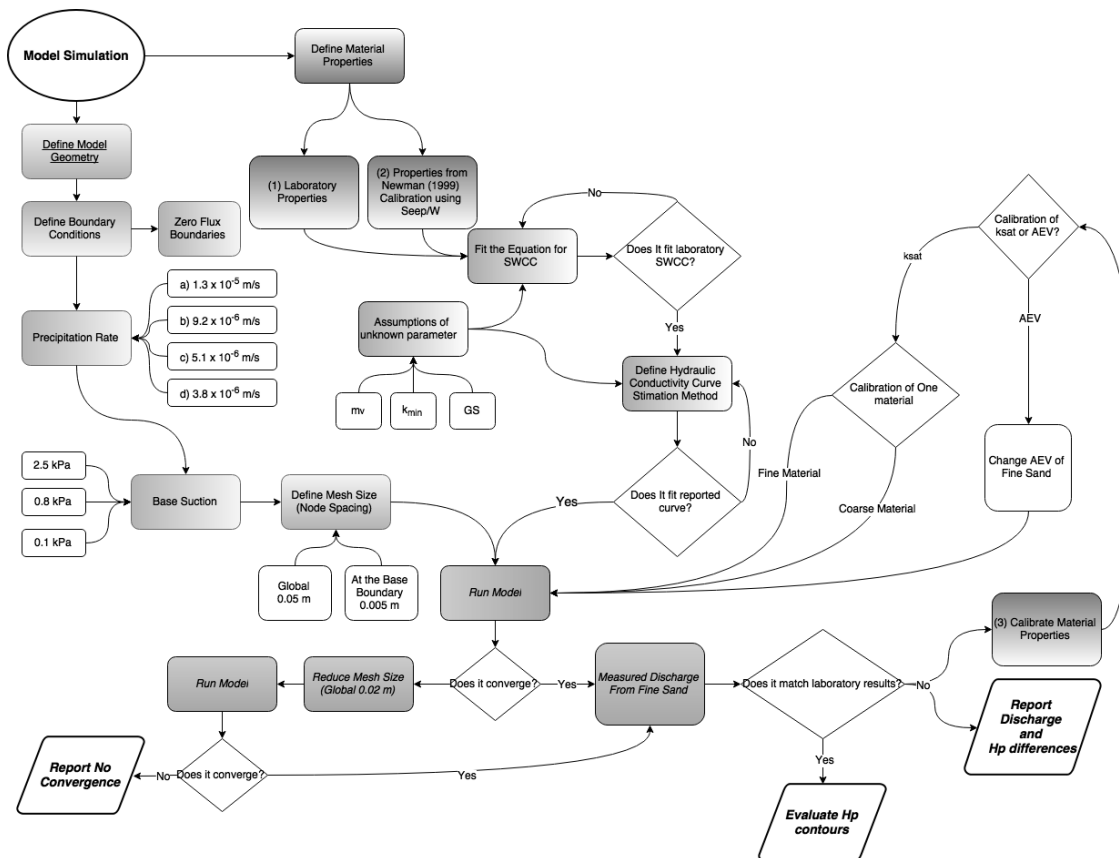


Figure 4.10 Methodology for Column-1

For the evaluation of the second column using waste rock material, the simulation process employs the same methodology as in Column-1, excluding the numerical model comparison, as this column has not been modeled previously. Figure 4.11 shows a diagram for the methodology used in the calibration process of Column-2.

- The first set of simulation uses the properties measured in the laboratory experiments by Herasymuik.
- The second set of simulations consisted in sensitivity analyses for each material k_{sat} in order to improve convergence between the numerical simulation and the laboratory experiment.

To evaluate and compare the correlation between the simulations and the laboratory results, the discharge flow from each simulation is compare with its respective laboratory measure. Additionally, to corroborate any numerical error, a vertical flux line was located at the contact between both materials to determine the amount of flow transfer between the materials. Furthermore, for the calibrated

simulations 2D pressure profiles with flux vectors are compared to evaluate the internal effect of change in precipitation and contact length.

From the calibration are selected the optimum characteristics (related to material properties) that correlate best to the laboratory experiment. Finally, the model is run for the different tests to obtain the pressure profile and the discharge comparison.

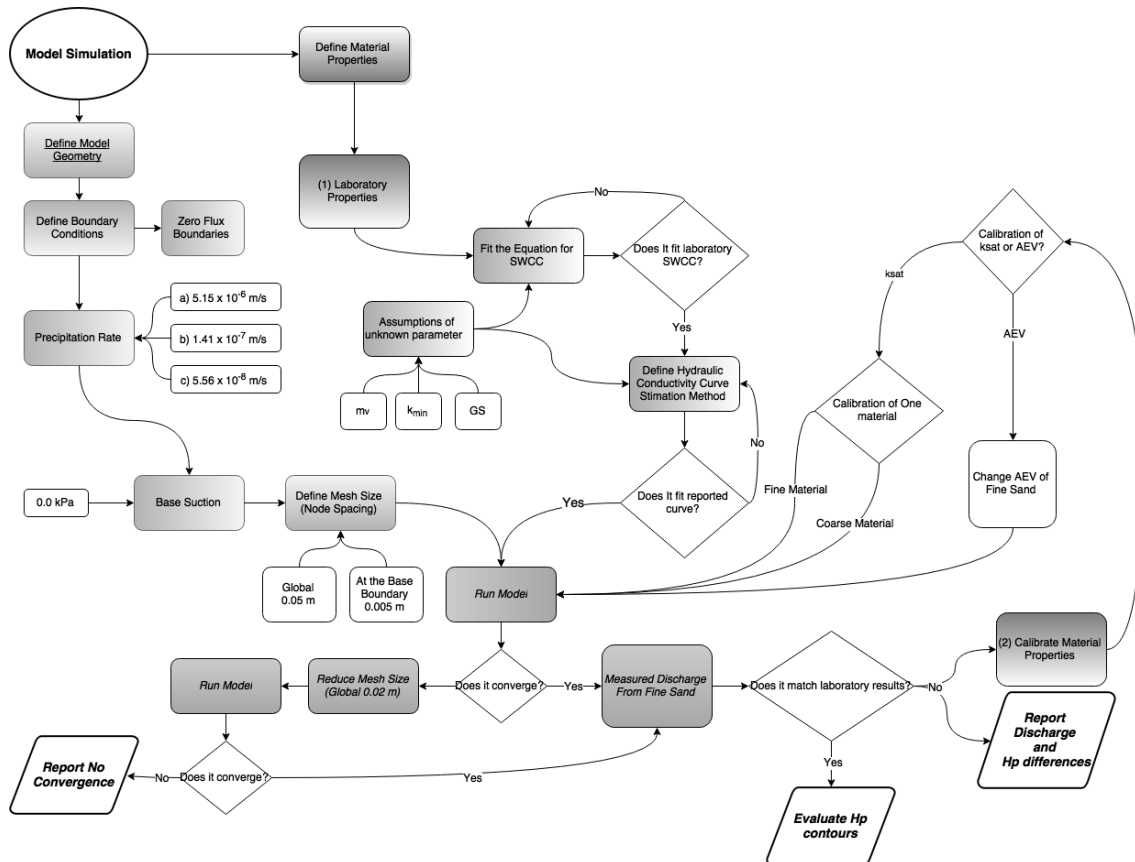


Figure 4.11 Methodology for Column-2

4.4.2. Modeling Assumptions

Certain assumptions are made in order to find reasonable solutions within the scope of the research. It is necessary to balance the computational efforts with the degree of accuracy of the model. The solutions for the PDEs, describing the seepage analysis with SvFlux, have the following assumptions:

- I. The model is in steady state condition.
- II. The materials are in unsaturated conditions and describe Fredlund and Xing (1994 A) equations for the SWCC and the hydraulic conductivity curve.
- III. The materials are continuous, homogeneous, and isotropic for each layer.
- IV. The evaporation and runoff at the top of the column is negligible.
- V. The density of the water leached is 9.8 kN/m^3 and a viscosity of 0.001 kg/m-s .
- VI. There are no effects on water pressure due to changes in temperature.
- VII. The effect of the acrylic walls on water flow is negligible.

4.4.3. Theory Adopted By the Numerical Integration for A Column Layered System

The simulation through numerical models recreates the conditions and results of the column experiments made by Newman. The models are made using commercially available software called SvFlux Version 7.0 from SoilVision Ltd. The software uses FlexPDA to solve Partial Differential Equations (PDE's) that describe water flow through the soil. The model runs under steady state conditions, as it was established in the column tests by Newman.

The following PDE governs water flow for a 2-D model, under steady state and no evaporation conditions, and for a heterogeneous, anisotropic, saturated-unsaturated soil.

$$\frac{\partial}{\partial x} \left[k_x^w \frac{\partial h}{\partial x} \right] + \frac{\partial}{\partial y} \left[k_y^w \frac{\partial h}{\partial y} \right] = 0$$

Where:

x,y= components on the horizontal and vertical direction, respectively.

k_i^w = hydraulic conductivity in the i-direction, m/s.

h = hydraulic head, m.

The PDE is derived by preserving the mass balance principle, and considering no volume storage is allowed due to the steady state condition. In other words, the amount of water coming into the system has to be equal to the amount of water coming out. For a steady state condition, it is assumed that there is no volume change in the material and the total stress is constant.

The model also satisfies Darcy's Law to describe the movement of flow for liquid water; the driving force is the change or the gradient in the Hydraulic Head (h). The generalized expression of Darcy's law for a saturated and unsaturated soil is expressed as (SoilVision Systems Ltd., 2012):

$$v_i^w = -k_i^w(\Psi) \frac{\partial h}{\partial i}$$

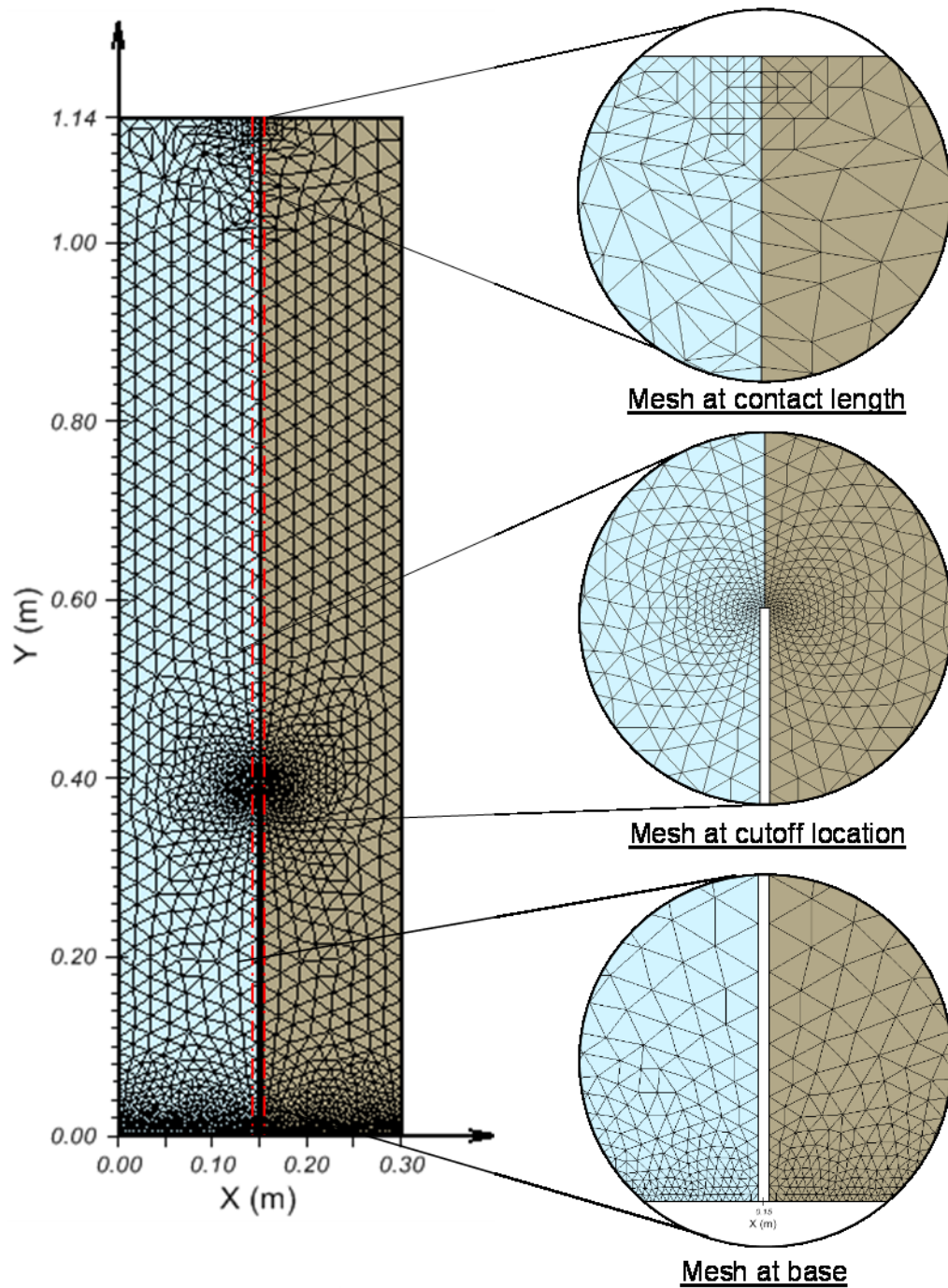
Where:

v_i^w = water flow rate in the i-direction.

$k_i^w(\Psi)$ = hydraulic conductivity in the i-direction as a function of the matric suction (Ψ).

h = hydraulic head, m.

The control errors for the dependent variables (for the column model, the variable is the total head) in accuracy and spatial accuracy (i.e. error limits for the solution) in each simulation are kept equal to 0.002 as suggested by the software manual for 2D models. In addition, the solution is found through a quadratic (second order) interpolation of the finite elements. The second order interpolation consists in a subdivision of the domain in triangular elements composed of six nodes. The nodes contain the information of the domain; they are spatially located on the vectors and the center of the sides of the element. Figure 4.12 illustrates the mesh generation and automatic refinement made at the vertical contact between the coarse and fine material, and the cut-off gap.



The numerical integration was done in the software SvFlux. The software comes with an automatic mesh generation and refinement algorithms starting from an initial

element size; the refinement finds a fast and precise convergence solution (SoilVision Systems Ltd., 2012). The simulation made during the analysis of Column-1 and Column-2 uses an initial mesh formed of triangular elements with nodes spaced at a maximum of 5.0 cm; at the base the mesh is refined for a maximum space between nodes of 0.5 cm. The model's geometry is set to the same scale as the laboratory experiment with a gap of 0.4 cm to recreate the cut-off between the materials. The cut-off was established for the four specific heights in Column-1 and for the one in Column-2. Additionally in Column-2, two feature lines are placed at 0.5 cm and 7.5 cm offset from the center of the column to evaluate the change in pressure with depth.

For steady state conditions, the model runs in a two stages analysis. First, the software solves the model in saturated conditions in order to establish initial conditions (i.e. head pressure distribution); for the second stage, the calculated solution is in unsaturated conditions. The calibration of the unsaturated properties of the materials, Saturated-Hydraulic-Conductivity (k_{sat}) and Air-Entry-Value (AEV), is made through a multi stage analysis, which consists in applying a deterministic range of values for k_{sat} and AEV for each case.

4.4.4. Model Boundary Conditions

The two-column models were built recreating similar boundary conditions as those established in the laboratory experiments. The case of the columns and cut-off were made of acrylic sheet with seals at the joints to restrain any leakage or infiltration. The model considers the side external boundaries, as well as the boundaries that recreate the cut-off as Zero-Flux boundaries.

At the top of the columns, the precipitation is applied to each half of the column. The model uses a climatic boundary condition to apply a constant precipitation flux, evenly along the top boundary in each material. At the base of the column, a drainage system was installed to each side of the column. The location of the outlet with respect to the base of the materials tested generated a negative pressure. The pressure at the base of the columns is set using pressure head boundary conditions.

In Column-1 the out-flux tubes were placed 0.25 m below the base of the materials, creating a suction of 2.5 kPa. In order to overcome the uncertainty of suction conditions generated with the gravel at the bottom of the coarse material, Newman proposed a sensitivity analysis to determine the effective suction that was in this material. The values used for the simulation are as follows:

- 2.5 kPa is the applied suction by the outlets in the laboratory experiment;

- 0.8 kPa corresponds to the AEV of the coarse material; and
- 0.1 kPa corresponds to a suction value below the AEV of the coarse material. Newman assumed this value to be residual suction of the gravel that controlled the desaturation process in the coarse side of the column.

In Column-2 the outlet tubes were placed at the same elevation of the base of the waste material, creating a boundary condition of 0.0 kPa of suction. Although the C-WR had an extremely low AEV, it controlled the desaturation process, as it was higher than the boundary condition generated by the outlets.

4.5. WATER FLOW SIMULATION RESULTS

This section presents the results from the simulation to recreate water flow in the two column experiments. The data shows the results of the numerical simulation from the experiments by Newman (1999). The results presented include:

1. Simulation of Column-1 using the laboratory properties; the calibration conditions from Seep/W by Newman; the calibration the Saturated-Hydraulic-Conductivity and Air-Entry-Value of the materials; and the lateral water flow between the materials
2. Simulation of Column-2 using the laboratory properties; the calibration from the Saturated-Hydraulic-Conductivity and Air-Entry-Value of the materials; and the lateral water flow between the materials
3. Pressure profiles along the center of the columns.

A short description and highlights from the result are provided after each set of results.

4.5.1. Water Flow in Sandy Material

The simulations of Column-1 consist of Fine Sand (i.e. BCS) and Coarse Sand (i.e. SS), under four precipitation rates and three contact lengths. The results are normalized by comparing in all cases the amount of flow discharging out of the BCS; the discharge is calculated and compared against the laboratory measures.

The results are grouped in the following manner: the first group relates the simulations *applying the properties and boundary conditions established during the laboratory experiment*. The second group relates the simulations *applying the properties determined by Newman (1999) using Seep/W and boundary conditions*

established during the laboratory experiment. The third group of result presents the *optimal correlation between the numerical simulation and laboratory* measures by changing k_{sat} of the materials.

All results also show the sensitivity analysis for changes in suction at the base of the SS. The simulations are carried out keeping a constant suction of 2.5 kPa for the BCS and varying the suction to 2.5 kPa, 0.8 kPa and 0.1 kPa for the SS.

4.5.1.1. SIMULATION USING LABORATORY MEASURED PROPERTIES

The results from the simulations using the parameters from the laboratory experiment (i.e. $k_{sat} = 6.2 \times 10^{-5}$ m/s for the BCS and 1.48×10^{-2} m/s for SS) are shown in Figure 4.13. The figure shows the results for each contact length, Test 1 (550 mm), Test 2 (750 mm), Test 3 (1000 mm), and Test 4 (1100 mm). Each graph relates the percentage of water discharge (i.e. discharge water at the base) from the BCS to the respective laboratory result in each suction case.

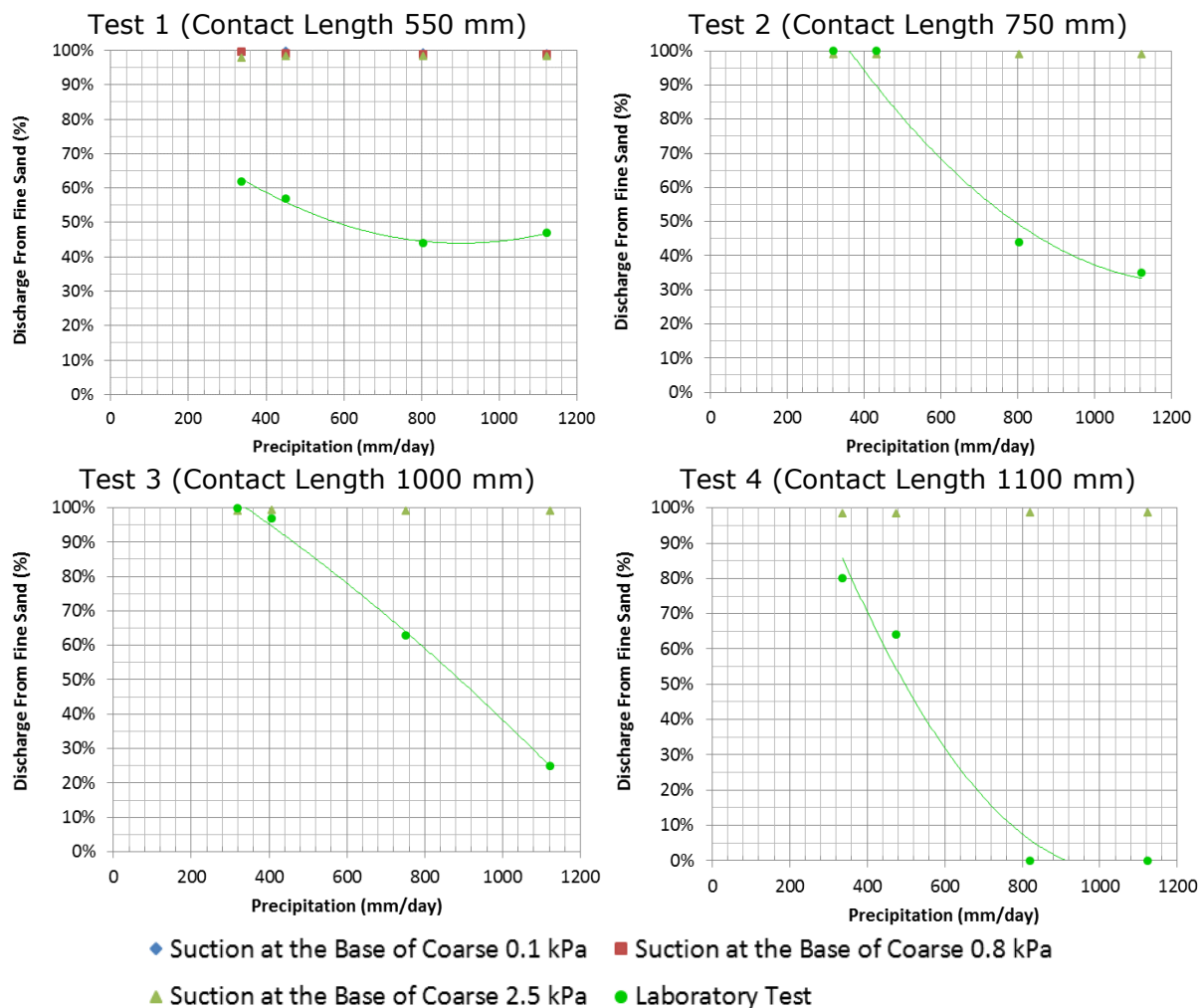


Figure 4.13 Discharge Flow from Fine Material Using the Laboratory k_{sat}

The results from the simulations using the configurations established in the column experiment do not correlate properly with the laboratory results. The increase in precipitation does not show a decrease in discharge from the fine sand as it is shown in the experiment where the preferential flow is changing from fine to coarse at precipitations greater than 800 mm/day.

The sensitivity analysis to evaluate the discharge on the coarse sand by changing suction at the base of the right side of Column-1 does not generate improvement in the correlation. Furthermore, Test 3 and 4 show fluxes over 100% as suction decreases and a gradient is formed between the bases of both materials. The error relates to a numerical equilibrium that the system must satisfy to generate the suction at the base. The SvFlux then attempts to satisfy the defined boundary conditions at the base that there is a water source from coarse sand that flows water into the column and transfers to the fine sand at the top of the cut-off. The effect of suction at the base vanished as the contact length decreases. Figure 4.14 shows the profile on Column-1 for tests 2 and 4 with details of the top of the cut-off.

The right side of Figure 4.14 (Test 4) shows water flow (purple and blue vectors) from the base of the coarse sand over the top of the cut-off into the fine sand due to a pressure gradient formed at the base between the two materials. This flow occurs due to the software limitation to define a constant head pressure and zero flux in i-direction for the same boundary, thus resulting in the increment of total flux in the system as the model assumes a water source at the base of the column.

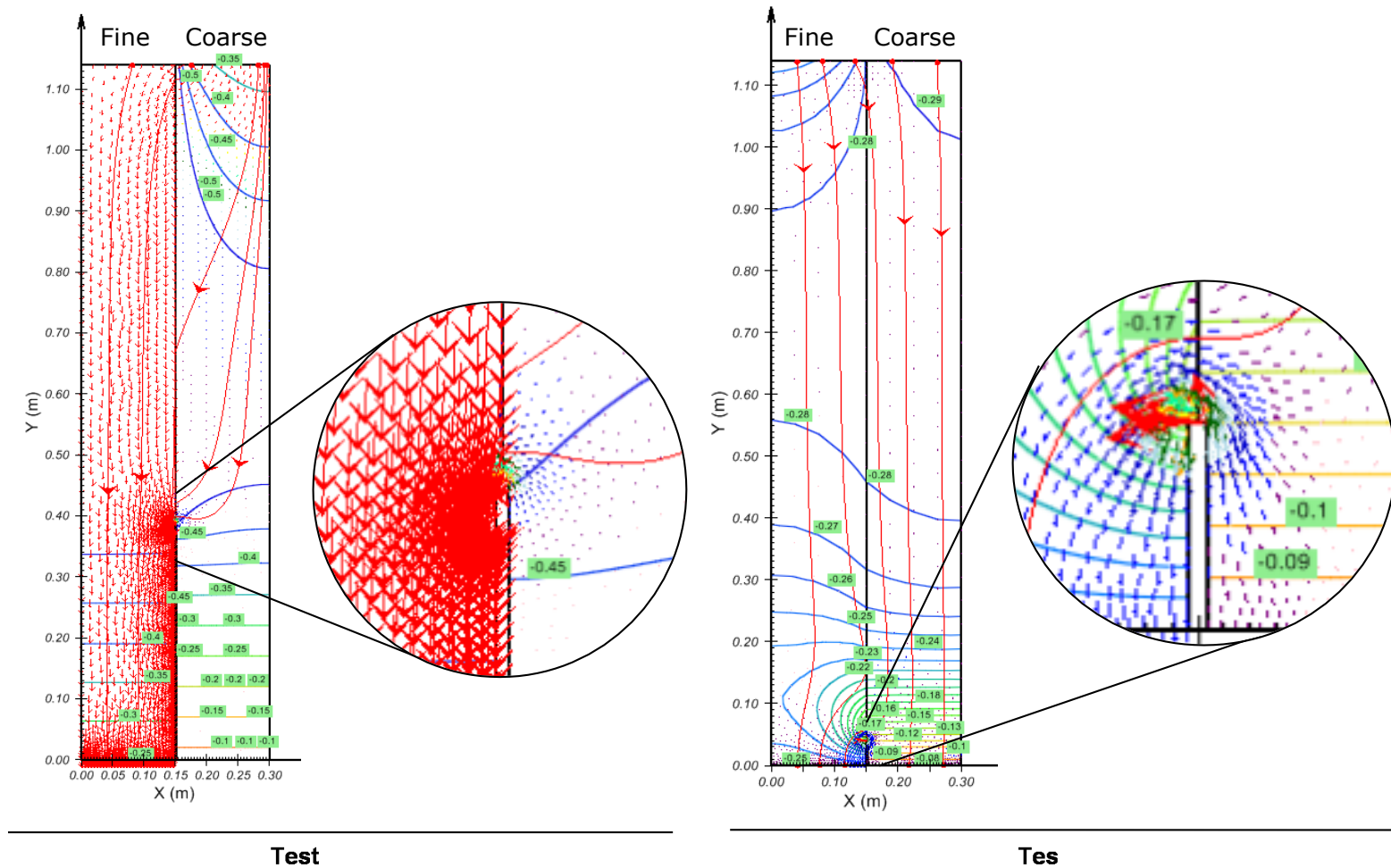


Figure 4.14 Matric Suction and Flux Vectors for Test 2 and 4 Under 450 mm/day (Flux c) Using A Base Suction of 0.8 kPa on the Coarse and 2.5 kPa on the Fine

As the objective to this study is limited to simulating the use of SvFlux, the correction in the simulation is made by subtracting from the amount of flow out of the fine. Figure 4.15 shows the results for Test 3 and Test 4 after applying a correction to the discharge on the fine sand.

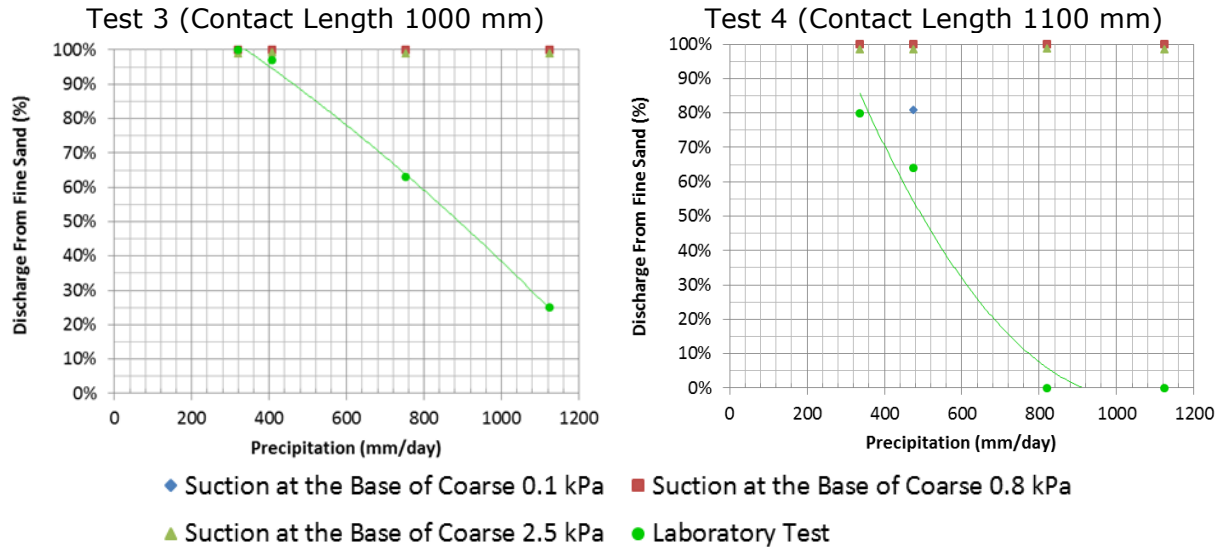


Figure 4.15 Corrected Discharge Flow from Fine Material Using the Laboratory k_{sat} for Test 3 and Test 4

The correction shows the total discharge being less than 100%. Nonetheless, the correction does not improve the correlation between the simulation and the laboratory results.

The simulation conditions resulted in an overestimation of water discharge from the fine material for all the cases when using the classification and characterization of the material described by Lori Newman for the Column experiment using BCS (i.e. Fine Sand) and SS (i.e. Coarse Sand). The average overestimation on the discharge is approximately 40% for all cases.

4.5.1.2. SIMULATION USING NEWMAN'S CALIBRATED PARAMETERS

Newman calibrated the model by changing only the k_{sat} of the fine sand (BCS). The properties in the SS were constant and equal to the laboratory measurement. The calibration simulations resulted in k_{sat} equal to $7.5 \times 10^{-6} m/s$; this is almost one order of magnitude lower than the laboratory measurement (equal to $6.2 \times 10^{-5} m/s$).

The results from the simulations using the parameters from the Newman's numerical calibration (i.e. $k_{sat} = 7.5 \times 10^{-6} m/s$ for the fine sand and $1.48 \times 10^{-2} m/s$ for the coarse sand) are shown in Figure 4.16. The figure shows the results for each contact length, Test 1 (550

mm), Test 2 (750 mm), Test 3 (1000 mm), and Test 4 (1100 mm). Each graph relates the percentage of water discharge (i.e. discharge water at the base) from the BCS to the respective laboratory result in each suction case.

The simulation that focused on the lowering of the k_{sat} of the fine sand shows a decrease of only 5% for Test 1 and Test 2. At Test 4 with the lowest precipitation and a suction of 0.1 kPa, the resulting discharge was almost 60%. This single result, despite having a 40% decrease due to the change in suction, could be related to the numerical instability that the software produces when attempting to satisfy the base boundary conditions.

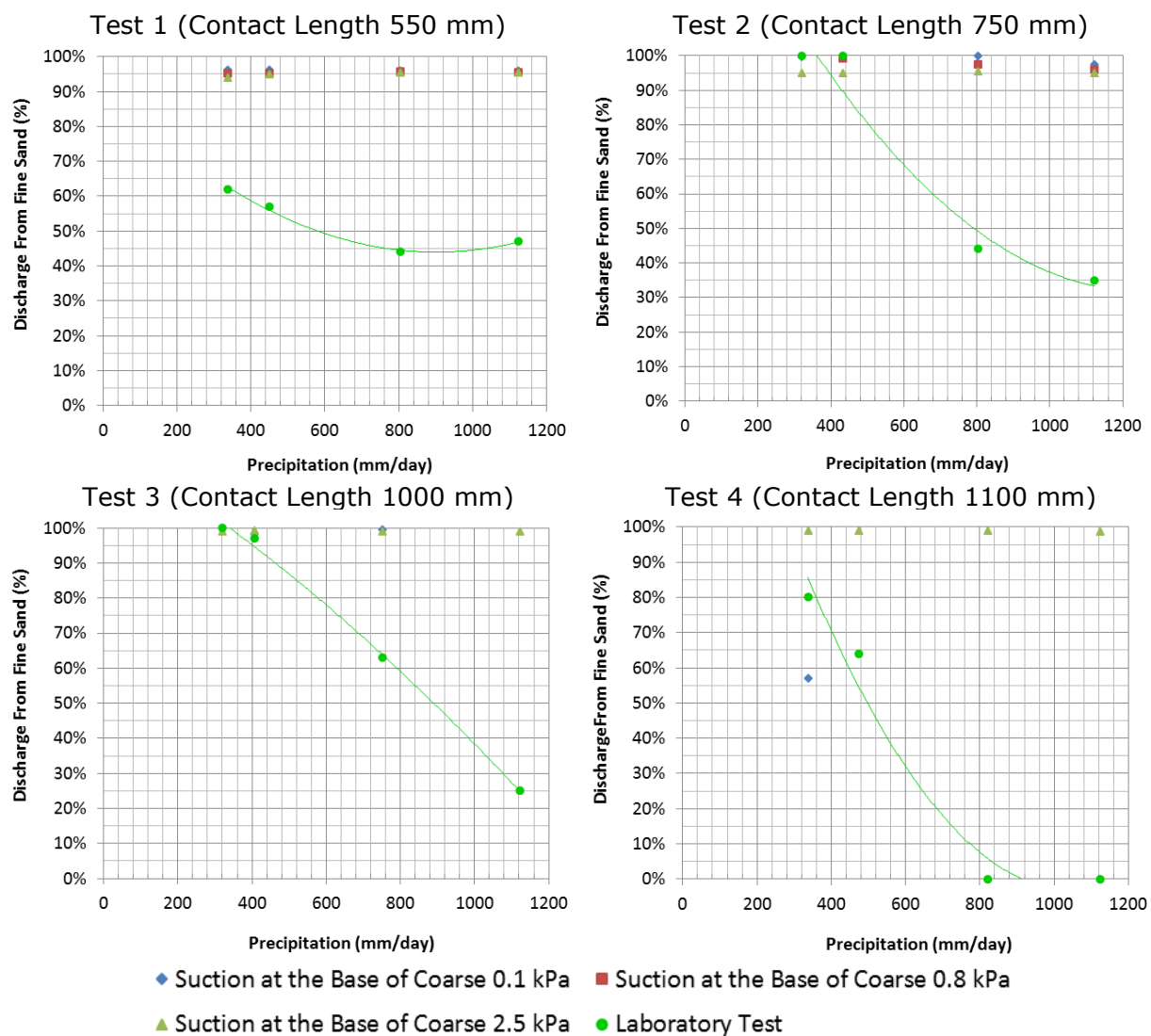


Figure 4.16 Discharge Flow from Fine Material Using k_{sat} From Calibrated Newman Simulation

Overall, the calibration proposed by Newman for the k_{sat} of the BCS does not improve the correlation of the simulations and the laboratory experiment. However, the problem in the correlation is probably related to the characteristics of the properties of the materials. The assembly of the materials in the column experiment can vary significantly from the characteristics of the permeability tests or the temple cell tests, which define the main properties that control water flow in unsaturated systems.

4.5.1.3. CALIBRATION OF COLUMN-1

The previous two simulations overestimate the discharge from the fine sand (BCS) with respect to the measures from the experiment. A back analysis of the material properties in the column model can improve the correlation to have a lower error (less than 10% difference to the laboratory measures). The Saturated Hydraulic Conductivity (k_{sat}) and the Air-Entry-Value (AEV) are two fundamental parameters that influence water flow in unsaturated conditions. These two parameters influence the estimation of the Hydraulic Conductivity Curve (HCC), and control the maximum permeability at saturation and the start of des-saturation in the materials, in other words, the point at which unsaturated water flow occurs.

The following results are limited to the influence in changes of the k_{sat} and AEV to achieve a correlation between the simulations and the laboratory experiment.

4.5.1.3.1. Sensitivity to Changes in k_{sat} for Beaver Creek Sand

The results from the simulations calibrating k_{sat} on the Beaver Creek sand (keeping $k_{sat} = 1.48 \times 10^{-2}$ m/s for the coarse sand) are shown in Figure 4.17. The figure relates the percentage of discharge (i.e. discharge water at the base) from the Beaver Creek sand at each suction case to the respective laboratory result.

The calibrations of the k_{sat} of the BCS increases the correlation of the discharge from the numerical simulation in Column-1, with respect to the simulations presented in section 4.5.1.1 and 4.5.1.2. Figure 4.17 shows preferential flow paths for the coarse sand (SS) at precipitation above 800 mm/day and for the fine sand (BCS) at precipitations below 800 mm/day in all tests. The average error with respect to the laboratory results are less than 7% for all cases. The effect of changing the suction value in the discharge is too low, resulting in an overlaying of the results for a base suction of 2.5 kPa, 0.8 kPa and 0.1 kPa from the base of the coarse sand.

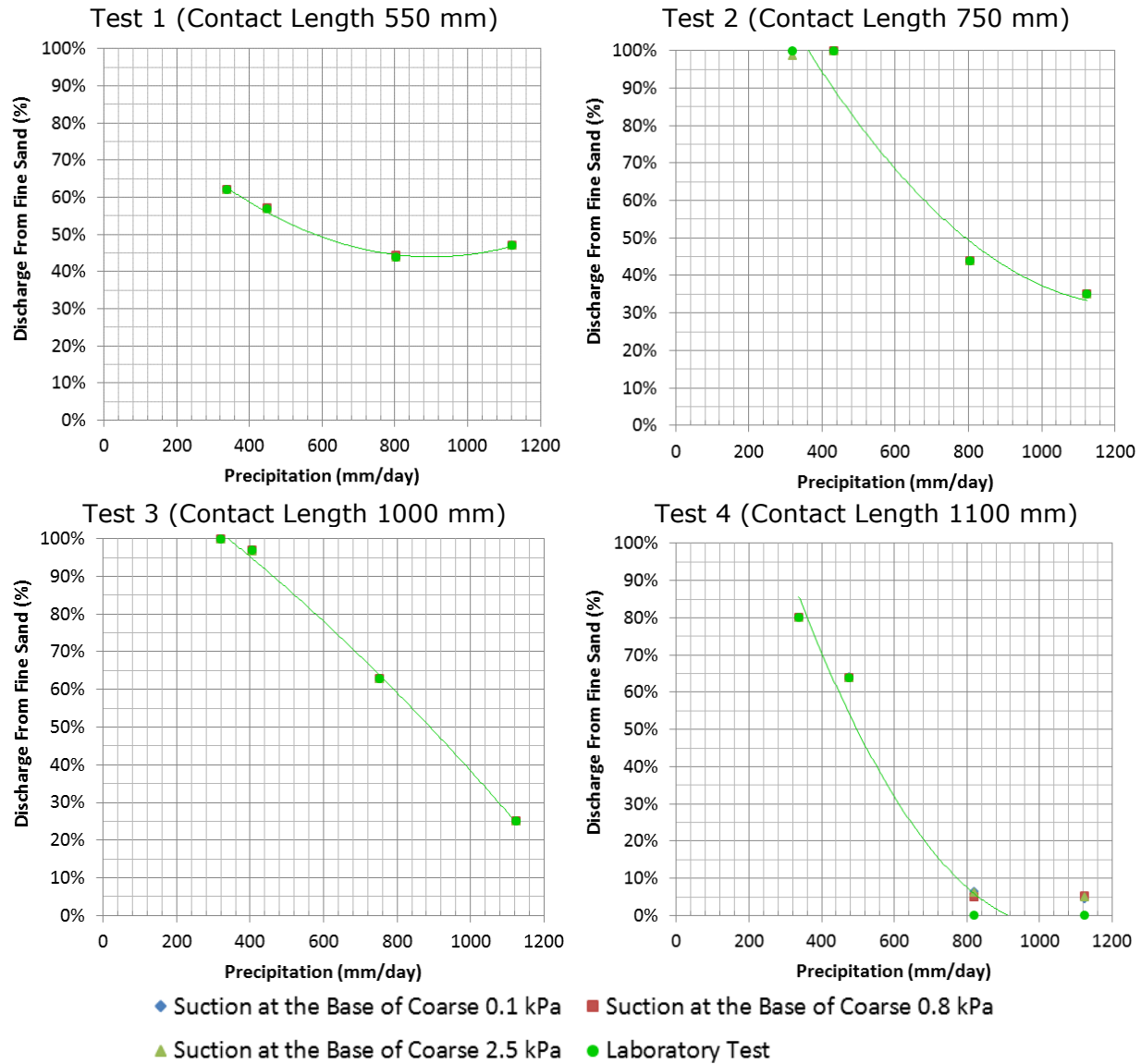


Figure 4.17 Discharge Flow from Fine Material by Calibrating k_{sat} on the Fine Sand

The highest divergence is for Test 4 (between 1% and 6% of the measured discharge) for fluxes above 440 mm/day. This increment error in Test 4 is related to the conditions explained previously where a gradient is formed between the two materials. The error found in the numerical simulations could not be solved by adjusting the k_{sat} of the fine sand; as k_{sat} became smaller in every iteration, the simulation had convergence difficulties. The improvement in convergence of the model was achieved through the calibration of k_{sat} ; however, the calibration does not result in a single value for the permeability. In other words, to achieve such high level of convergence, each case analysis had to be calibrated, resulting in multiple values for the same parameter. Nonetheless, the variance is small, in

the order of 10^{-10} ; however, this variance occurs as the range of values is in the order of 10^{-6} . A detail explanation of the calibration process of the BCS appears in Appendix A.

The calibration of each test required a particular calibration of the saturated hydraulic conductivity for the BCS, for each precipitation rate an average value is calculated with respect to the four tests; e.g. for a precipitation of 1120 mm/day (Flux a) the k_{sat} of the BCS was calibrated for the four contact lengths, this calibration resulted in slight variations of the k_{sat} with respect to the precipitation. **Figure 4.18** presents the average k_{sat} with respect to the different precipitation conditions with an error of less than 10%. The graph shows the average k_{sat} relation with the laboratory measure and range value established by Wilson (1990).

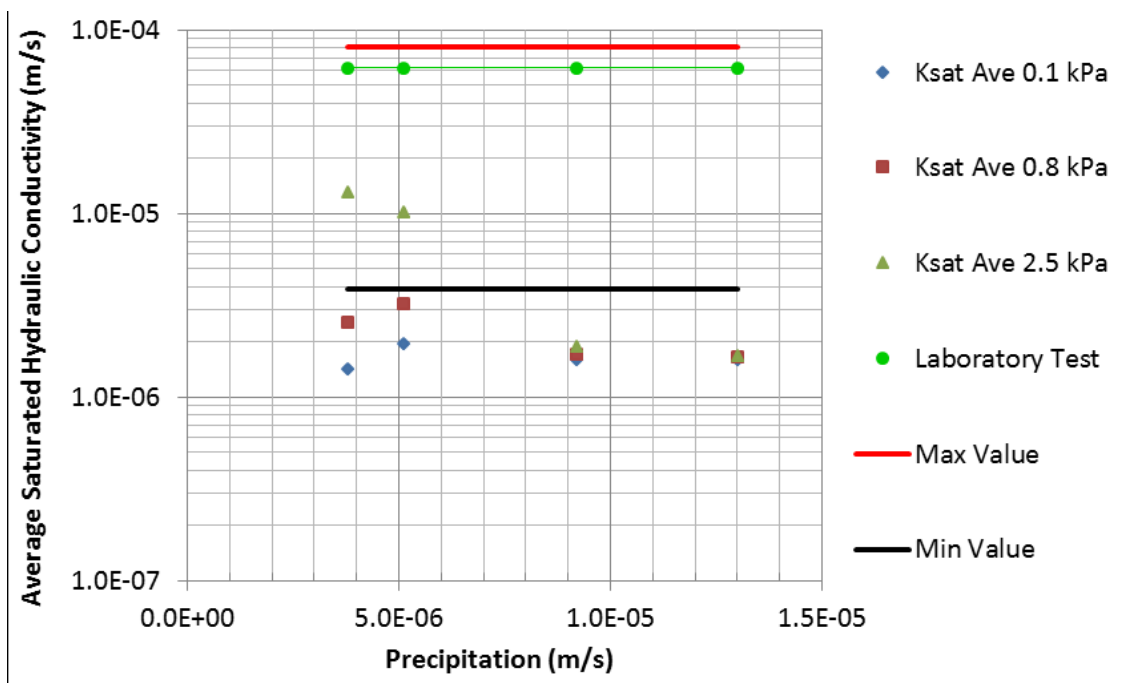


Figure 4.18 Change in k_{sat} with the Precipitation from Fine Sand Calibration to give a discharge within 10% difference using a Base Suction in the coarse of 0.1, 0.8, and 2.5 kPa

The sensitivity analysis of the k_{sat} for most cases shows that the model requires a value below the $3.9 \times 10^{-6} m/s$ to have significant effects on the preferential flow path. The value of k_{sat} in the BCS in the column experiment could be between $1.4 \times 10^{-6} m/s$ and $2.4 \times 10^{-6} m/s$. The level of accuracy available to measure k_{sat} in the field or in the laboratory is much lower with respect to the precision of k_{sat} from numerical modeling and back analysis. These differences lead us to consider that high precision in the numerical model is negligible due to the small scale. However, mathematical analysis shows that small changes in k_{sat} (in the order of 10^{-7}) can generate large changes in the preferential flow path of the

numerical model. Figure 4.19 shows sensitivity curves, describing the effect of changing k_{sat} in Column-1 for all the case analyses of Test 1 (See A). The legend in the figure relates the suction at the base of the coarse sand and the precipitation according to Table 4.1 where flux "a" is highest (1120 mm/day) and flux "d" the lowest (330 mm/day). The sensitivity curves start to move to lower values of k_{sat} as the contact length increases; in other words, with changes in the preferential flow path the k_{sat} becomes lower and lower. The calibration from the BCS in Column-1 results in a range between $1.4 \times 10^{-6} m/s$ to $2.4 \times 10^{-6} m/s$ for k_{sat} .

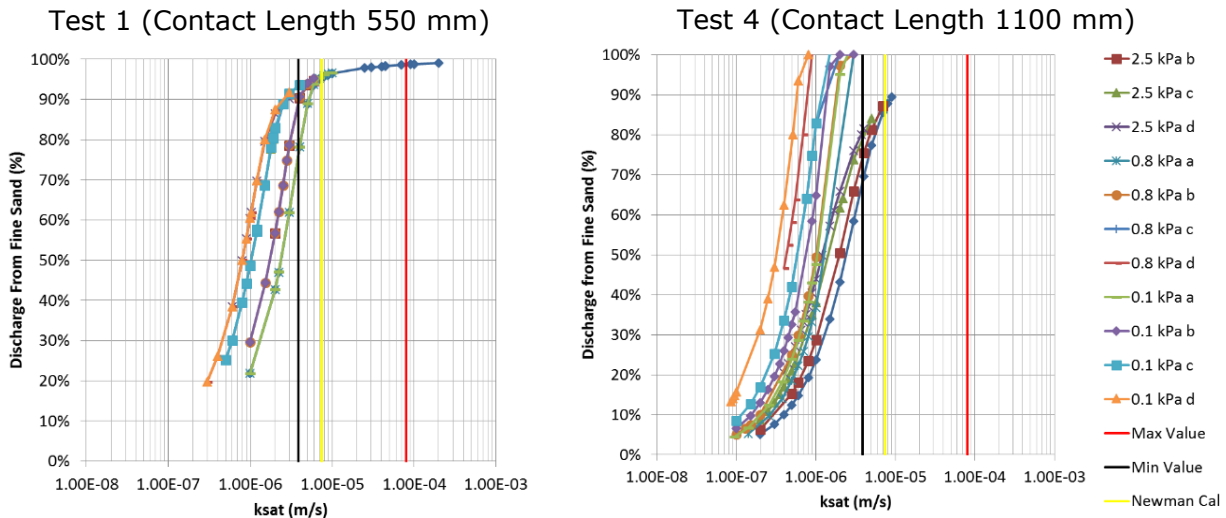


Figure 4.19 Change in Discharge from BCS Vs k_{sat} for Test 1 and Test 4

It should be expected that increases in k_{sat} generate increasing discharge from the BCS, making the BCS the preferential flow path of the system. However, the relevance is in the changes that occur due to a small increase of k_{sat} . With the example of Test 1 with a precipitation of 450 mm/day (flux "c"), if the k_{sat} is $1.0 \times 10^{-6} m/s$, then it could generate a discharge from the BCS of 50%; if the k_{sat} would be in fact $2.0 \times 10^{-6} m/s$, then the discharge increases to more than 80%. This is a 30% increase resulting from a small change of k_{sat} . Test 4 shows that the suction values at the base generate an impact on the calibration for the k_{sat} . The back analysis of Test 4 shows that increasing the contact length decreases all the values of k_{sat} ; similarly, if suction and precipitation decrease, the k_{sat} also decreases.

4.5.1.3.2. Sensitivity to Changes in k_{sat} for Silica Sand

The results from the simulations calibrating k_{sat} on the Silica sand (keeping $k_{sat} = 6.2 \times 10^{-5} m/s$ for the fine sand) are shown in Figure 4.20. The figure relates the percentage of discharge (i.e. discharge water at the base) from the Beaver Creek sand at each suction case to the respective laboratory result.

The calibrations of the k_{sat} of the SS do not improve the correlation for all the conditions tested in Column-1, nor affect the change in suction condition at the base of SS. From the 16 cases tested in Column-1, 11 cases correlate using an even base suction of 2.5 kPa, 4 cases for a suction of 0.8 kPa at the coarse, and 4 cases for 0.1 kPa of suction at the coarse. The cases that correlate correctly show the same trend to the column experiment; preferential flow occurs for the coarse sand (SS) at a precipitation above 800 mm/day and for the fine sand (BCS) at precipitations below 800 mm/day in all tests.

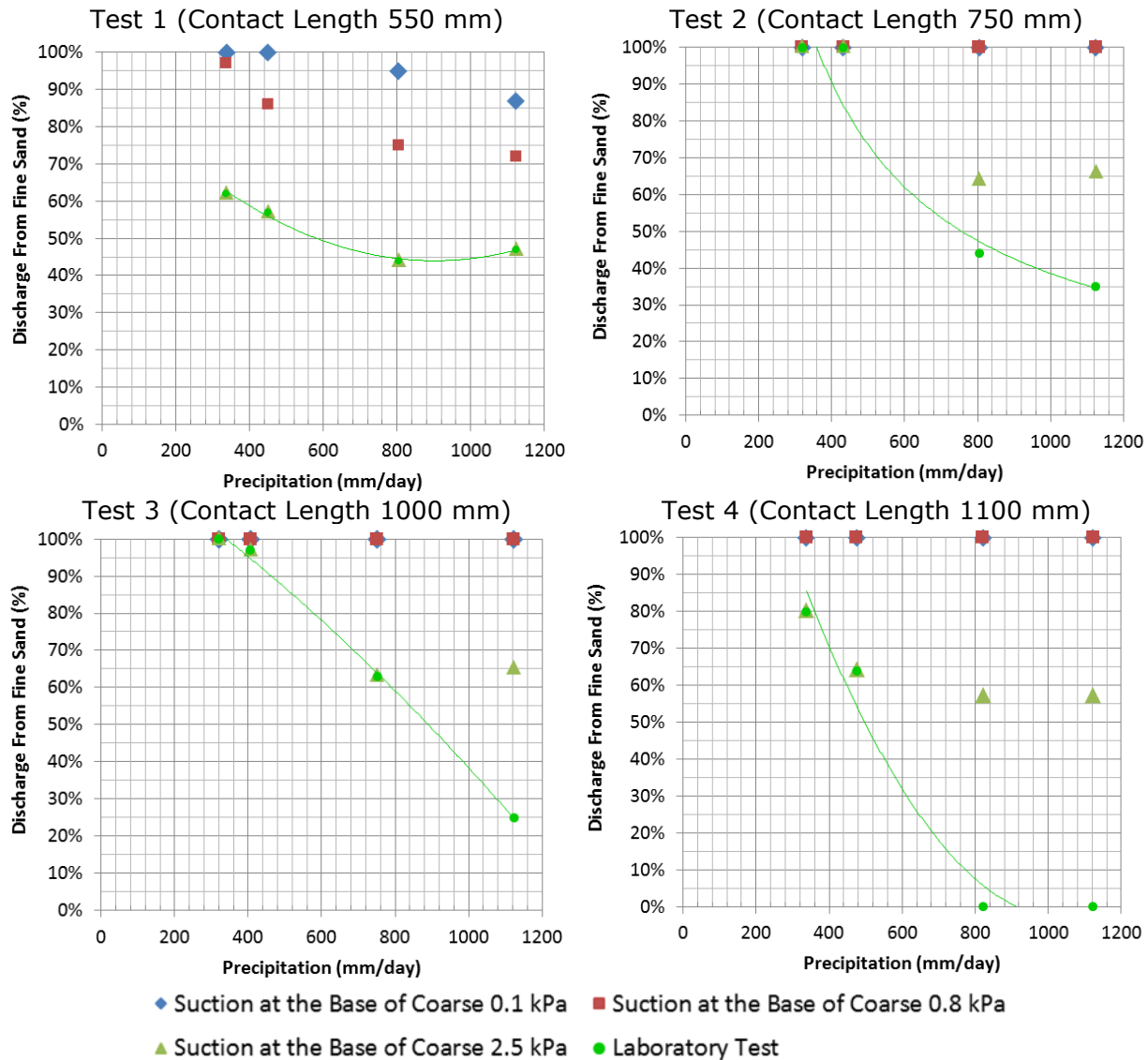


Figure 4.20 Discharge Flow from Fine Material by Calibrating k_{sat} on the Coarse Sand

Similarly as explain before for the calibration of the BCS (see **Figure 4.18**). The calibration of each test required a particular calibration of the saturated hydraulic conductivity for the SS, for each precipitation rate an average value is calculated with

respect to the four tests; e.g. for a precipitation of 1120 mm/day (Flux a) the k_{sat} of the SS was calibrated for the four contact lengths, this calibration resulted in slight variations of the k_{sat} with respect to the precipitation. Figure 4.21 presents the change in the average k_{sat} for the SS with precipitation (also averaged) for the conditions with an error of less than 10% with respect to the actual discharge. The graph shows the average k_{sat} relation with the laboratory measure.

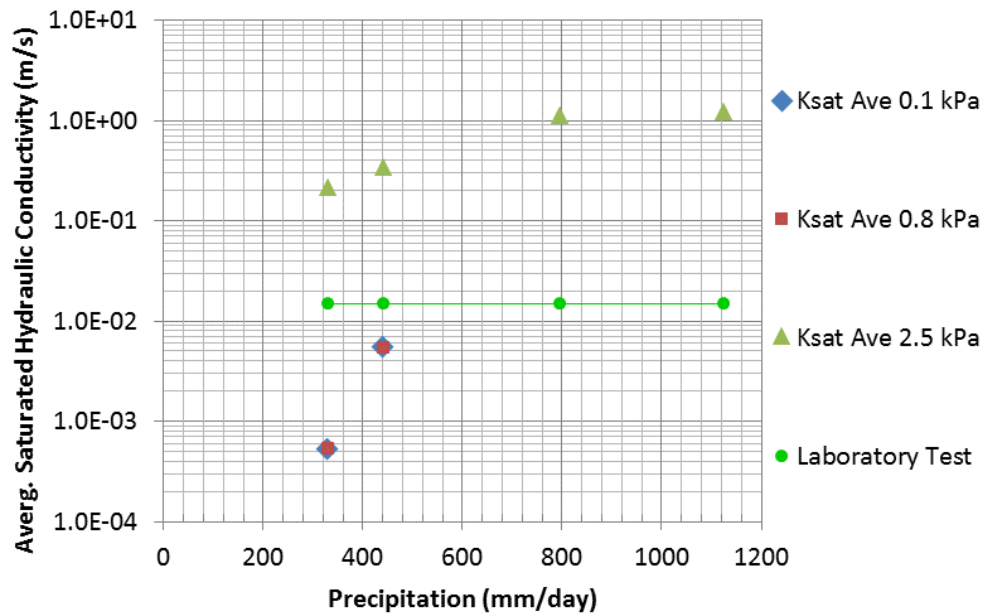


Figure 4.21 Change in k_{sat} with the Precipitation from Coarse Sand Calibration to give a discharge within 10% difference using a Base Suction in the coarse of 0.1, 0.8, and 2.5 kPa

The saturated hydraulic conductivity of the coarse sand was (for all cases) around three orders of magnitude higher than the measurement in the laboratory test. The calibration shows an average k_{sat} for all cases close to 1.0 m/s. This result is unreasonable for Medium Silica Sand. Furthermore, it should be expected that the value with respect to the laboratory measure be lower, because of the densification of the material due to the settlement that occurred while the barriers were lowered. The result from the calibration reflects more the behavior of a gravel material, such as that used for the filter at the base of the column to prevent the clogging of the drainage pipes.

The suction that allows the model to achieve more correlations is 2.5 kPa for the base of both materials. Figure 4.21 shows that k_{sat} increases with the increment of precipitation for the model to achieve a good correlation. The best correlation to the laboratory measures is achieved with a suction of 2.5 kPa, the required values of k_{sat} for the model, however, are unreasonable for precipitations greater than 440 mm/day. The

calibration of SS resulted in high values more related to gravel like material for Test 1 & 4. The results of k_{sat} for Tests 2 and 3 under 2.5 kPa of suction demonstrate a reasonable order of magnitude at $2.7 \times 10^{-1} \text{ m/s}$. The calibration also shows that increasing the difference of suction at the base and contact length reduces the convergence of the model; further detail of the calibration of the SS can be observe in Appendix A.

A variance in suction at the base of the model had a negative impact on the results. Less than half of the cases found convergence, of which those values are one order of magnitude lower than the laboratory measure but are reasonable for SS material. The difficulty of changing the k_{sat} of the SS to obtain a good correlation can be shown in Figure 4.22.

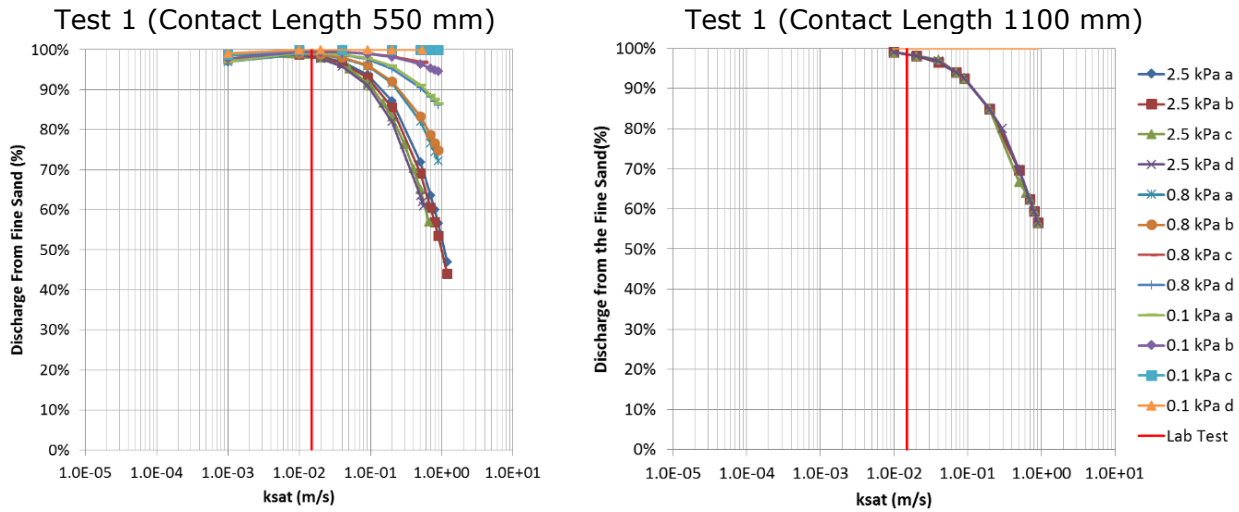


Figure 4.22 Change in Discharge from SS vs k_{sat} for Test 1 and Test 4

Figure 4.22 shows a completely different behavior in the back analysis of the SS than the behavior of the BCS. The curves show that increasing the k_{sat} decreases the discharge from the fine material (BCS); however, the decrease is not as significant as in the fine material, and in some cases, k_{sat} in the model is required to be unrealistic. Additionally, the reduction of k_{sat} lowers as the difference of suction at the base increases. The back analysis of Test 4 resulted in the same behaviour as Test 1; however, the numerical error of balancing the system (as shown in Figure 4.14) starts to increase as the base suction on the SS decreases.

4.5.1.3.3. Sensitivity in Changes of the AEV in the Beaver Creek Sand

The results from the simulations calibrating AEV on the Beaver Creek Sand (keeping constant the $k_{sat}=6.2 \times 10^{-5} \text{ m/s}$ for the BCS; and $k_{sat}=1.5 \times 10^{-2} \text{ m/s}$ and $AEV = 0.7 \text{ kPa}$ for

the SS) are shown in Figure 4.23. The model is run for the four tests, with their corresponding precipitation, and the change in suction at the base of the column for the SS.

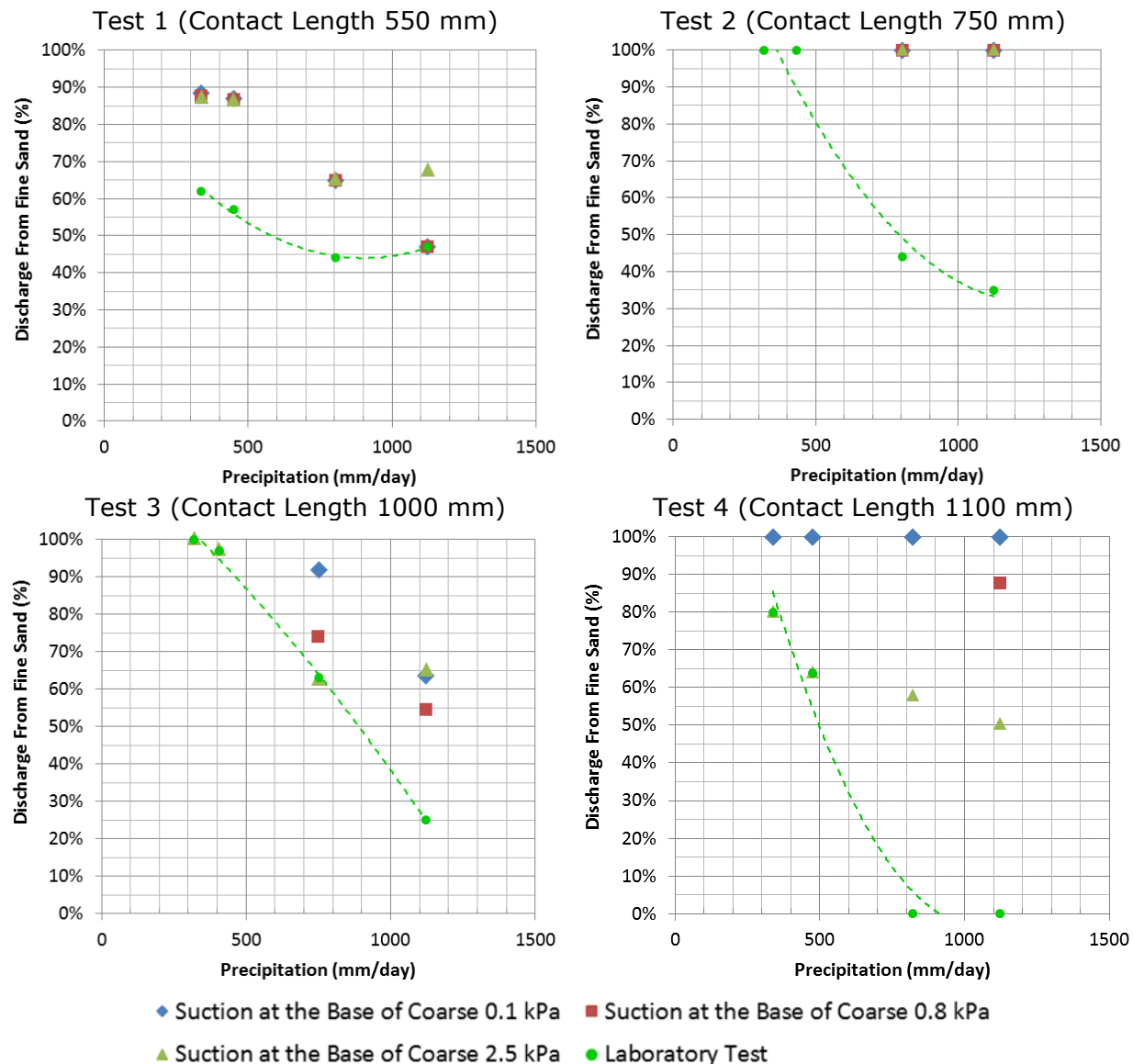


Figure 4.23 Discharge Flow from Fine Material by Calibrating AEV on the BCS

The calibration for the AEV in the BCS shows low correlations with the laboratory measurements. The previous results correspond to a variation of the AEV from 0.75 kPa to 3.2 kPa. The range was determined to be below the AEV measured from the SWCC (i.e. 3.8 kPa), because the simulations using laboratory properties (see section 4.5.1.1) overestimated the discharge from the BCS. The minimum value for the variation of the AEV relates to the AEV of the SS (i.e. 0.7 kPa); nonetheless, in most cases 0.86 kPa is the minimum AEV in which the model solved. The calibration shows AEVs below the laboratory

measure and the range determined by Wilson (3.0 kPa to 5.0 kPa), these low values allow a desaturation under a lower suction; however, most cases overestimate the discharge from the BCS. On the other hand, the results show that the change of suction at the base of the SS does not improve the correlation of the model. The results show that as the difference in suction increases, the correlation decreases.

Figure 4.24 shows the average calibration of the AEV for the BCS. The calibration of the model through back analyzing the AEV of the BCS resulted in errors ranging from 20% up to 100% for the best possible correlation (i.e. some cases, despite lowering the AEV, did not decrease the discharge from the BCS: for detailed calibration of the AEV see Appendix A). The average AEVs are taken from the results with a discharge of less than 10% error in Figure 4.23.

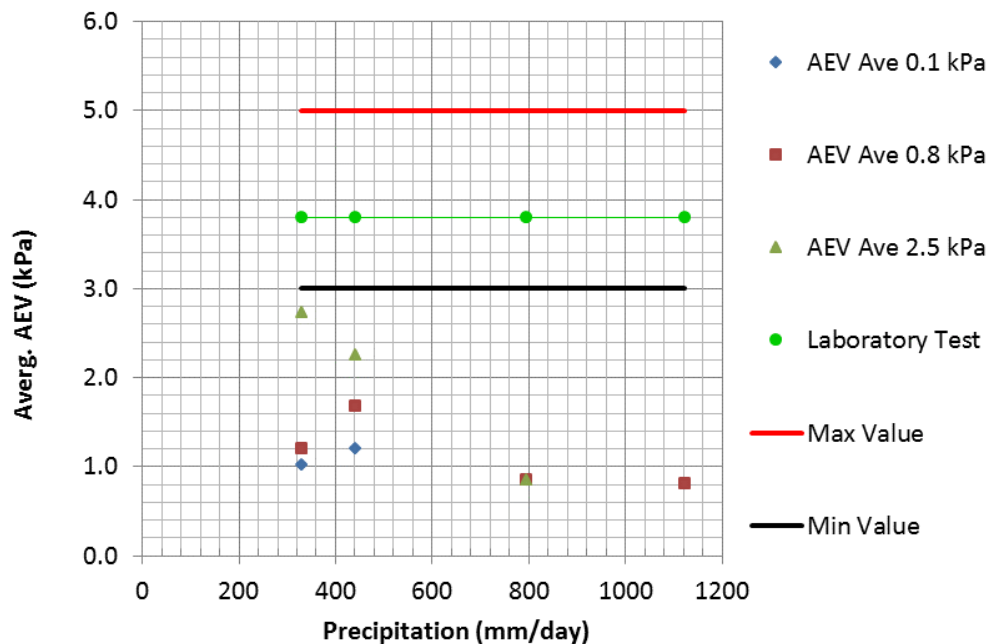


Figure 4.24 Average AEV per Flux from Fine Sand Calibration to give a discharge within 10% difference using a Base Suction in the coarse of 0.1, 0.8, and 2.5 kPa

Changes in the AEV of the Beaver Creek Sand did not show significant improvement in the calibration of the model as shown in Figure 4.23. In most cases, the discharge from the fine material did not lower below 80% despite lowering the AEV close to that of the Silica Sand, Appendix A shows the sensitivity analysis of the AEV for all the test and the maximum approximation to the laboratory results. The back analysis of the AEV in the BCS shows less affect in the preferential flow path in Column-1 than the saturated hydraulic conductivity.

4.5.2. Water Flow in Waste Rock Material

The simulations of Column-2 consist in Fine-waste-rock (F-WR) and Coarse-waste-rock (C-WR) under three precipitation rates and a single contact length. As in Column-1, the results are normalized by comparing in all cases the amount of flow discharging out of the fine material (i.e. F-WR); the discharge is calculated and compared with the laboratory measures.

No records were found for previous numerical simulations of Column-2; therefore, the results are grouped in the following manner: the first group relates to the simulations *applying the properties and boundary conditions established during the laboratory experiment*. The second group of result presents the *optimal correlation between the numerical simulation and laboratory* measures by changing the saturated hydraulic conductivity (k_{sat}) of each waste rock.

4.5.2.1. SIMULATION USING LABORATORY MEASURED PROPERTIES

The following results take into account the simulations of Column-2 using the laboratory parameters measured by Herasymuik (1996) and Newman (1999); see chapter 4.3.1. Figure 4.25 presents the changes in discharge from the F-WR with respect to the changes in precipitation.

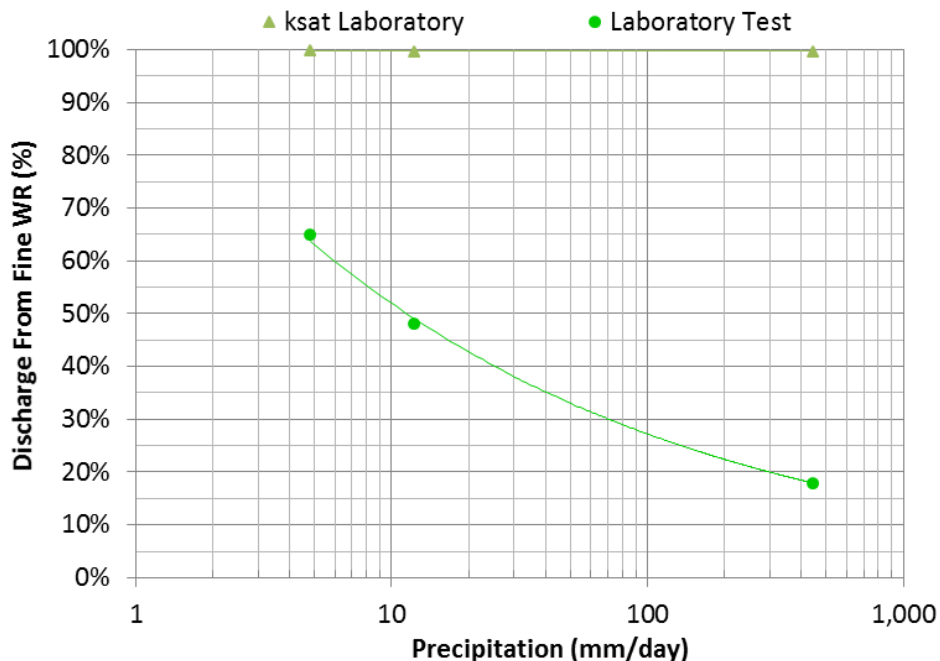


Figure 4.25 Discharge Flow from Fine-waste-rock using the Laboratory k_{sat}

The results from the simulations in the Column-2 using the material properties do not correlate with the laboratory results. In the three case simulations, the discharge from the F-WR is overestimated, maintaining almost a 100% preferential flow path through the fine material. Additionally, the change in precipitation does not seem to affect the discharge on the column.

The three precipitation rates for these simulations are below the k_{sat} of both materials. In order for the C-WR to be the preferential flow path at the highest precipitation rate (i.e. 445 mm/day), the column must develop a negative pressure below the suction at which both HCCs intersect. For such a condition to occur, the VWC has to increase to a point near saturation; however, as the precipitation is nearly one order of magnitude below the k_{sat} of the F-WR, it is not probable that the internal suction decreases so much under the experimental conditions. The other possible source of error is that if the k_{sat} of the F-WR is lower or the k_{sat} of the C-WR is higher than the laboratory measure, then the internal suction and the HCCs would match the preferential flow paths.

4.5.2.1. SENSITIVITY IN CHANGES OF THE SATURATED HYDRAULIC CONDUCTIVITY

The previous simulation has a low correlation to the measure discharged from the laboratory experiment. It is necessary to determine the conditions that would allow the numerical simulation to recreate with a low error (less than 10% difference to the laboratory measures) the water discharges. One method to improve the convergence of the model is to calibrate the material properties. In the following simulations, the back analysis of Column-2 is focused on the saturated hydraulic conductivity (k_{sat}) of the waste rock in order to modify the HCCs.

The results from the simulations calibrating k_{sat} on the Fine-waste-rock (keeping $k_{sat} = 1.0 \times 10^{-3}$ m/s for the Coarse-waste-rock) and calibrating k_{sat} on the Coarse-waste-rock (keeping $k_{sat} = 3.49 \times 10^{-5}$ m/s for the Fine-waste-rock) are shown in Figure 4.26.

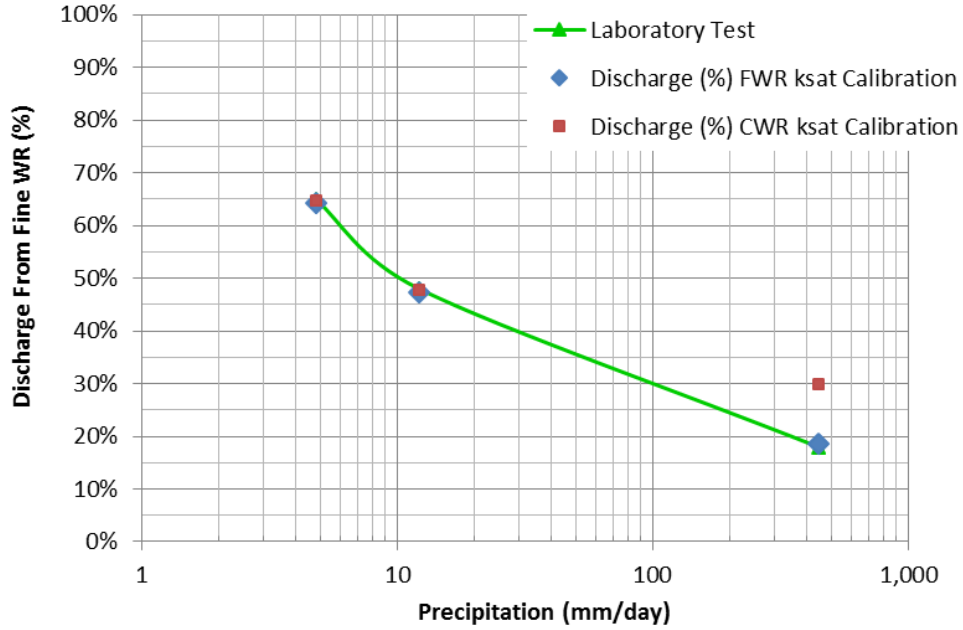
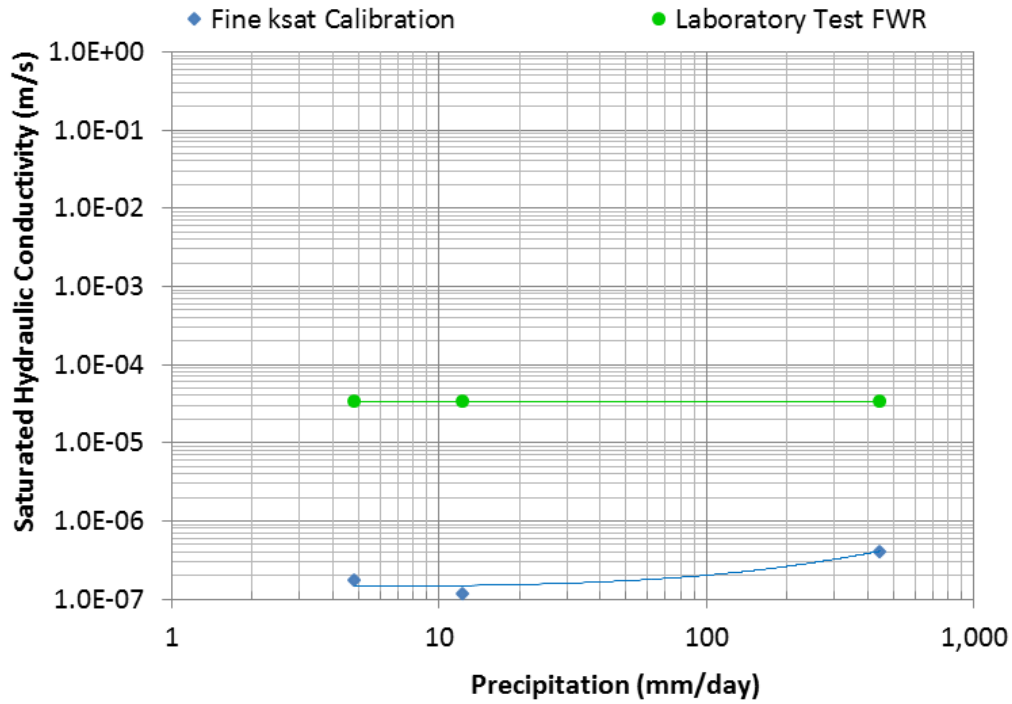


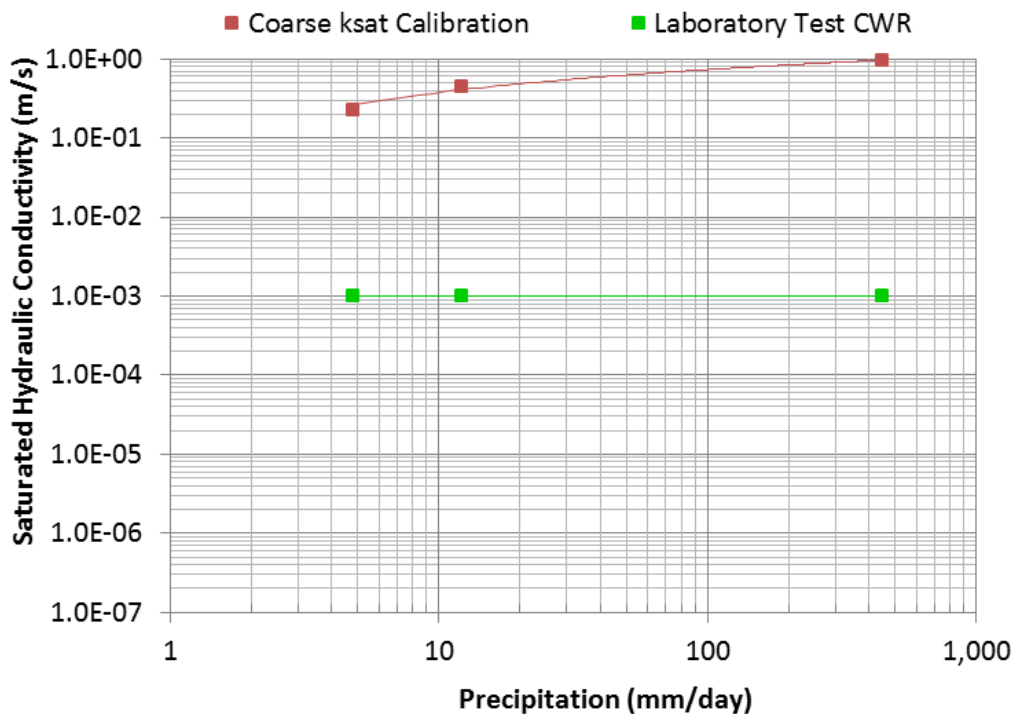
Figure 4.26 Discharge Flow from Fine-waste-rock by Calibrating k_{sat} on the Fine-waste-rock and on the Coarse-waste-rock

The calibrations of the k_{sat} of the F-WR and C-WR show an increment on the accuracy of the numerical simulation for Column-2, with respect to the simulations presented in section 4.5.2.1. Figure 4.26 shows preferential flow paths for the C-WR at fluxes above 5 mm/day. The controlling variable for the calibration is the discharge from the F-WR. The calibration resulted with differences in discharge of less than 1.0% with respect to the laboratory measurements, except for the C-WR at 445 mm/day. The waste rock in Column-2 shows high sensitivity to changes in k_{sat} during calibration. The sensitivity curves for the calibration of the F-WR result in high drops of discharge from the F-WR at k_{sat} below $5.0 \times 10^{-6} \text{ m/s}$. The maximum drop reaches 35% less discharge at changes of $1 \times 10^{-6} \text{ m/s}$ for the k_{sat} , detail information for the calibration process of Column-2 is in Appendix A. This drop similarly occurs for the sensitivity curve from the C-WR, for k_{sat} above $1 \times 10^{-3} \text{ m/s}$.

The calibration of the model for the experiment conditions in Column-2 is achieved through the calibration of k_{sat} ; however, each test case generates a different result. Figure 4.27 shows the calibration for the k_{sat} of the F-WR and C-WR. It presents the values of k_{sat} for each precipitation rate in Column-2, and the measured laboratory k_{sat} for comparison.



(a)



(b)

Figure 4.27 Calibrated ksats for F-WR (a) and For C-WR (b)

The numerical simulation in Column-2 required a different calibration of the waste rock k_{sat} for each of the applied fluxes. The calibration of the k_{sat} in the F-WR shows values

below the measured k_{sat} and a slight increase as precipitation increases. In contrast, in the calibration of the k_{sat} in the C-WR, the values are above the measured k_{sat} and the increment with precipitation is greater.

With respect to the F-WR, the sieve analysis classifies the material as sand with silt (SW-SM). Typically, this type of material can have a k_{sat} ranging from 10^{-3} m/s to 10^{-5} m/s. The result magnitude from the calibration of the k_{sat} in the F-WR has two to three orders of magnitude less than the minimum value and becomes unreasonable for this type of sand with such a low fine content.

A coarse gravel (GP) such as the C-WR should have a k_{sat} with an order of magnitude of greater than 10^{-3} m/s. The sensitivity analysis showed that the change in precipitation did not affect the relation between discharge and k_{sat} for the calibration of C-WR. This condition indicates that for every precipitation the model would require a different k_{sat} ranging from 0.22 m/s to 0.95 m/s. The calibration of the three simulated cases resulted in an average k_{sat} of 0.8 m/s. However, a k_{sat} of 1.77 m/s is needed to reach a discharge of 18% from the F-WR at the highest precipitation (Flux "a"), which is more related to gravel. Reducing this calibration to an acceptable value a k_{sat} of 0.95 m/s results in a discharge of 30%, increasing the difference to 12%. Considering this variance in the model for the Flux "a", the average calibration for the k_{sat} on the C-WR results in approximately 0.54 m/s.

4.5.3. Internal Responds For Sensitivity Models

Lateral transfer of water can occur in different zones of the contact zone in the column. Therefore considering only the discharge from each material could neglect the location where water transfers, and where water particles are punctually located generating the preferential flow path. Calculating the internal response using FEM requires a further understanding of the effect of precipitation and contact length between the materials.

The following results show the internal distribution of head pressure within each column. The figures show 2D pressure profile, stream traces and the velocity vector for a specific condition in the simulation of Column-1 and Column-2. Appendix A and Appendix A shows all the profiles from the simulation from Column-1 and Column-2 at the different tests conditions.

The following results satisfy (with less than 10% error) the correlation between the model and the laboratory; Newman's conclusions on the effect of change in precipitation and contact length are also satisfied by the pressure profiles from the simulations.

4.5.3.1. EFFECT OF CHANGE IN PRECIPITATION

Newman (1999) concluded that “preferential flow occurs through the fine if the precipitation was lower than the saturated hydraulic conductivity”. The laboratory results show that the preferential flow path becomes the fine material with the decrease of precipitation (Figure 4.5).

Column-1 was evaluated for four different precipitation rates applied at the top of the column, where each half of the column received an equal amount of flux under steady state conditions. Figure 4.28 shows the pressure distribution for the highest and lowest precipitation rates in Column-1 with a contact length of 550 mm between both materials.

The simulation shows that two gradients are formed in the contact zone, at the top of the column and top of the cut-off. The gradient of h_p between the materials is less than 1.0 kPa, but capable of generating a 100% lateral flow. This gradient increases as precipitation decreases, generating a higher lateral flow in the contact zone. At a higher precipitation, the VWC is increased in the system; consequently, the voids are filled and the suction decreases.

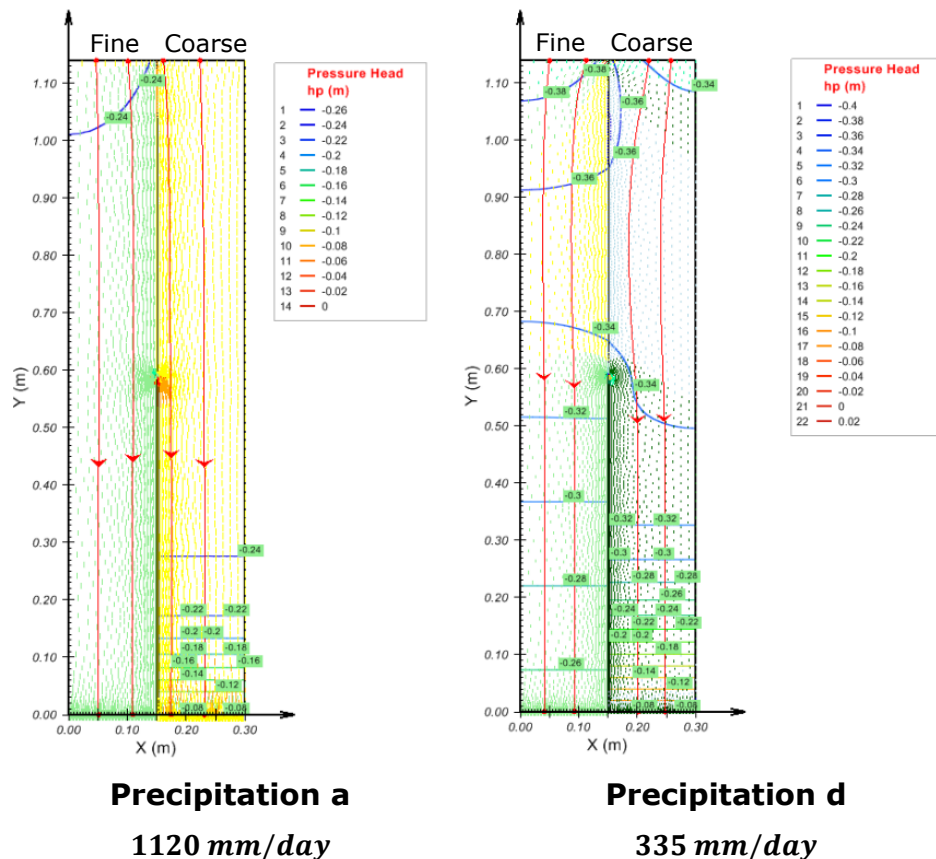


Figure 4.28 Change in Precipitation for Test 1 with a Base Suction of 2.5 kPa in the Fine Material and 0.8 kPa in the Coarse Material

The profile shows that a constant suction forms at the same elevation between the two mentioned gradients. This zone of equilibrium in suction decrease as precipitation decreases, Appendix A see the change in pressure with elevation for the different test in Column-1.

4.5.3.2. EFFECT OF CHANGE IN CONTACT LENGTH

Newman (1999) concluded that "increasing the contact length resulted in higher discharge from the coarse material, except in Test 3b" (1000 mm of contact length and a precipitation of 800 *mm/day*).

Column-1 was evaluated for four different contact lengths ranging from 550 mm to 1100 mm in a column with a total height of 1140 mm. Figure 4.29 shows the pressure distribution at a contact length of 550 mm and 750 mm for the lowest precipitation rate in the test (335 *mm/day*).

The simulations show that the change in contact length has an influence on the preferential flow path, as well as the magnitude of pressure developed within the column. Between Test 1 and Test 2 the simulations reveal that increasing the contact length to 200 mm, increases the discharge through the coarse sand.

This increment in the contact zone can have different outcomes with respect to the change in precipitation. Increasing the contact zone can decrease the head pressure (i.e., increasing the suction) if the precipitation is lower than the k_{sat} of the fine. However, if the precipitation is higher than k_{sat} of the fine, then the head pressure increases. On the other hand, the equilibrium suction is also affected by the change in the contact zone. This suction increases as the contact zone increases.

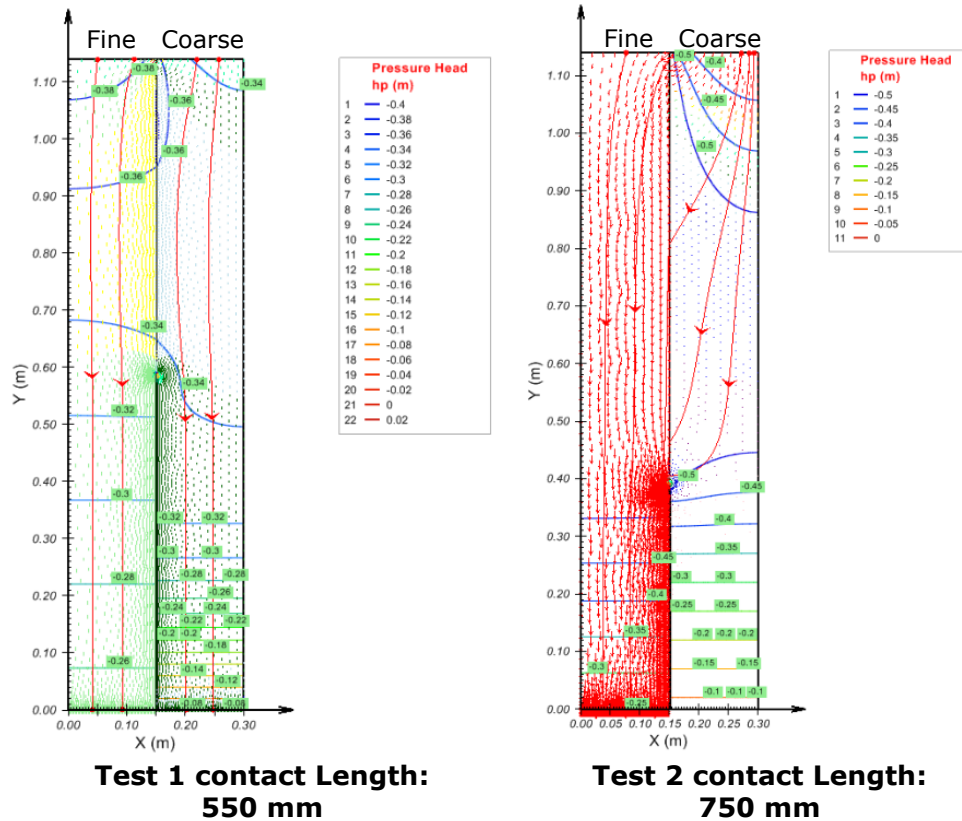


Figure 4.29 Comparison on the Change in Contact Length for a Precipitation of 800 mm/day with a Base Suction of 2.5 kPa in the Fine Material and 0.8 kPa in the Coarse Material

At a precipitation below $ksat$ of the fine, the equilibrium suction develops over a shorter distance as the contact length increases, detailed pressure profiles for Column-1 are presented in Appendix A.

The previous results have shown that for the lowest cut-off height (140 mm), the base boundary conditions have an effect in the water flow distribution (Figure 4.17 and Figure 4.20). This effect should be related to changes in precipitation due to the inclusion of suction at the base of the column. The numerical simulation for these conditions had the highest error, but still within the acceptable criteria defined for this investigation.

Figure 4.30 shows the results of the comparison between Test 3 and Test 4. When the four tests are compared, the top gradient is shown to increase with contact length. However, as mentioned before, the increment does not affect the increment in the zone of equilibrium. In addition, a high gradient formed at the base of the model to satisfy the boundary condition, resulting in a numerical error, as explained in section 4.5.1.1.

In Test 3 with a precipitation of 1120 mm/day, 25% of the precipitation discharges from the fine sand (BCS). The previous figure allows an interpretation that water was

transferred from the BCS at an elevation above 0.8 m. Water flows to the SS with a ratio between 25% and 50% as another gradient is formed at the top of the cut-off. The lower gradient moves water back to the BCS; meaning that despite the total discharge from the SS being 75%, the water that moved between the distance of the top and bottom gradient could be greater than the discharge.

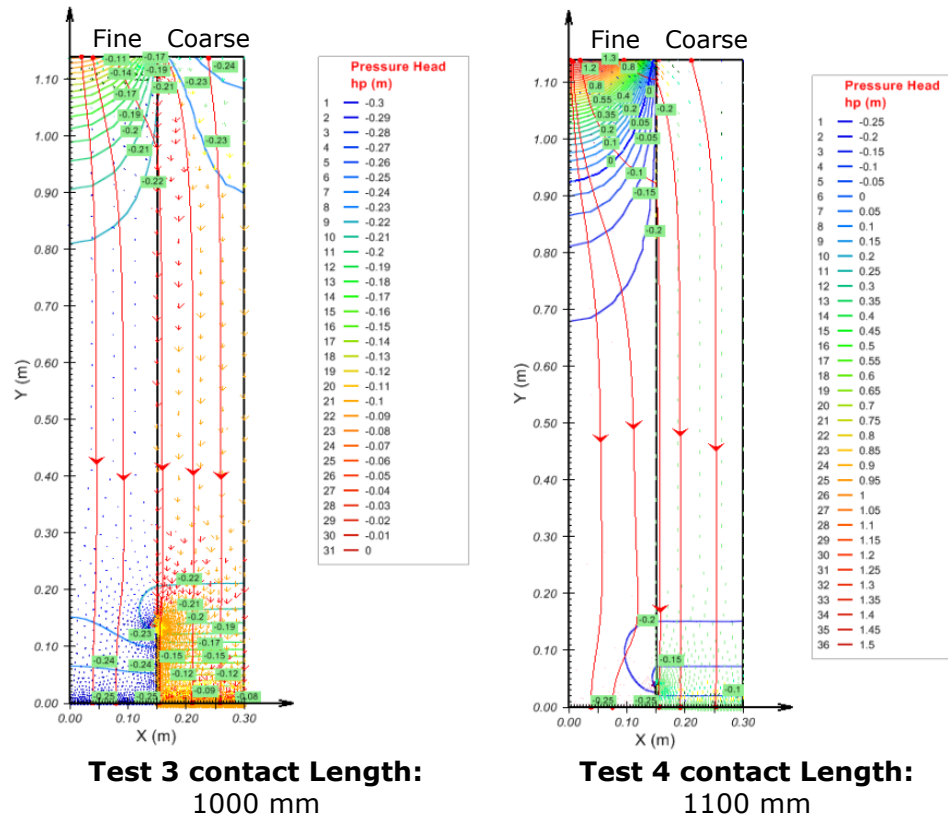


Figure 4.30 Change in Contact Length for a Precipitation of 1120 mm/day with a Base Suction of 2.5 kPa in the Fine Material and 0.8 kPa in the Coarse Material

4.5.3.3. EFFECT OF CHANGING PRECIPITATION ON WASTE ROCK

No previous models of Column-2 were found during the investigation. The following profiles allow clarification of the results from the laboratory experiment by Newman (1999). These profiles help to compare the conditions that control preferential flow path in Column-1 with the interaction of two materials with low AEV in Column-2.

Column-2 was evaluated for three different precipitation rates applied at the top of the column, where each half of the column receives the equal amount of flux under steady state conditions. Figure 4.31 shows the pressure distribution for the three precipitation rates in Column-2 with a contact length of 1000 mm between both materials.

At the highest precipitation rate applied in Column-2, the preferential flow path is the C-WR with a discharge of 78%. The profile reveals that most of the water transfer from the

F-WR to the C-WR occurs at the top 4.0 cm. In addition, above the cut-off there is gradient that also moves water traveling from the center of the F-WR to the C-WR. The head pressure profile shows a column with constant suction at every elevation. However, the small gradient allows that 62% of the applied water to the F-WR be transferred to the C-WR.

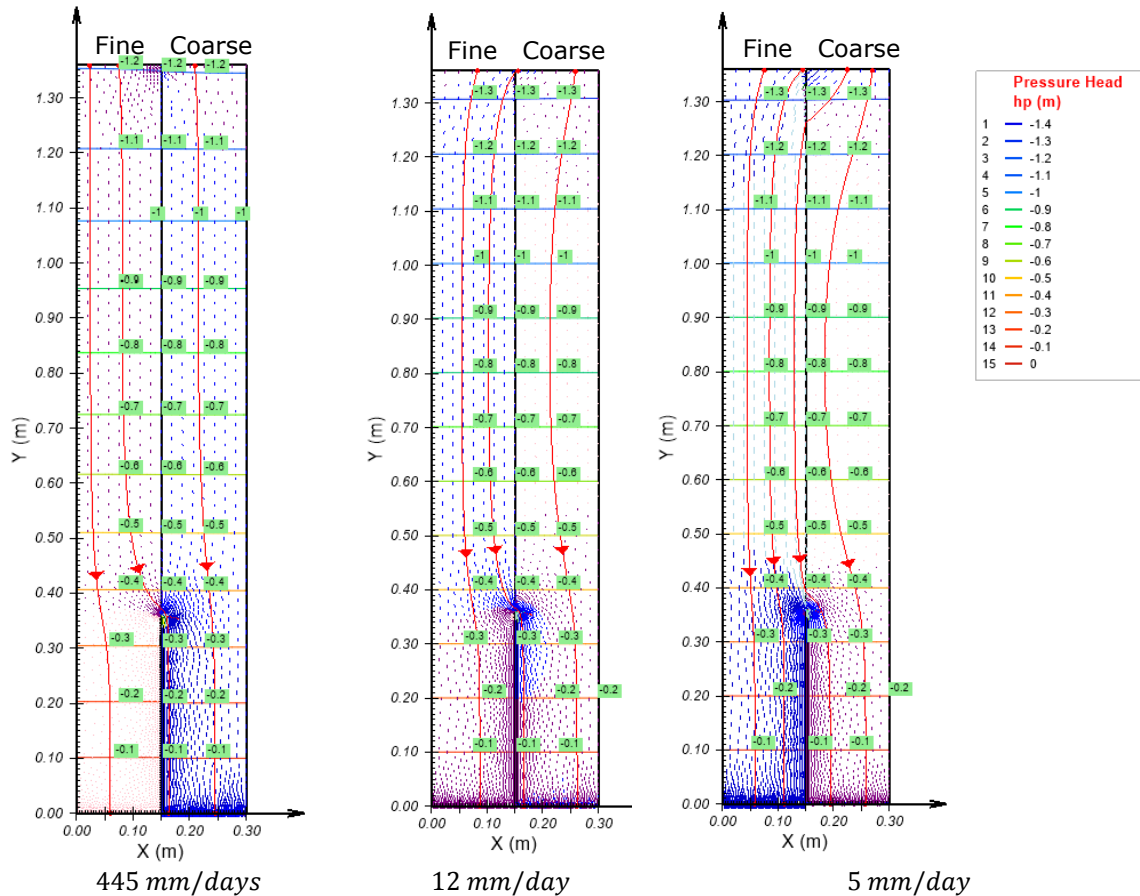


Figure 4.31 Comparison of Pressure Profiles for Column-2 at Different Precipitation Rates

Once the precipitation is lowered to 1.41×10^{-7} m/s, the discharge does not show a distinctive preferential flow path as close to 50/50 for each material. This ratio occurs as the gradients are small and developed over a really short distance; nonetheless, as mentioned before, the discharge is only one characteristic of the preferential flow path. The top 2.0 cm shows water transfer from the C-WR to the F-WR, but water is transferred back to the C-WR above the cut-off. This result showed that despite the discharge not showing a preferential flow path, water does flow more through the F-WR.

At the lowest precipitation, Column-2 shows that the preferential flow path is the F-WR. As in the second precipitation rate, a gradient is formed at the top 2.0 cm, transferring

water from the C-WR to the F-WR, and back again to the C-WR. The difference to the second case is that the gradient at the top of the cut-off is not strong enough to transfer back most of the water that was already moved into the F-WR, resulting in a 65% discharge from the F-WR.

Similar to the results in Column-1, the effect of increasing the precipitation rate in the Waste Rock Column shows that as water flux decreases, the preferential flow path switches from the C-WR towards the F-WR.

4.5.4. Highest Correlation Conditions for the Column Experiment

The calibration of the k_{sat} in the Beaver Creek Sand (BCS) offers reasonable results for Column-1, even though that the calibration results are below the minimum k_{sat} range given by Wilson (1990). The sensitivity analysis of the k_{sat} for most cases shows that the model requires a value below the $3.9 \times 10^{-6} \text{ m/s}$ to have significant effects on the preferential flow path. A k_{sat} of $2.4 \times 10^{-6} \text{ m/s}$ for BCS represents most of the cases of the simulation calibration.

As mentioned before, there is no clear indication of which suction is controlling the discharge on the Silica Sand. However, at 0.1 kPa and 0.8 kPa, there is a higher consistency with respect to 2.5 kPa. Therefore, it may be said that the discharge from the silica sand was controlled either by the AEV of the silica sand and/or by the gravel filter at the base. Nonetheless, considering that the silica sand should have a higher AEV than the gravel, it is more reasonable to expect that water flow be controlled by the sand at around 0.8 kPa.

The results presented in Table 4.4 show the difference in the discharge from the BCS between the model and the laboratory results. The correlation from the simulation to the experiment increases with an increase in the contact length. However, at Test 4 the correlation drops to 0.6 due to the high variance generated by the base boundary conditions. The average difference to the laboratory is around 11% by excluding Test 4.

Table 4.4 Simulation Results and Comparison to the Laboratory Test for Column-1

Contact Length		Applied Flux (mm/day)		Fine Discharge (% of total precipitation)	Discharge Difference (Model – Experiment)
1	550 mm	Flux (a)	1123	49%	2%
		Flux (b)	804	64%	20%
		Flux (c)	449	87%	30%
		Flux (d)	337	89%	27%

Table 4.4 (continue) Simulation Results and Comparison to the Laboratory Test for Column-1

Contact Length		Applied Flux (mm/day)		Fine Discharge (% of total precipitation)	Discharge Difference (Model – Experiment)
2	750 mm	Flux (a)	1123	49%	14%
		Flux (b)	804	63%	19%
		Flux (c)	432	86%	-14%
		Flux (d)	320	91%	-9%
3	1000 mm	Flux (a)	1123	54%	29%
		Flux (b)	752	73%	10%
		Flux (c)	406	113%	3%
		Flux (d)	320	133%	0%
4	1100 mm	Flux (a)	1123	87%	87%
		Flux (b)	821	100%	100%
		Flux (c)	475	101%	37%
		Flux (d)	337	101%	21%

The calibration of the waste rock (WR) from Golden Sunlight Mine was achieved for all the tested cases in the column experiment with low variation. The calibration for the Fine-waste-rock (F-WR) had a much lower variance ($\text{Var}=2.4\text{E-}14$) than the Coarse-waste-rock ($\text{Var}=0.14$). Nonetheless, the order of magnitude in each material range highly varies. At a k_{sat} equal to 0.54 m/s for the C-WR, the Column-2 simulations give a better correlation for precipitations below 12 mm/day. Variance of the material structure between both the column and the falling head test could be related to the two orders of magnitude difference of the simulation and the laboratory results.

Table 4.5 Simulation Results and Comparison to the Laboratory Test for Column-2

Contact Length		Applied Flux (mm/day)		Fine Discharge (% of total precipitation)	Discharge Difference (Model – Experiment)
1	1000 mm	Flux (a)	445	54%	36%
		Flux (b)	12	54%	6%
		Flux (c)	5	54%	-11%

As mentioned before, the model remains unaffected from changes in precipitation. The discharge increases maintaining the same proportions (i.e. same percentage of discharge). Since the k_{sat} of the C-WR is approximately 0.54 m/s, the preferential flow path would be through the F-WR, regardless of the three precipitation conditions.

The change in pressure profiles from Column-1 and Column-2 using the final calibrated properties can be observed in A and A, respectively.

4.6. ANALYSIS AND DISCUSSION

The principal objective of this study is to produce a numerical simulation of water flow in an unsaturated system of two columns with two vertical layers. This study works as a stepping-stone towards the simulation of a more complex model, consisting in the experiment with the three Meso-scale panels. The previous section of this chapter gave a brief description of the experiment from two column experiments conducted by Newman (1999). With Newman's description of the column geometry and material characteristic, a model was created for each column and was tested under the same experimental conditions. Section 4.5 shows a detailed description of the results along with the patterns and relationships between the different characteristics of the column and material properties. The simulation of these two columns provides a base understanding of the mechanism that controls water transfer in unsaturated systems constituted from materials with contrasting hydraulic properties. Furthermore, the simulations generate an internal description of the behavior of the materials from summing this kind of system to different climatic conditions.

The material properties described by Newman for the Beaver Creek sand (BCS) and Silica Sand (SS) are consistent with the general characteristics for these kinds of soils. The relation of change in VWC and suction measured through Temped Cell fitted consistently with the Fredlund & Xing regression for the SWCC. This fit provided a reliable estimation of the hydraulic conductivity curve using the SWCC.

The simulation of Column-1 and Column-2 started in a consideration of a model with the same characteristics of geometry and material properties that were considered during the laboratory experiment. The initial simulation considered the different contact conditions between the two materials as well of the different precipitation conditions applied to each test. The experiment presented by Newman (1999) was conducted in a controlled environment with proper care to reduce any of the possible variability that could occur. Nonetheless, the model did not have a close correlation to the experimental results. If we

have the proper tools and all the information from the experiment, it should be expected that only small differences could occur due to any numerical error. However, in all testing conditions, the discharge from the BCS was greatly overestimated, and no condition was found to allow a preferential flow path through the coarse material. This result lead to questioning three possible sources of error: first, the software may have numerical errors from the defined PDEs; secondly, the mathematical theory may not be describing accurately the flow mechanisms; or thirdly, the material characteristics are not consistent with the experiment.

The first possible error is unlikely as the software used for the simulations has been validated numerous times and compared to others (like Seep/W). The second possible source is beyond the scope of this study; however, it is also highly unlikely as the experiment and materials do not show any distinctive characteristic that makes this experiment an exceptional model (see Chapter 2). Still, it is known that investigations had been conducted and that others are currently underway to improve the regressions of the SWCCs or the HCCs, resulting in a variety of methods to obtain both curves. The third possibility seems more reasonable as the hydraulic properties depend on various characteristics that can be altered depending on the conditions of the sample.

The hydraulic material properties that control water flow in an unsaturated system rely on various characteristics such as size distribution, grain size distribution, density, organic material content, clay content, and mineralogy on the pore-water retention behavior. Density might have played an important role in the hydraulics characteristic of the materials. The energy of compaction of the materials within the columns was not consistent; Column-1 had a compactive energy of 133 kN/m^3 for the sandy material, while Column-2 was 67 kN/m^3 for the waste rock. A difference in density could have occurred if the compactive energy used in the permeability test (to obtain the k_{sat}) varies from the compactive energy used in the placement of the materials inside the column. The change in the compactive energy could have led to differences in the void ratio, changing the hydraulic properties between both samples of the same soil, including the AEV (See Chapter 3).

The model with the laboratory measurements for k_{sat} and AEV in the column was within the range, but this setup of the model shows low correlation. The second attempt to model Column-1 considering Newman's calibration did not show much improvement, despite the fact that the k_{sat} in the BCS was lowered one order of magnitude. There is a high difference between Newman's and the updated model using SvFlux. The SvFlux model has a higher refinement on the meshing properties, and could be a factor that makes the model

less accurate with respect to Newman's. Variation on the mesh can result in differences in the solution of numerical models, especially when solving highly non-linear equations. In all the tests, the SvFlux model using Newman's calibrated parameter results in an overestimated discharge from the BCS. Nonetheless, with respect to the first modeling attempt, the decrease in k_{sat} shows a slight decrease in the discharge from the BCS, showing a slight improvement in the correlation.

The improvement in the correlation of the model was examined by a back analysis process of the k_{sat} of the BCS and the SS, as well as the AEV of the BCS. The possible variability presented in k_{sat} of the BCS had a greater impact in the modeling of the first column, while the changes in k_{sat} of the SS and AEV show less effect in most cases on the preferential flow path (see Figure 4.17, Figure 4.20, and Figure 4.23). This third attempt to recreate Column-1 was achieved by decreasing the k_{sat} of the BCS below $3.9 \times 10^{-6} m/s$ (minimum range defined in previous studies). Lowering k_{sat} , the model achieved a correlation with less than 7% difference. The sensitivity curves for the model show that small changes (in the order of $10^{-7} m/s$) in k_{sat} can modify up to 30% the preferential flow path of the numerical model (Appendix A shows the sensitivity analysis of k_{sat} in Column-1). The k_{sat} is a high variable soil property, which can vary over one order of magnitude even in homogeneous soils; studies have shown that the methodologies to determine this variable can have errors of one order of magnitude (Nagy, et al., 2013). This sensitivity analysis for water flow in unsaturated conditions demonstrates the level of precision that simulations require for an accurate model. However, Nagy (et al, 2013) shows that current methodologies and procedures are still far away from having a reliable precision.

The difference in level of accuracy from determining k_{sat} directly or through numerical modeling leads us to consider that there is no need to have a high level of precision in the numerical model. However, the results from the calibration of Column-1 show the high sensitivity of preferential flow in unsaturated condition to any changes in k_{sat} . Considering that the average value for k_{sat} in the BCS is $2.4 \times 10^{-6} m/s$, the simulations of Column-1 resulted in errors between 0% to 30% for Test 1, 2 and 3 and 20% and 100% for Test 4. As such, the permeability acting in the column experiment could have been modified through the testing process.

In Column-2 the model was initially run using the classification and characterization of the material described by Newman (1999) and Herasymuik (1996) for the Waste Rock from Golden Sunlight. The simulation using the measured laboratory properties resulted also in overestimations of the discharge from the fine grain material (i.e. F-WR) for all the cases. In contrast, the calibration of Column-2 resulted in a change of the k_{sat} on the coarse

grain material. In order to decrease the discharge from the F-WR, the k_{sat} of the C-WR was increased over two orders in magnitude, ranging between 0.22 m/s and 0.95 m/s. The calibration of the C-WR resulted in correlations with less than 12.0% difference for Flux "a" and less than 1.0% for fur Flux "b" and "c". At a k_{sat} equal to 0.54 m/s for the C-WR, the waste rock column simulations provide a better correlation for precipitations below 12 mm/day. Variance of the material structure between the column and the falling head test could be related to the two orders of magnitude difference between the simulation and the laboratory results. The calibration in Column-2 remained unaffected from changes in precipitation. However, this condition results from the three precipitation fluxes being below the k_{sat} of both materials. As such, if the precipitation increases above the k_{sat} of the F-WR the effect of changing precipitation could increase, as observed in Column-1.

The simulation of the columns revealed that considering only the total discharge from each material neglects in some cases the real preferential flow path of the system as shown in Figure 4.28 and Figure 4.31. The h_p profile allows the examination of the internal behavior of flow within the system. The profiles have shown that gradients develop at the top of the column and top of the cut-off in which water initially transfers to one material at the top and flows back to the original material. In between these two gradients, a zone of equilibrium suction develops; this zone decreased to zero the lateral flow. The zone of equilibrium suction changes with precipitation due to changes in the gradients, decreasing with the precipitation. Similar behavior of the preferential flow path resulted in both columns using Sandy materials and Waste Rock.

The results from the simulation in Column-1 and Column-2 have shown that each test condition requires a particular calibration to recreate the water flow conditions from the experiments. The numerical model decreases errors from simulations by adjusting and improving the model detail and mesh characteristics. However, the results did show high susceptibility to changes in the saturated hydraulic conductivity of the material.

4.7. CONCLUSIONS

The simulation of the two column experiments to recreate the conditions and results of water flow of the unsaturated soils, under steady state conditions, was carried out in a two dimensional numerical model using SvFlux. The conclusion from the simulation can be summarized as follows:

- Column-1 made from sandy materials and Column-2 made from Waste Rock were calibrated within the scope of this thesis, with an error less than 10%. However,

limitation of these calibrations were found as each testing conditions resulted in a particular calibration.

- The optimal calibration from Column-1 was achieved by decreasing the k_{sat} of the fine material (BCS) to $2.4 \times 10^{-6} \text{ m/s}$, whereas, to the contrary, in Column-2 the calibration was achieved by increasing the k_{sat} from the coarse material (C-WR) to 0.54 m/s.
- There is no clear indication as to which suction is controlling the discharge on the SS; however, at 0.1 kPa and 0.8 kPa there is higher consistency compared to 2.5 kPa. As such, it may be said that the discharge from the SS was controlled either by the AEV of the SS and/or the Gravel filter at the base. The SS should have a higher AEV than the gravel; thus, it is more reasonable to expect the sand at around 0.8 kPa to control the water flow.
- Despite incomplete instrumentation during a laboratory experiment, numerical modeling allows the prediction of the internal response of the soil under the conditions tested. The analysis of the change in suction, flux distribution and streamlines validates the mechanism that lead to a specific discharge. Furthermore, the models display patterns that lead to predictions as these patterns occur with the back analysis in the calibration process.
- The hydraulic properties measured through laboratory testing did not correlate to the conditions of the materials within the columns. k_{sat} is a highly variable soil property that can range several orders of magnitude for the same soil. In the simulation of water flow in unsaturated conditions, the input properties in the model should match the conditions of the experimental model. E.g. the grain size distribution, SWCC, and k_{sat} should be measured under the same conditions as the material placed within the experimental column, having equal density and soil structure. This repetition would reduce the uncertainty from the material properties within the numerical models.
- As the waste rock layering tends to be at the angle of repose (approximately 37°), then the presented simulations have limited validity, so further study should be conducted on modeling an incline layering system in order to describe water flow and preferential flow path in an incline system in unsaturated conditions.

CHAPTER 5 NUMERICAL MODEL OF WATER FLOW MODEL IN INCLINE LAYERED SYSTEM

5.1. INTRODUCTION

Three Meso-scale experiments were made at the University of British Columbia in 2009 to identify the flow mechanisms in incline coarse and fine layers of waste rock, under unsaturated conditions. The “difficulties in knowing the location of existence of coarse and fine layers within a waste rock dump” lead to developing the laboratory test program to investigate flow paths, Andrina (2009). The three panels were built using 10 mm thick acrylic sheets: the first panel was composed of seven alternating layers of fine acid rock (F-AR) and coarse acid rock (C-AR); the second panel had an equal configuration as the first panel plus a top-layer of coarse limestone (C-L); the third panel had nine layers with different arrangements including fine limestone (F-L). The materials used in the panel were taken from Grasberg Mine in Indonesia and the grain size were scaled to match the field conditions.

This chapter presents the numerical simulation of the three Meso-scale experiments by Andrina using SvFlux. The data presented include the results of the following:

1. Simulation of laboratory experiment of Panel-1, Panel-2, and Panel-3.
2. Simulation of Panel-1 applying four pairs of material properties from different investigations of water flow studies.
3. Calibration and comparison of the models to the laboratory results.

5.2. OBJECTIVES

The objective of this study is to examine water flow paths in an unsaturated system of a three incline layering system under steady state condition in a two-dimensional space using numerical modelling. The use of a numerical model allows the evaluation of the effect of precipitation and base suction in the preferential flow path under unsaturated conditions for waste rock. The simulation of the first panel is run considering the laboratory properties described from the experiment; followed by a calibration of the material properties to increase the correlation. The second and third panel are run considering three material

properties: the first analysis is based on the initial properties from the experiment; the second analysis is based on calibration from the first panel; and the third analysis based on calibrated properties of the first panel and calibrating the top layer.

An additional objective was set through the course of this investigation in order to compare the effect of different materials under the same condition from Panel-1. Three simulations are conducted in Panel 1: the first two analyses are using the calibrated material properties discussed in Chapter 4 from Newman's Column experiment, including the sandy materials and waste rock material from Sunlight Mine; and third analysis is using Tailing Beach Sand and Devon Silt, materials characterized in research from colleagues at the University of Alberta (Abdulnabi, 2015; Kouakou, 2014; Torghabeh, 2013).

The three main objectives of this study are as follows:

- I. Evaluate the effect in controlling water flow in the numerical model by altering the Air-Entry-Value (AEV) or the Saturated-hydraulic-conductivity (k_{sat}).
- II. Calculate the internal response of the Meso-scale experiments, considering the head pressure distribution, flow velocity, and movement of water particles.
- III. Evaluate the effect of precipitation and suction on the model in the Meso-scale experiments.
- IV. Compare the discharge results and suction response between the numerical model and the laboratory results by Andrina (2009).

The following analyses are for Panel-1, Panel-2, and Panel-3 evaluated under the same steady state conditions used in the experimental stage. Each experiment is run for different configurations of precipitations rates (i.e. 2mm/day, 5 mm/day, and 10 mm/day), and different suction at the base (i.e. 0.0 kPa, 2.0 kPa and 4kPa).

5.3. MESO-SCALE PANEL EXPERIMENT

In 2009, Andrina at University of British Columbia presented her results for a Meso-scale experiment for three panels. The object of the experiments consisted in understanding the flow mechanism for incline layers of waste rock, as well as assessing the effect of inclination and of rainfall intensity on the flow path. The study was made by applying different precipitation rates to three Meso-scale panels and measuring the discharge water at the base. Additionally, each panel contained instrumentation at different elevations allowing the evaluation of the change in matric suction. The panels were composed of inclined interbedded layers of waste rock materials from Grasberg Mine in Indonesia. The

first panel used seven interbedded layers of fine and coarse acid rock. The second panel included a horizontal layer of coarse limestone overlaying the incline layers; the objective of this experiment was to evaluate the effect of an alkaline solution on the leachate quality. The third panel used nine interbedded layers of coarse and fine acid rock, and layers of coarse and fine limestone as shown in Figure 5.1.

The three panels had an inclination of 37° for the inner and outer slope. This took into account the typical inclination found in the layers formed within the waste rock embankments due to the process of end-dumping. The height of Panel-1 was 1.5 m, Panel-2 was 2.0 m, and Panel-3 was 1.5 m. The layers inside each panel had 25 cm length and 25 cm width and inclined 37° . A drainage system was placed in each layer to collect the leachate from each precipitation simulation. A filter material was placed at the base of each layer to control clogging of the drainage system, the height of this filter ranged between 30 cm to 50 cm. Acrylic strips of 1 cm height and 1 cm width were also installed at the base in the contact between layers to prevent crossover flow.



Figure 5.1 Meso-Scale Experiment for Panel-3 (Andrina, 2009)

The application of different suction conditions at the base of the panel used lysimeters in the drainage system. The lysimeters generated a suction of 0.0 kPa, 2.0 kPa, and 4.0 kPa.

The first panel composed of F-AR and C-AR had a simulated precipitation on top of the panel starting from layer two (L-2) to layer seven (L-7) and along the outer slope up to

minimum elevation of 0.5 m from the base. The instrumentation in Panel-1 was located at 0.5 m and 1.0 m elevation in each layer. The collection of the water discharge from each layer was taken at the base of the panel (L1 to L7) and along the inner slope (S1 to S3). The second panel had the same configuration as Panel-1 with an additional 50 cm horizontal layer of C-L. The simulated precipitation was located on top of the panel starting 25 cm away from the inner slope and along the outer slope up to minimum elevation of 0.5 m from the base. The instrumentation in Panel-2 was located at 0.5 m, 1.0 m, and 1.5 m elevation in each layer. The collection of the water discharge from each layer was taken at the base of the panel (L1 to L7) and along the inner slope (S1 to S4). The third panel had the same height as Panel-1 with additional two inclined layers of waste rock. The simulated precipitation was located on top of the panel starting from layer two (L-2) to layer seven (L-9) and along the outer slope up to a minimum elevation of 0.5 m from the base. The instrumentation in Panel-3 was located at a 0.5 m and 1.0 m elevation in each layer. The collection of the water discharge from each layer was taken at the base of the panel (L1 to L9) and along the inner slope (S1 to S3).

The Figures 5.2, 5.3 and 5.4 present the characteristics from the three Meso-scale experiments conducted by Andrina (2009).

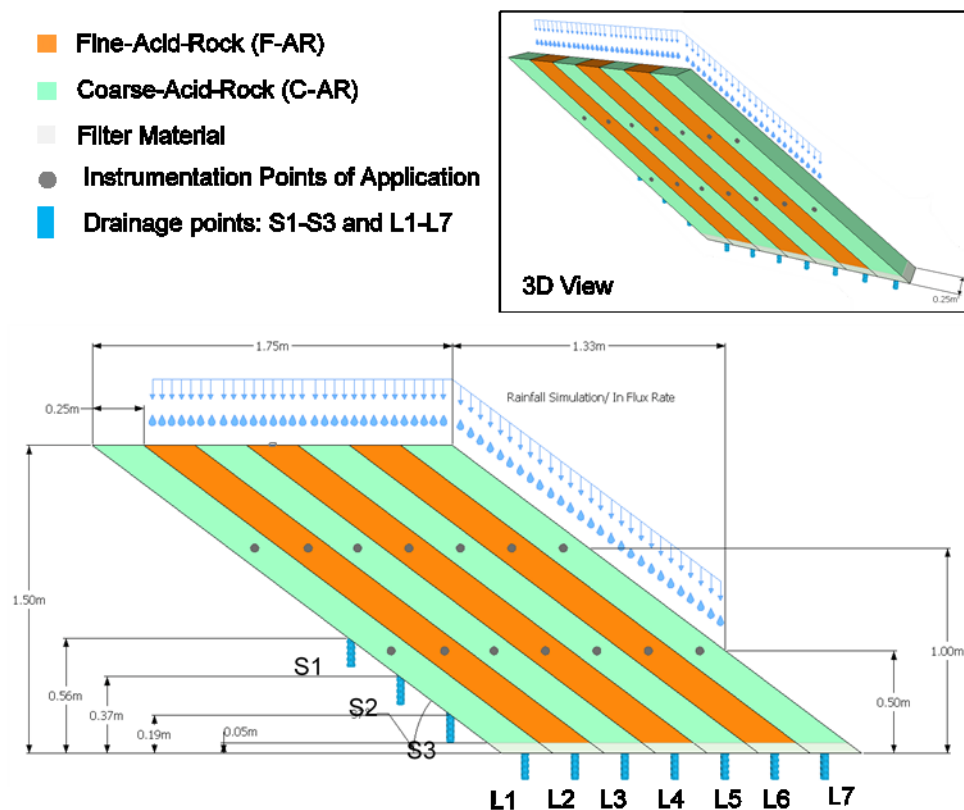


Figure 5.2 Physical Characteristics of Panel 1
Geometry, Material, Instrumentation, Drainage Points (Andrina, 2009)

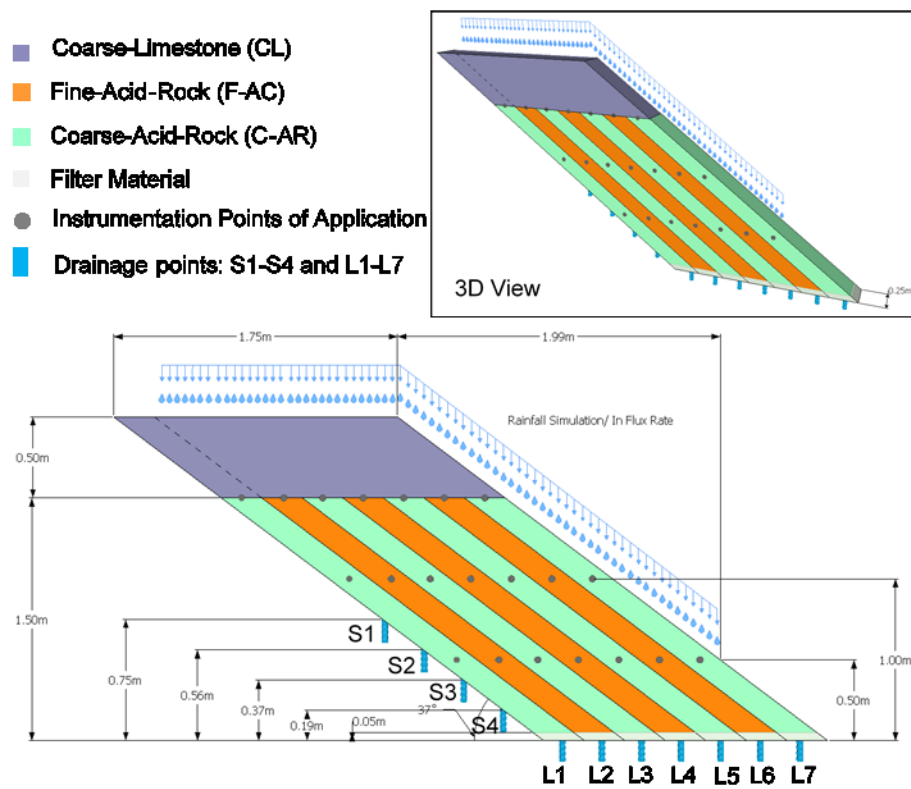


Figure 5.3 Physical Characteristics of Panel-2
Geometry, Material, Instrumentation, Drainage Points (Andrina, 2009)

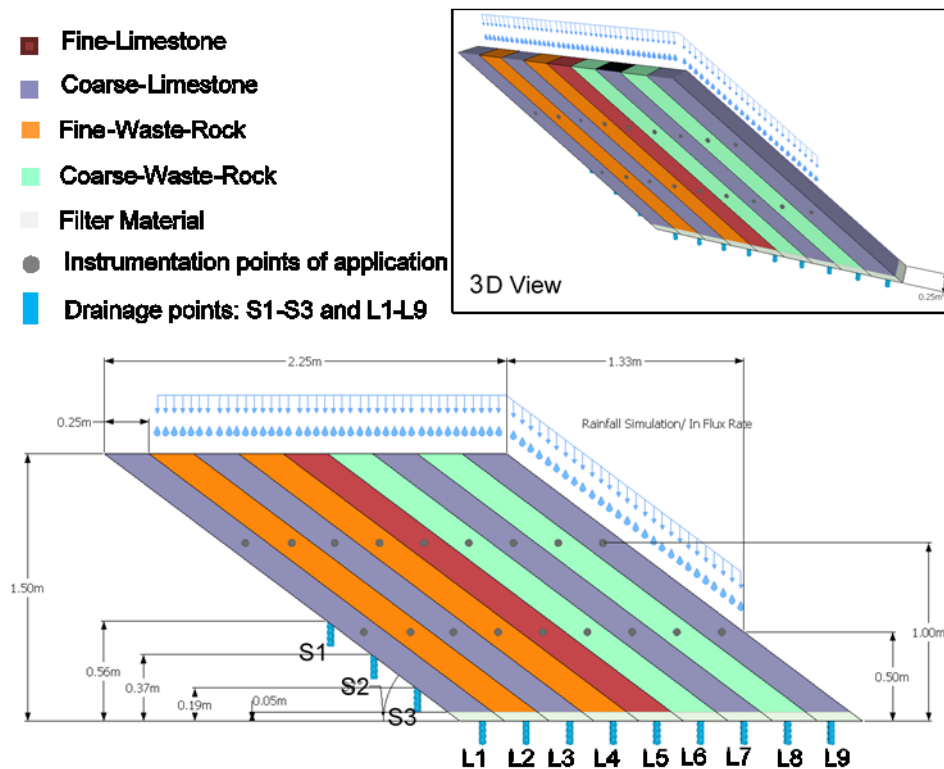


Figure 5.4 Physical Characteristics of Panel-3
Geometry, Material, Instrumentation, Drainage Points (Andrina, 2009)

The evaluation of water flow in the Meso-scale experiments had changes in the boundary conditions for the top and bottom of each panel (Table 5.1). The top boundary had a simulated precipitation of constant flux rate, establishing the steady state conditions in the experiment. The flux rate for the panels was 2 mm/day, 5 mm/day, and 10 mm/day. The selected precipitation rates were below the k_{sat} of the waste rock materials, and account for different climate types. The base boundary corresponds to the suction lysimeters; the panels had a constant suction applied in each layer at the drainage points L1 to L9. The drainage point in the inner slope (S1-S4) did not have suction.

The set-up from each panel allowed nine boundary conditions (Figure 2.26). However, for Panel-1, six tests were carried out, evaluating the effect of change in precipitation and suction on the discharge of the panel. In Panel-2 and Panel-3, three tests evaluated the effect of change in precipitation. Additionally, Panel-3 ran a test at a lower suction.

Table 5.1 Testing Conditions for Each Panel

Panel	Test	Suction (kPa)	Precipitation (mm/day)
1	III	0	10
	IV	2	2
	VI	2	10
	VII	4	2
	VIII	4	5
	IX	4	10
2	VII	4	2
	VIII	4	5
	IX	4	10
3	IV	2	2
	VII	4	2
	VIII	4	5
	IX	4	10

The Meso-scale was covered at the top of the panel with aluminum foil to allow approximately zero loss of water due to evaporation. On the other hand, the simulated

precipitation allowed a uniform flux for every layer, reaching a uniformity coefficient between 97% and 99%, Andrina (2009).

5.3.1. Material Properties

The materials in the experiment of the three panels came from the waste rock embankment in Grasberg Mine. The waste rock dump in the mine showed two distinctive types of materials: acid rock and limestone. The scaling of the experiment to the field conditions in the mine was made by crushing the materials and reducing the particle size of the waste rock. The fine fraction was crushed approximately to the size of the Run-of-Mine (size for processing mine ore), resulting in most particle sizes passing sieve #4. On the other hand, the particle size in the coarse fraction ranged between 10 mm to 25 mm, the maximum particle size being 10% of the layer thickness. The characterization of the materials was made according to ASTM standards.

The model's hydraulic properties, such as the soil water characteristic curves (SWCC), were measured using pressure cell tests, and the saturate hydraulic conductivities (k_{sat}) were measured using a constant head test and falling head test. The gradation of the waste rock does not show a significant difference between the acid rock and the limestone as shown in Figure 5.5. The coarse grain material resulted in a well graded coarse gravel (GW), while the fine grain was a poorly graded coarse gravel (GP).

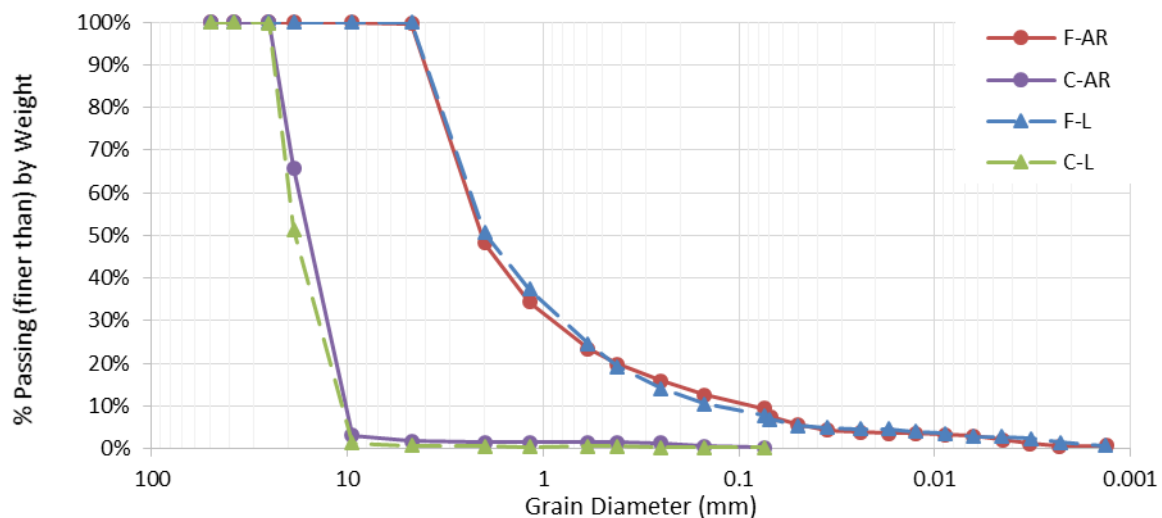


Figure 5.5 Grainsize Distribution Curve for Waste Rock in Meso-scale Panels

The properties used in the simulation of the three panels were measured through laboratory experiments (Andrina, 2009). Andrina stated that both the coarse and fine materials share the same unsaturated properties due to the small difference of the grain

size distribution. Table 5.1 presents the material properties of the materials used for the models of the three panels.

The values in Table 5.2 show the initial parameters for the simulations. The range of values for the AEV and k_{sat} are taken into account for the calibration of the model.

Table 5.2 Material Properties for Simulation

Properties\Material	Coarse-waste-rock (C-AR and C-L)	Fine-waste-rock (F-AR and F-L)
k_{sat} (m/s)	$1.0 \times 10^{-2} \leftrightarrow 1.5 \times 10^{-2}$	$3.9 \times 10^{-4} \leftrightarrow 8.0 \times 10^{-4}$
AEV (kPa)	0.025	1.42
Sat. VWC	0.37	0.44
Sat Suction (kPa)	0.01	0.01
GS	2.5	2.5

The Soil Water Characteristic Curve (SWCC) for the fine fraction is a fit between the values measured from a Tempe Cells test (Andrina, 2009) and Fredlund & Xing Equation (Fredlund & Xing, 1994 A). The SWCC for the Coarse-waste-rock was estimated from the Fredlund and Xing equation. The Figure 5.6 shows the SWCC for both Acid rock and Limestone materials.

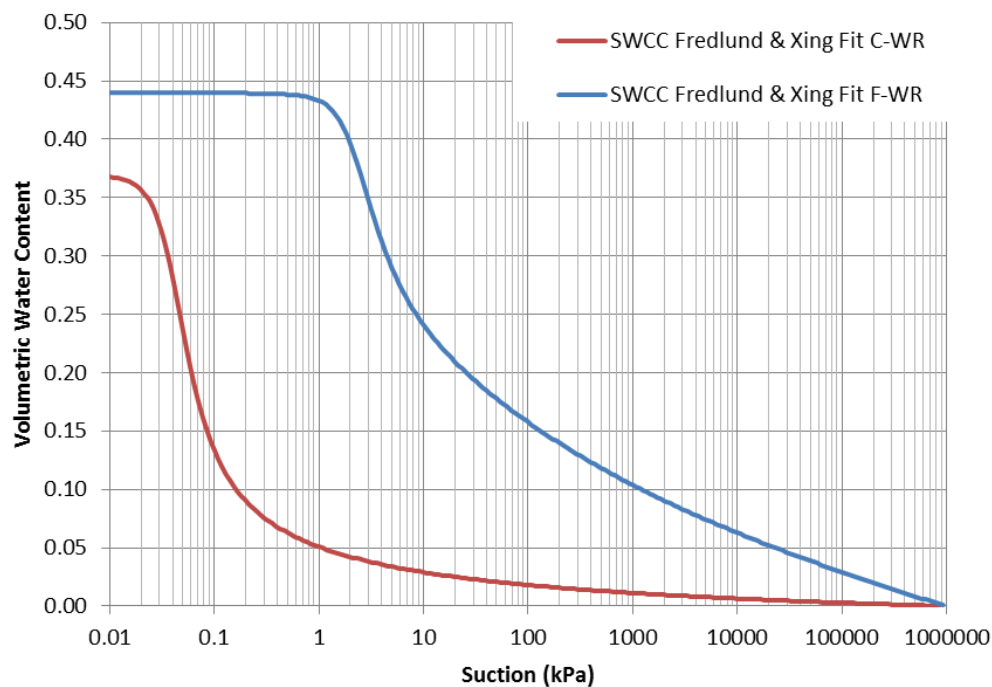


Figure 5.6 SWCC for Waste Rock in Meso-scale Experiment

Figure 5.7 shows the hydraulic conductivity curve for both Waste rock materials. The Hydraulic-Conductivity-Curves are estimated from the SWCC using Fredlund & Xing's equation (Fredlund & Xing, 1994 A). The simulations of Panel-1, Panel-2, and Panel-3 assume a minimum hydraulic conductivity (k_{min}) for all materials of $1 \times 10^{-10} m/s$. This magnitude is reached at the residual suction, this magnitude is verified not to reach k_{min} for any of the simulated cases (i.e. the internal suction of the material during the steady state analysis was lower than the residual suction).

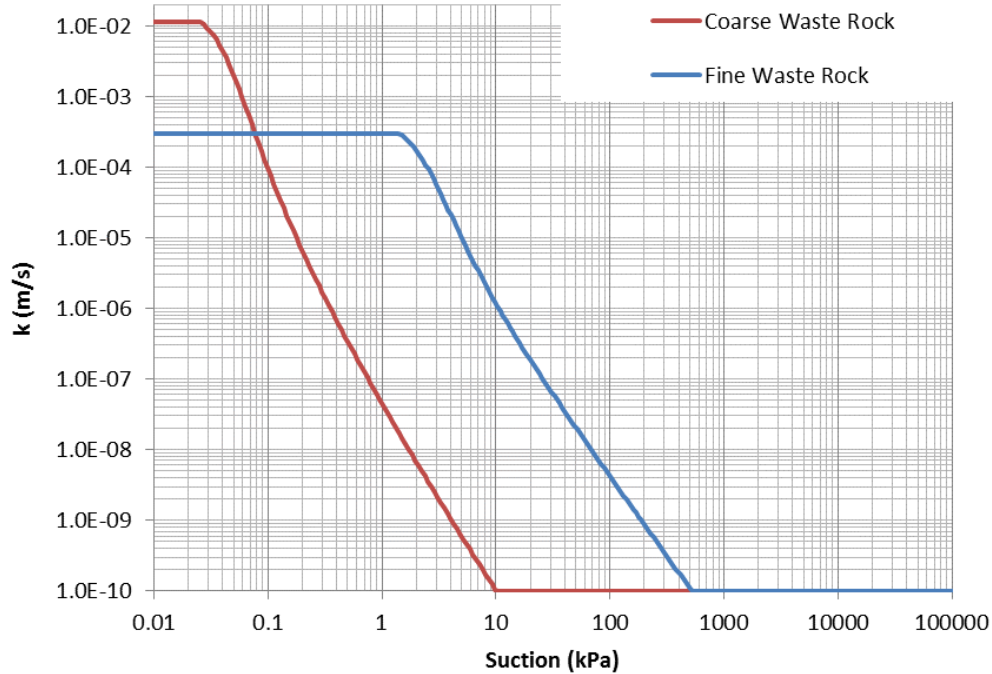


Figure 5.7 Hydraulic-Conductivity-Curves for the Meso-scale Experiment Estimations Using Fredlund & Xing (1994)

5.3.2. Experiment Results

During the laboratory experiments, once the test reaches a steady state condition, the water was collected from each drainage point (Table 2.7). This allowed a view of the preferential discharge point with respect to the location and material characteristics. The following results are presented as the percentage of flux with respect to the total precipitation rate applied at the top of each panel. The Figures 5.8, 5.9, 5.10 show the total outflow from drainage points with respect to the coarse and fine waste rock. In Panels 1 (Figure 5.8) the total discharge from the layers of fine grain (F-AR) includes drainage points L2, L4, and L6; for the layers with coarse grain (C-AR), the drainage points are S1, S2, S3, L1, L3, L5, and L7. The discharge points in Panels-2 are the same as in Panel-1. The total outflow from the layers with F-AR includes drainage points L2, L4, and L6; for the layers

with C-AR, the drainage points are S1, S2, S3, L1, L3, L5, and L7. In Panel-3 (Figure 5.9) the results are grouped in four materials (F-AR, C-AR, F-L, and C-L) and two grain sizes (Fine-waste-rock and Coarse-waste-rock).

Andrina confirmed that every layer received the same rainfall application rate by calculating the uniformity coefficient using Christiansen's formula (Andrina, 2009). Her calculation resulted in a uniformity coefficient between 97% and 99%, indicating high confidence in the boundary condition at the top of the panels. The result from the experiment showed that precipitation had an influence in the preferential discharge points. The result from the different tests lead Andrina to conclude that gravitational flow was the dominant flow mechanism as rainfall rate increased.

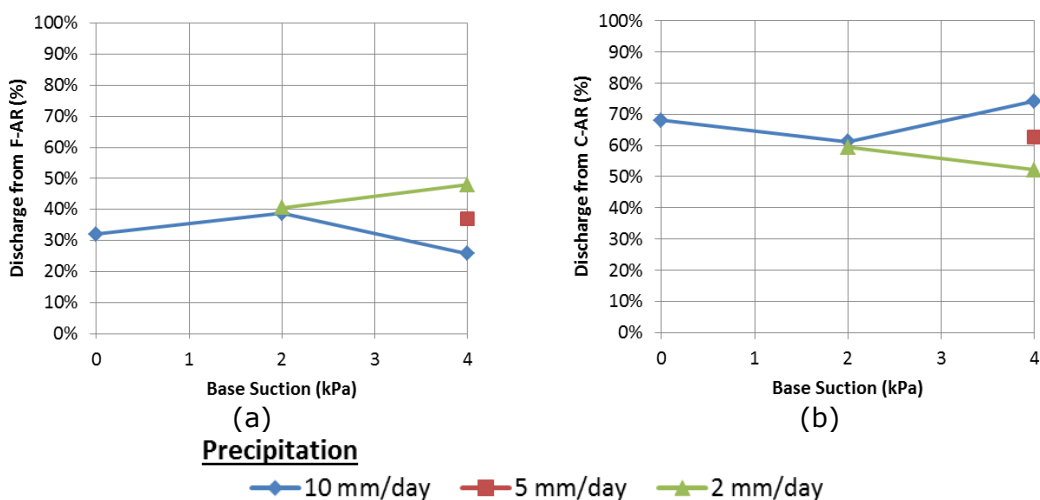


Figure 5.8 Discharge Flow of the Fine (a) and Coarse (b) Waste Rock in Panel-1 after Andrina (2009)

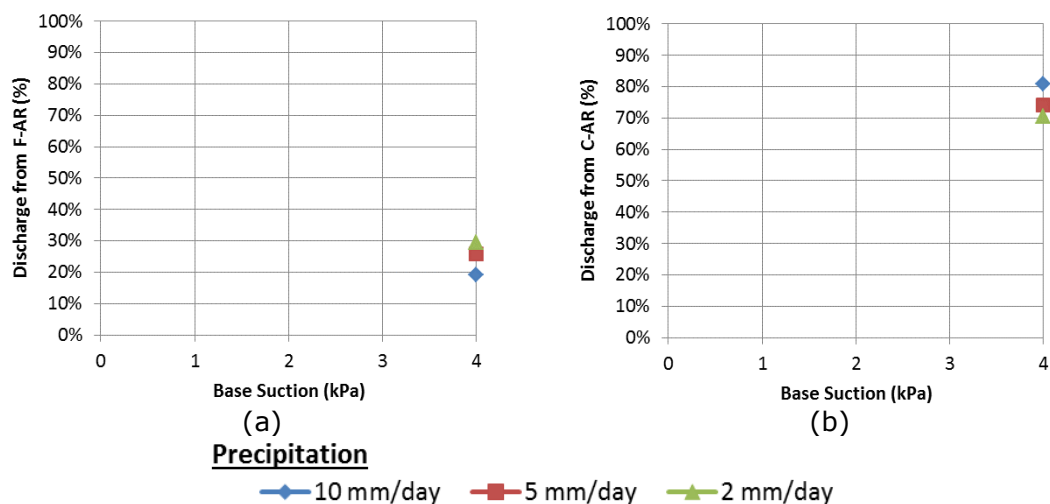


Figure 5.9 Discharge Flow of the Fine (a) and Coarse (b) Waste Rock in Panel-2 after Andrina (2009)

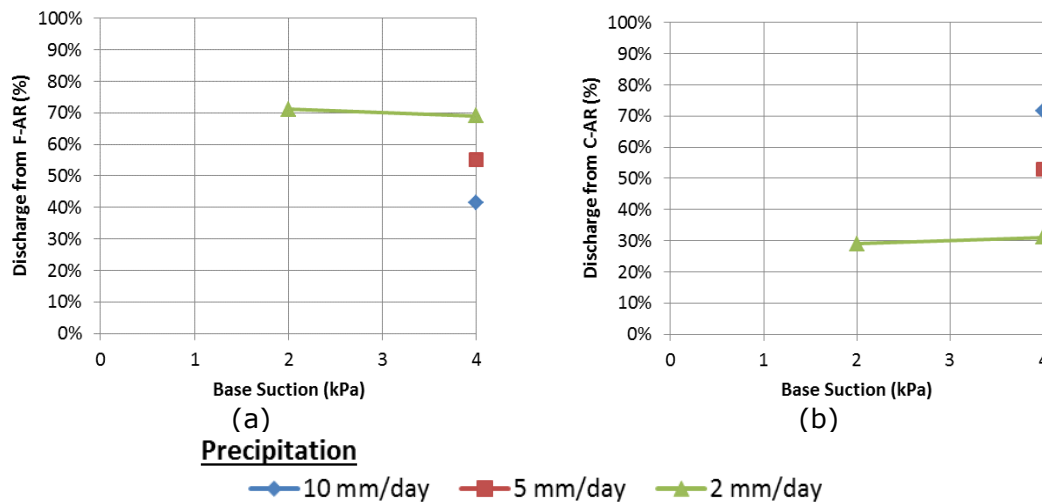


Figure 5.10 Discharge Flow of the Fine (a) and Coarse (b) Waste Rock in Panel-3 after Andrina (2009)

The matric suction during the experiment was measured from the installed instrumentations prior the installation of the lysimeters (i.e. for a base suction of 0.0 kPa). Figure 5.11 shows the matric suction for a precipitation of 2 mm/day and 10 mm/day in Panel-1 and at an elevation of 0.5 m and 1.0 m in Panel-3. Andrina reported that the experimental results showed matric suction between 0.1 kPa and 0.2 kPa in layer 6 from Panel-1. In Panel-2, the matric suction increased from 0.3 kPa to 0.6 kPa (Andrina, 2009, pp. 279-280). The matric suction increased toward the outer layer (L7 for Panel-1 and Panel-2, and L9 for Panel-3).

The results from the Meso-scale experiments show that external factors, such as precipitation and suction, have an effect on the internal conditions or mechanism that influence water flow within the system. Three models are created to simulate the experimental conditions and responses achieved during the laboratory experiment of the Meso-scale Panels. The following section describes the characteristics and assumptions present in order to achieve acceptable correlations between a numerical model and the laboratory experiment.

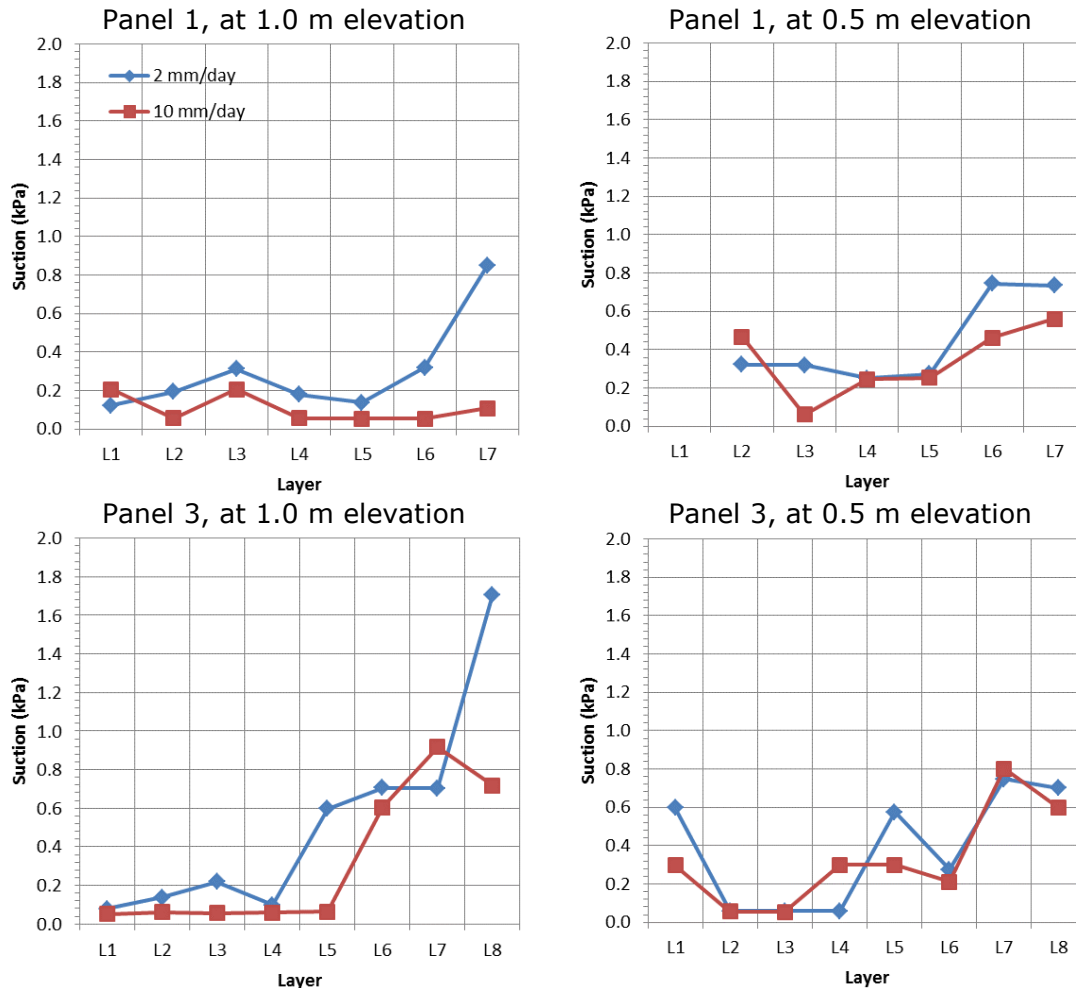


Figure 5.11 Measured Matrix Suction from Panel-1 and Panel-3 at 0.5 m and 1.0 m Elevation for 2 mm/Day and 10 mm/Day (Andrina, 2009)

5.4. NUMERICAL MODEL

The simulation of the column experiment using waste rock from Golden Sunlight Mine (i.e. Column-2) is the first step towards describing the mechanism that controls water flow in waste rock embankments. The simulations showed the effect that changes in precipitation have in a water flow regime. Mechanisms like the gradients formed at the top between the contact zones of both materials. These gradients in suction are relatively small (less than 0.4 kPa), with almost no changes in h_p for the same elevation, and are capable of generating high lateral flow between the materials.

The simulations of Column-2 show a decrease in suction with elevation, contrary to the measured matrix suction in the panel experiments; furthermore, the magnitude of suction was much greater in the column. The geometry of the column experiment has

limitations; it differs from the conditions in which a waste rock embankment is placed (i.e. the vertical orientation of the layers) or is affected by external factors, such as precipitation. The simulation of the three panels improves the descriptions of the mechanisms that controls water flow within waste rock.

The following section presents the methodology and description of the model characteristics for the three Meso-scale Panels using SvFlux from Soil Vision System Ltd.

5.4.1. Model Methodology

The methodology to evaluate the convergence of the numerical model with respect to the three Meso-scale experiments is conceptually the same as the methodology used in the simulation of the Column experiments (see section 4.4.1).

Initially to establish the model geometry, the general characteristics of the three experiments were identified (i.e. dimensions, drainage, precipitation boundaries, suction boundaries, impermeable boundaries, contact boundaries, and material boundaries) allowing the generation of a distinctive model for each panel. The simulation is compared to the laboratory result to evaluate the convergence between the numerical model and the experiment.

The convergence of the panels is controlled by two conditions based on the volume discharge from system. The calculation of the discharge is a percentage of total precipitation rates applied at the top of the panel. The first condition compares the sum of the discharge from the layer with equal material to the measures from the laboratory experiment, e.g., in Panel-1 the total outflow from fine layers is equal to the sum of water draining from L-2, L-4, and L-6. The second condition uses the "Pearson Product moment correlation coefficient" (PPMCC) to compare the difference in the discharges between each single layer from the model and the experiment. The minimum convergence of the model is set to be with a total discharge difference of less than 10% and a PPMCC greater than 0.8.

The simulations of the Meso-scale experiments started by recreating Panel-1, which is the simplest model from the three panels, and serves as the base of the other two. Panel-1 was modeled considering the discharge points from the internal slope in the first layer (i.e. S1, S2, and S3); it was observed that the characteristics of the collection points would require a 3D analysis. This condition was simplified by excluding the drainage points in the inner slope; the water collected from these points in the experiment was added to the volume collected in the first layer (L-1), thereby conserving the water balance in the system. With the defined characteristics of the model, the simulation of Panel-1 is run with the material properties from the laboratory measures, i.e. the descriptive characterization

made by Andrina (2009) for the Acid Rock. In each simulation condition of Panel-1, the volume discharging from each layer is recorded to evaluate the convergence from each case.

The high differences between the simulated results and the laboratory measures resulted in the calibration of the material properties by back analyzing the model. The back analysis of Panel-1 is made through the calibration of the Air-Entry-Value (AEV) and the saturated hydraulic conductivity (k_{sat}) for the F-AR and C-AR. The properties are calibrated individually for each test condition using an iterations process by adjusting AEV until the closest correlation with the laboratory results is achieved and before having convergence difficulties. The change on the AEV is independent for each material, i.e. the calibration of the AEV in the C-AR consisted in varying the AEV while keeping the other properties equal to the values measured in the laboratory. The AEV of the F-AR decreases from 1.4 kPa up to 0.067 kPa; in contrast, the AEV of the C-AR increases from 0.026 kPa and 0.78 kPa. On the other hand, the k_{sat} affects the preferential flow path in the system as it is shown in the simulation of the column experiment in Chapter 4. The calibration of the AEVs in the acid rock is made by using the maximum and minimum values of k_{sat} , to assess the effect of the k_{sat} on the preferential flow path as summarize in Table 5.3.

Table 5.3 Simulation Cases for Back Analysis of the AEV

Case	F-AR		C-AR	
	k_{sat} max.	k_{sat} min.	k_{sat} max.	k_{sat} min.
1	x		x	
2	x			x
3		x	x	
4		x		x

The calibration of k_{sat} resulted similar to the back analysis of the AEV. The magnitude of k_{sat} in each material varies while the other properties remain constant. The variation of k_{sat} is taken from the range of values determine by Andrina (2009). The k_{sat} of the F-AR varies between $3.9 \times 10^{-4} m/s$ (k_{sat} min.) to $8.0 \times 10^{-4} m/s$ (k_{sat} max.); the k_{sat} of the C-AR varies between $1.0 \times 10^{-2} m/s$ (k_{sat} min.) to $1.5 \times 10^{-2} m/s$ (k_{sat} max.). Furthermore, the calibration of each k_{sat} was run for the maximum and minimum values of k_{sat} of the material (Table 5.4).

Table 5.4 Simulation Cases for Back Analysis of the k_{sat}

Case	k_{sat} max.	k_{sat} min.
1	x	
2		x

The back analysis of each test in Panel-1 results in four values for the AEV of each material and in two values for the k_{sat} . This method entails eight back analyses in each test for the AEV and four in each test for the k_{sat} . The multiple approaches generate a bigger sample size to find the optimum conditions in which the model would satisfy the laboratory results. The approaches to achieve convergence result in different degrees of correlation. The results in each test are averaged and compared to define the material properties that describe most of the laboratory results.

The simulation of Panel-2 initiates with a model applying the material properties measured through laboratory testing. As it occurs with Panel-1, the model did not have a good correlation to the laboratory results. As this model involves an additional horizontal layer of C-L, the back analysis is completed only for the limestone material.

Panel-3 has a different arrangement of the layer of Panel-1 and Panel-2, adding a higher complexity by including coarse and fine limestone between the incline layers, thus resulting in four materials. Considering that the acid rock and limestone share similar properties with respect to the grain size distribution, the simulation of Panel-3 is limited to three cases to evaluate the convergence with a model. The first case applies to the model using material properties measured through laboratory testing for both the acid rock and limestone. The second case consists of applying the material properties from the laboratory to the limestone, and the calibrated properties of the Acid Rock from Panel 1. The third case consists in applying the material properties from the laboratory to the fine limestone (F-L); the calibrated properties for F-AR and C-AR from Panel 1; and C-L equal to the calibration of C-AR. As mentioned, C-L and C-AR share similar characteristics.

Finally, in order to demonstrate the application of the numerical model to different materials Panel-1 is modeled using the three different sets of material properties for the fine and coarse fraction of the layers. The first and second set of material properties include the calibrated simulations from the column experiments presented in Chapter 4 for the sandy material (BCS and SS) and the waste rock from Golden Sunlight (F-WR and C-WR). The third set of the material properties uses Tailing Beach Sand and Devon Silt, materials characterized in research from colleagues at the University of Alberta (Abdulnabi, 2015) (Kouakou, 2014) (Torghabeh, 2013).

In the modelling of the three panels, the parameters evaluated taken during the simulations include the discharge percentage in each layer with respect to the total precipitation flux; the profile calculation of change in h_p , flux vectors and stream traces; and the change in matric suction at the elevation equal to the laboratory instrumentation.

5.4.2. Model Assumption

Certain assumptions are made in order to find reasonable solutions in the model to recreate the Meso-scale experiment for Panel-1, Panel-2, and Panel-3 using numerical simulations. It is necessary to balance the computational efforts with the degree of accuracy of the model. The solutions for the PDE's, describing the seepage analysis with SvFlux, have the following assumptions:

- I. The model is in steady state condition.
- II. The materials are in unsaturated conditions and describe Fredlund and Xing's equations for the SWCC and the hydraulic conductivity curve.
- III. The materials are continuous, homogeneous, and isotropic.
- IV. The suction applied at the base of the panel is equal for all layers.
- V. The rainfall applied at the top of the panel is equal for Layers (for L2 to L7 for Panel-1 and Panel-2; and for L2 to L9 for Panel-3).
- VI. The internal slope in Layer-1 is impermeable.
- VII. The total drainage at the base of Layer-1 takes into account the collected water from the drainage systems at the internal slope.
- VIII. The filter material at the base of each layer of 3cm to 5 cm is negligible.
- IX. The evaporation and runoff at the top of the panel is negligible.
- X. The density of the water leached is 9.8 kN/m^3 and a viscosity of 0.001 kg/m-s .
- XI. There are no effects on water pressure due to changes in temperature.
- XII. The effect of the acrylic walls on water flow is negligible.

5.4.3. Theory Adopted for the Numerical Integration for A Column Layered System

The Meso-scale experiments made by Andrina (2009) are simulated through numerical models to recreate the conditions and results. The simulation is made using commercially available software called SvFlux Version 7.0 from SoilVision Ltd. The software uses FlexPDE to solve Partial Differential Equations (PDEs) that describe water flow through the soil. The model runs under steady state conditions, as it was established in the experiments.

The following PDE governs water flow for a 2-D model, under steady state and no evaporation conditions, and for a heterogeneous, anisotropic, saturated-unsaturated soil.

$$\frac{\partial}{\partial x} \left[k_x^w \frac{\partial h}{\partial x} \right] + \frac{\partial}{\partial y} \left[k_y^w \frac{\partial h}{\partial y} \right] = 0$$

Where:

x, y = components on the horizontal and vertical direction, respectively.

k_i^w = hydraulic conductivity in the i -direction, m/s.

h = hydraulic head, m.

The PDE is derived by preserving the mass balance principle, while considering that no volume storage is allowed due to the steady state condition. In other words, the amount of water coming into the system has to be equal to the amount of water coming out. For a steady state condition, it is assumed that there is no volume change in the material and the total stress is constant.

The model also satisfies Darcy's Law to describe the movement of flow for liquid water; the driving force is the change or the gradient in the Hydraulic Head (h). The generalized expression of Darcy's law for a saturated and unsaturated soil is expressed as (SoilVision Systems Ltd., 2012):

$$v_i^w = -k_i^w(\Psi) \frac{\partial h}{\partial i}$$

Where:

v_i^w = water flow rate in the i -direction.

$k_i^w(\Psi)$ = hydraulic conductivity in the i -direction as a function of the matric suction (Ψ).

h = hydraulic head, m.

The control error for the dependent variables (i.e. total head) in accuracy and spatial accuracy (i.e. error limits for the solution) in each simulation is kept equal to 0.002 as suggested by the software manual for 2D models. In addition, the solution is found through a quadratic (second order) interpolation of the finite elements. The second order interpolation consists in a subdivision of the domain in triangular elements composed of six nodes. The elements of the models have a maximum spacing between nodes of 5.0 cm. The model runs with an automatic mesh refinement algorithm; nonetheless, refinement of the mesh was established at the basal drain and the precipitation boundaries with nodes spaced 1.0 cm. Also, at the elevation of the instrumentation the nodes are spaced 2.0 cm. Figure 5.12 illustrates for Panel-1 the mesh generation and refinement made at the base boundary, the precipitation boundary, and the location of instrumentation. The differences of the mesh configuration in Panel-2 and Panel-3 are related to the change in geometry of the model. The refinement at the elevation of instrumentation allows improving the comparison of head pressure distribution between the model and the experiment.

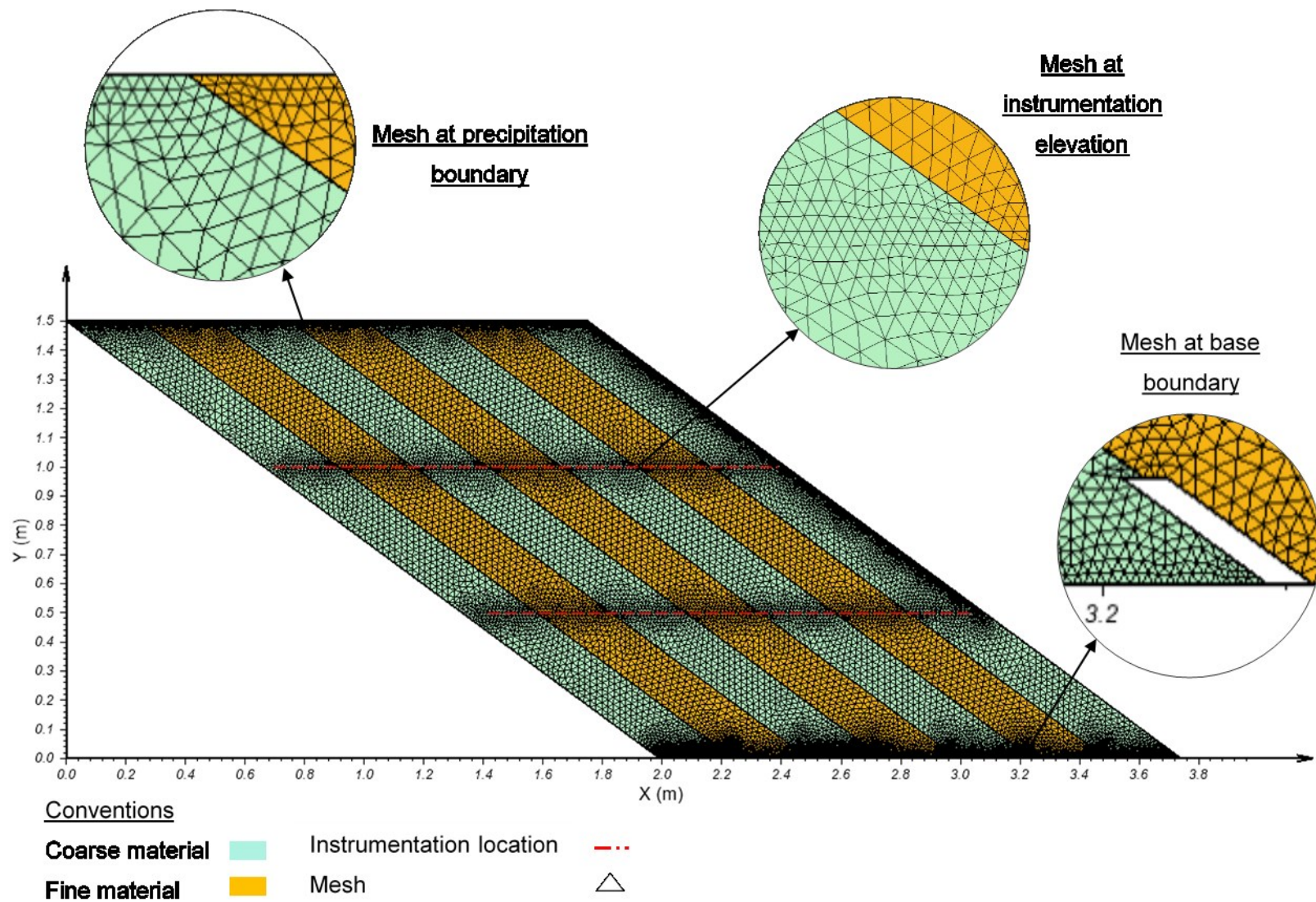


Figure 5.12 Mesh Geometry for Panel-1

For steady state conditions, the models runs in a two stages analysis. First, the software solves the model in saturated conditions in order to stablish the initial conditions (i.e. head pressure distribution); for the second stage, the calculated solution is in unsaturated conditions. The calibration of the unsaturated properties of the materials; Saturated-Hydraulic-Conductivity (k_{sat}), and Air-Entry-Value (AEV) are made through a multi stage analysis, which consists in applying a deterministic range of values for k_{sat} and AEV for each case.

5.4.4. Model Boundary Conditions

The Meso-scale models are built by applying similar boundary conditions as were established in the laboratory experiments. The numerical model has three types of boundary conditions:

- Climate: specifying the precipitation flux and runoff conditions at the top of the panels. This boundary allows the application of a constant flux evenly in the top boundary.
- Pressure Head: specifying the suction produced by the lysimeters at the base of each layer. The suction is applied to the model as a negative head pressure in each layer.
- Zero Flux: specifying the boundaries where water cannot break through. The structure of the panels and division at the base between the materials were made of acrylic sheet with seals at the joints to restrain any leakage or infiltration. The model considers the external boundaries and the division strips as Zero-Flux boundaries.

The layout of the panel experiments ensured three precipitation conditions and three base suctions. Each panel was tested under different combinations of precipitation and base suctions to evaluate water flow in waste rock in unsaturated condition. All panels were composed of layers of waste rock with a cross section of 25 cm X 25 cm and inclined at 37°. The first and second panel had seven layers, while the third panel had two additional layers. The height of the first and third panel was 1.5 m, while the second panel had an additional 50 cm of horizontal layer on the top incline layers.

The model for each of the three panels has a drainage boundary at the base of each layer that enables the measurement of the water outflow. The drainage boundary applies suction equally to the one exerted by the lysimeters installed during the Meso-

scale experiment. Figure 5.13 shows the geometrical characteristic applied to the model in Panel-1, and similarly to Panel-1 and Panel-3.

The Meso-scale experiment had installed acrylic strips at the base and at the internal slope of Layer-1. The strips located at the base of the panels are placed between the contacts of the layers to avoid water crossover; these strips are represented in the model by a gap of 1.0 cm width, 2.0 cm vertical height and incline 37° (Figure 5.13). The strips located in the slope collected water at different elevations of L1; nonetheless, these strips are considered negligible, as it does not affect the head pressure distribution and preferential flow path.

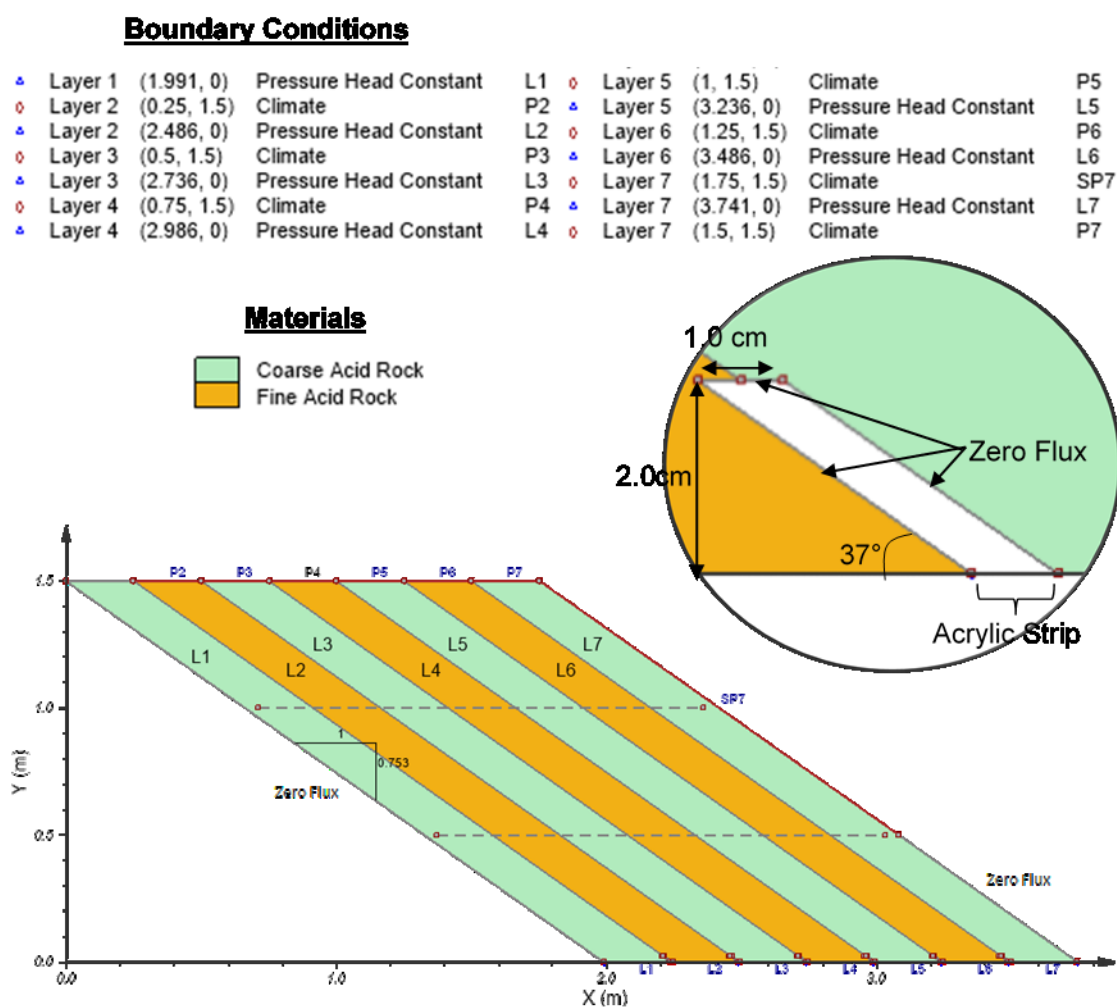


Figure 5.13 Boundary Conditions and Geometry of Panel-1

Following the definition of the material characteristics, geometry, boundary conditions, mesh geometry, and convergence criteria, the simulation results for three models are shown in the following sections.

5.5. SIMULATION OF PANEL-1

The following results present Panel-1 simulation under six test conditions. The simulation is evaluated for two cases to obtain optimum convergence. The first case analyses correspond to a model applying equal material characteristics to the laboratory measures. The second case analyses have an adjustment of the material properties to improve convergence.

The model of Panel-1 is also evaluated using three additional sets of material properties, the description of the model, comparisons and analyses are found in Appendix A.

5.5.1. Simulation Applying Experimental Conditions and Measure Properties

The solution of the first case analyses shown in Figure 5.14 shows the total discharge flow from the fine and coarse layers from the simulated results (F-AR and C-AR) and laboratory measurements ("F-AR lab" and "C-AR lab"). The total outflow is calculated as a percentage of the total applied rainfall rate for 2 mm/day, 5 mm/day and 10 mm/day.

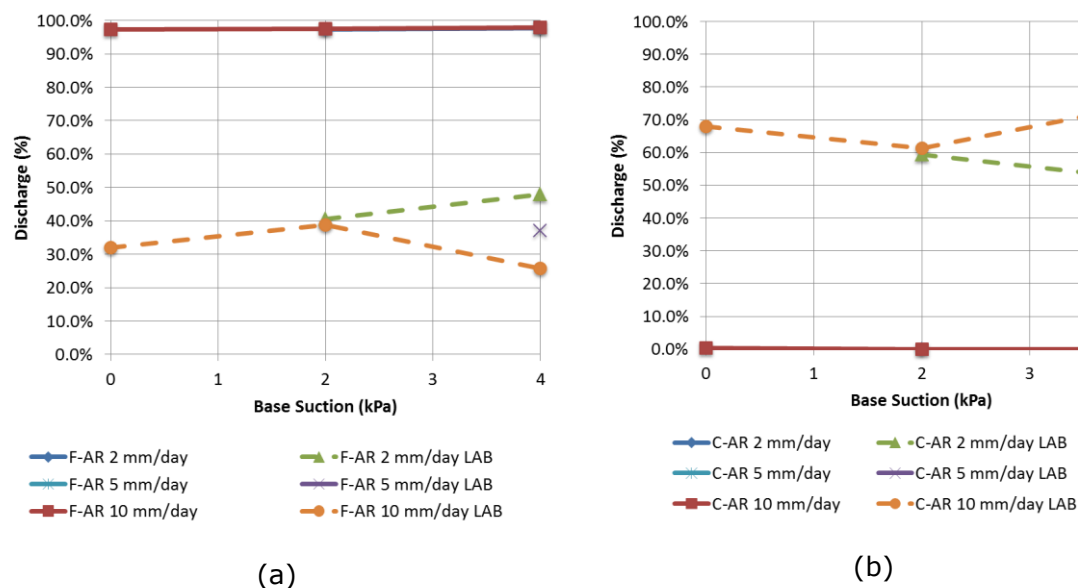


Figure 5.14 Simulation of Total Outflow for Panel-1 under Laboratory Conditions for the Fine Layers (a) and Coarse Layers (b)

It can be seen in Figure 5.13 that under the laboratory condition the numerical simulation for Panel-1 overestimates the discharge from F-AR and underestimates the discharge from C-AR. The simulated condition shows preferential flow in the fine layers, maintaining almost 99% of the total flow. Flow in the fine layers and coarse layers are constant regardless of the change in Flux rate and base suction.

On the other hand, it should be noticed that the laboratory results for a base suction of 4.0 kPa and 10 mm/day are misleading. The laboratory results show that increasing the base suction from 2.0 kPa to 4.0 kPa, results in 15% less discharge from F-AR. The increment of the base suction should increase the hydraulic conductivity of the material, thus resulting in increased discharge through the F-AR.

The high divergence between the numerical simulation and the laboratory measurement suggests that the model is not generating a proper head pressure distribution. The simulation shows high head pressure gradients at the top of layers 3 and 5, driving the water from the coarse layers to flow into the fine layers. Figure 5.15 shows the computed head pressure contours for a rainfall rate of 10 mm/day and 4.0 kPa of suction.

The unsaturated condition of the waste rock generates negative head pressure distribution. The suction decreases with depth until it reaches the base boundary condition of 4.0 kPa. The numerical simulation shows that high gradients of suction are generated between the coarse and fine layers at the top of the panel. The gradient decreases with depth and reaches a constant h_p at an elevation below 0.4 m for layers one to five.

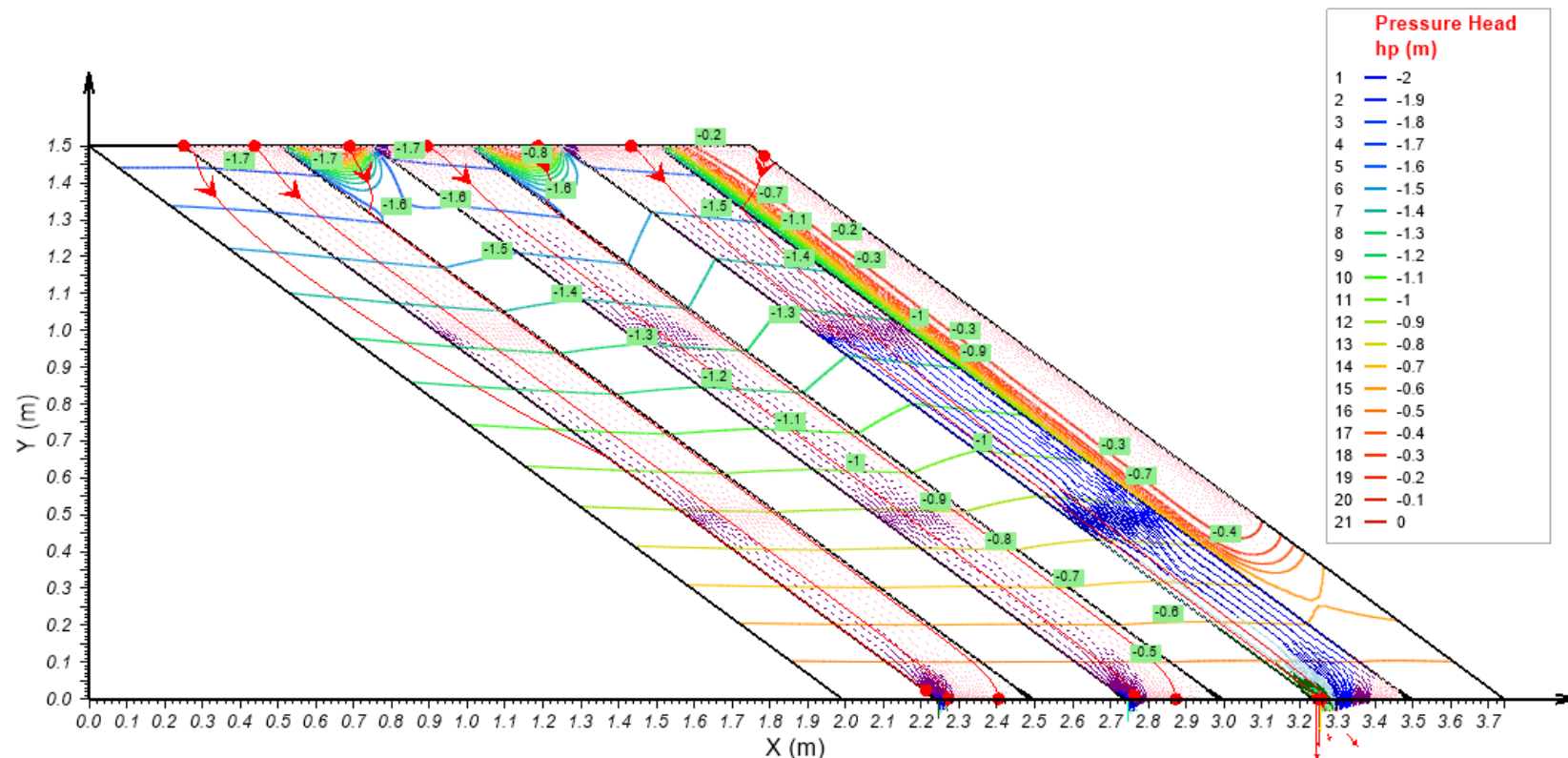


Figure 5.15 Head Pressure, Streamtraces and Flux Vector for Panel-1 for 10 mm/Day and 4 kPa of Suction

The flux vectors in Figure 5.15 revealed that the layers of F-AR draw water from the adjacent layers due to the low permeability in the C-AR under unsaturated conditions. This flow shows that the geometrical distribution of the interbedded layer can increase the amount of water flowing through individual layers. Furthermore, layer 5 is acting as a capillary barrier as all the precipitation that infiltrates layer 6 and 7 flows downwards in the direction of the layer.

The numerical simulation of Panel-1 has no correlation to the experimental results (i.e. measure properties, geometry, and boundary conditions) using the reported conditions by Andrina (2009). This divergence from the simulation could be related to the following:

- The boundary conditions: the *boundary conditions* have an important role in the head distribution and could not have been well defined in the model or not well identified in the experiment. However, the precipitation boundary had a uniformity coefficient (calculated in the experiment by Andrina) above 97%. Still, the base suction is part of the variable's inspect in the model.
- The material properties: the measurements of the *material properties* are not an accurate representation of the conditions in which the layers were placed in the panel.
- The mathematical formulation: the *mathematical formulation* that describes water flow in unsaturated conditions requires improvement or further detail, as some conditions might not be modelled numerically. The analysis of the mathematical formulation would require extensive experimental data (not available at the time) beyond the scope of this experiment.
- The geometry of the model: *geometrical aspects* can alter the head distribution due to changes in inclination and height of the panel; the width of the layers; the distribution of the layering system; the drainage system; and the rainfall simulation. Nonetheless, the geometry is not a characteristic that should be altered in order to improve convergence of a model; as the geometry is the essence of the problem to be solved. Nonetheless, the model should be as simple as it is accurate. The discharge points in the inner boundary of the first layers are not considered, as it these points do not affect the outcome of the model formulation.

5.5.2. Simulation of Panel-1 with Calibrated Properties

The numerical model of Panel-1 requires calibration due to the low correlation in the simulations from using the material properties measured in the laboratory experiment. The second case analysis of Panel-1 shows the improvement of the model by the calibration of the material properties, increasing AEV of the C-AR to 0.54 kPa. Detailed information in the calibration process and values are referenced in Appendix A. Figure 5.16 shows the discharge results from F-AR and C-AR in Panel-1 after the calibration of the AEV for the tests conducted in the laboratory experiment. Figure 5.16 also shows the results from the laboratory experiment for each test in Panel-1.

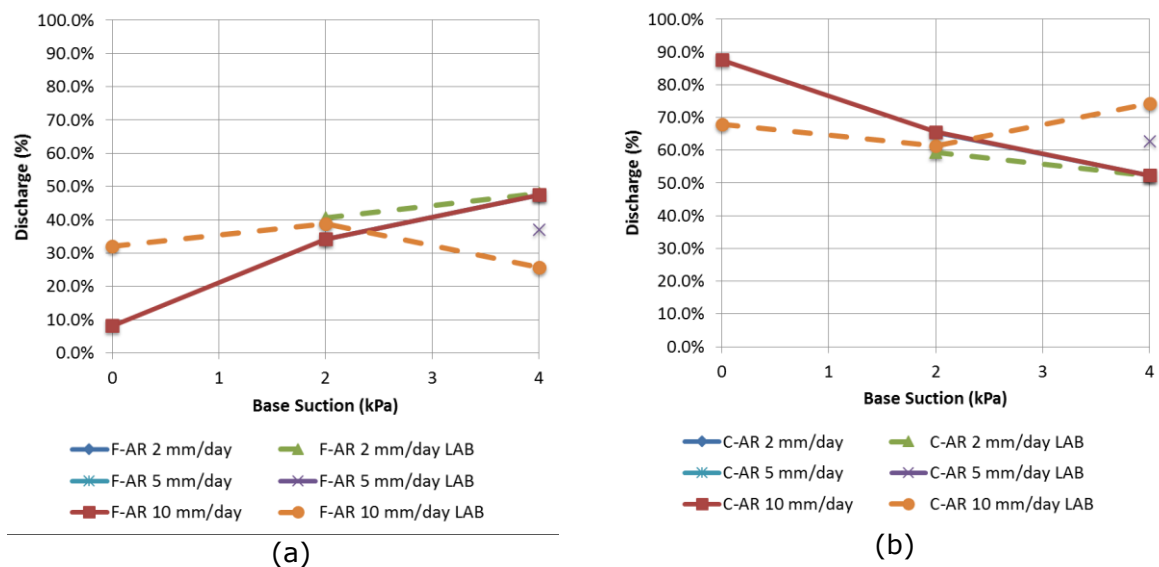


Figure 5.16 Simulation of Total Outflow for Panel-1 Using Calibrated Parameters in the Acid Rock for the Fine Layers (a) and Coarse Layers (b)

The results from the simulation produce a high improvement in the correlation of Panel-1. The calibrated parameters of the Acid Rock decreased the discharge from the fine fraction and increased the discharge from the coarse fraction. Despite that there is a higher divergence at a suction of 0.0 kPa, the model shows an expected trend of increment in discharge from the F-AR with increment of suction. This trend is also evidenced at a precipitation of 2 mm/day, where the model has the highest convergence for two suction conditions.

The simulations applying a base suction of 2.0 kPa and 4.0 kPa have the same percentage of total discharge, regardless of the precipitation amount, as occurred in the laboratory experiments. The amount of discharge increased, but the proportion

resulted equally for the three cases. Andrina expressed that the impact in increasing the precipitation did not have significant impact in the individual layers.

In the model, the mesh was refined at the elevations where the instrumentation was located in the experiment of Panel-1. The matric suction as shown in Figure 5.16 in the simulations is measure for the six tests in Panel-1, as it was measured in the experiment.

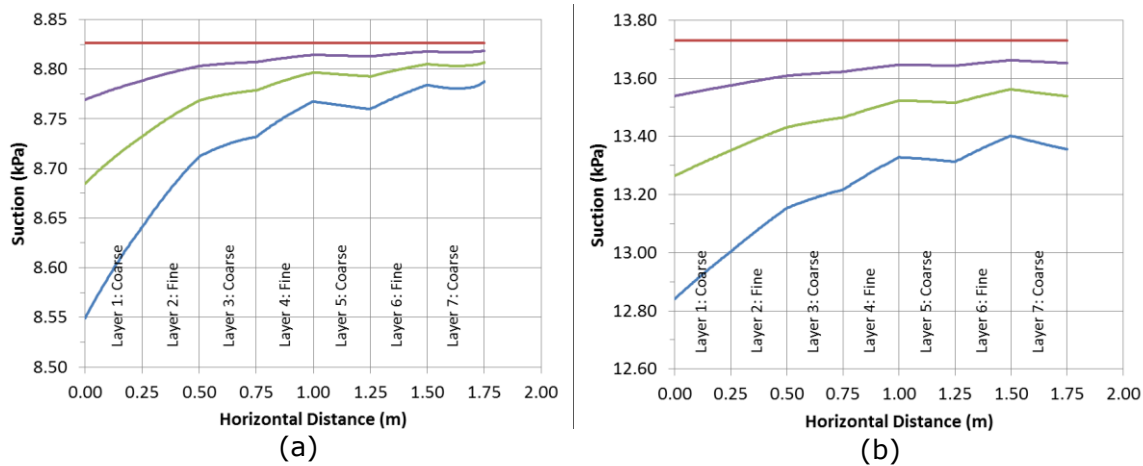


Figure 5.17 Simulated Matric Suction at 0.5 m (a) and 1.0 m (b) Elevations Applying a Base Suction of 4.0 kPa

The change in suction with distance is extremely low, but enough to generate changes in the preferential flow path of 30%. The changes from layer one to seven range between 0.1 kPa to 1.0 kPa. This variance at elevation increases with the precipitation rate and does not increase with the base suction (e.g. at 50 cm for 10 mm/day). The result from the simulations diverge from the measurements in the laboratory (see Figure 5.11). In the model there is approximately a constant increment of matric suction from Layer 1 to Layer 7. The increment is greater in the first two layers and starts to decrease; nonetheless in every layer of F-AR the increment in suction peaks, while the C-AR drops. These changes in suction become less significant as the precipitation decreases; nonetheless the suction increases with precipitation.

The previous curves demonstrate that change in suction is related to the precipitation, the base suction, the materials, and elevation. In all tests suction increases towards the outer slope of the panel; however, the rate of change is not constant. The first Layer has the highest change in suction among the coarse layers, while in Layer 3, there is a lower change and less again to Layer 5 and 7. In the fine

layers, suction always increases towards the outer slope. With respect to the elevation, the magnitude of suction at 1.0 m is highest.

The effect of precipitation on the suction reveals that higher precipitations generate lower magnitude of matric suctions; however, the rate of change is greater at higher precipitations. Similarly, base suction influences the magnitude of matric suction in the system. The increment of base suction increases the internal suction of the panel and also the ratio of increment in suction.

The simulations reveal that the first two layers are the preferential discharge zones. The streamlines show that water flows to the discharge points below the zone of applied precipitation as shown in Figure 5.18. However, the path is not exclusively a gravitational flow. The flow-vectors display that water shifts through the fine layers once breakthrough occurs between the contact zones as can be seen in Figure 5.19 and Figure 5.20.

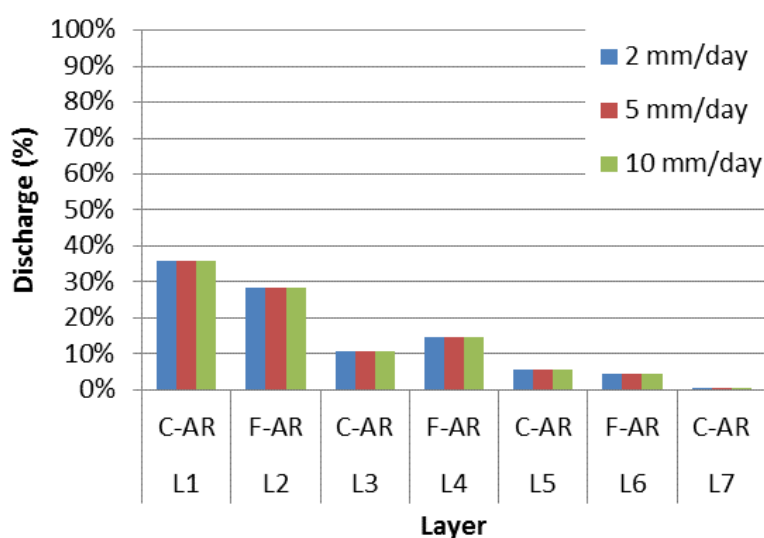


Figure 5.18 Contrast Discharge at Three Precipitation Rates in Panel-1
Applying a Base Suction of 4.0 kPa

The velocity vector shows the preferential flow path through the F-AR (L2, L3, and L4). However, the flow does not occur through the entire length of the layer, rather only below the area of precipitation. The increment of precipitation generates a slight change on the h_p profile, increasing suction for all the layers. At 2 mm/day the h_p is constant at the same elevation, but at 10 mm/day there are slight increases at the same elevation. The suction at the top has an increment of 1.0 kPa for a precipitation of 2 mm/day compared to 10 mm/day. However, this increase does not affect the discharge percentage for any layer (Figure 5.18).

The results in Figure 5.18 reveal that the relative discharge is not affected by changes in precipitation; in addition, the simulations show minor changes in the preferential flow path. Figure 5.19 and Figure 5.20 shows the profile of Panel-1 for a precipitation of 2 mm/day and 10 mm/day; with a base suction of 2.0 kPa. The simulations show low influence on the h_p distribution; therefore, the base suction has a greater effect on the preferential flow in Panel-1 as a variable affecting the model. Figure 5.21 shows the profile of Panel-1 for a precipitation of 10 mm/day, and a base suction of 0.0 kPa. Figure 5.22 shows the profile of Panel-1 for a precipitation of 10 mm/day, and a base suction of 4.0 kPa. Additional profiles of Panel-1 are found in Appendix A.

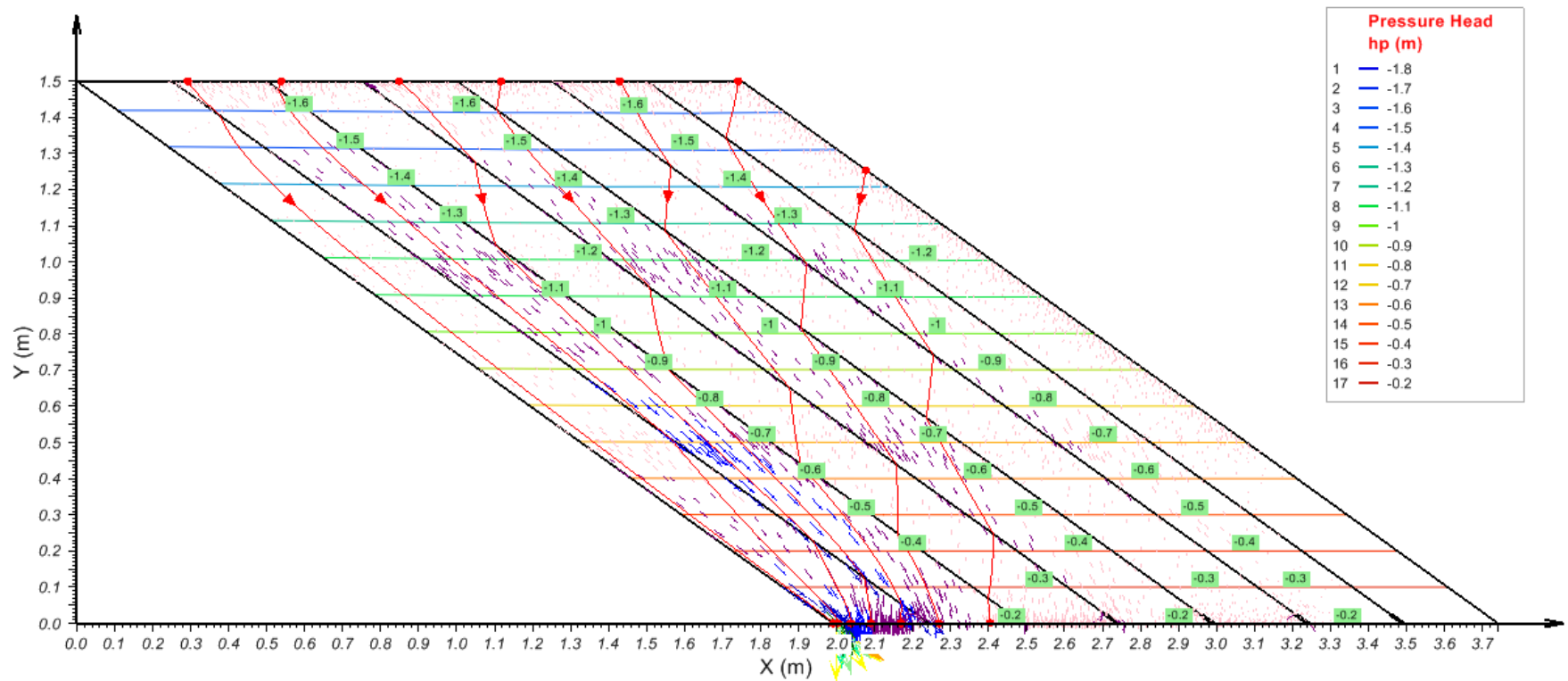


Figure 5.19 Simulation of Panel-1 using Calibrated Parameters under a Precipitation of 2 mm/day and a Base Suction of 2.0 kPa

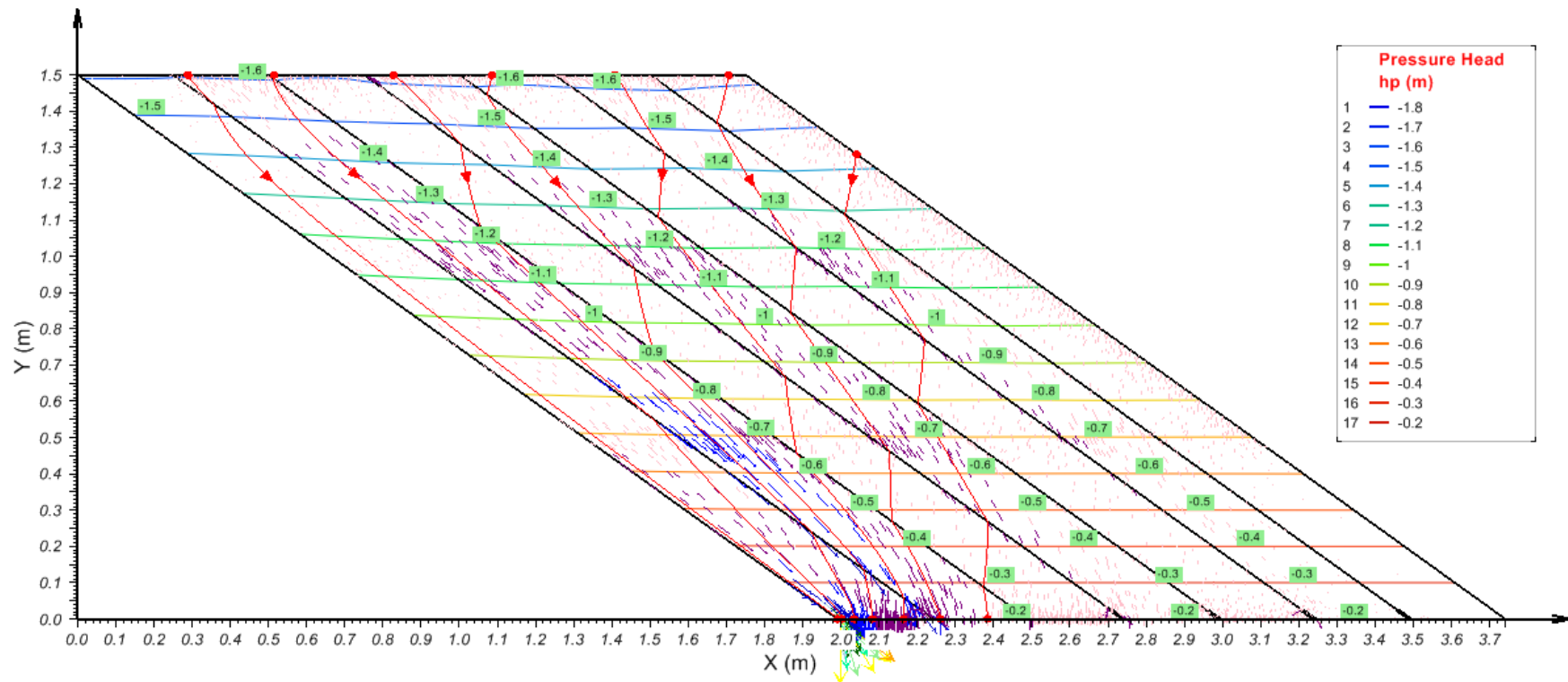


Figure 5.20 Simulation of Panel-1 using Calibrated Parameters under a Precipitation of 10 mm/day and a Base Suction of 2.0 kPa

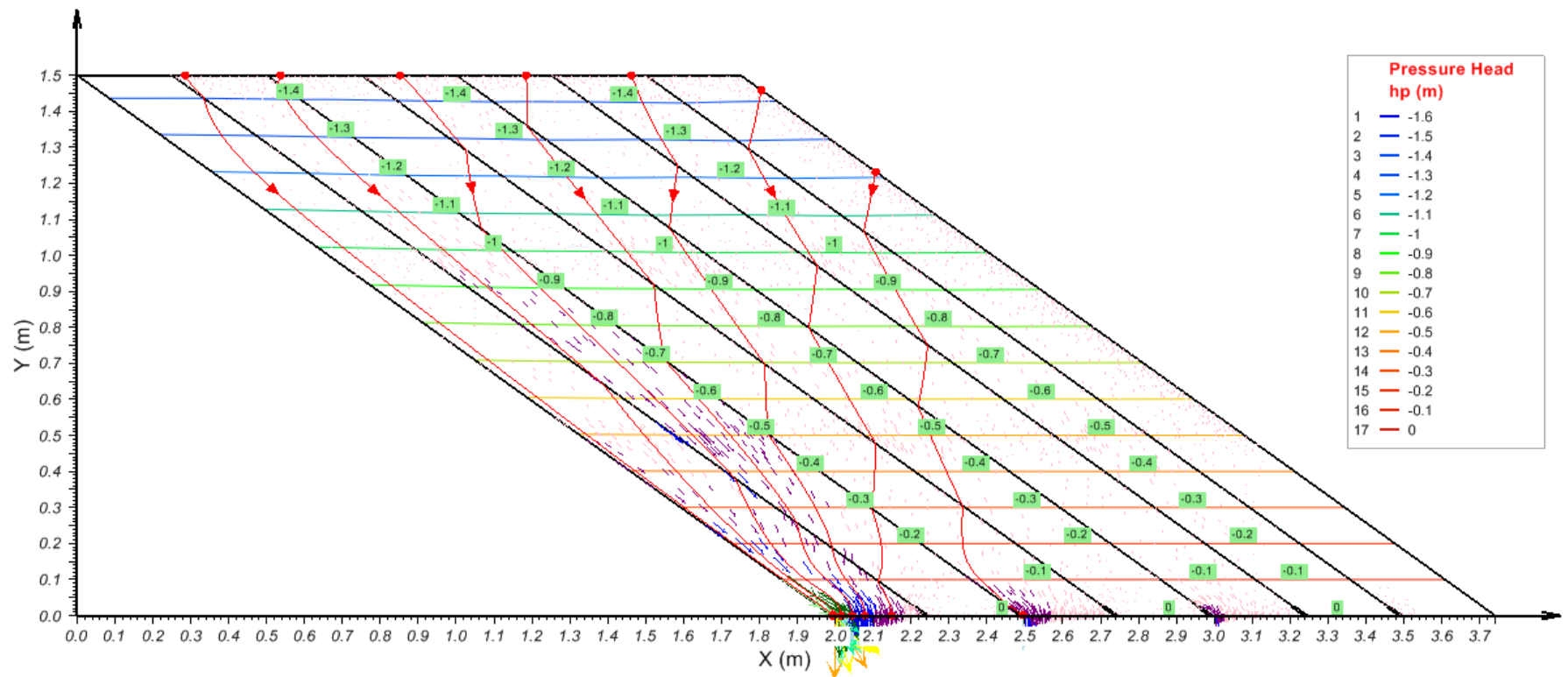


Figure 5.21 Profile Simulation of Panel-1 using Calibrated Parameters under Base Suction of 0.0 kPa and a Precipitation of 10 mm/Day

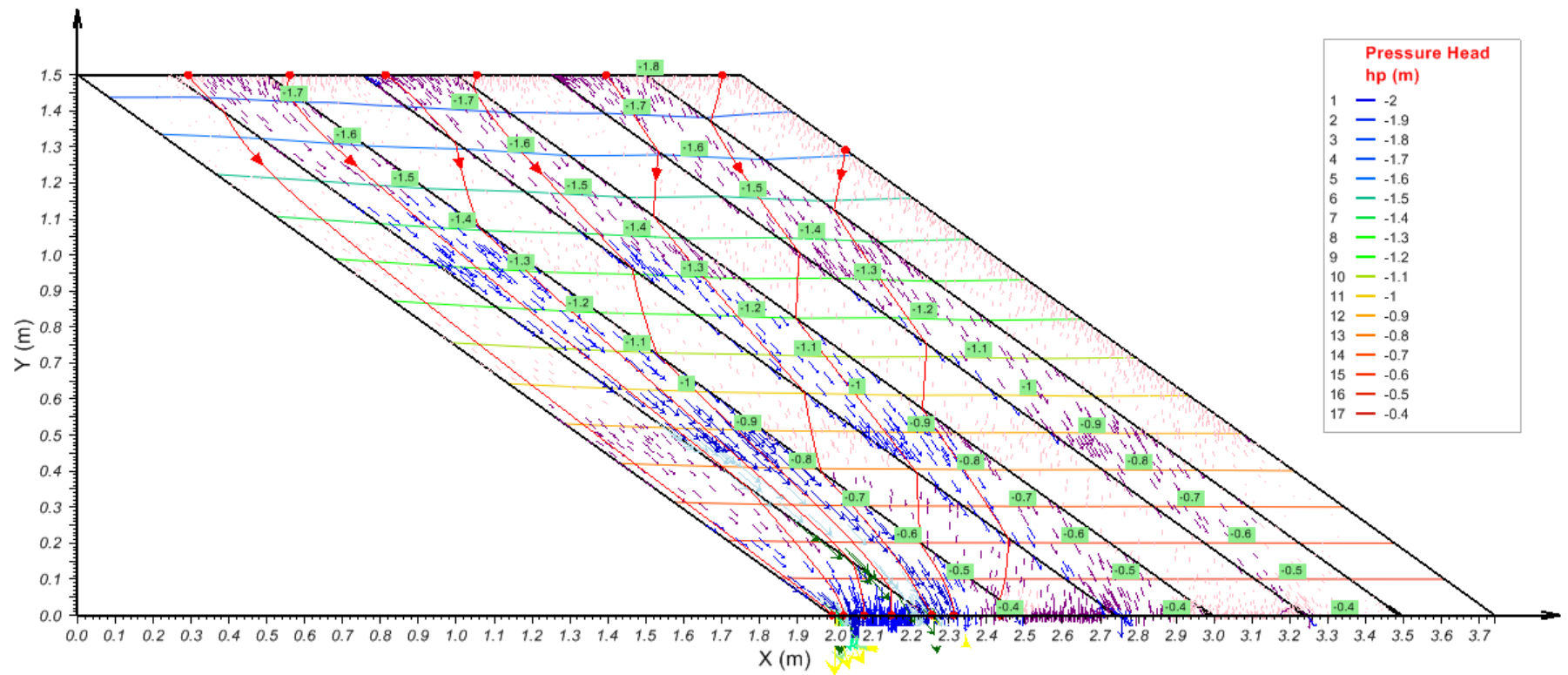


Figure 5.22 Profile Simulation of Panel-1 using Calibrated Parameters under a Base Suction of 4.0 kPa and a Precipitation of 10 mm/Day

A change in suction has a major impact on the water flow through the panel. As suction increases, more water flows through the fine layers and for a longer distance. The increment in suction distributes water through all the layers. Comparing h_p at the same elevations, there is a change in suction equal to the difference in suction applied at the base.

Figure 5.23 shows a relationship between the discharge and suction to the material properties. The histogram reveals that decreasing suction generates an increment in the discharge from the C-AR, while this decrease generates lower discharge from the F-AR.

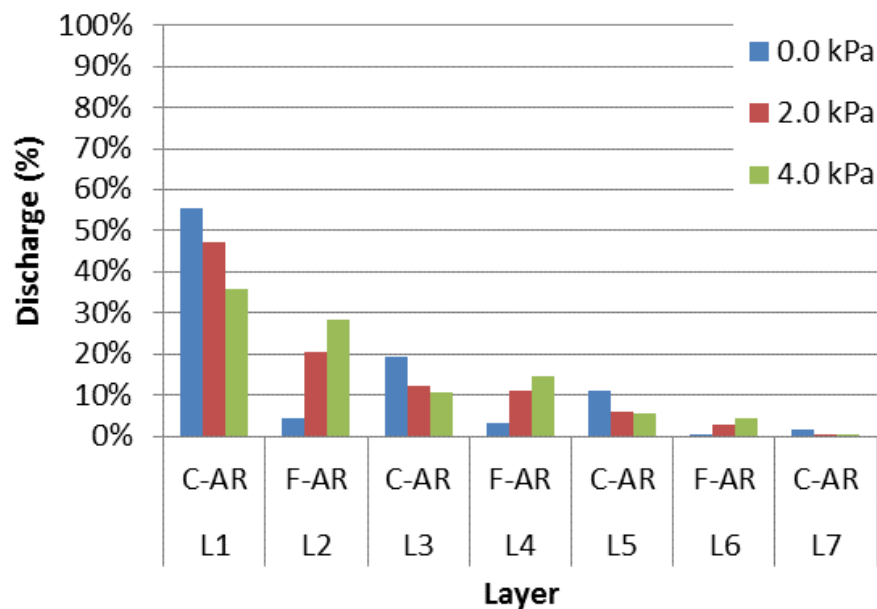


Figure 5.23 Water Flow in the Discharge Points at a Precipitation of 10 mm/Day

The increase in suction decreases the discharge in the C-AR and increases in the F-AR. These changes in discharge decrease with the increase of suction and distance to L7, as shown in Figure 5.23. Suction changes the preferential discharge material from coarse to fine; at 0 kPa to 4 kPa, the total discharge from the coarse layers decreases from 87% to 52%.

5.6. SIMULATION OF PANEL-2

The following results present Panel-2 simulation under three test conditions, for a precipitation of 2 mm/day, 5 mm/day and 10 mm/day under a base suction of 4.0 kPa. The simulation is evaluated for three cases to obtain optimum convergence.

- The first case analysis correspond to a model applying the equal material characteristics of the laboratory measures.
- The second case analysis consist in applying the material properties from the laboratory for the C-L, and the calibrated material properties from Panel-1 for the Acid Rock.
- The third case analysis apply the calibrated material properties from Panel-1, and assumes the C-L properties are equal to C-AR. The assumption in the third case is based on the similarity between the grain size distributions of the materials.

Figure 5.24 summarizes the results of total discharge from the fine and coarse layers in Panel-2 for the simulation of the three case analyses and the experimental results.

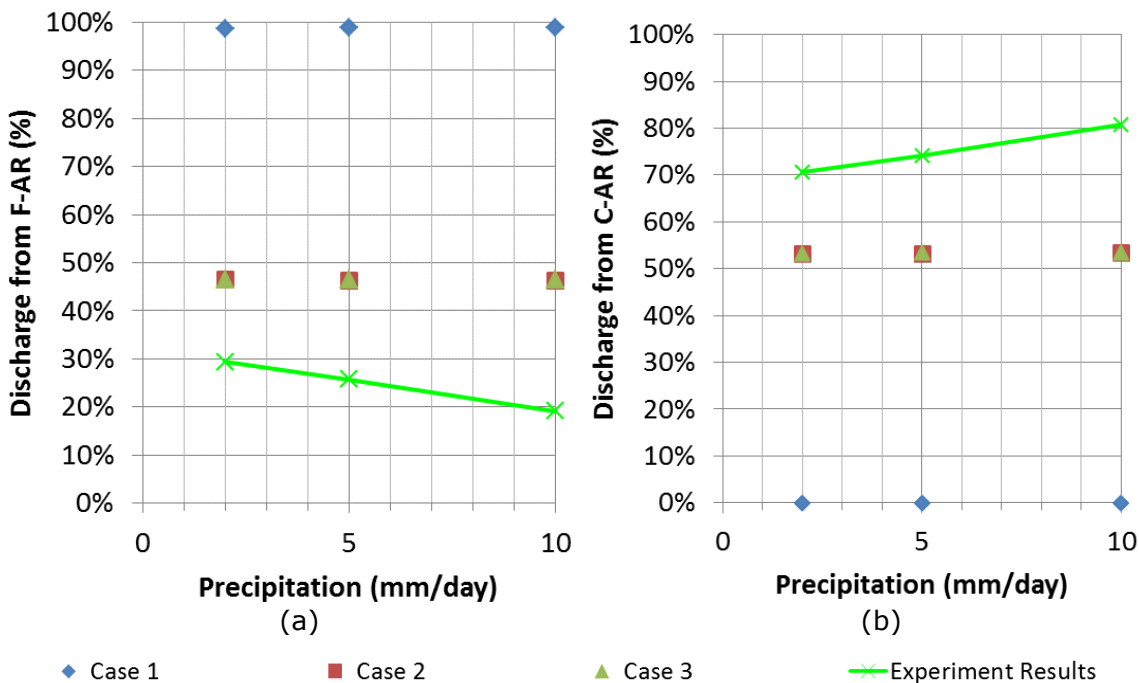


Figure 5.24 Simulation of Total Outflow for Panel-2 under a Base Suction of 4.0 kPa for the Fine Layers (a) and Coarse Layers (b)

The simulation of Panel-2 using the measured properties from the experiment results in a high overestimation of the discharge of the F-AR. The three test results are not influenced by changes in precipitation as they occur with the simulation of Panel-1; the discharge volume increases with precipitation but the proportions remain equal for the system. Nevertheless, the experimental results did not have any high contrasting differences in discharge. In the three tests, the difference was less than 10%.

Applying the properties calibrated from Panel-1 (Case 2) indicates a 53% improvement in the discharge response from the simulation of Panel-2. Also, the model does not display any effects in the proportions in the discharge with respect to changes in precipitation; the ratio results in approximately 50/50 discharge from each material. Furthermore, the results from Panel-1 under the same testing conditions (i.e. base suction of 4.0 kPa) only have a 1% discharge difference to Panel-2. This result indicates no external influence from adding the top material in the preferential discharge points.

The simulation results from the third case analysis are equal to the discharge in Case 2. The results from the third attempt to improve convergence of Panel-2 show that calibrating the two hydraulic properties used in this research (i.e. AEV, and k_{sat}) for the top layer does not have any effect on the preferential discharge points of the simulations. This lack of effect was verified also through a sensitivity analysis of AEV and k_{sat} over the C-L, resulting in zero change in the preferential discharge points or the preferential flow path in the system.

The flow paths from the simulation show that water flow in the horizontal layer flow through a gravitational mechanism (see streamlines in Figure 5.25 and Figure 5.26). Once the flow reaches the contact zone between the acid rock and the limestone, the flow follows the inclination of the panel until breakthrough occurs between the layers of higher permeability. On the other hand, the flow path changes with respect to the location of the precipitation and discharge points. Infiltration from the precipitation at layer seven show a gravitational flow, despite having the same h_p distribution as the first two layers (L1 and L2).

The internal response of the model shows no significant change in the h_p distribution (Figure 5.25 and Figure 5.26) with respect to Panel-1; the differences found between both panels at equal elevation are simply related to the inclusion of precipitation through the top of layer 1. The simulated profiles demonstrate that a zone of equilibrium suction forms at the contact zone between the incline layers and the horizontal layer. This zone tends to have the maximum suction for both materials (limestone and acid rock). In both materials, the suction increases towards the contact zone reaching a maximum between 17 kPa to 18 kPa. Both materials show a contrary relation between the elevation and the suction developed in the system; in the limestone, maximum suction is at the lowest elevation, while in the acid rock suction is at the highest elevation.

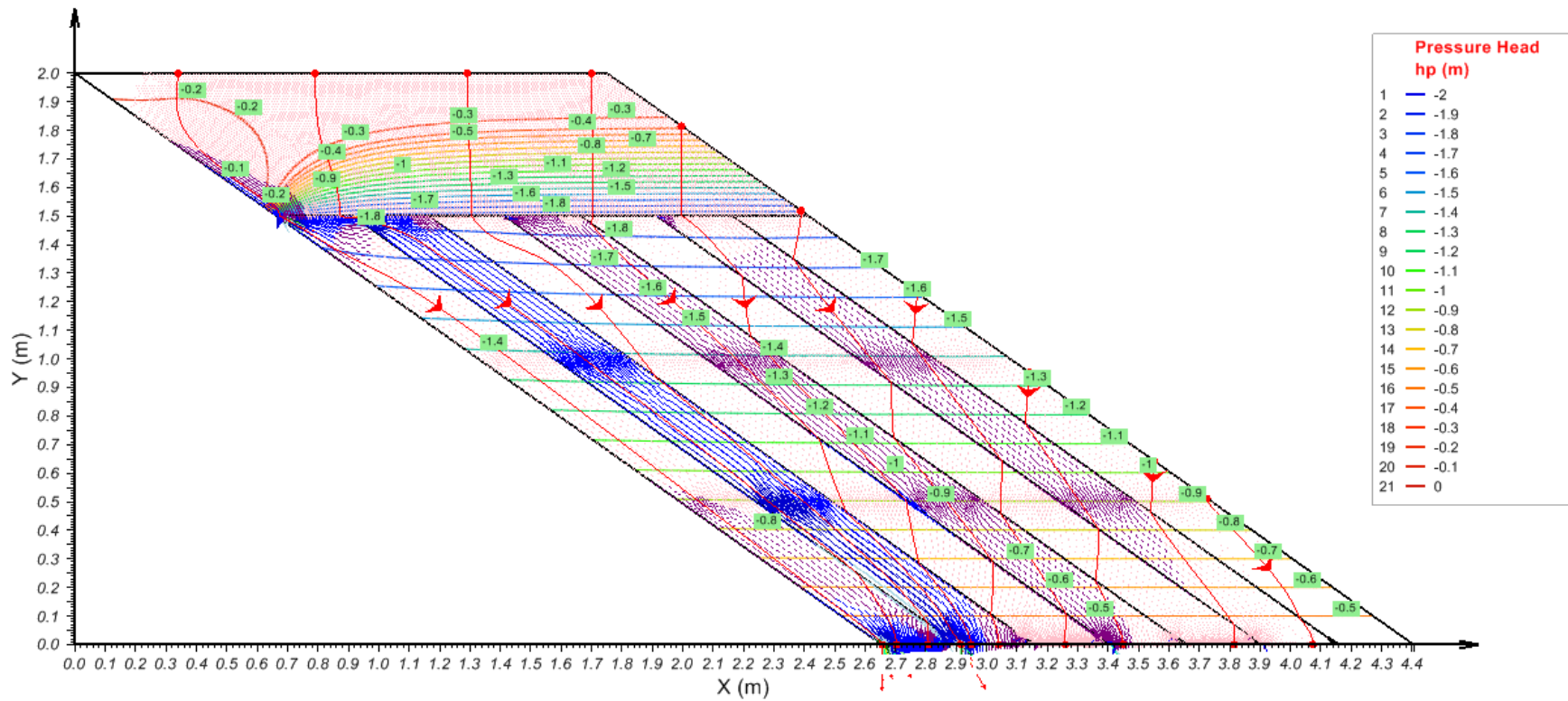


Figure 5.25 Simulation in Panel-2 at a Precipitation of 2 mm/day and 4 kPa of Base Suction for Case 3

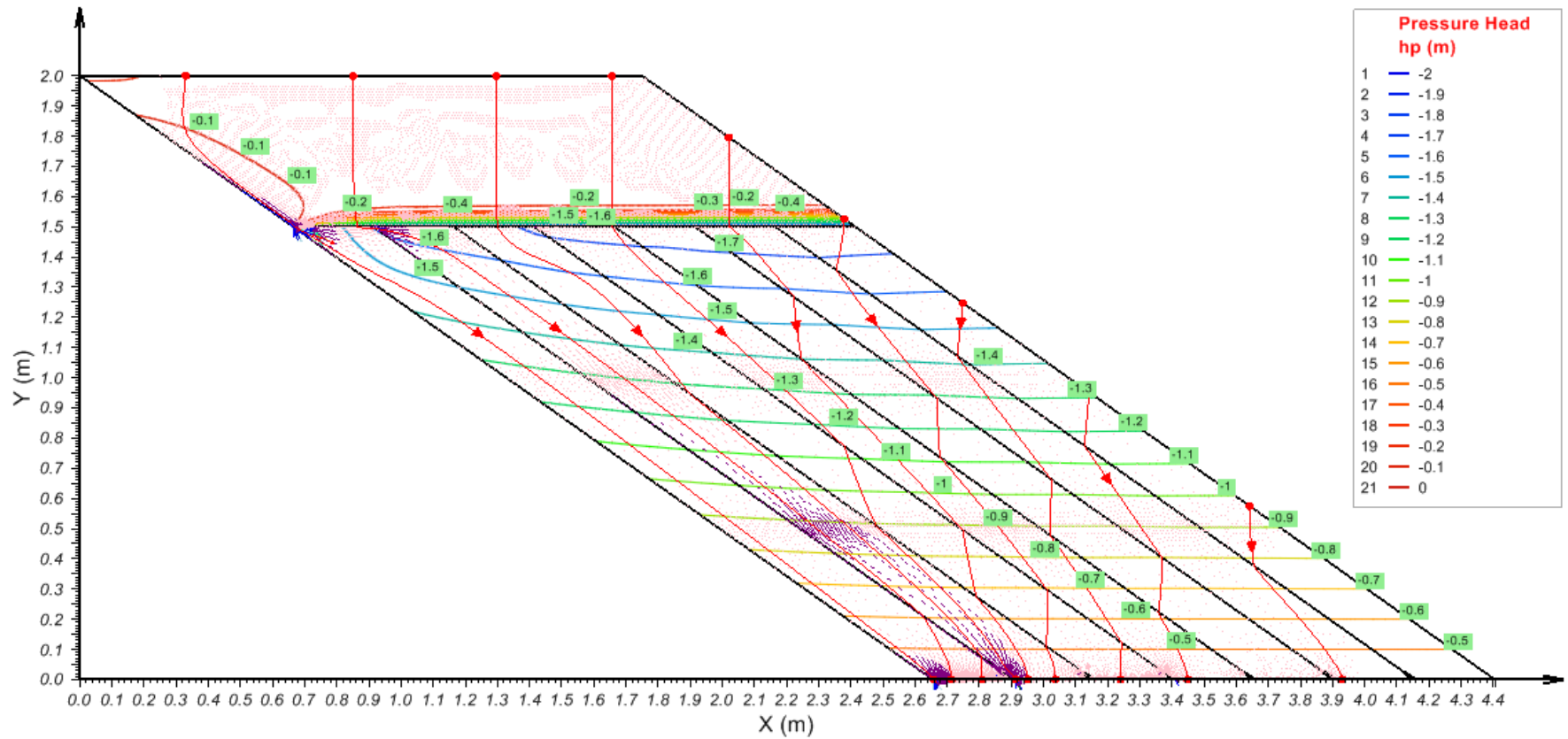


Figure 5.26 Simulation in Panel-2 at a Precipitation of 10 mm/day and 4 kPa of Base Suction for Case 3

The three tests show no significant relation between the precipitation and the h_p distribution within the acid rock. However, the limestone shows that increasing the precipitation changes the h_p distribution. Higher precipitation rates have a lower suction as shown in the simulated profiles of Panel-2 in Appendix A. The maximum change in suction at the same elevation is 4.0 kPa, being lower and closer to the first layer and increasing toward the outer layers.

On the other hand, the simulations display changes in the flux vectors with precipitation. Despite the precipitation not affecting the preferential discharge points, the flow paths change. Increasing the precipitation reduces the flux from the F-AR in layers four and six.

5.7. SIMULATION OF PANEL-3

The following results show the Panel-3 simulations under four test conditions, which differentiates changes in the base suction and precipitation. Similar to Panel-2, the three case simulations are run to obtain optimum convergence. The first case analysis correspond to a model applying material characteristics equal to the laboratory measures. The second case analyses consist in applying the material properties from the laboratory for the limestone, and the calibrated material properties from Panel-1 for the Acid Rock. The third Case analysis applies the calibrated material properties from Panel-1, and assumes the C-L properties equal to C-AR. The assumption in the third case is based on the similarity between the grain size distributions of the materials.

Figure 5.27 summarizes the results of total discharge from the fine and coarse layers in Panel-3 for the simulation of the three case analyses and the experimental results. Unlike the previous two models, the discharge in Panel-3 occurs throughout four materials.

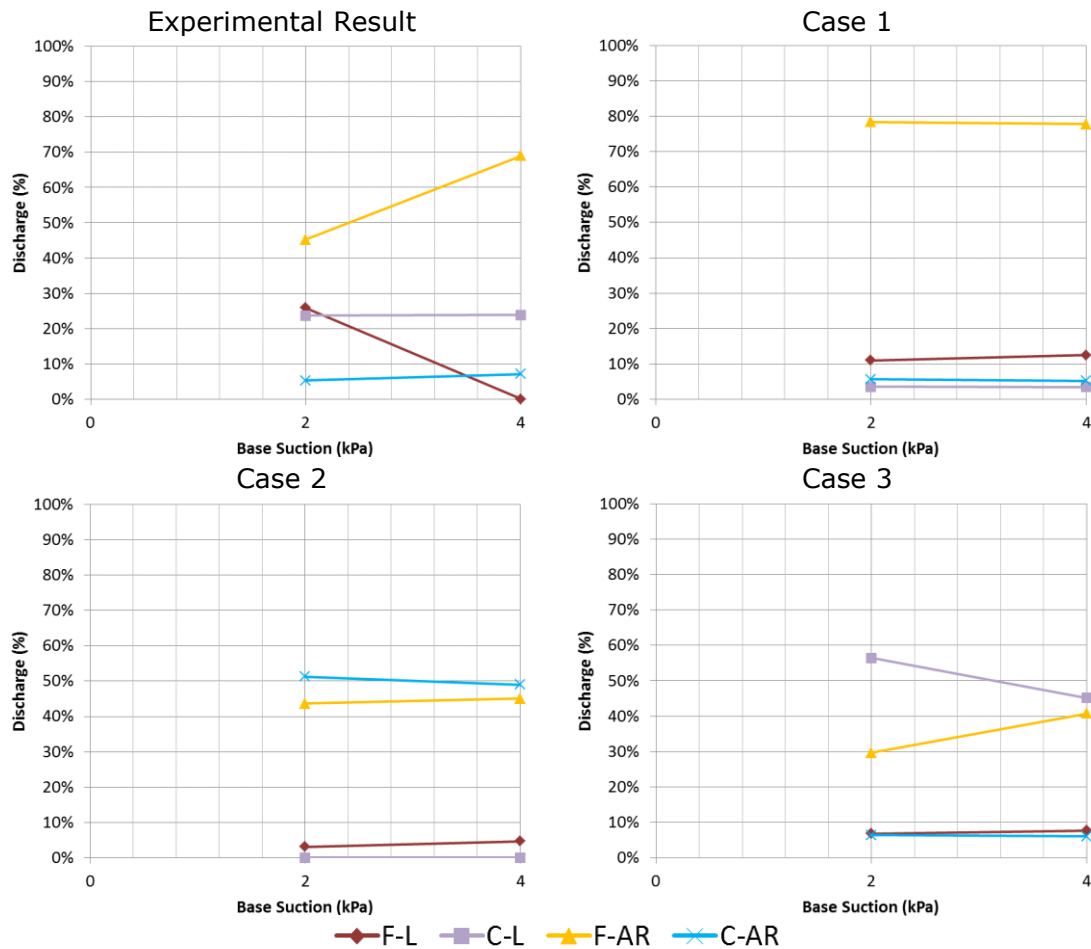


Figure 5.27 Total Outflow for Panel-3 for a Precipitation of 2 mm/Day in the Experiment Results and the Three Simulation Cases

In the experimental result, suction generates a low impact in the discharge from the coarse grain materials (C-L and C-AR). In contrast, in the fine grains the increase in suction causes a drop of the discharge from the F-L, which proportionally increases the F-AR. The change in discharge demonstrates that a breakthrough occurs from F-L to the F-AR; thus, F-AR becomes the preferential discharge material with 70% discharge. Under the tested conditions, the high change in discharge from the fine grain materials might only be possible for an AEV in the limestone lower than the AEV in the acid rock, despite the Fine-waste-rock having grain size distribution similar to the same SWCC.

In addition, the number of layers that each material had and the arrangement of the layer with respect to the precipitation points affect the preferential discharge distribution. The experimental results show that F-AR has a higher discharge than F-L, but the C-L has a higher discharge than C-AR. Nonetheless, the discharge does not

represent the internal preferential flow path through the system as gravitational flow occurs at a low elevation.

The three cases made to recreate the laboratory results (i.e. discharge percentage) did not show good correlation and no relation of discharge with suction. Case 1 displays the F-AR as the main discharge material (over 70%), followed by the F-L and the coarse grain (C-AR and C-L with less than 10%). Case 2 increases the AEV of the C-AR from 0.05 kPa to 0.57 kPa, resulting in the C-AR as the preferential discharge material (about 50%) followed by the F-AR (with over 40%) leaving C-L and F-L with less than 10% discharge. In the final attempt (Case 3), after increasing the AEV on C-AR and C-L from 0.05 kPa to 0.57 kPa, the preferential discharge material becomes C-L (with over 50%), then F-AR (between 30% and 40%), and with less than 10% F-L and C-AR. Additionally, Case 3 shows that both C-L and F-AR are affected by suction. From the three simulations run for Panel 3, only 4.0 kPa and 2 mm/day achieve a good overall correlation (Figure 5.36) using the measured laboratory properties. The main variance on the discharge occurred in the first for layers (L1 to L4). The simulations did not show significant change in the total discharge from all the materials due to changes in suction. However, in Case 3 the F-AR did show the same trend as in the laboratory experiment, increasing around 10% instead of the 25% measured in the experiment.

Although the model has a low correlation to the laboratory experiment in the preferential discharge points, the simulations locally can display the same response as in the experiment as shown in Figure 5.28 and Figure 5.29. In the outer layers (L6 to L9), both model and experiment have very low discharge, in L9 between 5% and 0%. The main variance occurs toward the inner slope where the simulations show high discharge from L1 and L2, while the experiment showed that the principal discharge occurs in the fine material in the center of the panel (i.e. L4-L5). This difference occurred due to the defined material properties in the model, as the experiment results indicate that layer L4 and L5 are acting as a capillary barrier, preventing any water breaking through the first layers. However, the simulations show breakthrough at an elevation of 50 cm approximately. The two layers should have an AEV higher than 1.4 kPa in order to generate the capillary barrier over the inner layers.

The tests conditions in Panel-3 indicate the effect of the change in base suction in the system. The increase in suction generates a higher flux through the first five layers, prioritizing the fine grain layers (L2, L4, and L5). As the precipitation increases, the breakthrough flow between layers also starts to be longer between the layers. Figure 5.27 shows that in Case 3 the increment in suction increases the discharge from

the F-AR (layers L2 and L3), while it decreases the discharge from the C-L (layers L1, L3, L7, and L9); the discharge in F-L and C-AR remains approximately constant. However, as previously mentioned, the preferential discharge points do not take into account the preferential flow path of the system. In Figure 5-24 the simulations of Case 3 reveal that increasing the base suction of the system increases the preferential flow path through the F-L. The flux vectors reveal that water moves through the entire length of the layer up to an elevation of 0.1 m where the final breakthrough occurs and water flows to the F-AR in L4.

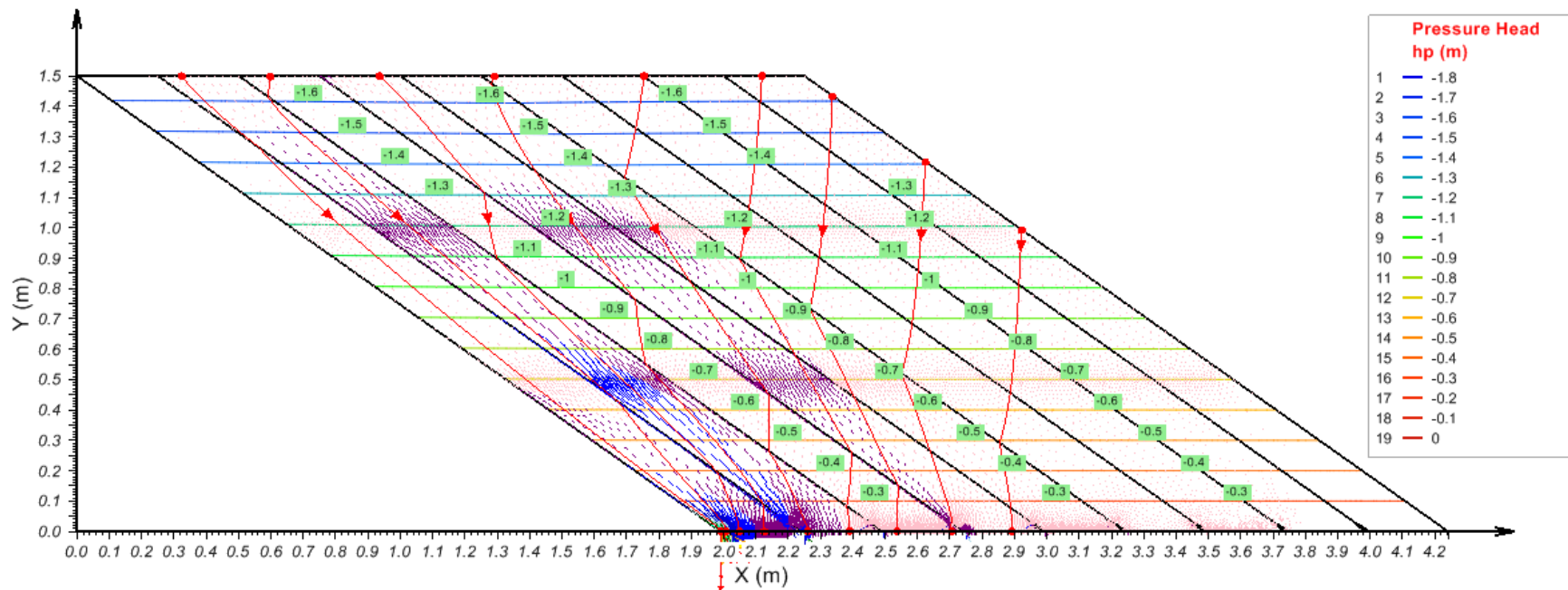


Figure 5.28 Simulation of Panel-3 under at a Base Suction of 2 kPa and a Precipitation of 2 mm/Day for Case 3

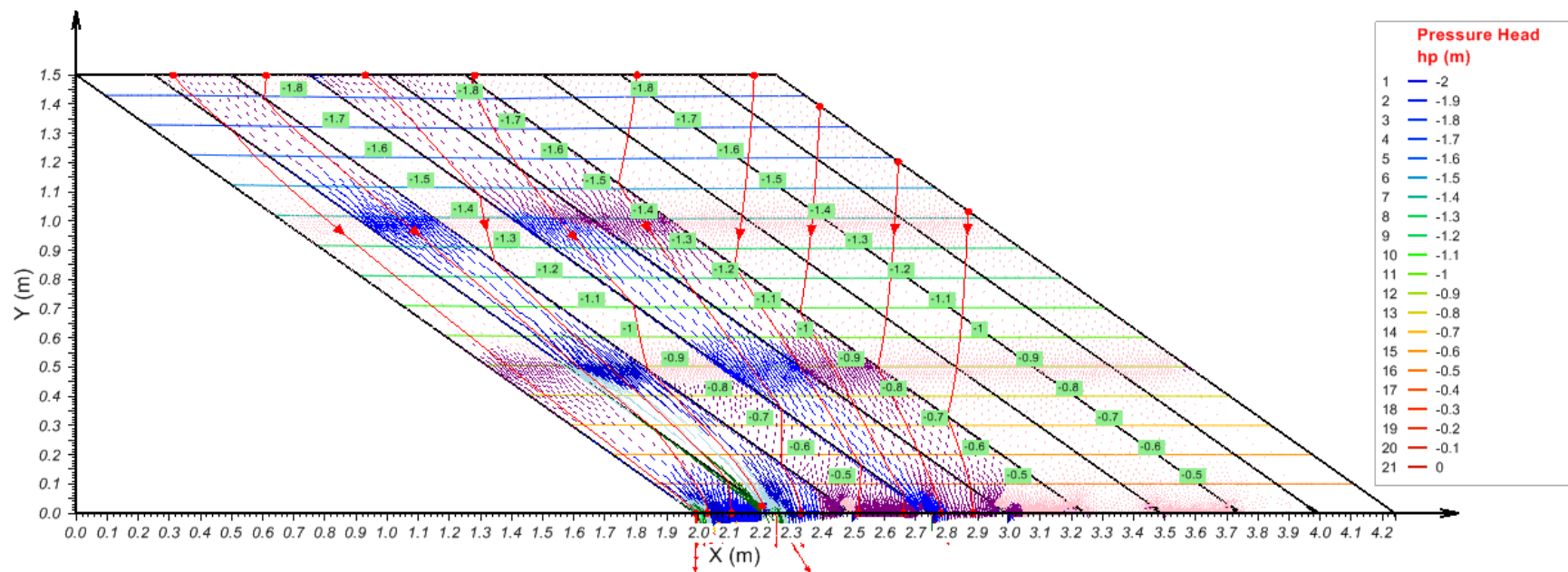


Figure 5.29 Simulation of Panel-3 under at a Base Suction of 4 kPa and a Precipitation of 2 mm/Day for Case 3

The simulations show that the increase in suction generates change in the discharge from the materials similar to the observed result from the simulation of Panel-1. For C-L and C-AR, the discharge decreases, while for F-AR and F-L, discharge increases as shown in Figure 5.30. This change is reduced significantly towards the outer slope (right side of the panel) up to a point where change in suction does not affect the discharge.

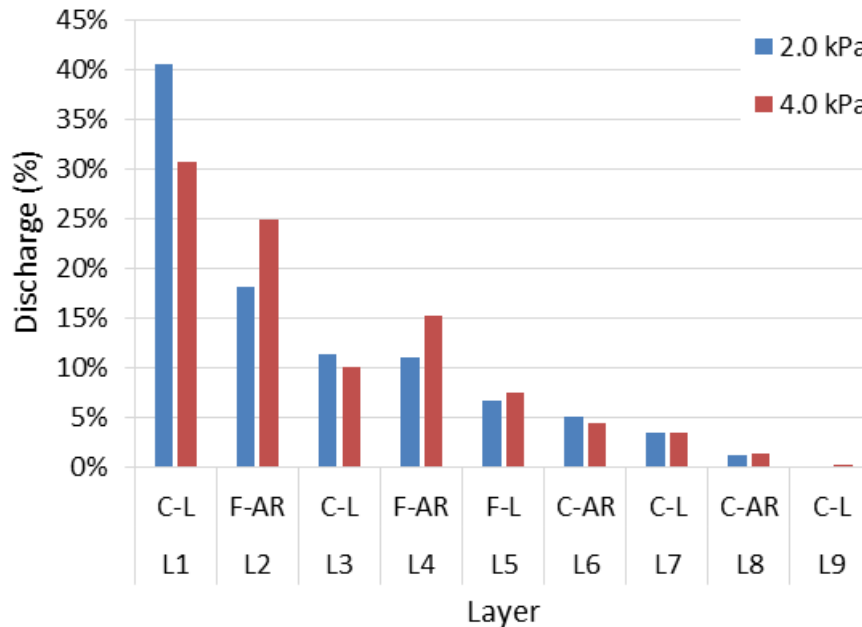


Figure 5.30 Water Flow from the Discharge Points for a Suction of 2.0 kPa and 4.0 kPa at a Precipitation of 2 mm/Day in Case 3, Panel 3

The experiment results in Panel-3 show that precipitation affects the discharge from the material as shown in Figure 5.31. Increasing precipitation increases the discharge from the Limestone and decreases discharge from the acid rock. The results revealed that at a precipitation close to 7 mm/day, the C-AR and F-L could have the same discharge as well for the F-AR and C-L. In other words, an increase in precipitation can lead to drastic change in the preferential flow path for the waste rock.

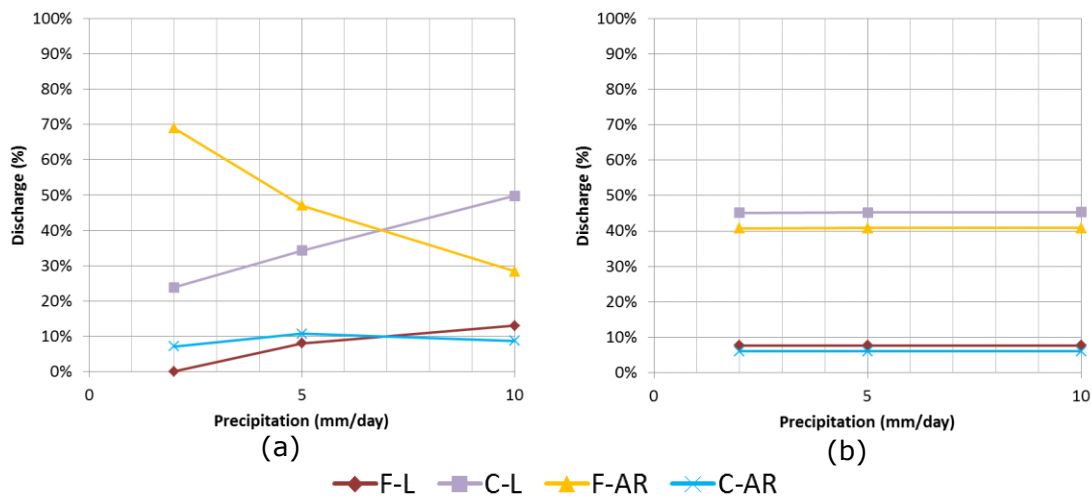


Figure 5.31 Total Outflow for Panel-3 for Base Suction of 4.0 kPa in the Experiment Results (a) and the third Simulation Cases (b)

As it occurs in the simulation of Panel-1 and Panel-2, the models are not affected by the changes in precipitation. The increase in precipitation results in an increase of the volume, which keeps the same proportionality for all the simulated cases. This result indicates a low correlation with the total discharge from the model and the experiment. Nonetheless, it should be noted that for a precipitation of 10 mm/day in Case 3, the model simulates the order in which the materials have predominant discharge. This simulation occurs due to the number of layers and the increment in the AEV of the material, generating a higher permeability under the unsaturated conditions.

Similar to the previous panels, despite the precipitation not having any effect in the preferential discharge point, the internal behaviour of the panel changes. The simulation in Panel-3 displays a small sensitivity from the changes in precipitation that are revealed in the change in suction, see Appendix A for all simulation results for Panel-3. The increment of precipitation generates a slight decrease in the suction of the system. The reduction of suction becomes less uniform with elevation as the precipitation increases. The uniformity is loss as the suction in the inner layer is lower than the outer layers in the panel. Nonetheless, the difference in suction is not significant but capable of altering the preferential flow path. The simulation shows the fine layers with the highest suction along the same elevation. This increment in suction decreases the permeability of the material, resulting in a breakthrough from the fine layers toward the inner layers. This response is contrary to the experimental results in which the materials must have a lower suction that allowed higher permeability values with respect to the coarse material, driving the water from the adjacent layers towards the fine material.

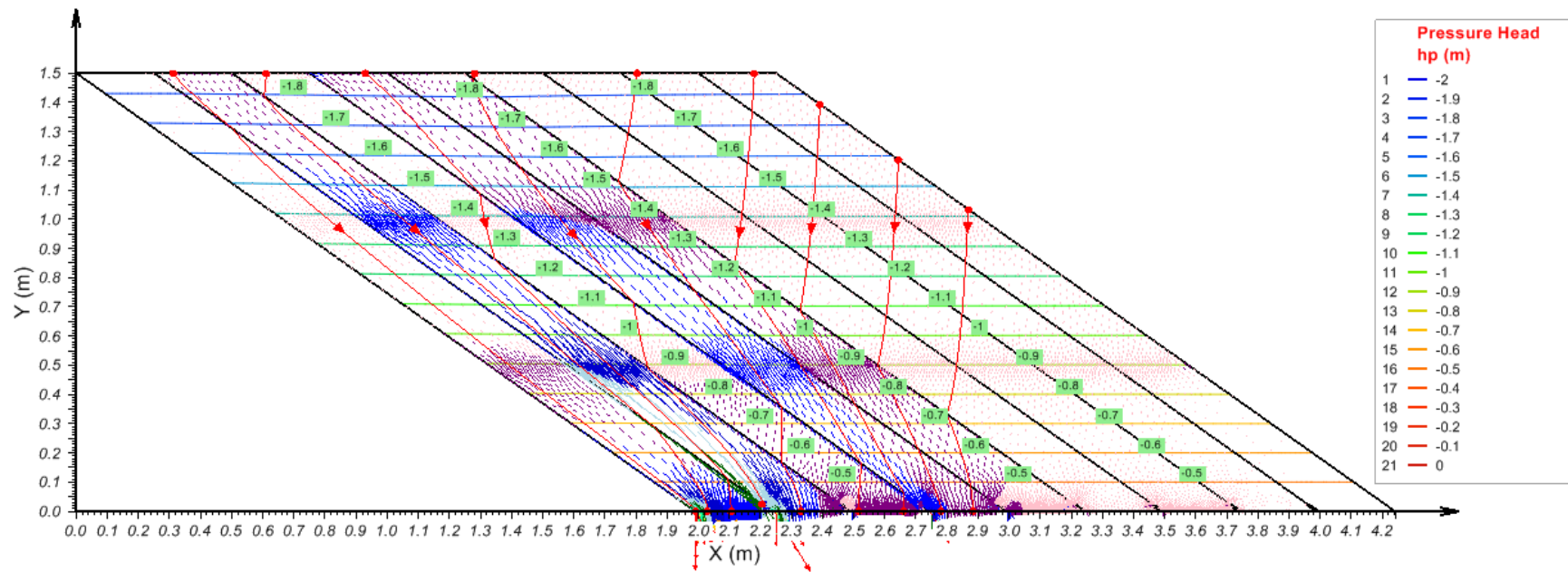


Figure 5.32 Simulation of Panel-3 under a Precipitation of 2 mm/day and a Base Suction of 4.0 kPa For Case 3

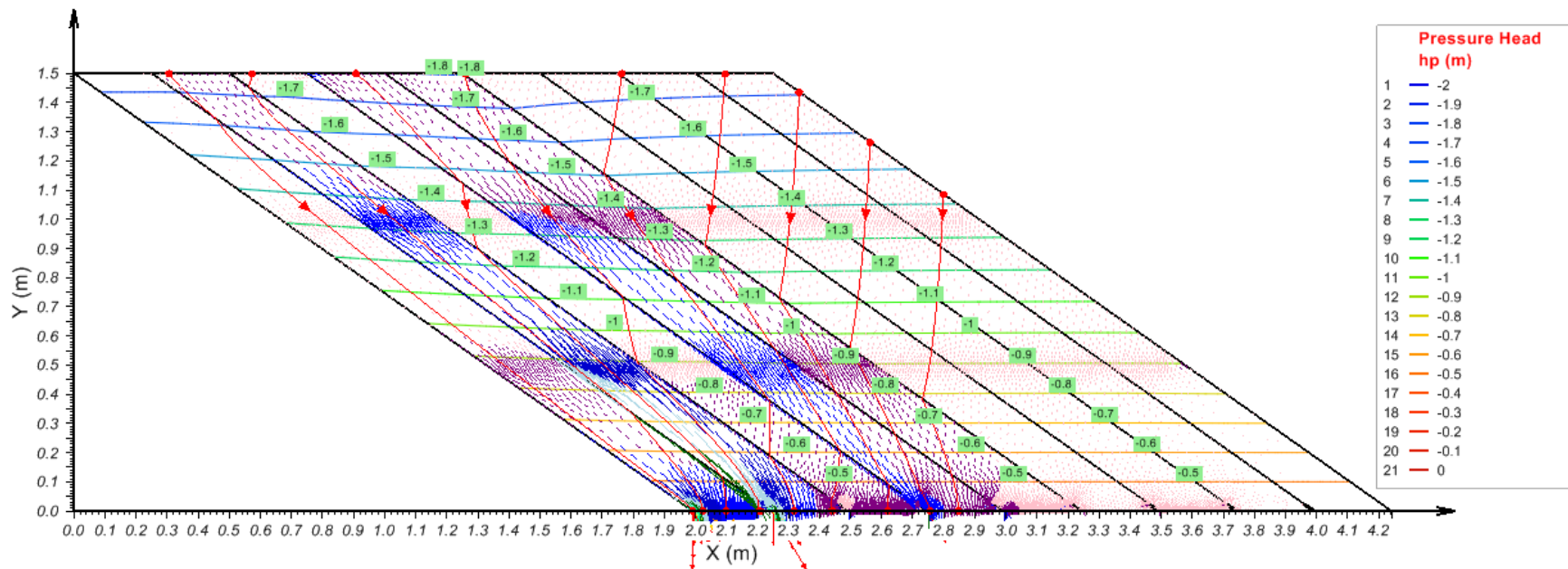


Figure 5.33 Simulation of Panel-3 under a Precipitation of 10 mm/day and a Base Suction of 4.0 kPa For Case 3

The only distinguishing feature of Panel-3 with respect to the others is the thicker layer of fine grain material in the center of the panel. This double layer generates a peak of increasing suction, acting as a capillary barrier within the panel. The simulations show peaks of approximately 8.0 kPa and 13 kPa at 50 cm and 100 cm elevation from the base of the panel. Appendix A shows additional simulated profiles for Panel-3. The increase in suction causes a decrease in permeability in the fine layers; however, the suction in the outer layer is not low enough to increase the permeability and generate a preferential flow path through the coarser layer (L6 to L9). The suction conditions develop in the system under steady state conditions and show that the magnitudes of suction in the HCCs have a higher permeability in the fine grain material, infiltrating all the water from the outer layers. Also, the simulations illustrate that at lower elevation, the gradient in suction decreases, resulting in a lower difference in permeability between layers. Despite of the change in suction the preferential flow path remains the same.

5.8. ANALYSIS AND DISCUSSION

The principal objective of this study is to examine the water flow paths in an unsaturated system of the three presented panels using two-dimensional space numerical models. The numerical models were created based on the experiments conducted by Andrina (2009). These experiments had a system composed of waste rock and a simulated precipitation. The system addresses different boundary conditions based on climate and base suction for unsaturated water flow. A specific methodology was provided to evaluate the different conditions from the experiment into the models, allowing the validation of the results. The methodology followed two modeling programs.

The first program is based on the validation of the three Meso-scale experiments. The initial modelling of Panel-1 has the simplest characteristics of geometry and composition; Panel-2 increases the complexity by building up from the initial geometry of Panel-1 and adding one material to the composition. The initial modeling program ends in Panel-3 with the highest complexity. The final panel holds a more accurate composition, resembling the characteristics found in the waste rock embankment at the mine; the embankment is made up of four materials and a more random arrangement of the layering system.

The second program of analysis presented in Appendix A describes the water flow mechanism in four material types for Panel-1. The selected materials for this

characterization included the waste rock from the Grasberg Mine (from first modelling program); waste rock from Golden Sunlight Mine (from Column-2 in Chapter 4); sandy materials (from Column-1 in Chapter 4); and, in the last model, two materials holding properties of Tailing Beach Sand and Devon Silt.

5.8.1. Modelling Of Meso-scale Panels

The previous sections showed the numerical results of the three models and a description of the trends displayed from the different tests. The results from the simulations were compared with the experimental result. The calibration of the models is based on calculating the difference of the total discharge flows from each material to the experimental results, as well as evaluating the correlation (PPMCC) of the discharge in each layer.

The simulation of the three panels required an evaluation under different conditions, due to the low convergence of the model while applying the same material properties from the characterization of the waste rock from Grasberg Mine. The simulation of Panel-1 was used as the initial calibration of the acid rock to improve the convergence of the model. The result from the calibration of the geotechnical properties shows that calibrating the AEV of the materials improves the convergence of the model. In the acid rock, the AEV that gives better convergence is from the coarse grain material (i.e. C-AR).

Furthermore, the calibration reveals the sensitivity of the simulation for any changes. The materials in the model are considered homogeneous and isotropic, making a significant assumption on the natural condition and even in controlled experimental conditions. The fabric of the materials has a high relevance in unsaturated water flow, as the connection of the voids relates to suction developed between particles. Testing samples under different conditions in the field or, in this case, in the experiment can lead to different material behaviors. The simulation of Panel-1 shows that slight variations occurred between the assembly of the Meso-scale Experiment, the measure of the SWCC with Temple Cell, and the measure of the saturated hydraulic conductivity using falling head test. On the other hand, the applied boundary conditions may have made slight differences in the expected values in the experiment, making the back analysis not only sensitive to the properties but also the specific boundaries (a possibility that goes beyond the objective of this research project as it becomes highly speculative with limitless possibilities).

The model of Panel-1 showed that four out of the six testing conditions display a good correlation between the total discharge from the F-AR and the C-AR. The two

cases with low correlation are for a precipitation of 2 mm/day and a base suction of 4.0 kPa and for 10 mm/day and a base suction of and 0 kPa. The difference in the first case could be related to the experimental measures, since under the experimental conditions of 2 mm/day the experiment is showing a decrease in flow from the F-AR when increasing suction. These results do not match with the relationship between the HCC of the waste rock materials and the suction conditions developed in the panel. The second case confirms the previous statement where lower suction generates less flow through the fine material. In this case, the model satisfies the retention of the water in the fine layers, thus resulting in the first layer of C-AR being the preferential discharge point.

The convergence of the panel from the individual discharge is high for precipitation above 5 mm/day (Figure 5.34). The correlation shows that lower precipitations and low suction values decrease the convergence of the flow path drastically, despite the total discharge flow matching the experimental results.

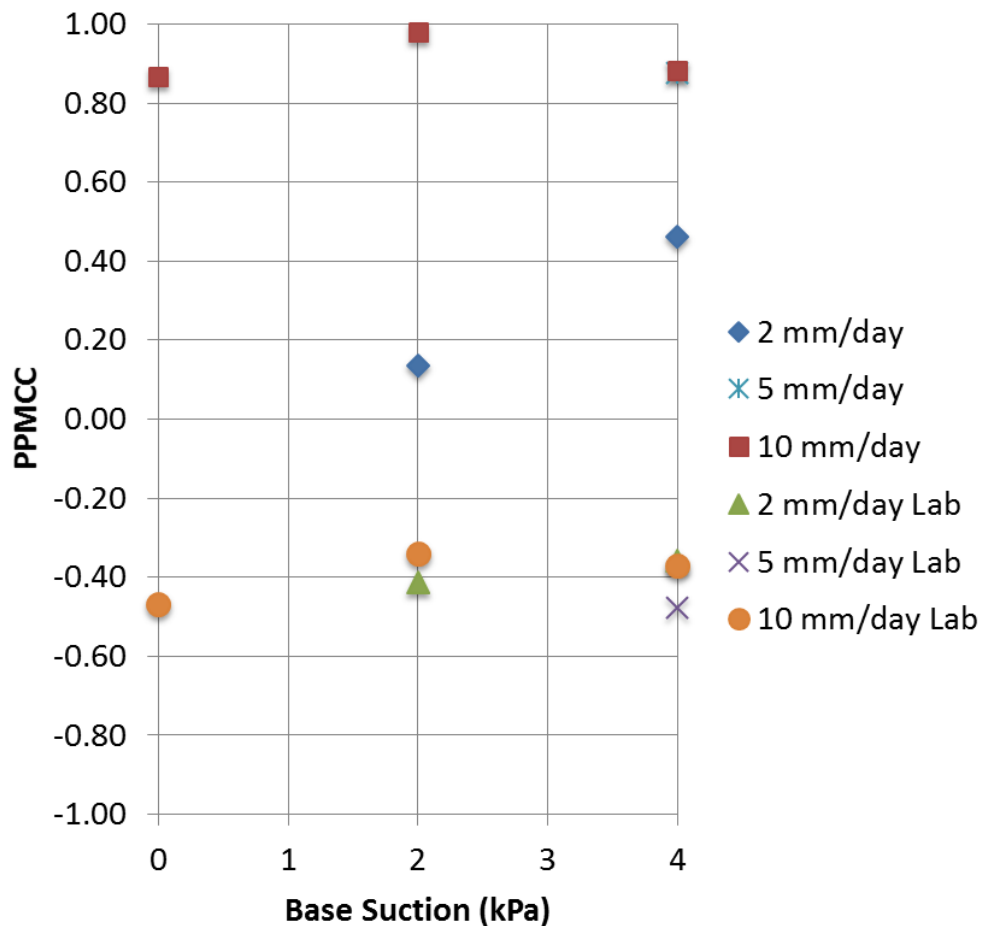


Figure 5.34 Correlation between Simulation and Experiment in Panel-1

The results from the simulations of Panel-1 and Panel-2 do not display any response in the total discharge from changes in precipitation. This response of the numerical model exposes an existing or new variable that has not yet been identified as responsible for the effect of precipitation on discharge in the system. Internally, there is no significant change in the h_p distribution (as shown in Figure 5.25 and Figure 5.26), the differences found between both panels at equal elevation are just related to the inclusion of precipitation through the top of layer 1. At the contact zone between the horizontal layer and the incline layers, however, there is shift in the h_p distribution in the system. This shift shows higher suction at a lower elevation in the horizontal layer, contrary to the developed suction below the contact zone. This suction distribution generates purely gravitational flow, as the precipitation increases the VWC and decreases suction.

The simulations using the properties from Panel-1 show that a change in precipitation changes the suction within the panel, Appendix A shows profile of Panel-2 using the calibrated properties of Panel-1. The increment on precipitation makes water to ponding at the contact zone between the horizontal and incline layers. This pond increases the VWC at the base of the horizontal layer (150 cm elevation), generating a tighter gradient of suction. Once water reaches the incline layers, the suction starts to decrease as water infiltrates. Then again, higher precipitation decreases suction. The simulation exposed a maximum gradient in suction of 4 kPa, and this change decreases as it moves closer to the outer slope. Additionally, the profiles show an increase in suction with the elevation: at 50 cm suction reaches around 9 kPa, at 100 cm around 14 kPa, and at 150 cm 18 kPa.

The simulations of Panel-2 followed three case analyses to improve the convergence based on the calibration in Panel-1. These cases show an improvement in convergence, though not as accurate as Panel-1. The result reveals that an additional calibration of the top limestone does not affect the discharge flow. In other words, the flow path below the horizontal layers would remain the same regardless of the characteristics of the horizontal layer, but only if this material does not alter the infiltration flow. The proof of this statement is that the results from the total discharge in Panel-1 and Panel-2 are the same under the same boundary conditions. However, the model overestimates the discharge from the fine material. The results indicate that Panel-2 requires an additional calibration of the materials from Panel-1 in order to improve the convergence of the system. This requirement means that the hydraulic characteristic of the acid rock in both panels was different. In spite of the difference in

the total discharge, the PPMCC resulted in high values for precipitation above 5 mm/day (Figure 5.35).

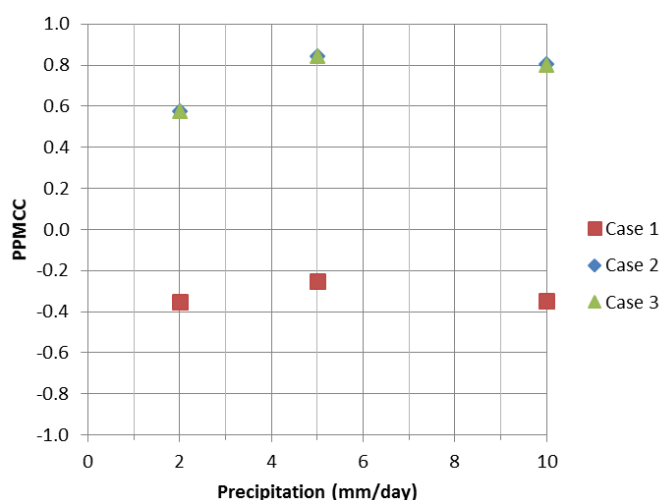


Figure 5.35 Correlation between Simulation and Experiment at 4.0 kPa of Suction in Panel-2

The model in Case 1 shows negative correlation and low response to changes in precipitation. Despite Case 2 and Case 3 demonstrating that the model has low response to changes in the precipitation in the total discharge, the correlation of the individual layers is affected by precipitation. Panel-2 shows that increasing the precipitation has an effect on the correlation, and despite the overall discharge having a variance of approximately 20%, the difference in the individual layers between the laboratory and simulation is low (8% average). As previously mentioned, the change in material properties from the horizontal layers does not affect the preferential flow path of the system, and thus the respective correlation from each test in Case 2 and Case 3 remains constant.

The simulations of Panel-3 were also run for three case analyses to validate the model, improving the correlations and convergence. In the three analyses, the fine grain material shared the same HCC; but only in Case 1 and Case 3 do they have equal AEV for the coarse grain materials. Case 2 has the calibrated properties from the C-AR with a higher AEV.

The calibration of the Acid Rock resulted in an improvement on the convergence of total discharge in Panel-1 and Panel-2; however, Panel-3 shows low improvement in Case 2 and Case 3. Contrary to the first two panels, the discharge in Panel-3 occurs in four types of materials, thus increasing the complexity in finding convergence in the whole system. The analysis shows that correlation increases with suction: at low precipitation, Case 1 had higher correlation followed by Case 2 and Case 3. Only in

Case 1, at one of the four tests, was the convergence reasonable. At a suction of 4.0 kPa and a precipitation of 2 mm/day, the model displays the lowest differences of total discharge flow (an average difference of 10%), although the model shows 20% less discharge from the C-L. The correlation of all layers results in a PPMCC above 0.9 as shown in Figure 5.36. Between the three models, only Panel-3 shows better correlation using the laboratory parameters. This situation occurs due to the assembly or placement of the materials. As mentioned before, changes in the fabric of the materials (between the testing of material properties and the Meso-scale test) could generate variances in the hydraulic properties that control the flow mechanisms. The results from the simulations indicate uncertainty on either the properties of the materials or the boundary conditions used in the laboratory experiment.

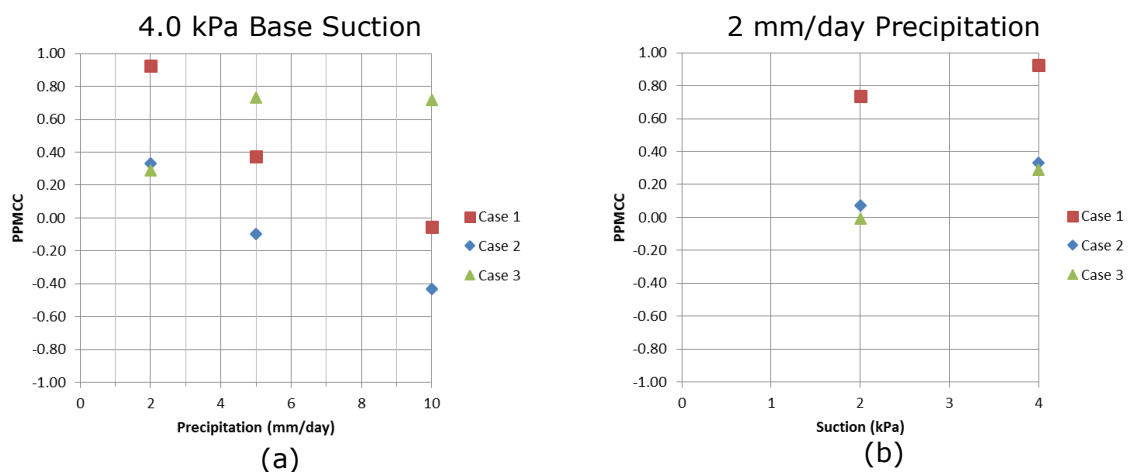


Figure 5.36 Correlation between Simulation and Experiment with Respect to the Change in Precipitation (a) and Change in Suction (b) for Panel-3

The flow path in Panel-3 shows initial preferential flow through the fine materials; however, the preferential discharge was through the coarse material, as shown in the profiles from Appendix A. This occurred due to the breakthrough of flow between fine layers and underlying coarse layers. The transfer flow occurs at the points where permeability of one material is greater than the other due to change in suction. The magnitude of suction that develops in the infiltration is near the point of intersection between both HCCs of the materials. If the internal suction decreases with elevation in the system, then the preferential flow path could switch between layers.

The contrast of the model and the experiment shows correlations of less than 0.4 and even generates negative correlations. Nonetheless, for Case 1 and Case 2, the decreasing precipitation increases the correlation. At 2 mm/day in Case 1, the correlation reaches 0.9, and this match provides the difference in discharge of 5% on

average. In Case-3, the increase of the AEV in coarse materials generates a correlation of 0.7, but it does not show a relation with precipitation.

The model of Panel-1 is also tested using three additional sets of material properties (See Appendix A for the detail results of Panel-1 under different material properties). Test 2 involves sandy material of lesser grain size than the original panel; Test 3 involves waste rock from another mine site; and Test 4 uses finer materials than the other tests. The comparison of the four tests predicts the water flow that could occur in Panel-1 testing different materials, and also validates the mechanism of water flow from another waste rock material. Figure 5.37 and Figure 5.38 shows the comparison of the simulation results between the four materials with respect to the change in precipitation and suction respectively.

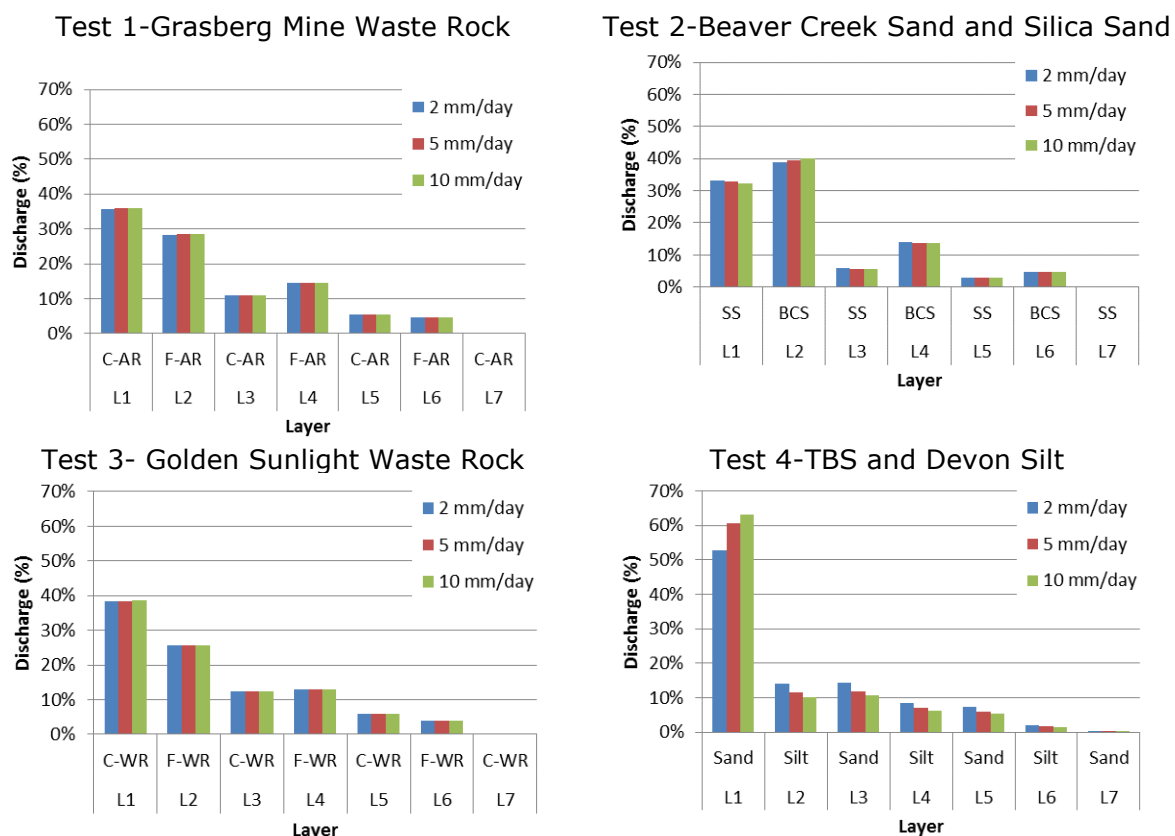


Figure 5.37 Contrast Discharge from Four Material Sets in Panel-1 under Three Precipitation Rates and Applying a Base Suction of 4.0 kPa

The results from Panel-1 show little effect of the precipitation on the preferential discharge points. The only significant change occurs using Tailing Beach Sand and Devon Silt (Test 4). These two materials show that increasing the precipitation generates an increasing discharge from the first layer (i.e. coarser material) and decreases discharge from the other six layers, regardless of the material

type. This changes in discharge occurs due to the low difference between k_{sat} from the fine material and the precipitation rates. The precipitation builds an uneven h_p distribution with the elevation generating vertical flow through the whole panel. Contrary to the other simulations, both vertical and parallel flow to the layers occurs. Similarly, using Beaver Creek Sand and Silica Sand (Test 2), the h_p is uneven but it normalizes in the lower 30 to 40 cm. thus allowing water discharge to be more distributed along the layers.

The simulations also show the effect of change in suction in Panel-1 for the different testing materials, as shown Figure 5.38. Similarly to the previous models, base suction has a greater impact on the discharge than the change in precipitation does in the discharge. The results show similar response in all tests, where discharge from the fine material increases as the suction increases.

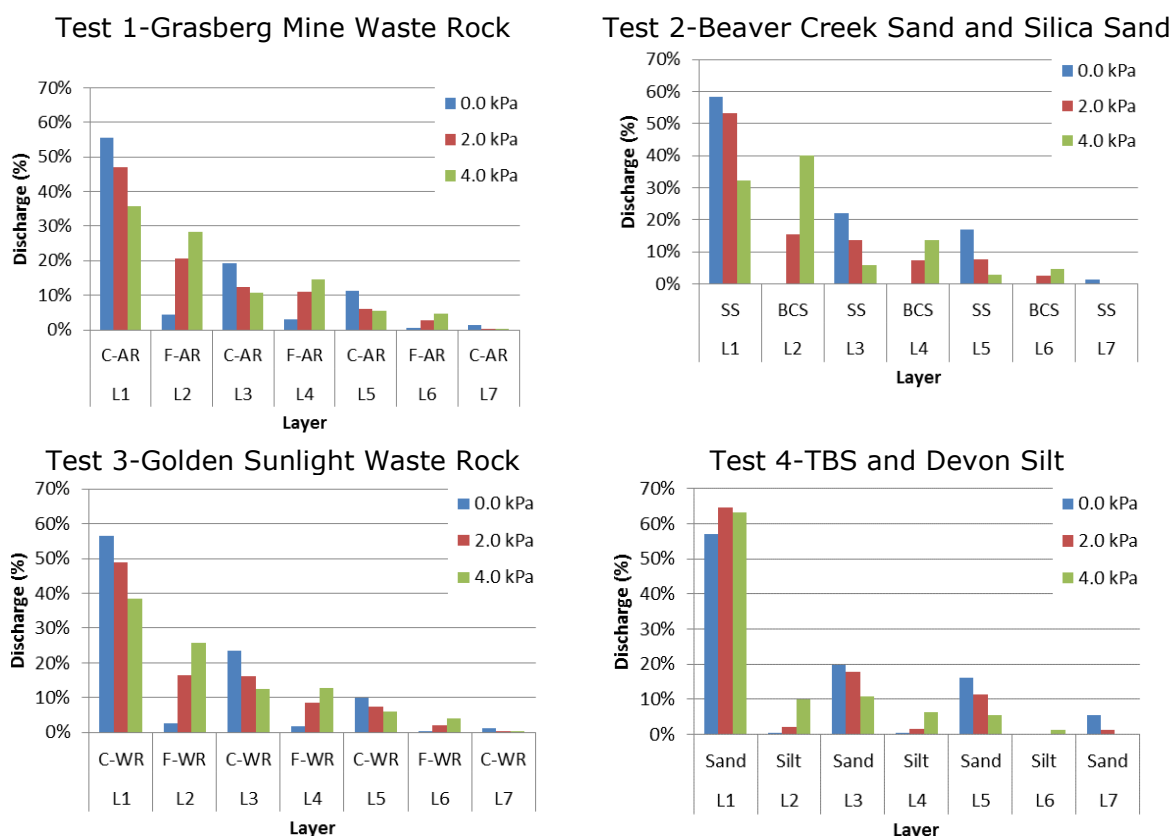


Figure 5.38 Contrast Discharge from Four Material Sets in Panel-1 under Three a Base Suction and at a Precipitation of 10 mm/Day

The simulation using waste rock materials shows similar discharge patterns even though the difference in the AEV between each set of materials is lower in Test 1 than in Test 3. In addition, the four tests show that changes in suction modify the

distribution of discharge in the system. At a lower suction, the difference in discharge from the fine layer and the adjacent coarse layer increases. Finally, it is clear that suction plays a more important role in coarser grain material, as the magnitude of the AEV in this type of material is generally very low. A small change in suction can generate a faster change in VWC and consequently a change in permeability.

5.8.2. Numerical Model Comparison

Despite that the results display some differences in the validation of the model. The numerical model allows observing additional information, this information generates trends that corroborate or contradict the observations from the Meso-scale experiments. The following points discuss the difference between the model and experiment from Panel-1:

- The numerical model for Panel-1 shows that most of the outflow occurs in the first two to three layers, regardless of the change in suction and precipitation rate, while the laboratory results demonstrate that low precipitation rates and suction affect the flow path. At a lower suction, most outflow occurs in the middle layer (i.e. layers 4 and 5). Another contrast is observed for a specific precipitation rate. As suction decreases, the outflow in the first layers increases.
- The model confirms that increasing precipitation has a minor impact on the discharge of individual layers. However, there are small changes in the h_p distribution close to the infiltration zone.
- With respect to the relation between discharge and the base suction, the simulations concur with the experimental data that the discharge is not only related to the base suction, but also to the material characteristics.
- The model confirms that the materials properties affect the distribution and change in the matric suction. On the other hand, the internal suction of the model differs greatly in magnitude and distribution with respect to the measurement of the instrumentation (Andrina, 2009, p. 281). However, the precision of the instrumentation might have played a role in the differences. Furthermore, the simulation shows a correlation between low suction and low precipitation as demonstrated by previous researchers (Andrina, 2009, p. 279)
- In the experiment, layer seven (L7) resulted in significant variation in matric suction (Andrina, 2009, p. 278). The model reveals that the variation in L7 occurs at lower elevation, and it is proportional to the change in precipitation and suction.

The objective for the Meso-scale Experiment of Panel-2 was to assess the effect of alkaline solution on the leachate quality from the coarse limestone on top of the dipping layers. The experimental objective evaluated the chemical behaviour more than water flow in the unsaturated system. The objective of the simulation in this panel was limited to the flow analysis. The following points discuss the difference between the model and experiment from Panel-2:

- The model and experiment register higher discharge in L1 and L2. As Andrina (2009) mentioned, "the change in geometry, placed 2/3 of the application points above the lower slope and collection drains". However, the model shows that this occurs furthermore because of the breakthrough of flow parallel to the inclined layers and not only due to gravitational flow. In addition, the model shows that only at the top horizontal layer the flowing mechanism is purely gravitational.
- The discharge in the experiment was related to the precipitation conditions. The experiment showed the discharge from the first layer (L1) increased with the precipitation due to vertical flow. In contrast, the model did not show an increase in the proportion of discharge with respect to precipitation.
- Overall, the experiment and model results have high divergence. The discharge from the simulation of Panel-2 was not influenced by the change in AEV and k_{sat} of C-L in the horizontal layer. If the change in water flow between Panel-1 and Panel-2 is not controlled by the addition of the top horizontal layer of C-L, then the material properties from the acid rock in the incline layers could have changed between Panel-1 and Panel-2.

Panel-3 had a higher resemblance to the field conditions found in the waste rock at Grasberg Mine. The following points outline the difference between the model and experiment from Panel-3:

- In the experiment, the middle layers of fine material (L4 and L5) acted as a capillary barrier that modified the flow distribution in the system (Andrina, 2009, p. 292). However, only in Case 1 does the model resemble this preferential flow; Case 2 and Case 3 show that increments of AEV from the coarse grain material increase the permeability enough to drive the flow across the middle layers.
- The model does not display changes due to increasing precipitation as in the experimental results. In the experiment, the fine layers show less discharge

with increasing precipitation, and gravitational flow dominates through the coarse layers (Andrina, 2009, p. 268).

- The flow mechanism revealed by the model resembles the experiment at low precipitation rates where flow parallel to the incline layers dominates due to the capillary forces (Andrina, 2009, p. 269). On the other hand, the model shows vertical flow in the coarser materials, but does not indicate discharge. The main point of discharge from the outlets is located below the precipitation zone (Andrina, 2009, p. 273).
- The model validates that water flow reaching the middle fine layers (L4 and L5) is due to gravitational flow (Andrina, 2009, p. 291) from the precipitation applied to the coarse grain layers (L6 to L9).
- The model shows that the distribution of discharge increases towards the first layer (L1) for Cases 2 and Case 3 similarly, as occurs in the experiment with a precipitation of 5 mm/day. In Case 1, the model shows that discharges decrease from the center fine layer (L4 and L5) towards the sides of the panel, as similarly occurs in the experiment with a precipitation of 2 mm/day.

5.9. CONCLUSIONS

The simulation of the three Meso-scale experiments to recreate the conditions and results of water flow in unsaturated soils, under steady state conditions, was carried out in a two-dimensional numerical model using SvFlux. The conclusion from the simulation can be summarized as follows:

- The simulation of the three panels allows for the examination in detail of the mechanism that controlled water flow in unsaturated conditions. The simulations show the changes in head pressure, flux, and trajectory of water particles in the system and allow both visualizing and explaining of the preferential flow path for the three panels. The models demonstrate that gravitational flow occurs in areas where coarse material predominates, while flow parallel to the layers occurs through the fine material. There are differences in the preferential discharge model and experiments; however, internally the models satisfy the internal response of the experiment according to the interpretation made by Andrina.
- The discharge from the models displays no sensitivity to change in precipitation, and contradicts previous studies of flow in unsaturated

conditions. Nonetheless, the models exhibit changes in the preferential flow path inside the system. On the other hand, the change in the base suction shows significant effect on the preferential flow path as suction. The increment of suction increases the flow through the Fine-waste-rock and decreases proportionally the flow through the Coarse-waste-rock.

- The simulation of the Meso scale experiment Panel-1 shows that the measured laboratory properties did not adjust to the conditions inside the panel. The model is required to calibrate the material properties in order to recreate the preferential discharge flow.
- The simulation of an incline layering system in unsaturated conditions requires high detail in the measured properties and definition of the boundary conditions. In this study, the models were created based on a laboratory experiment that gives ideal conditions for the characteristics of the material and the geometry layering system. However, even under this idealization, the modeling of unsaturated flow has high complexity, and can result in extreme difference to the physical model.
- The calibration of the Acid Rock shows the high sensitivity of the model to changes in the Air Entry Value of the materials. The back analysis of the materials illustrates a 50% change in the preferential flow by adjusting the Air Entry Value on either material by less than 0.5 kPa. This sensitivity is critical in the measurement of the SWCC for modelling procedures, especially in modelling flow in coarse material such as waste rock.
- The mechanism of flow in an unsaturated system of two or more materials is not dictated by the magnitude itself of the hydraulic properties, but rather the relationship between them, as long as the flux rate is below permeability. The reach of the calibration procedure for the waste rock limits the result from this analysis. Other calibration methods through the adjustment of different parameters could decrease the divergence between a numerical model and the experiment.
- The results from the four tests in Panel-1 using different material properties demonstrate the significance of the relationship between the precipitation rate and the hydraulic properties. The results from the simulations using different materials reveal that despite that the materials having different characteristics, coming from different mines across the world, or having deposits of fine sands, the discharge for the specific conditions of

precipitation and suction values did not have extreme differences. The results show the same tendency of increasing the preferential flow path through the fine material at a higher suction.

CHAPTER 6 CONCLUSIONS

The mechanism of water flow in unsaturated soil conditions has been investigated here. A methodology was established and applied to evaluate unsaturated flow in soil and on waste rock under different external conditions of precipitation and suction. The analysis started with reviewing the principles behind water flow in an unsaturated system and its usage in finite element methods. A software program that applied these principles was used to analyse five experimental models. The models involved two column experiments, becoming the bridge towards a more complex model of three incline layering systems. The specific conclusions of the research program are as follows:

- The two column models showed a good correlation to the experimental results. The discharge difference was kept below a 10% margin. The simulations allowed estimating the internal response of the two soil layers after applying different precipitation fluxes. In order to validate the two models a calibration methodology was followed in each column. The calibration of the model was achieved by altering two hydraulic parameters in the materials: the Air Entry Value and the saturated hydraulic conductivity. The models showed higher improvement of the correlation by calibrating the hydraulic conductivity curves of the materials through the saturated hydraulic conductivity. The changes with respect to the laboratory measures resulted in decreasing the k_{sat} of the Beaver Creek Sand to $2.4 \times 10^{-6} \text{ m/s}$ in Column-1 and increasing the k_{sat} from the Coarse-waste-rock to 0.54 m/s in Column-2. The calibration in each test shows the existing variability between the characteristics of the material properties inside the column and the laboratory testing to measure the hydraulic properties. Furthermore, the calibration shows that small changes in the saturated hydraulic conductivity can lead to change of over 40% in discharge of an unsaturated flow model.
- The incline layering system offers a better representation of the mechanism that controls preferential flow path in waste rock embankments. The assumption of verticality in the models reduces the effect of change in gradients at low precipitation rates.
- The experiments were run under ideal conditions and in a controlled environment; however, the simulation of the five experiments showed very

small correlation of the model by applying the measured hydraulic properties. In each case, a calibration is required to find a convergence between the model and the experiment. The low correlation of the numerical models with the field results when applying the laboratory properties indicated the magnitude of variability in analysis of water flow in unsaturated conditions when using these numerical models. Consequently, these methods of analysis should be used carefully, understanding their high assumptions and limitations when analyzing seepage in unsaturated conditions.

- The hydrology of waste rock embankments can become extremely complex depending on the construction method. The end-dumping method generates a random stratigraphy that does not describe a continuous flow path. The understanding of the different aspects and material properties that relate to the mechanism of water flow through an unsaturated system can help to improve the practice of construction or remediation to control the generation of ARD in waste rock embankment.
- The three Meso-scale experiments were modeled under different testing conditions. The validation of these models was assessed by the difference in total discharge from each material with respect to the experimental results, and by using the Pearson Product Moment Correlation in the discharge from each layer. The model for Panel-1 displays differences in total discharge of less than 5% with a correlation of 0.98. As the complexity of the experiment increased, the models display higher difference with the total discharge, but with good correlation above 0.8. Panel-3 had the most complex geometry of the three panels and the model showed the lowest convergence.

6.1. FURTHER RESEARCH

While this study indicates the mechanism controlling the water flow in unsaturated conditions in a two dimensional space, analysis and further work should be conducted in three dimensional models, probably in the embankment investigation carried by Andrina (2009) to assess the difference between a numerical model and site investigation.

The research in this study did not identify which variable in the mechanism generated mode influence in the preferential flow path of the system. A multivariable analysis of the three panels could help determine the variable that influence mostly the discharge from the model.

Finally, laboratory testing should be made for the hydraulic properties from samples taken from a model experiment that analysed water flow in unsaturated conditions. This model should be run in numerical simulation to evaluate the relevance of the fabric during testing and understand the effect of disturbing samples in testing material properties.

APPENDIX

A. BACK ANALYSIS OF KSAT FOR BCS IN COLUMN-1

The Figure A.1 shows the result from the back analysis of the k_{sat} in the four tests in Column-1 for the Beaver Creek Sand (BCS, i.e. Fine sand). The back analysis is measured with respect to the discharge from the BCS. The values of k_{sat} are compared with respect to the changes in suction, precipitation, and the maximum and minimum values (Wilson, 1990).

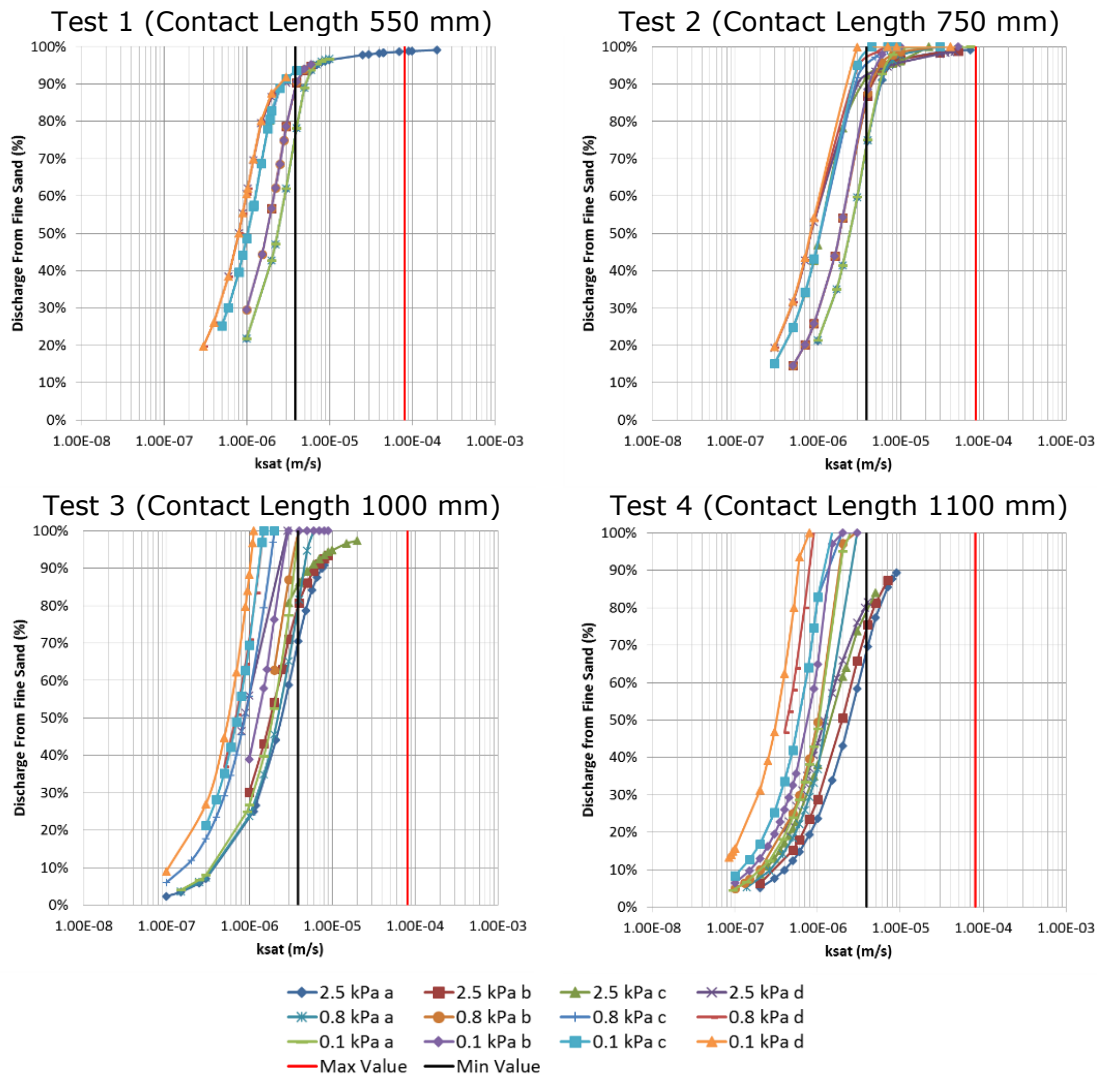


Figure A.1 Back Analysis Results from BCS in Column-1 for a Suction of at the Coarse Base of 0.1, 0.8, and 2.5 kPa; and a Precipitation of 1120 mm/day (a), 800 mm/day (b), 440 mm/day (c) and 330 mm/day (d)

Figure A.2 shows the k_{sat} of the Fine sand from the calibration simulations. The sensitivity curves shows the calibrated k_{sat} for the BCS for all the simulated conditions with respect to the measured value in the laboratory ($6.2 \times 10^{-5} m/s$) and the range established by Wilson (Wilson, 1990) between $3.9 \times 10^{-6} m/s$ and $8.1 \times 10^{-5} m/s$.

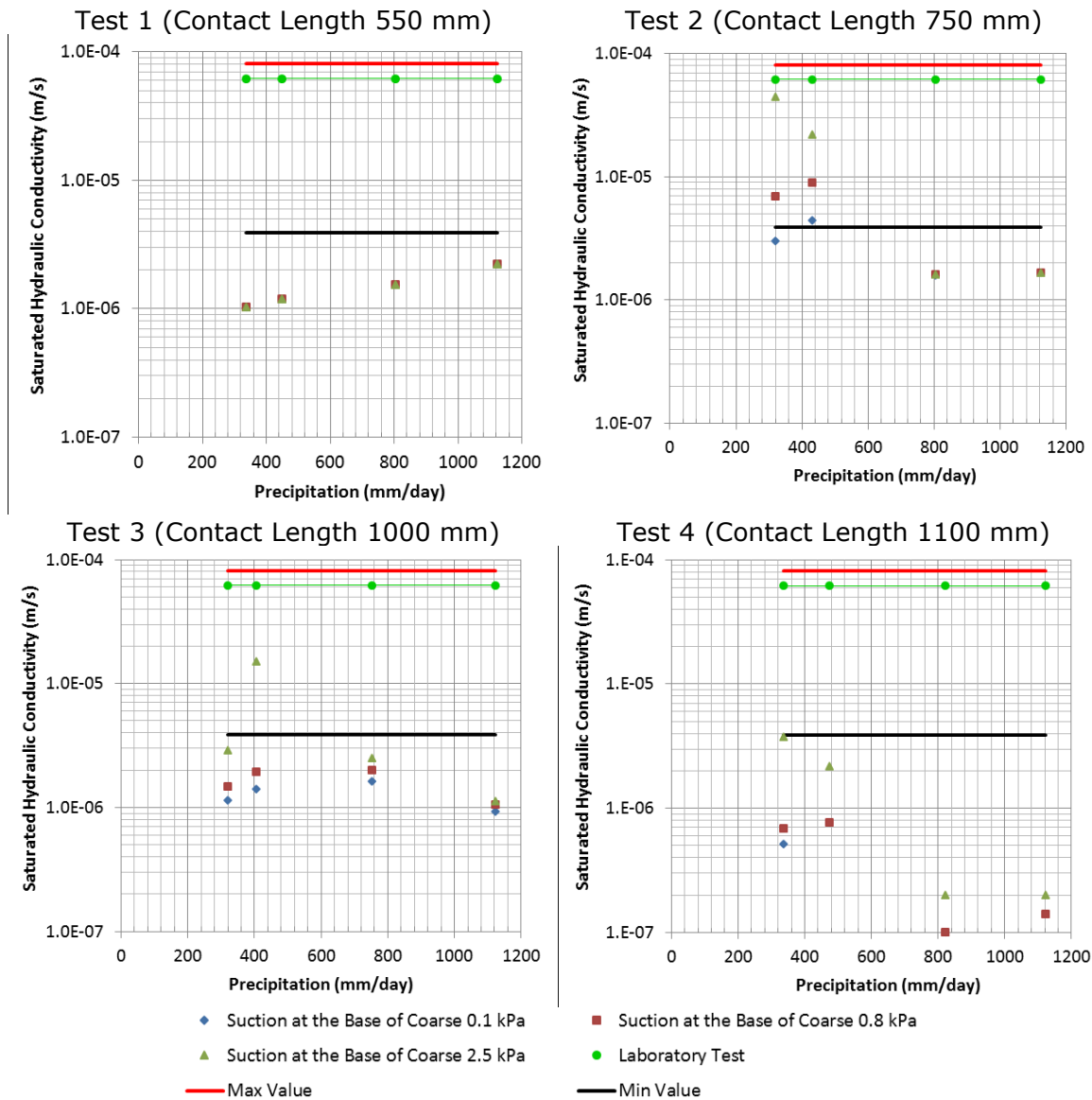


Figure A.2 Calibrated Saturated Hydraulic Conductivity for Fine Sand

The calibration of the Beaver Creek Sand k_{sat} seems reasonable despite being lower than the minimum range value by Wilson (1990). The sensitivity analysis with respect to the suction did not show significant variance to determine the controlling suction of discharge in the coarse sand, as all cases converged within an acceptable error (less than 10%).

highest error was at Test 4 (a) (b) with an average of 7% overestimation of discharge from the BCS. The sensitivity analysis of the k_{sat} for most cases shows that the model requires a value below $3.9 \times 10^{-6} \text{ m/s}$ to have significant effects on the preferential flow path.

The average of the k_{sat} on the Beaver Creek Sand for a suction of 0.1 kPa at the base of the Coarse sand is $1.5 \times 10^{-6} \text{ m/s}$ with a standard deviation of $1.1 \times 10^{-6} \text{ m/s}$. For a suction of 0.8 kPa, the average is $2.1 \times 10^{-6} \text{ m/s}$ with a standard deviation of $2.4 \times 10^{-6} \text{ m/s}$. For 2.5 kPa, the average is $6.5 \times 10^{-6} \text{ m/s}$ with a standard deviation of $1.2 \times 10^{-5} \text{ m/s}$.

B. BACK ANALYSIS OF KSAT FOR SS IN COLUMN-1

The following figure shows the result from the back analysis of the k_{sat} in the four tests in Column-1 for Silica Sand (SS, i.e. Coarse sand). The back analysis is measured with respect to the discharge from the BCS. The values of k_{sat} are compared with respect to the changes in suction, precipitation, and laboratory measure.

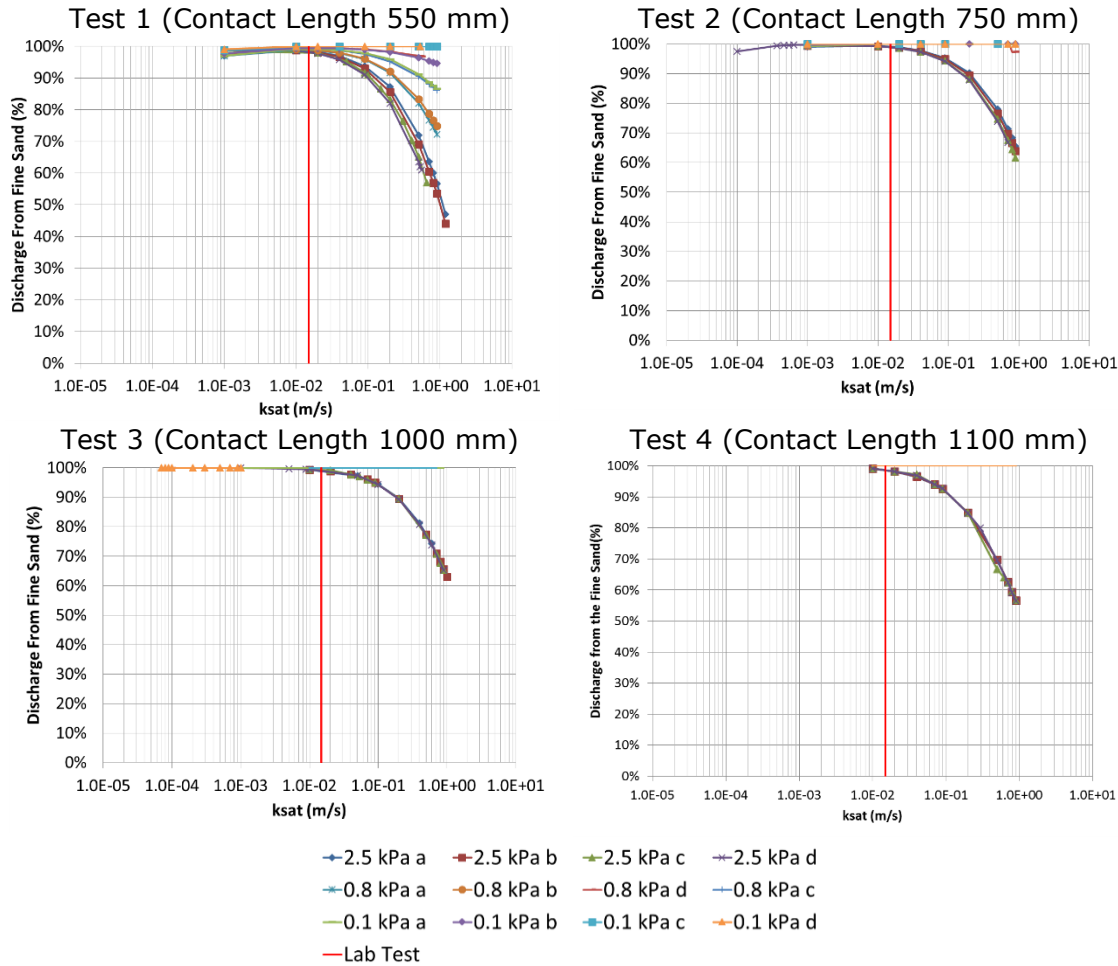


Figure B.1 Back Analysis Results from SS in Column-1 for a Suction of at the Coarse Base of 0.1, 0.8, and 2.5 kPa; and a Precipitation of 1120 mm/day (a), 800 mm/day (b), 440 mm/day (c) and 330 mm/day (d)

The range of values in the back analysis of the SS k_{sat} is between 1.0×10^{-3} m/s and 1.0 m/s. The range is selected between the extreme possible values that a material of this type could reach for the hydraulic properties. In all tests, the discharge from the BCS starts to decrease at a k_{sat} greater than the measurements in the laboratory (i.e. 0.015 m/s). However, this effect also decreases as the suction at the base of the SS decreases, and a

higher gradient of suction is formed at the base of the column. The simulation showed that only in Test 1 with a suction of 2.5 kPa at the base is it possible to model a preferential flow path through the SS; however, to achieve 8% preferential flow, the k_{sat} has to be at the extreme of 1.0 m/s .

Figure B.2 presents the k_{sat} of the Coarse sand related to the discharge results in Figure 4.20. The graphs show the calibrated k_{sat} for all the simulated conditions that are closest to the laboratory results and its relation to the measured value in the laboratory ($1.48 \times 10^{-2} \text{ m/s}$).

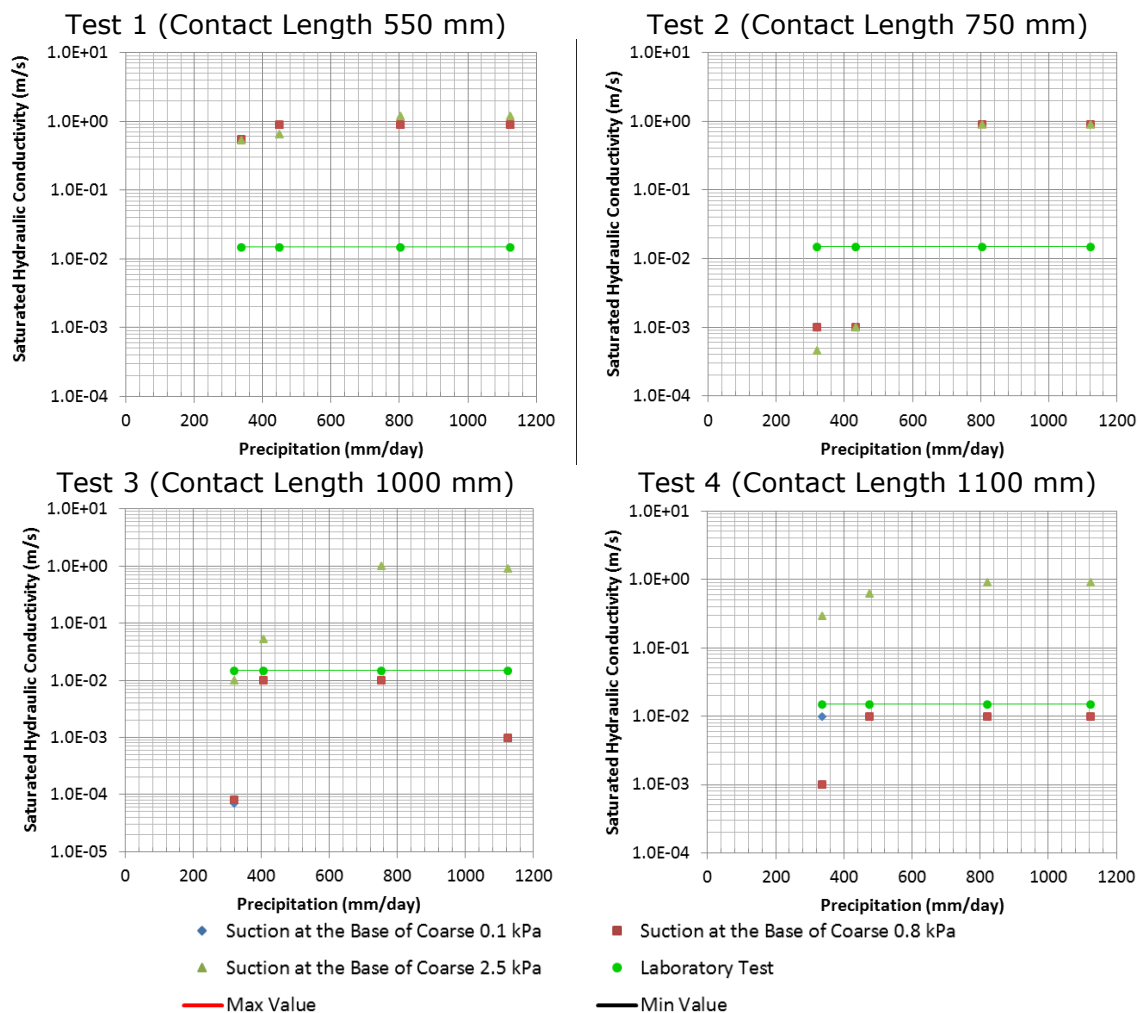


Figure B.2 Calibrated Saturated Hydraulic Conductivity for Coarse Sand

Considering the calibrations with less than 10% discharge error, the average of the k_{sat} on the Silica Sand for a suction of 0.1 kPa and 0.8 kPa at the base of the Coarse sand is $3.0 \times 10^{-3} \text{ m/s}$ and at 2.5 kPa, the average is 0.71 m/s . These results relate to the

displacement of the HCC; as k_{sat} decreases, the levels of suction decrease to maintain the same permeability of the material.

C. BACK ANALYSIS OF AEV FOR BCS IN COLUMN-1

The following figures show the result from the back analysis in the four tests in and its relation to the changes in suction, precipitation, and laboratory measurement.

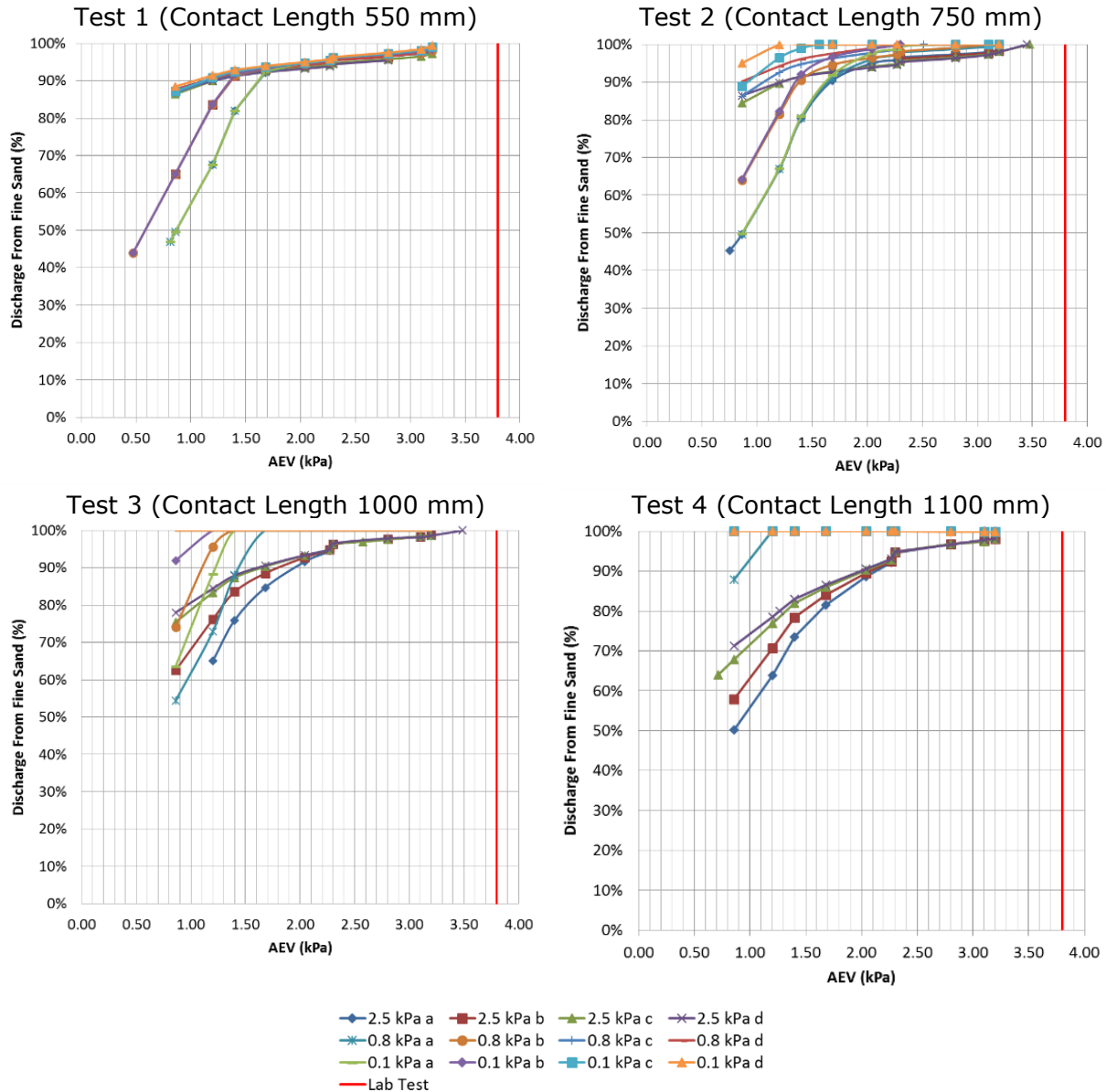


Figure C.1 Back Analysis of AEV for the BCS in Column-1 for a Suction of at the Coarse Base of 0.1, 0.8, and 2.5 kPa; and a Precipitation of 1120 mm/day (a), 800 mm/day (b), 440 mm/day (c) and 330 mm/day (d)

The back analysis of the AEV for the BCS is within a range of 0.6 kPa and 3.5 kPa. This range varies from the proposed values by Wilson (1990) in which the AEV for the BCS was established to be between 3.0 kPa and 5.0 kPa. The back analysis shows that the model

maintains a preferential flow in the BCS for AEV above 3.5 kPa. The use of the AEV calculated from the measured SWCC resulted in an overestimation of the preferential flow path through the BCS (see section 4.5.1.1). The sensitivity curves for the AEV show a decreasing discharge for AEV below 3.5 kPa; for Tests 1 and 2, the drop in discharge increases at of 1.6 kPa of suction, while for Tests 3 and 4, the drop increases less and starts at an AEV of 2.1 kPa.

On the other hand, it is noticeable that decreasing suction at the base affects the calibration of the AEV for the BCS. As suction decreases, the change in discharge is lower at lower AEVs.

D. BACK ANALYSIS OF k_{sat} FOR WR IN COLUMN-2

Figure D.1 shows the result from back analyzing k_{sat} from the Fine-waste-rock (F-WR) and Coarse-waste-rock (C-WR) in Column-2. The back analysis is measured with respect to the discharge from the F-WR. The values of k_{sat} are compared with respect to the changes in precipitation and laboratory measurements. Figure D.1 show the change in discharge from the F-WR with changes in k_{sat} for the F-WR (a) and the C-WR (b).

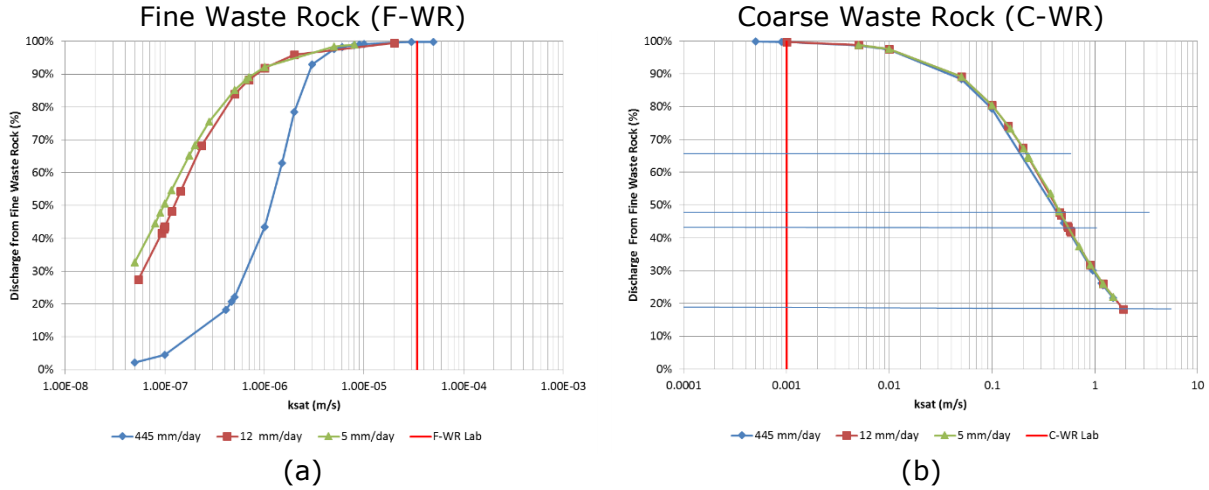


Figure D.1 Back Analysis of F-WR k_{sat} (a) and C-WR k_{sat} (b) for Waste Rock in Column-2 for a Suction of at the Base of 0.0 kPa; and a Precipitation of 445 mm/day (a), 12 mm/day (b), and 5 mm/day (c)

The calibration of the k_{sat} for the F-WR (Figure D.1 a) shows a decrease in discharge from the F-WR with decreasing k_{sat} . The effect from changes in k_{sat} can vary greatly; a variation of $1 \times 10^{-6} m/s$ can decrease the discharge from 5% up to 35%. Once the k_{sat} is smaller than the precipitation, the discharge decreases significantly from the F-WR with small changes in k_{sat} . The decrease in discharge from the F-WR results in higher discharge from the C-WR. In order for the model to maintain the balance from decreasing the k_{sat} in the F-WR and increasing the discharge on the C-WR, the column internal pressure should increase. The increase has to lower the suction in order that permeability of the C-WR is higher than the F-WR under unsaturated conditions. Similarly, if the k_{sat} of the C-WR is increased, the head pressure has to reduce to increase the suction. This reduction goes to a point where the permeability of the F-WR is greater than the C-WR, in order for the F-WR to be the preferential flow path.

The calibration of the k_{sat} for the F-WR shows a similar tendency of discharge vs k_{sat} at a precipitation of 12 mm/day and 445 mm/day. At the highest precipitation in Column-2,

the change of k_{sat} shows a high decrease in the F-WR discharge. In contrast, in the calibration of the k_{sat} for the C-WR, there is no influence in the precipitation.

In addition, the calibration displays a total discharge (Figure D.2) being less than the applied precipitation. This difference occurs due to numerical errors in the mesh. The results from the calibration of the F-WR show an increment in the error as the k_{sat} decreases; on the contrary, in the case of the C-WR, the error increases with the increment of k_{sat} . These errors reach a maximum of 20% at the highest precipitation, but decrease as the precipitation decreases. One way to overcome this numerical error is to measure the lateral flow at the contact zone, this measurement allows to indirectly calculate the total flow in each side of the column, and consequently, results in a secondary reading of the discharge flow with respect to the total precipitation. The secondary reading allows the correction of the total discharge to have a 100% reading, preserving the mass balance of the system. Furthermore, these readings were verified by applying a flux section close to the base and measuring the total discharge, which was equal to the total precipitation.

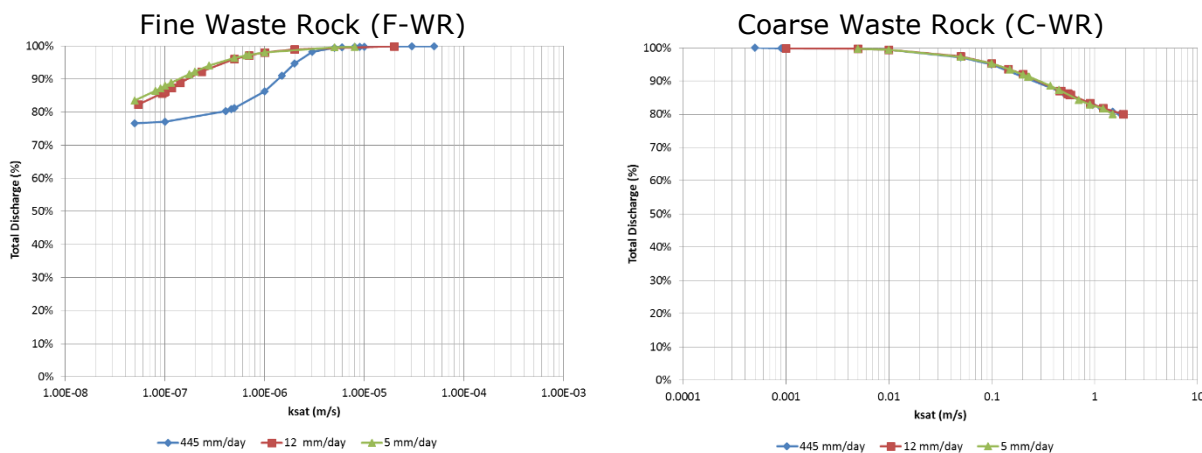


Figure D.2 Total Discharge from the Back Analysis of F-WR and C-WR in Column-2

E. WATER FLOW TRANSFER IN SANDY SOIL

The calibration of the k_{sat} from Column-1 and Column-2 allows the evaluation of the effect of lateral flow of water between the two materials. The following results are presented as a percentage of the flux applied to each half of the column (i.e. one half of the total applied flux to the column; see Table 4.1 Column-1). For example, 30% lateral flow *to the fine sand* is the percentage of the flux applied to the SS moved into the BCS at the contact length. The following figures show the simulation results for each precipitation rate and contact length. Each case evaluates the three different base suctions in the coarse sand. The vertical axis in each graph indicates water transfer from the SS to the BCS for values above 0% axis (blue zone), and water transferring from the BCS to the SS for values below 0% (red zone). Figure E.1 illustrates the results in each test and flux rate for the lateral water transfer after iterating k_{sat} of the Beaver Creek sand.

Figure E.1 shows that as the k_{sat} in the BCS increases, the lateral transfer to the fine sand increases, changing the flow from the coarse to the fine. The analysis showed the possible changes in water transfer through the system, ranging from 60% to the coarse sand up to 100% through the fine sand. This variation can occur by altering k_{sat} of the fine sand approximately one order of magnitude. For Tests 1 and 2, k_{sat} can range between $3.0 \times 10^{-7} m/s$ and $2.0 \times 10^{-4} m/s$; Tests 3 and 4 range between $3.0 \times 10^{-7} m/s$ to $7.0 \times 10^{-5} m/s$. The effect of increasing the contact length results in a lower k_{sat} for an equal discharge or lateral flow. For example, at a precipitation rate of $1.3 \times 10^{-5} m/s$ in Test 1, having a Fine Sand k_{sat} equal to $4.0 \times 10^{-5} m/s$ results in a discharge of 42% from the fine sand, while for Test 4, k_{sat} is equal to $2.5 \times 10^{-5} m/s$ for a discharge of 42%. The precipitation has an impact on the calibration of Column-1 and the transfer flow from one material to the other. The change in precipitation generates a responds where at lower flux rates, the required k_{sat} decreases for the model. This responds of the model results in the displacement of the lateral flow with the change in k_{sat} to lower values (left side). The sensitivity analysis regarding the difference in base suction at the column shows the lateral transfer in Tests 1 and 2 to be unaffected by changes in precipitation; contrary to Tests 3 and 4 where the variability increased as the flux rate decreased (with a higher intensity).

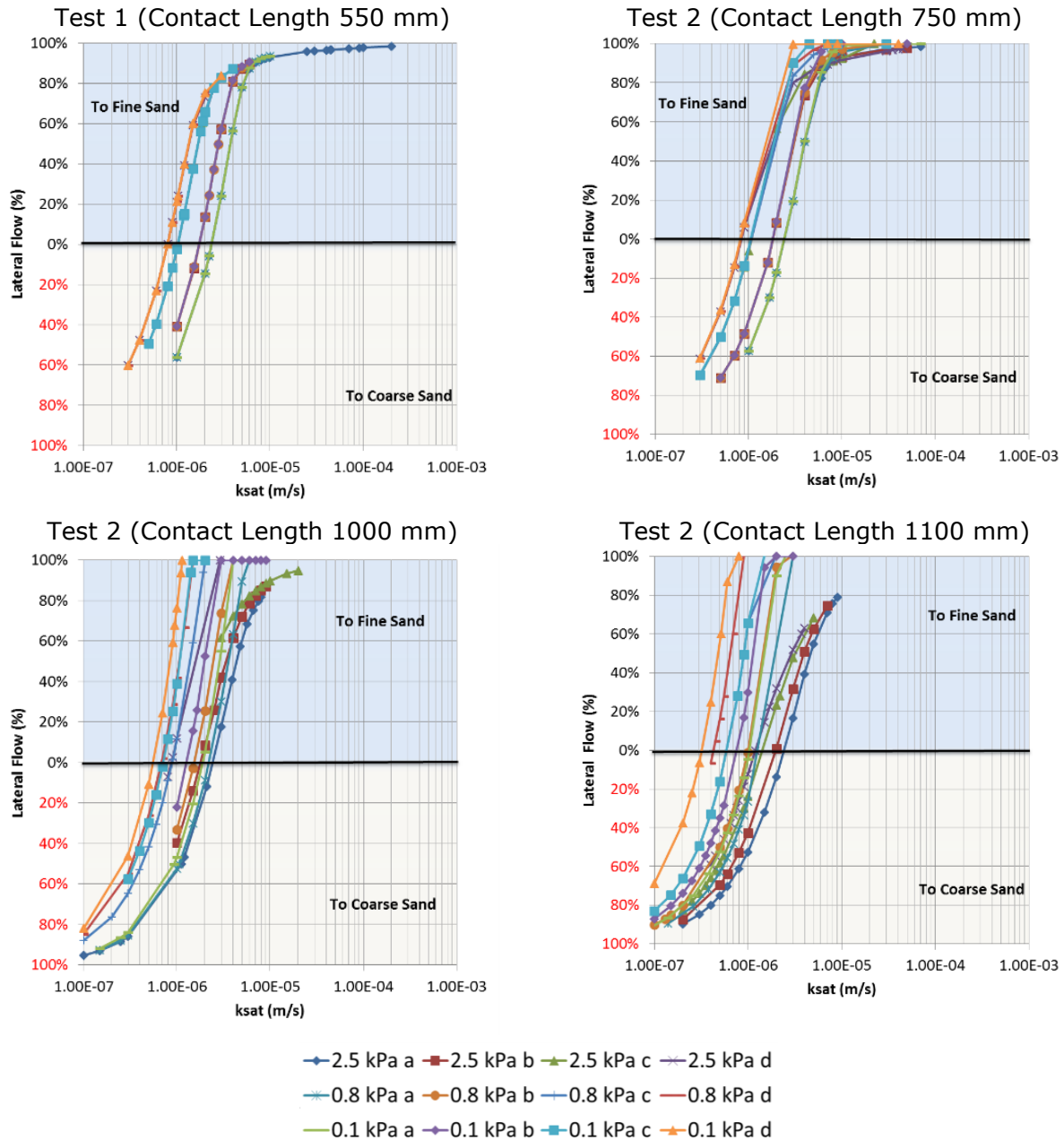


Figure E.1 Sensitivity Curves for Lateral Flow with Changes k_{sat} from BCS for a Suction of at the Coarse Base 0.1, 0.8, and 2.5 kPa; and a Precipitation of 1120 mm/day (a), 800 mm/day (b), 440 mm/day (c) and 330 mm/day (d)

Figure E.2 illustrates the percentage of water transfer using the k_{sat} calibration of the Beaver Creek sand. The calibration shows the preferential flow path through the fine sand only under flux rates below 750 mm/day, and through the coarse sand for fluxes above 800 mm/day.

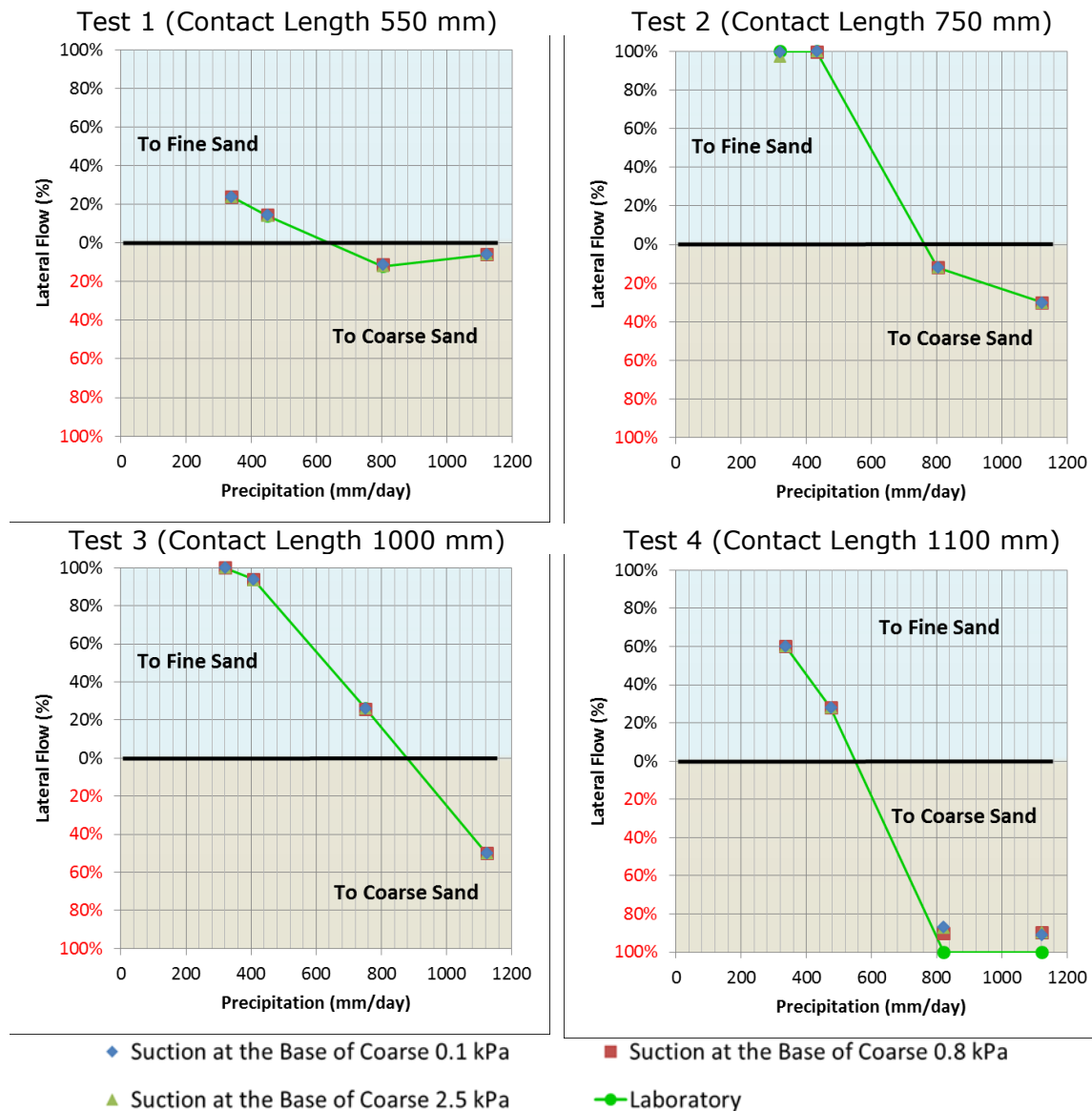


Figure E.2 Lateral Flow in Column-1, Comparison between Laboratory Results, and Model Calibration of k_{sat} from BCS

The calibration of the model enabled the recreation of the lateral flow from Column-1 by adjusting the k_{sat} for the BCS. The model also mimics the results for the three suction conditions at the base boundary of the column; however, as the contact length increased, the drop of suction generated small numerical instabilities. In contrast, the calibration of the k_{sat} from the coarse sand requires large values of k_{sat} to generate preferential flow through the SS. Figure E.3 shows the results in each test and flux rate for the lateral water transfer after iterating the k_{sat} from SS.

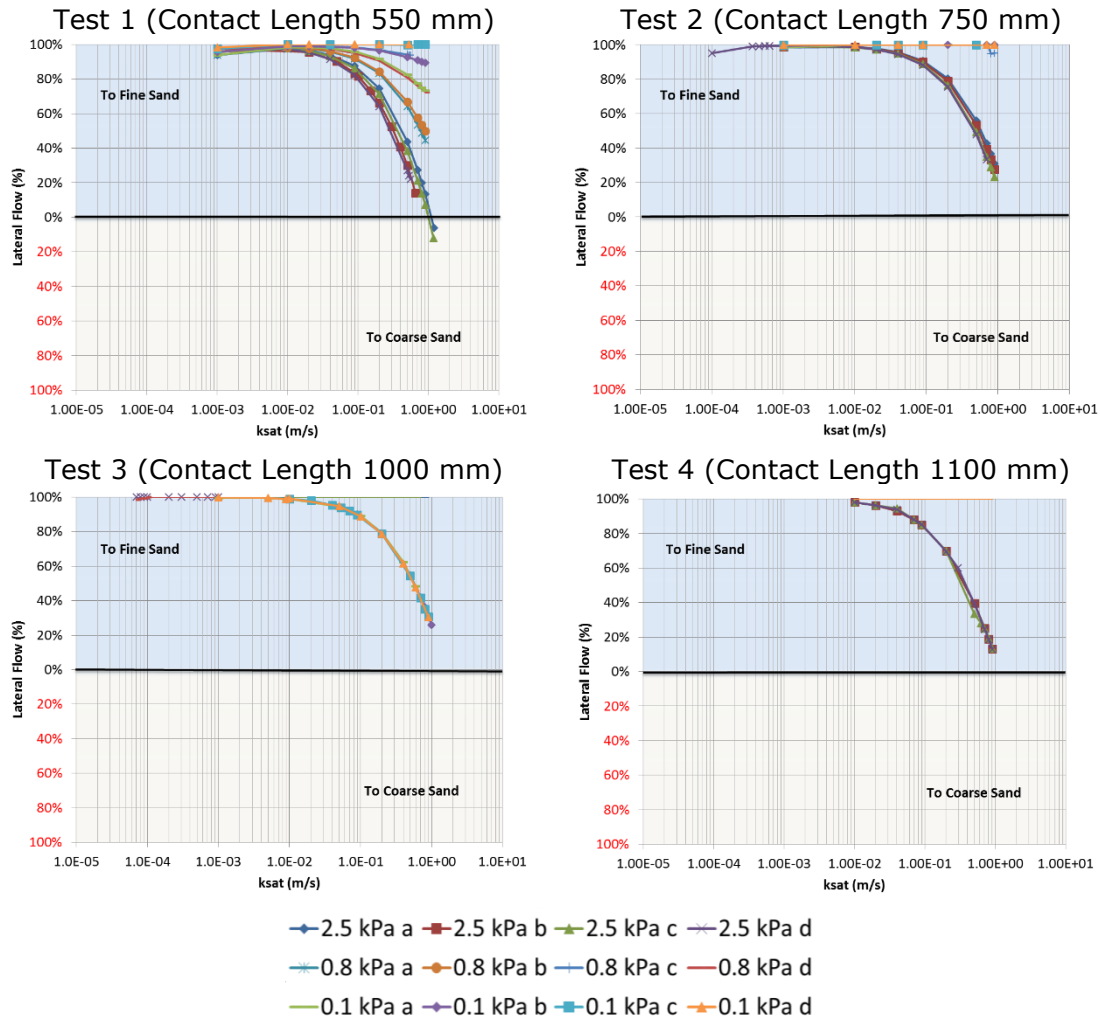


Figure E.3 Sensitivity Curves for Lateral Flow with Changes k_{sat} from SS for a Suction of at the Coarse Base of 0.1, 0.8, and 2.5 kPa; and a Precipitation of 1120 mm/day (a), 800 mm/day (b), 440 mm/day (c) and 330 mm/day (d)

Figure E.3 shows that increasing the k_{sat} for the SS decreases the lateral transfer to the BCS, changing the flow from the fine to the coarse sand. The simulations show possible changes in water transfer through the system, ranging from 100% to the fine sand up to 10% through the coarse sand. However, in order to generate a small drop of flow from the BCS, the increment in the k_{sat} of the SS is of two orders of magnitude. These increments lead to unrealistic hydraulic properties for the characteristics of the coarse sand in the Column (above 1.0 m/s for k_{sat}).

Figure E.4 shows the closest correlation of the model from the sensitivity curves. The results showed that as the suction at the base of the SS decreased, the correlation drops.

The optimum correlation is for equal base suction at the base of 2.5 kPa by calibrating k_{sat} of the SS.

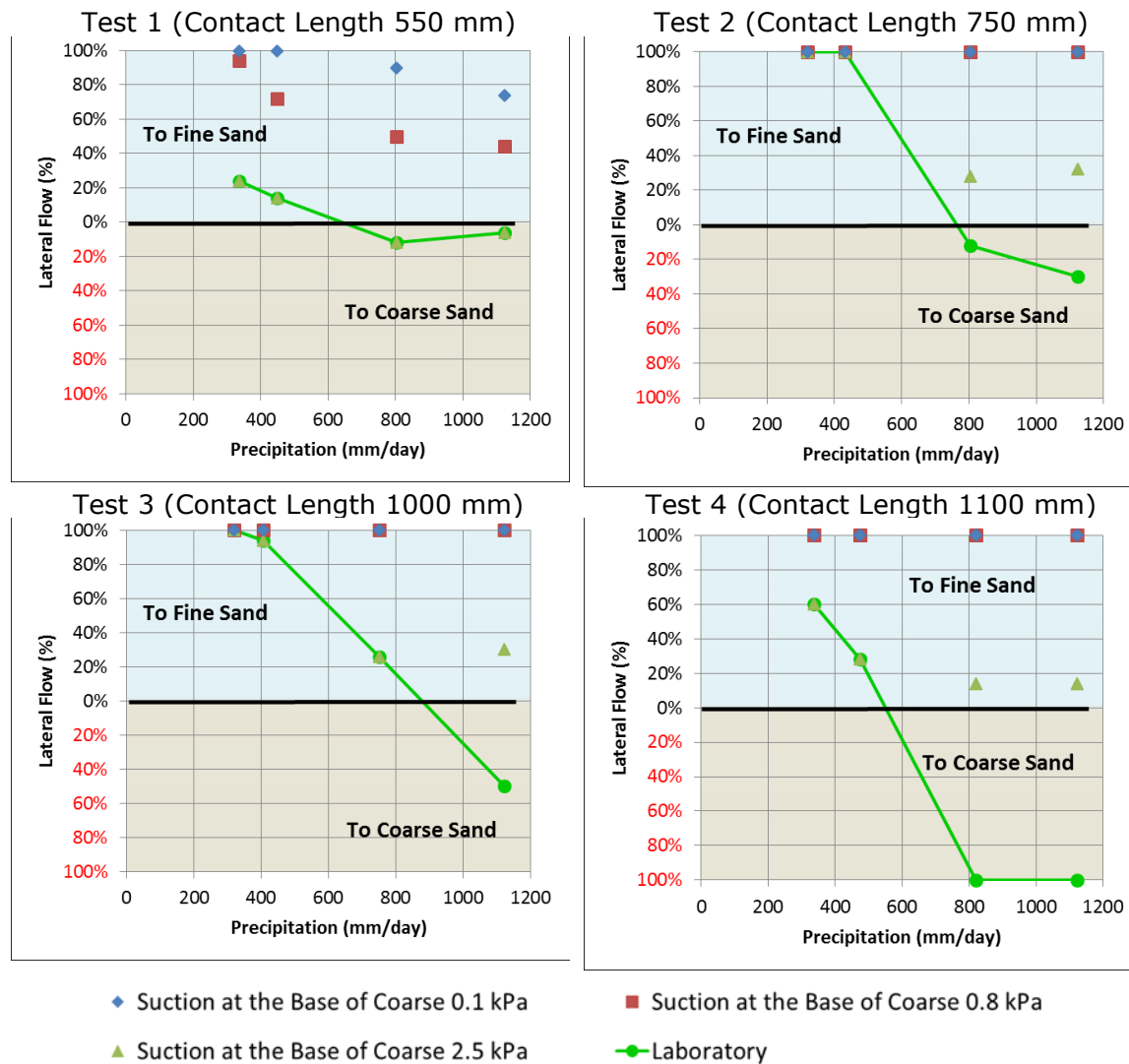


Figure E.4 Lateral Flow in Column-1, Comparison between Laboratory Results, and Model Calibration of k_{sat} from SS

The calibration of the model allowed for a few cases to recreate the lateral flow from Column-1 by adjusting the k_{sat} for the SS. The reduction of suction at the base resulted in a lateral transfer to the BCS of 100% when the material has a contact length above 750 mm. Below 750 mm, the decrease in suction at the base has a slight improvement of the correlation as k_{sat} approximates 1.0 m/s.

The lateral transfer in Column-1 is improved by calibrating the hydraulic properties of the materials. The comparison of the two approaches in this investigation achieves the

optimum calibration of the column by reducing the k_{sat} of the BCS to $2.4 \times 10^{-6} \text{ m/s}$. This calibration results in a change of the relation between the hydraulic conductivity curves in Column-1.

F. WATER FLOW TRANSFER IN WASTE ROCK

The following results show the lateral flow in Column-2 from the simulations calibrating the saturated hydraulic conductivity (k_{sat}) from the Waste Rock materials. The back analysis of each material (Figure F.1) illustrates the lateral flow resulting from changes in k_{sat} for each material. The range of values for the k_{sat} in the F-WR varies in three orders of magnitude, between $5.0 \times 10^{-8} m/s$ to $5.0 \times 10^{-5} m/s$, while for the C-WR, the k_{sat} varies between $5.0 \times 10^{-4} m/s$ to $2.0 m/s$. The range selected for each calibration is beyond the typical values for these materials with respect to the classification ASTM D 2487 (SW-SM and GP for F-WR and C-WR, respectively).

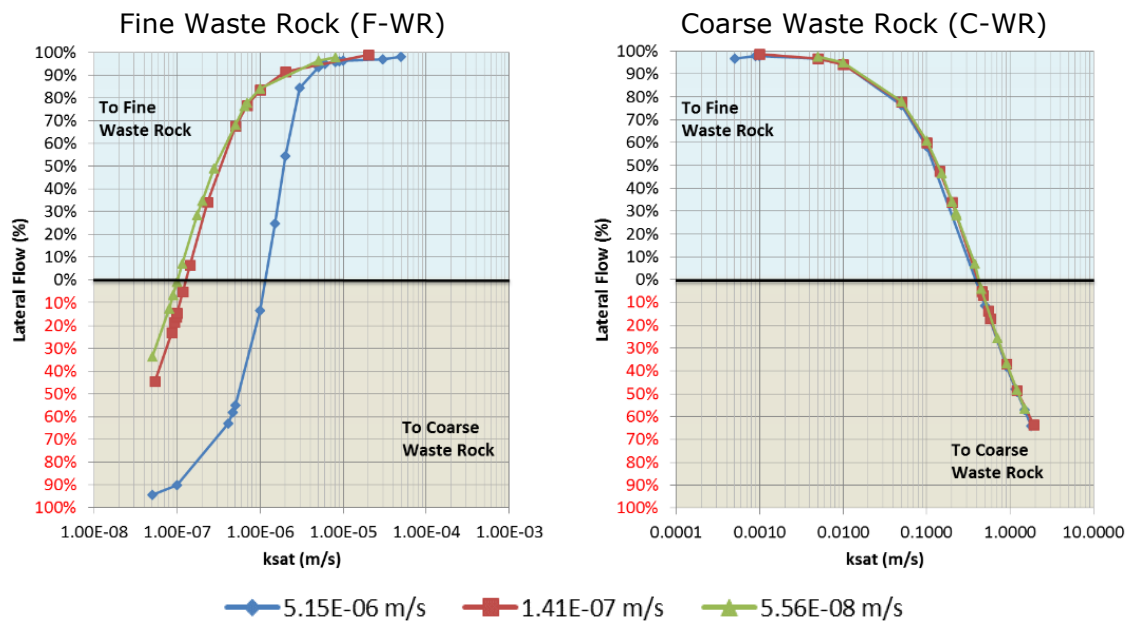


Figure F.1 Water Transfer between Coarse Sand and Fine Sand from Iteration of k_{sat} for the Fine-waste-rock and Coarse-waste-rock

The lateral flow from F-WR shows that increments in k_{sat} decrease flow from the C-WR and transfer to the F-WR at small variances. The analysis showed the possible changes in water transfer through the system, ranging from 90% to the C-WR up to 100% through the F-WR. This variation can occur by altering k_{sat} of the Fine-waste-rock approximately two orders of magnitude in difference. The calibration of F-WR shows that at higher precipitation rates, the lateral transfer is impacted more than low precipitation. The right graph shows the lateral flow to the C-WR by incrementing k_{sat} in C-WR, changing the flow from the fine to the coarse. The analysis showed the possible changes in water transfer through the system, ranging from 100% to the F-WR up to 70% through the C-WR. Overall, the simulations

show that lateral flow is more sensitive to changes in the k_{sat} from the F-WR than from C-WR.

The following results present the lateral flow of water between the waste rock materials and Golden Sunlight Mine. The lateral flow is calculated as a percentage of the flux applied to each half of the column (i.e., one half of the total applied flux to the column; see Table 4-1 Column-2). The results indicate water transfer from the coarse sand to the fine sand for values above 0% axis (i.e. blue zone) and water transferring from the fine sand to the coarse sand for values below 0% (i.e. red zone). The simulated solutions using the laboratory parameters, the numerical calibration by Newman, and the proposed k_{sat} calibration are as follow:

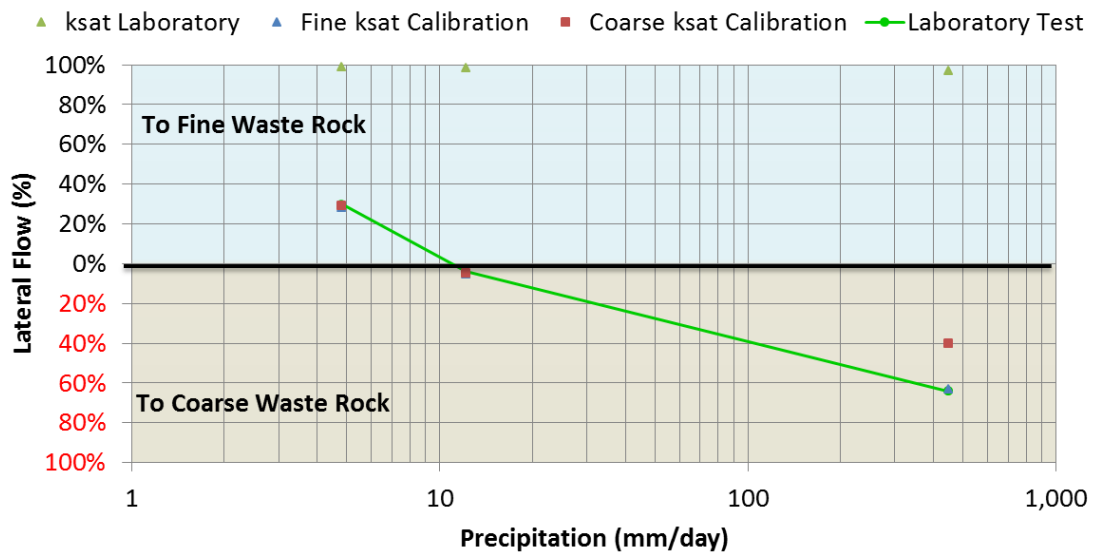


Figure F.2 Lateral Flow in Column-2, Comparison Between Laboratory Results, Model with Laboratory Properties and Model Calibration of k_{sat} from F-WR, C-WR

The laboratory results showed in Column-2 that lateral flow increases to the C-WR as precipitation increases. The simulation using the laboratory properties overestimated the lateral flow from F-WR to C-WR (Figure F.2). Under this condition, almost all the precipitation applied to the C-WR is transferred laterally. The calibration of the k_{sat} for each material helps to improve the correlation of the model with errors of less than 1.0%.

G. PRESSURE PROFILES IN COLUMN-1 USING SANDY SOILS

The following figures show the change in pressure with elevation; the profiles are located at 5 mm and 75 mm from the center of the column. The results are from simulations using the average precipitation from Table 4.1; Flux (a) = 1120 mm/day, Flux (b) = 800 mm/day, Flux (c) = 440 mm/day, and Flux (d) = 330 mm/day. The results take into account the calibrated condition for Column-1. The differential suction at the base is generated by 2.5 kPa at BCS and 0.8 kPa at SS. The calibrated properties for the BCS consider a k_{sat} of $2.4 \times 10^{-6} m/s$ and $0.015 m/s$ for the SS.

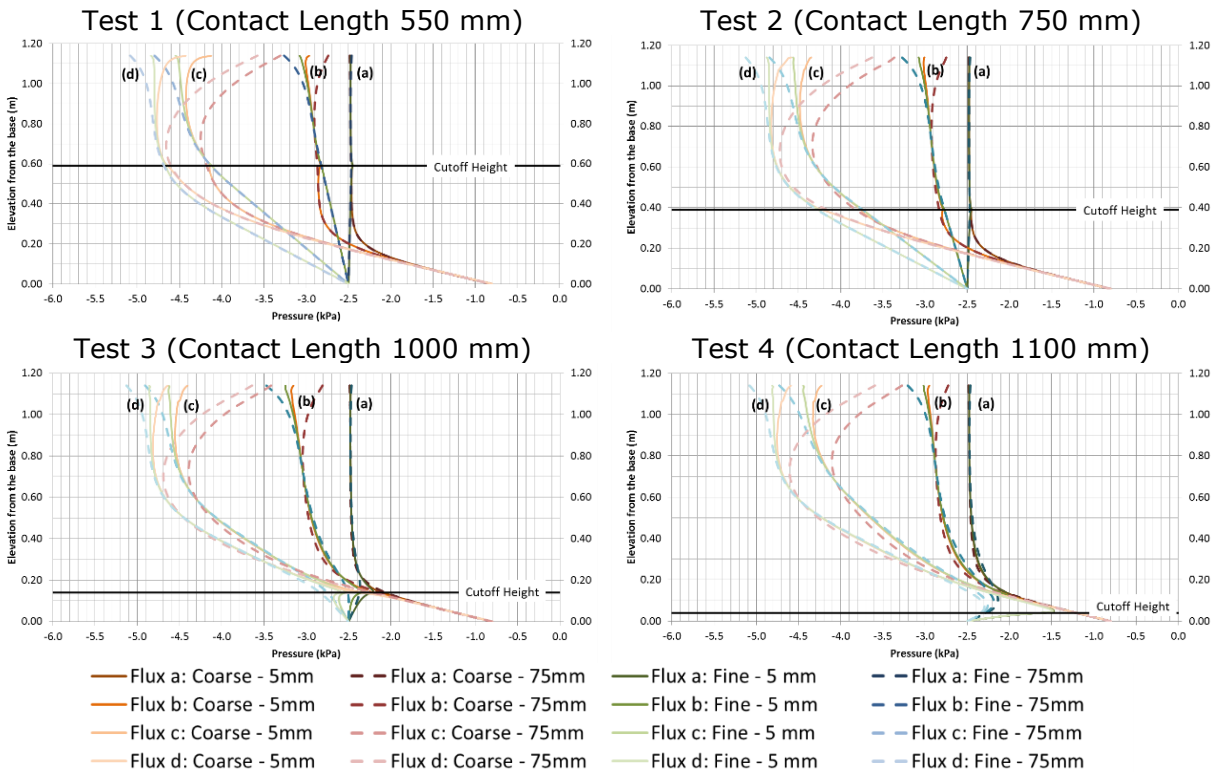


Figure G.1 Change in Suction at Calibration of k_{sat} in BCS-Test 1, 2, 3, And 4 for a Suction of at the Coarse Base of 0.8 kPa; and a Precipitation of 1120 mm/day (a), 800 mm/day (b), 440 mm/day (c) and 330 mm/day (d)

The initial unsaturated conditions established at the beginning of the tests demonstrate that the materials reach a suction at the AEV. Once the precipitation rate is applied in steady state conditions, the internal suction of the system changes. It is expected that if the precipitation rate is below the hydraulic conductivity, then the initial suction of the system should not change, as there is no change in VWC. If the VWC increases or decreases, the materials should decrease or increase the suction levels, respectively. However, the nature of this model generates lateral transfer of water between the two

materials; thus, the precipitation could be below the hydraulic conductivity, but a gradient between the two materials would generate water flow from one material to the other. The increment in flow in one material due to lateral flow could result in changes of VWC.

The precipitation rates increase the VWC, resulting in a reduction of the hydraulic conductivity. The increment in VWC fills the pores, reducing the hydraulic conductivity of the soil and its matric suction.

In all tests, the pressure profiles show constant suction in the column at the highest precipitation; as the precipitation decreases, the suction in the system increases. At the top of the column for precipitation "b", "c", and "d" changes in suction occurred due to the precipitation rates. In the BCS, suction starts to decrease with height and toward the center of the column. In the top 0.2 m, a quick drop of suction occurs, followed by an almost constant suction at 0.8 m; at the lowest 0.6 m, suction decreases constantly, reaching the base suction of 2.5 kPa. The response of the SS from precipitation in the top 0.2 m is contrary to that at the BCS; at the top 0.2 m, suction increases towards a lower elevation and the center of the column. This condition revealed that the main gradient in the column is formed at the top, resulting in the higher lateral flow from the SS toward the BCS.

The boundary conditions causes the system to satisfy the suction at the base, resulting in change of suction below the height of the cut-off. At the base of the coarse sand (right side of the column), the suction reaches a minimum of 0.8 kPa, while in the Fine Sand, higher suction is develop to reach 2.5 kPa. The curves show that higher suction is generated in the column for lower precipitation rates, as follows:

$$\text{Suction Flux "a"} < \text{Suction Flux "b"} < \text{Suction Flux "c"} < \text{Suction Flux "d"}$$

The different tests show that an equilibrium in suction occurs on both material where the gradient between both materials is close to zero. The equilibrium occurs at an elevation between the top of the cut-off and the top of the column, increasing towards the center of the column. The distance of equilibrium suction increases with precipitation and contact length (Table G.1).

Table G.1 Longitude of Equilibrium Suction for Colum-1 (m)

Test	Contact Length (m)	Precipitation (mm/day)			
		1120	800	440	330
1	0.55	0.84	0.5	0.15	0.25
2	0.75	0.84	0.69	0.5	0.45
3	1.0	0.99	0.93	0.65	0.7
4	1.1	1.04	0.97	0.8	0.8

Finally, it can be observed that equilibrium suction can continue below the top of cut-off, but it starts to change as the system starts to satisfy the base boundary conditions. The length in which a constant suction is formed below the cut-off is reduced as the cut-off decreases.

H. PRESSURE PROFILES IN COLUMN-2 USING WASTE ROCK

The figure presents the change in suction with elevation for each material at 5 mm from the center of the column and at 75 mm (center of each side) from the center of the column. Contrary to Column-1, the Waste Rock column was tested with a 0.0 kPa base suction; this condition reduced the effect of having a gradient near the base due to the boundary conditions.

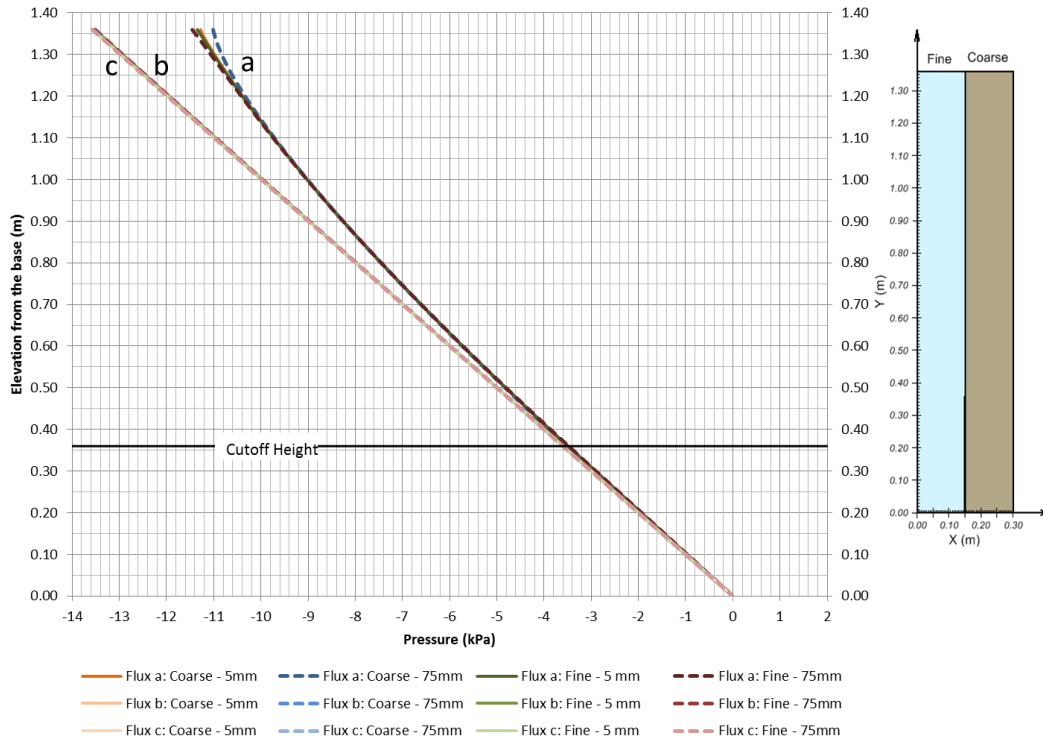


Figure H.1 Change In Suction at Calibration Of k_{sat} In C-WR for a Suction of at the Base of 0.0 kPa; and a Precipitation of 445 mm/day (a), 12 mm/day (b), and 5 mm/day (c)

The pressure profile shows a constant increment of suction and the same magnitude for both materials at the same precipitation. It also shows a slight decrease in suction for the highest precipitation of 445 mm/day; the decrement starts at the top cut-off with a slight exponential decrease up to the top of the column.

I. PROFILE RESULTS FROM SIMULATION IN COLUMN-1

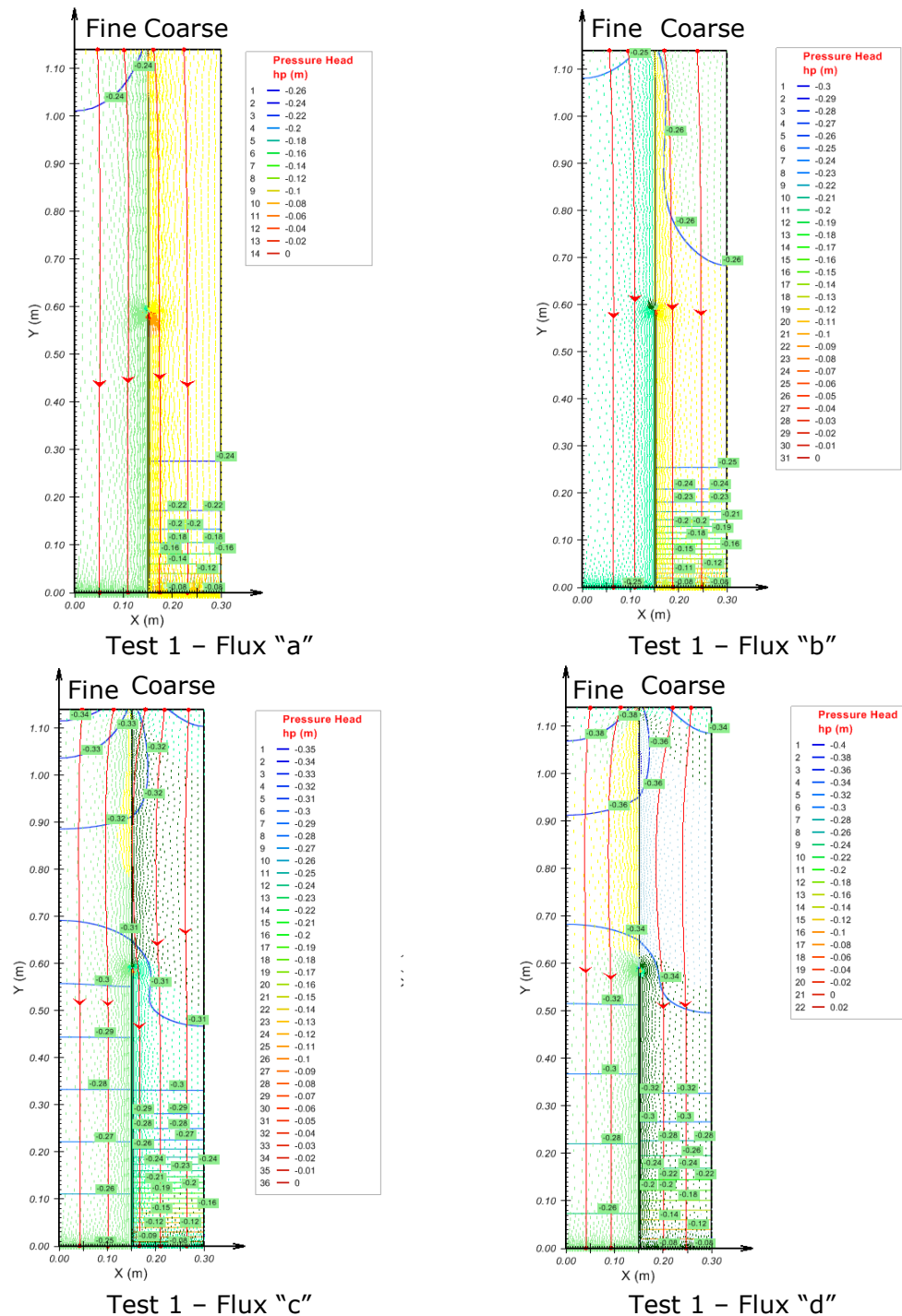
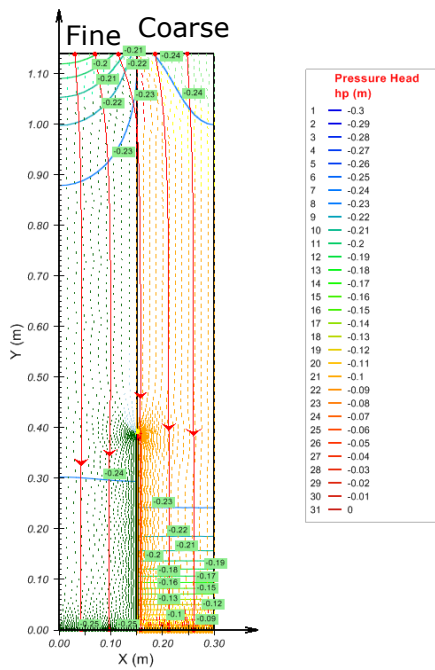
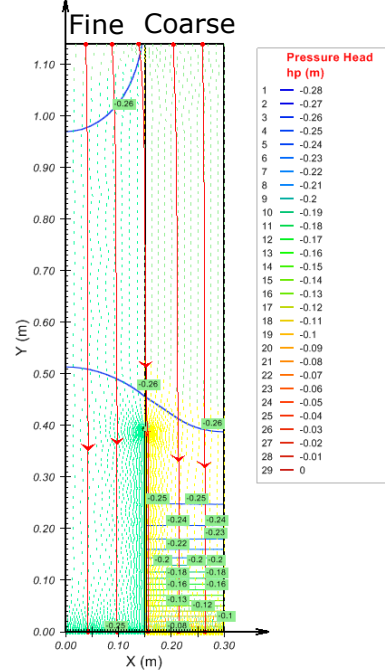


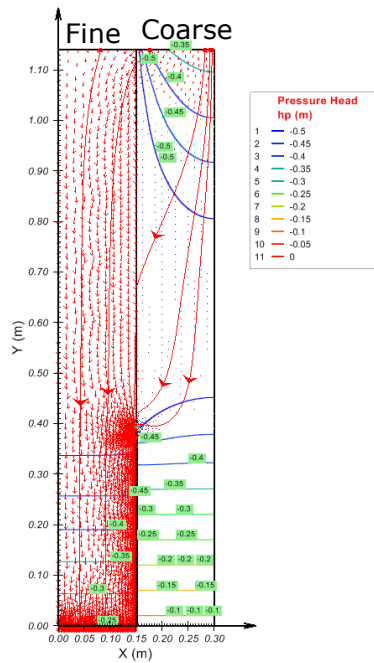
Figure I.1 Results from Test-1 with A Contact Length of 550 mm for for a Suction of at the Base of 0.8 kPa and a Precipitation of 1120 mm/day (a), 800 mm/day (b), 440 mm/day (c) and 330 mm/day (d)



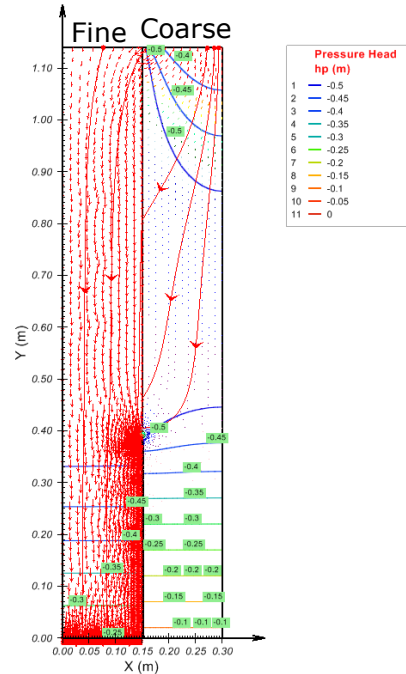
Test 2 - Flux "a"



Test 2 - Flux "b"

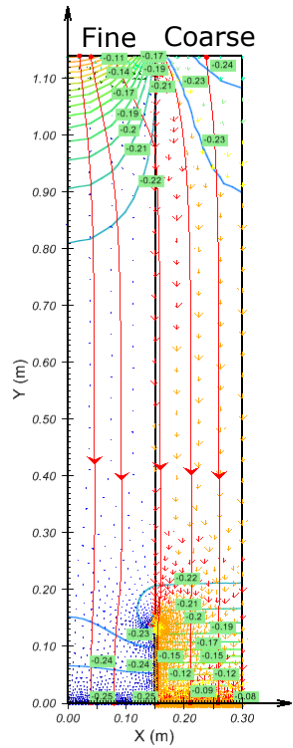


Test 2 - Flux "c"

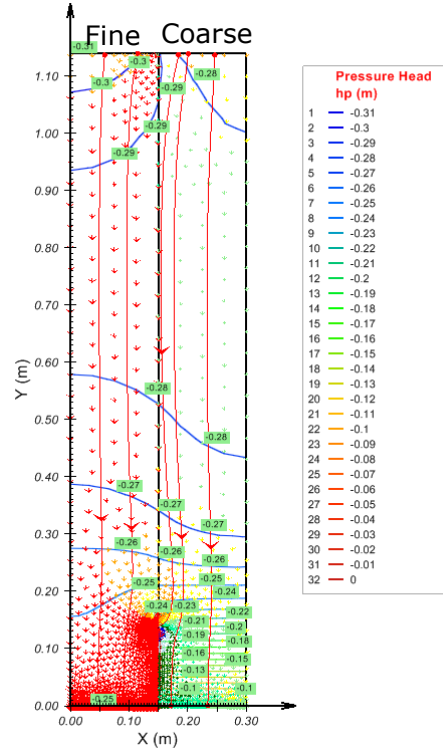


Test 2 - Flux "d"

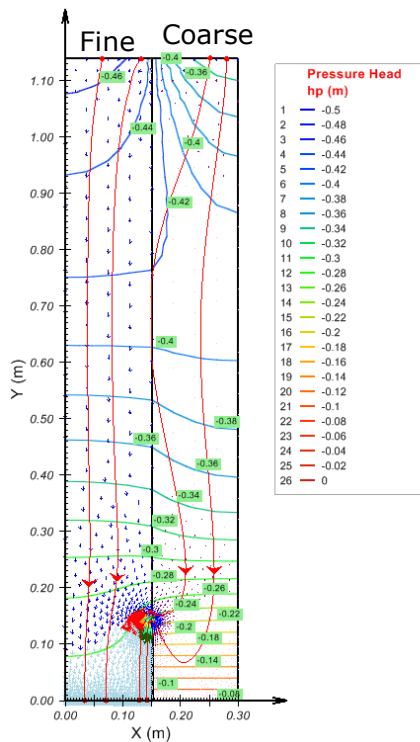
Figure I.2 Results from Test-2 with A Contact Length of 750 mm for for a Suction of at the Base of 0.8 kPa and for Precipitation of 1120 mm/day (a), 800 mm/day (b), 440 mm/day (c) and 330 mm/day (d)



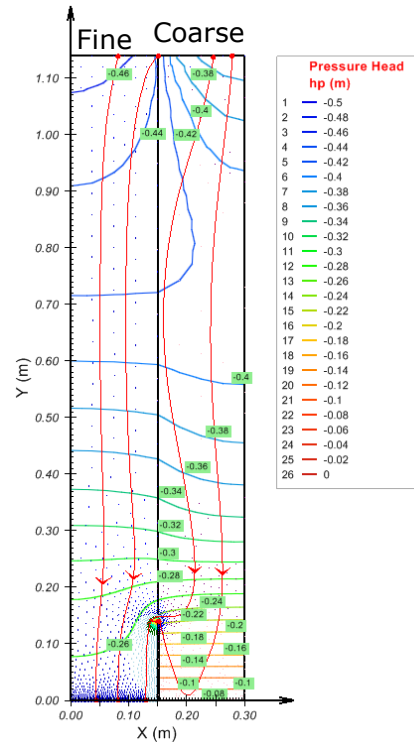
Test 3 - Flux "a"



Test 3 - Flux "b"

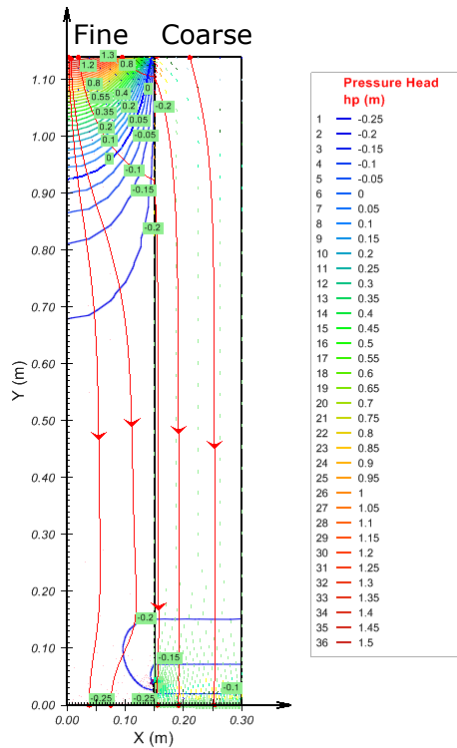


Test 3 - Flux "c"

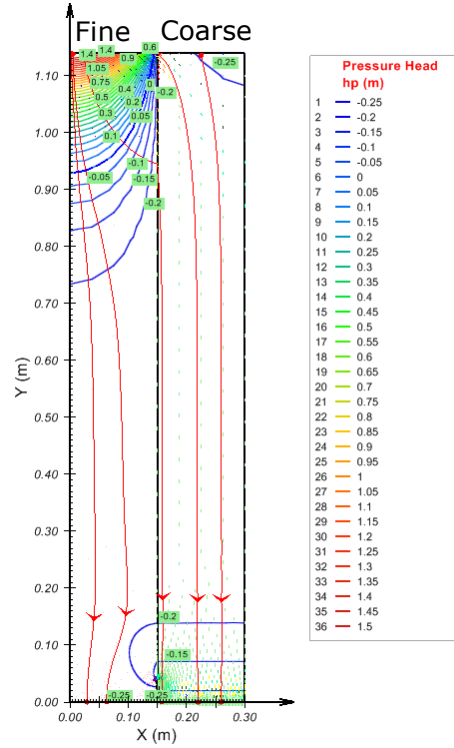


Test 3 - Flux "d"

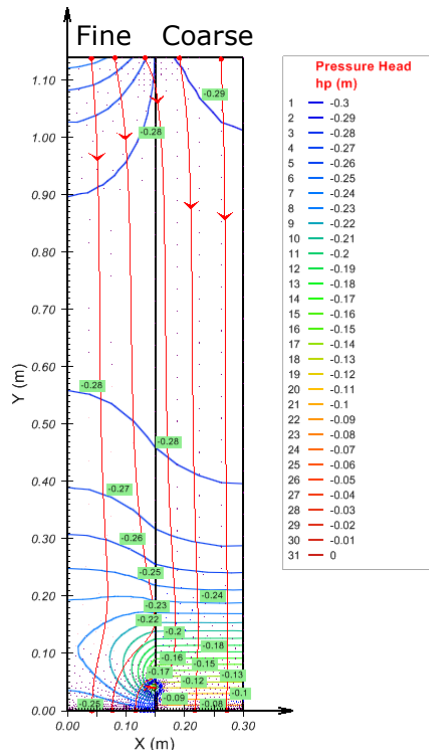
Figure 1.3 Results from Test-3 with A Contact Length of 1000 mm for for a Suction of at the Base of 0.8 kPa and for Precipitation of 1120 mm/day (a), 800 mm/day (b), 440 mm/day (c) and 330 mm/day (d)



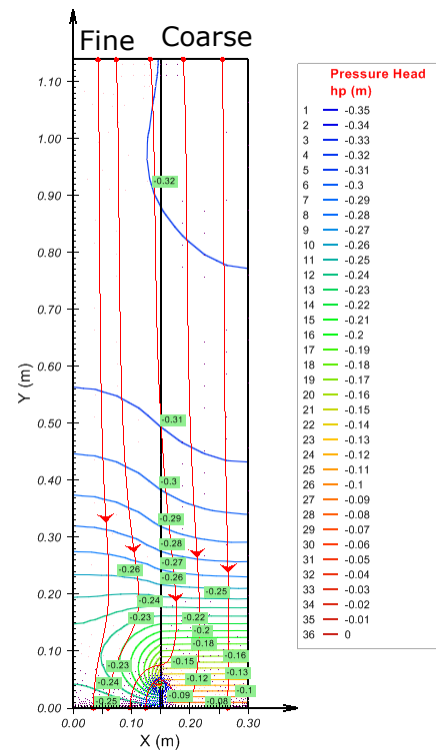
Test 4 – Flux "a"



Test 4 – Flux "b"



Test 4 – Flux "c"



Test 4 – Flux "d"

Figure 1.4 Results from Test-4 with A Contact Length of 1100 mm for for a Suction of at the Base of 0.8 kPa and for Precipitation of 1120 mm/day (a), 800 mm/day (b), 440 mm/day (c) and 330 mm/day (d)

J. PROFILE RESULTS FROM SIMULATION IN COLUMN-2

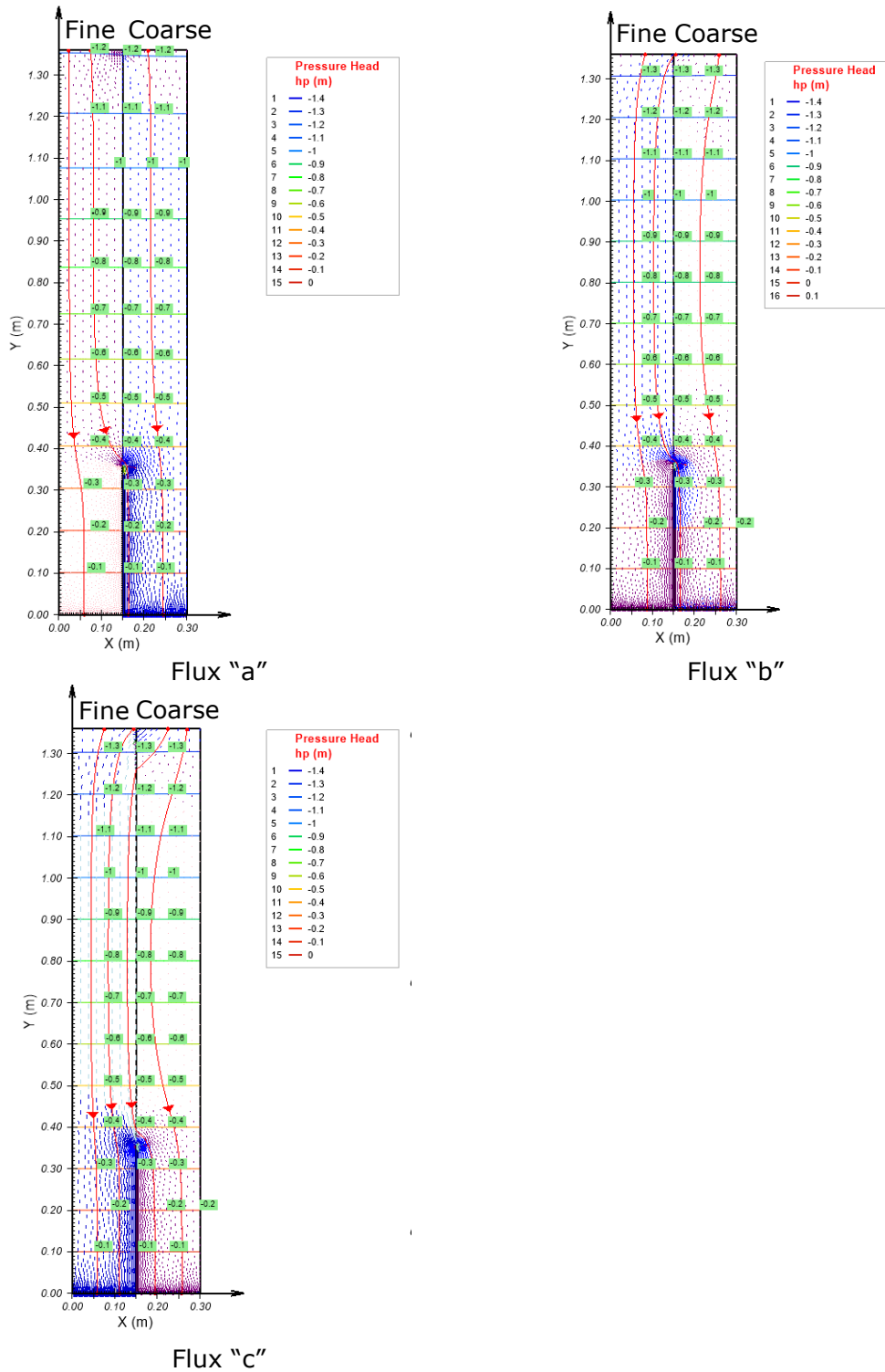


Figure J.1 Results from Column-2 with A Contact Length of 1000 mm for a Suction of at the Base of 0.0 kPa; and a Precipitation of 445 mm/day (a), 12 mm/day (b), and 5 mm/day (c)

K. CALIBRATION OF ACID ROCK IN PANEL-1

Improving the result from the previous model requires a calibration of one or more variables. The calibration is made through a back-analysis process, consisting in changing the independent variables to obtain the same total discharge for each material. The calibration is focused in the material properties as the main characteristic affecting the convergence of the model.

The calibration of the geotechnical properties of the waste rock will be limited to the Air-Entry-Value (AEV) and the Saturated-Hydraulic-Conductivity (k_{sat}). It is assumed these two properties are the most relevant in unsaturated flow. The waste rock materials have a low AEV due to the large particle size, and it can result in difficulty determining these suction values. The uncertainty of k_{sat} is due to a high variability that can result from the relationship between the conditions of the materials placed in the panels and the conditions in the permeability tests. The back analysis of Panel-1 is applied to the six test conditions used in the laboratory experiment.

I. BACK ANALYSIS OF AEV

The back analysis of Panel-1 is run for four cases representing the extreme combination with respect to the range of k_{sat} (see Table 5.3). Figure K.1 summarizes the results of total discharge calibrating the AEV of the F-AR between 1.42 kPa and 0.074 kPa. The range for the iteration process was determined randomly, starting from the laboratory and decreasing gradually until the convergence had an error of less than 10%.

The simulation of Panel-1 applying laboratory properties with an AEV equal to the laboratory (1.42 kPa) resulted in a total outflow from the fine layers of 98%. Consequently, the AEV of the F-AR needs to be lower, decreasing the flow in the fine layers and incrementing the flow in the coarse layers. The previous statement assumes the condition that the AEV of the C-AR is constant at 0.025 kPa.

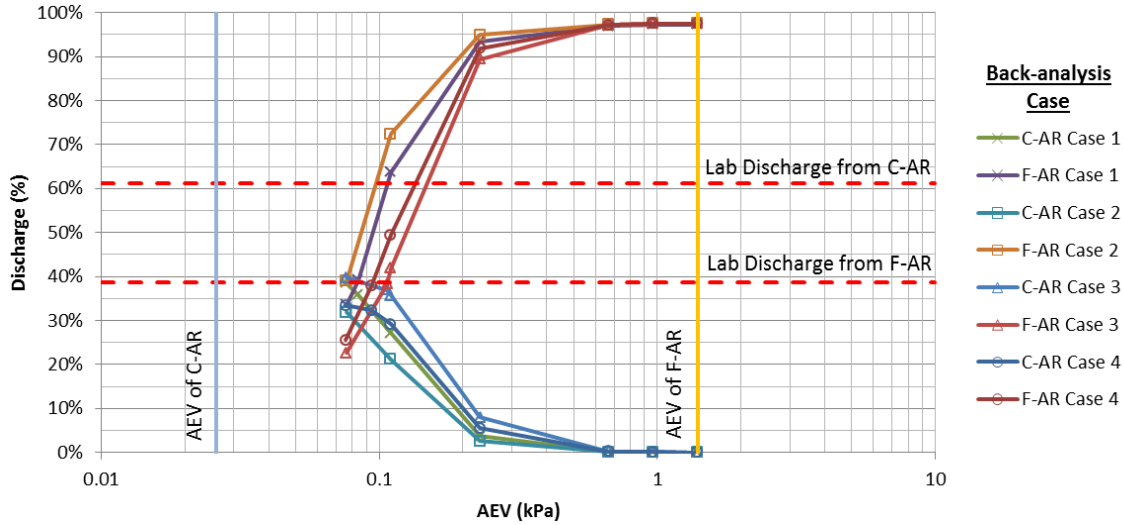


Figure K.1 Calibration of The AEV from the F-AR in Test VI (10 mm/Day and A Suction of 2.0 kPa)

The sensitivity analysis shows a rapid decrease in discharge from the F-AR at an AEV below 0.23 kPa. The decreased rate of discharge from the F-AR is much higher than the increment from the discharge from the C-AR. At 0.1 kPa, the increment rate becomes very low, generating an error in the amount of total discharge.

Figure K.2 summarizes the results of total outflow calibrating the AEV of the C-AR between 0.025 kPa and 0.78 kPa. The simulation of Panel-1 applying laboratory properties with an AEV equal to the laboratory (0.025 kPa) resulted in a total outflow from the coarse layer equal to 1.2%. Contrary to the calibration of the AEV for the F-AR; the AEV of the C-AR needs to be higher, increasing the flow in the coarse layers and decreasing the flow in the fine layers. The previous statement assumes the condition that the AEV of the F-AR is constant at 1.42 kPa.

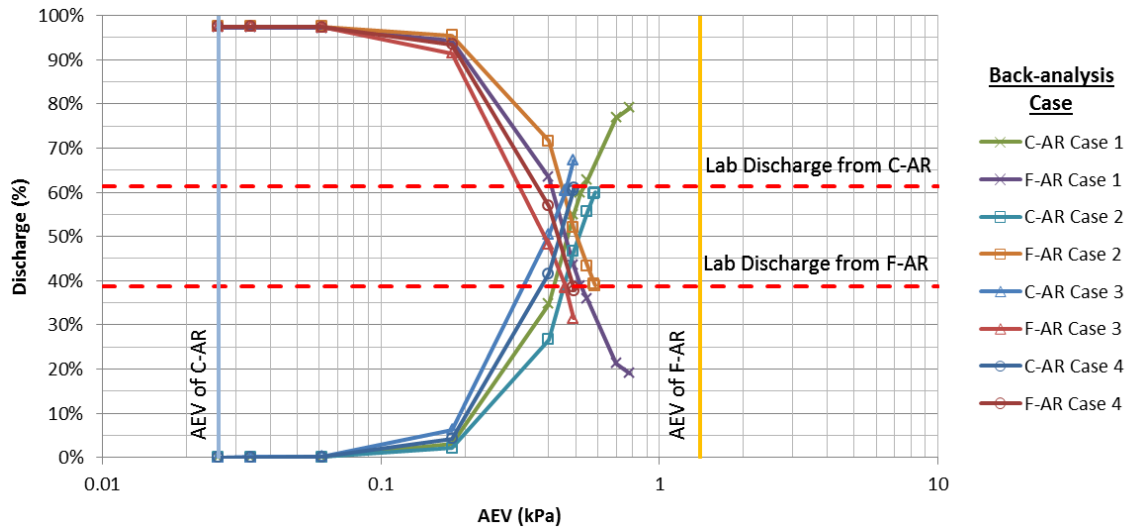


Figure K.2 Calibration of The AEV from the C-AR in Test VI (10 mm/Day and A Suction of 2.0 kPa)

Contrary to the sensitivity analysis of the F-AR, the increment in the AEV decreases the discharge from the F-AR and increases it in the C-AR. At an AEV of 0.18 kPa, there is a rapid decrease of discharge on the F-AR and a residual increment of the C-AR. The changes keep the total discharge close to 100%. In the test at 0 kPa of suction at the base, the sensitivity curves move to the left, decreasing the AEV for the same discharge percentage. This causes the rapid drop of discharge from the F-AR to start at an AEV of 0.026 kPa. Both approaches show a drop in outflow with small changes in the AEV. The back-analysis of the AEV in the F-AR shows a change in outflow of 50% from 0.1 kPa to 0.2 kPa. For the back-analysis of the AEV in the C-AR, the results show a change in the outflow of 50% from 0.2 kPa to 0.5 kPa.

The correlation of each case shows the variance of the discharge from all the layers between the laboratory and the simulation. Figure K.3 shows the correlation of the discharge from the seven layers between the model and the laboratory experiment in the back analysis of the F-AR and the C-AR. The discharge of the model is taken from the results using the AEV with the highest PPMCC in each case in Test VI. A perfect correlation would have a relation 1:1 for each point (i.e. objective line). The sensitivity analysis of the AEV in Case 1 at Test VI, assumes a maximum k_{sat} of $8.0 \times 10^{-4} \text{ m/s}$ for the F-AR and a maximum of $1.5 \times 10^{-2} \text{ m/s}$ for the C-AR.

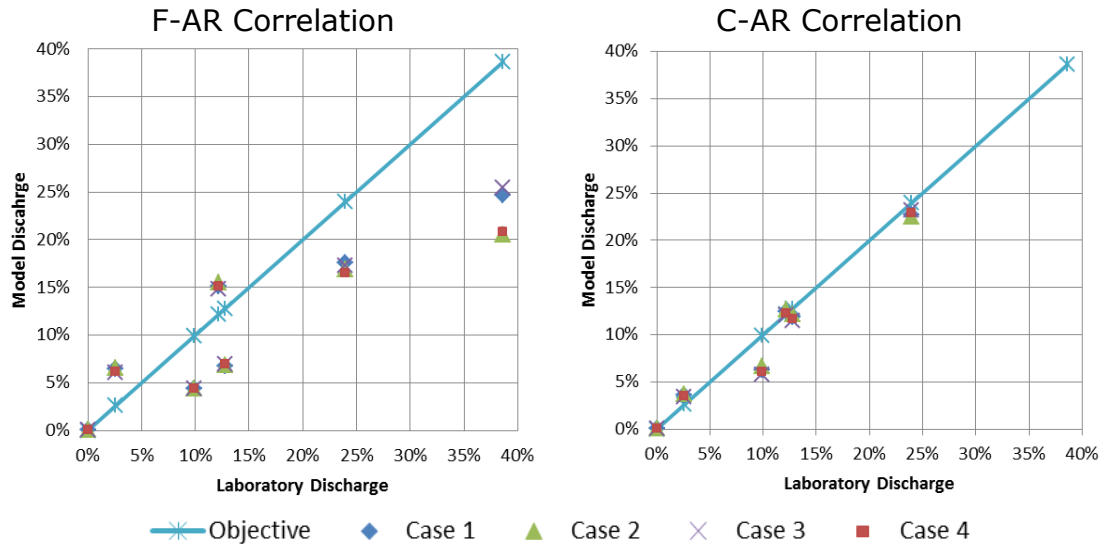


Figure K.3 Panel-1 Correlations for 10 mm/Day and 2.0 kPa Suction

The correlation is shown to be closer in the back analysis of the C-AR for all cases. The back analysis of the C-AR indicates increments in AEV as the suction increases, resulting in a constant AEV of 1.4 kPa in the F-AR. The increment increases as precipitation increases. At 10 mm/day, the C-AR can have an approximate minimum of 0.2 kPa and a maximum of 0.9 kPa. Contrary for the back analysis of the F-AR, with a constant AEV of 0.024 kPa for the C-AR, the variance is small despite changes in precipitation and base suction with values around 0.1 kPa

The summary of the back analysis of the AEV following the F-AR and C-AR is shown in Table K.1 and Table K.2, respectively. The values represent the average result from the four cases analysis in the AEV with respect to the k_{sat} (see Table 5.3).

Table K.1 Calibration Results for AEV of the F-AR

Test	Suction (kPa)	Rainfall	AEV(kPa)	Discharge Difference		PPMCC
				F-AR	C-AR	
III	0	10 mm/day	0.097	0.5%	34.5%	0.78
IV	2	2 mm/day	0.075	0.2%	7.1%	0.14
VI	2	10 mm/day	0.105	0.5%	27.1%	0.90
VII	4	2 mm/day	0.080	0.4%	8.4%	0.35
VIII	4	5 mm/day	0.082	0.2%	26.5%	0.85
IX	4	10 mm/day	0.068	0.4%	45.5%	0.87

The calibration of the AEV for the F-AR showed values up to two orders of magnitude lower than the measurements from the SWCC and close to the AEV of the C-AR to achieve a good correlation to the experiment. None of the six tests achieves both a low difference and acceptable correlation. Furthermore, it is not likely to have an AEV too low for the F-AR.

Table K.2 Calibration Results for AEV of the C-AR

Test	Suction (kPa)	Rainfall	AEV(kPa)	Discharge Difference		PPMCC
				F-AR	C-AR	
III	0	10 mm/day	0.157	0.3%	0.2%	0.16
IV	2	2 mm/day	0.501	0.2%	1.4%	0.17
VI	2	10 mm/day	0.514	0.1%	1.1%	0.99
VII	4	2 mm/day	0.544	0.5%	0.9%	0.47
VIII	4	5 mm/day	0.628	0.2%	0.7%	0.88
IX	4	10 mm/day	0.790	0.3%	0.9%	1.00

The calibration of the AEV for the C-AR, shows values one order of magnitude higher than those measured from the SWCC. In all tests, the error is below 2%, and Test VIII, VI, IX, three of the six tests, gave good correlation. The two optimal values of AEV occur in the back analysis for a precipitation of 5 mm/day and 10 mm/day, at a suction of 4.0 kPa and 2.0 kPa, respectively. The results from test IX show good correlation (low discharge difference and a high correlation) from the calibration; however, the laboratory measurement from the Meso-scale panel is not reasonable, because the discharge indicates lower magnitude from the F-AR at a higher suction.

The correlations and difference of each test correspond to the specific characteristics of the material properties applied to the model. The calibration that results in the most optimum correlation is found in the AEV of the C-AR; the average AEV from Test VI and VIII resulted in a suction of 0.57 kPa. Both test calibrations satisfy the criteria defined in this thesis.

After the first calibration, a second attempt of calibration was pursued to improve the convergence of the other four test tests. The second order calibration consisted in modifying the AEV of the F-AR and the k_{sat} of both materials assuming an AEV of 0.57 kPa for the C-AR. However, changes in the saturated hydraulic conductivity and the AEV of the F-AR could improve the correlation of Test VII and Test IV. These changes decreased the PPMCC of Test VI to approximately zero.

II. BACK ANALYSIS OF k_{SAT}

The improvement of convergence of Panel-1 is also verified by back analyzing the k_{sat} of the materials. The calibration is made by changing the k_{sat} of one material, while keeping the rest of the material properties constant. Nevertheless, the simulations are run for the maximum and minimum magnitude of the k_{sat} of both fine and coarse acid rock.

Figure K.4 summarizes the results of total discharge calibrating k_{sat} of the F-AR between $3.9 \times 10^{-4} m/s$ and $8 \times 10^{-4} m/s$. The simulations are run for a k_{sat} in C-AR equal to $1.0 \times 10^{-2} m/s$ and $1.5 \times 10^{-2} m/s$.

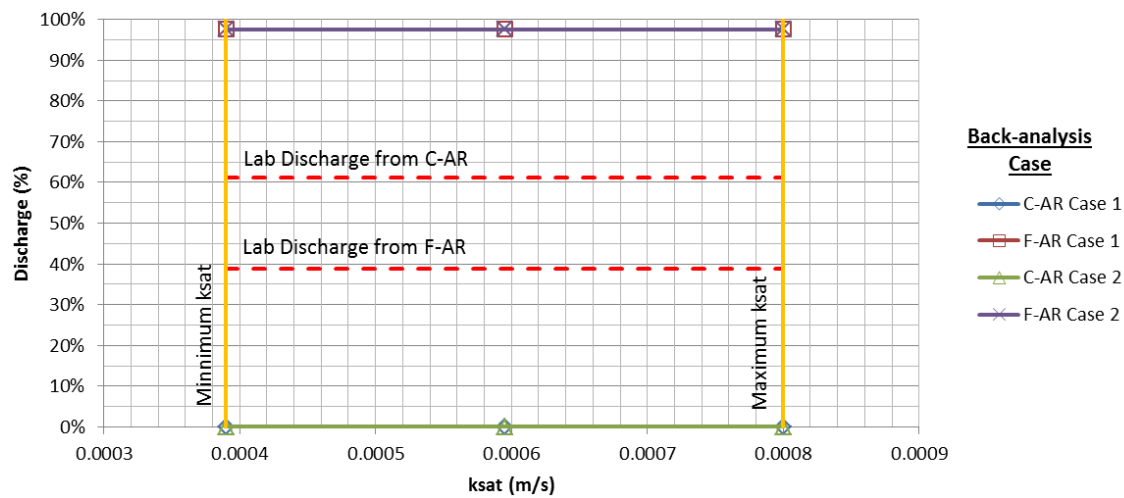


Figure K.4 Calibration Of The k_{sat} from the F-AR in Test VI
- 10 mm/Day and a Suction of 2.0 kPa

Figure K.5 summarizes the results of total discharge calibrating k_{sat} of the C-AR between $1.0 \times 10^{-4} m/s$ and $1.5 \times 10^{-4} m/s$. The simulations are run for a k_{sat} in C-AR equal to $3.9 \times 10^{-4} m/s$ and $8 \times 10^{-4} m/s$.

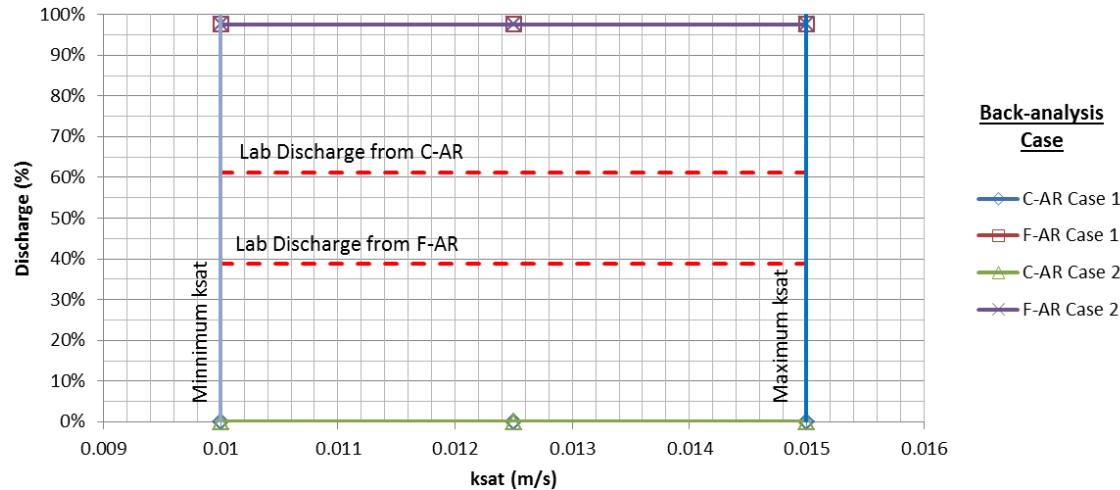


Figure K.5 Calibration Of The k_{sat} From the C-AR in Test VI
- 10 mm/Day and a Suction of 2.0 kPa

In all the tests of Panel-1, the calibration of the k_{sat} between the ranges defined by Andrina (2009) has negligible effect in the total discharge. Nevertheless, it should be kept in mind that the preferential flow in the model is sensible to change in k_{sat} at different magnitudes of AEV. This effect occurs in the calibration of the column model (see Chapter 4) and it is indirectly shown in Figure K.1 and Figure K.2.

III. DISCUSSION AND ANALYSIS FOR THE BACK ANALYSIS

The back-analysis of the AEV allowed an improvement in the convergence of the model with respect to the laboratory results. Nonetheless, calibrating the AEV of the C-AR makes a better convergence. The analysis shows the smallest difference in the total discharge from the fine layers and the coarse layers is 0.1% and 0.2%, respectively. In contrast, the calibration of the F-AR only results in a small difference for the discharge from the fine layer, while the difference is between 7% and 45% for the coarse layers. The back-analysis for the k_{sat} of the materials does not results in changes of the outflow from the layers. The different analysis shows a constant outflow and the results have a high difference with respect to the laboratory measurements.

The acid rock shows high sensitivity to changes in AEV. The calibration of the AEV in the F-AR resulted in values fifteen times smaller than the laboratory measurement; nonetheless, the calibration only allows an approximation of the discharge of the F-AR while the difference in discharge from C-AR increased with precipitation. These differences showed that changing the AEV resulted in a conflict to the principle of "conservation of mass" in the model; as the sum of the total discharge from the F-AR and C-AR is less than a 100% of the applied precipitation. This occurs as the materials in the panel have such a

small permeability, that they do not allow water to infiltrate the layers. SvFlux controls this condition by allowing the excess water to runoff, maintaining the principle of “conservation of mass”. The difference in discharge shows that the model could not manage the amount of precipitation, thus resulting in 30% to almost 50% of runoff water as the AEV of the F-AR decreased.

The calibration of the C-AR resulted in AEV values twenty times greater than the laboratory measurements. The calibration in each case has reasonable values with difference in discharge of less than 2%. Additionally, the simulations show Test VI, VIII, and IX with a PPMCC approximating one (i.e. high correlation).

The laboratory results in Test IX seem unreasonable for the AEV, as the results are indicating lower discharge from the F-AR at higher suction. As the suction at the base increases, the internal h_p in the panel increases; consequently, the ratio in difference of the permeability between C-AR and F-AR becomes smaller. Then the permeability of the F-AR starts to increase with respect to the permeability of the C-AR. The calibration from Test VI and VIII has reasonable solutions, with an AEV of 0.51 kPa and 0.63 kPa respectively. The two tests have an approximate difference of 0.1 kPa in the calibration of the AEV for the C-AR. This might not be significant; however, it was observed during calibration that small changes in the AEV can affect significantly the water regimen in unsaturated systems. If the AEV in Test VI increases to 0.6 kPa, there is an insignificant drop of the correlation of less than 2%; however, the difference in the total discharge increases significantly from 1% to 15%. This increase similarly occurs in Test VIII. If the AEV drops to 0.5 kPa, the correlation has an insignificant drop but the discharge difference increases to over 10%.

Overall Test VI resulted in a higher correlation than Test VIII; however, as Test VIII was run in Panel 2 and Panel 3, the calibration of the Acid Rock takes into account the average AEV between both calibrations.

The AEV parameters that best described water flow in Panel 1 is with an AEV of the F-AR equal to 1.4 kPa and a calibrated AEV of the C-AR equal to 0.57 kPa. Figure K.6 shows the change in the hydraulic conductivity curves between the estimation considering Andrina’s laboratory measurements (F-WR initial and C-FW initial) and the calibration of the AEV through back-analysing Panel-1 (F-WR Calibrated and C-FW Calibrated).

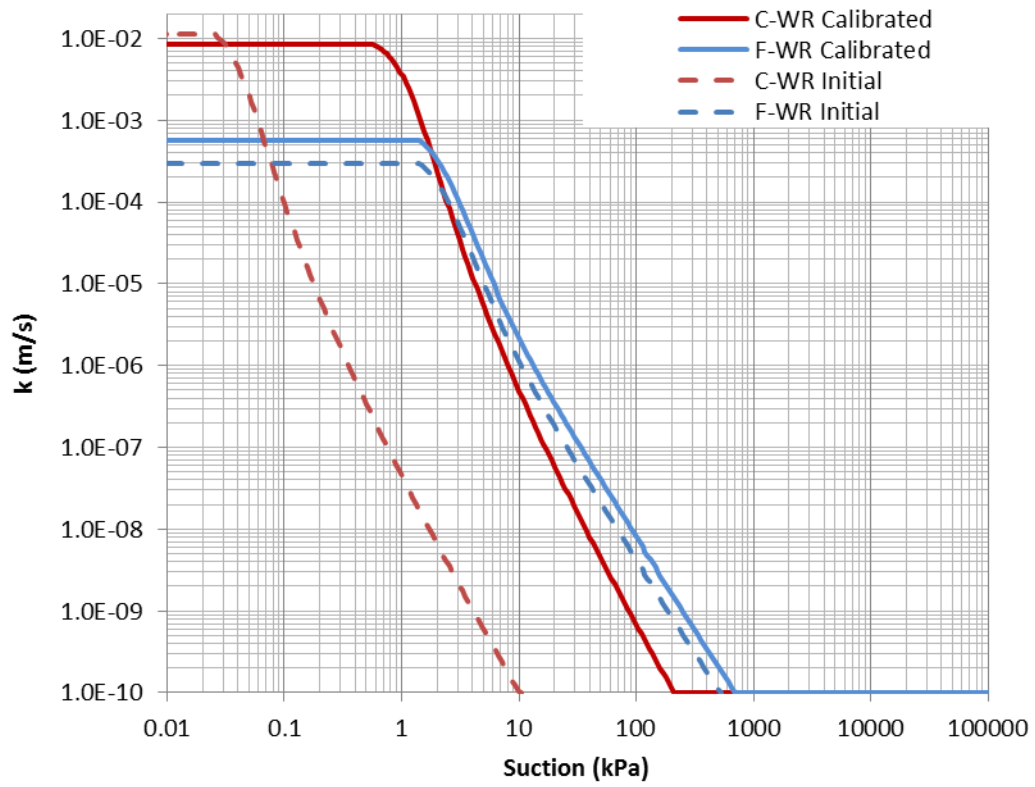


Figure K.6 HCCs after Calibration of the Acid Rock in Panel-1

L. SIMULATION PROFILES IN PANEL-1

The following figures show the profile of h_p , flow vectors and stream traces from the simulations in Panel-1 using the calibrated properties for the acid rock.

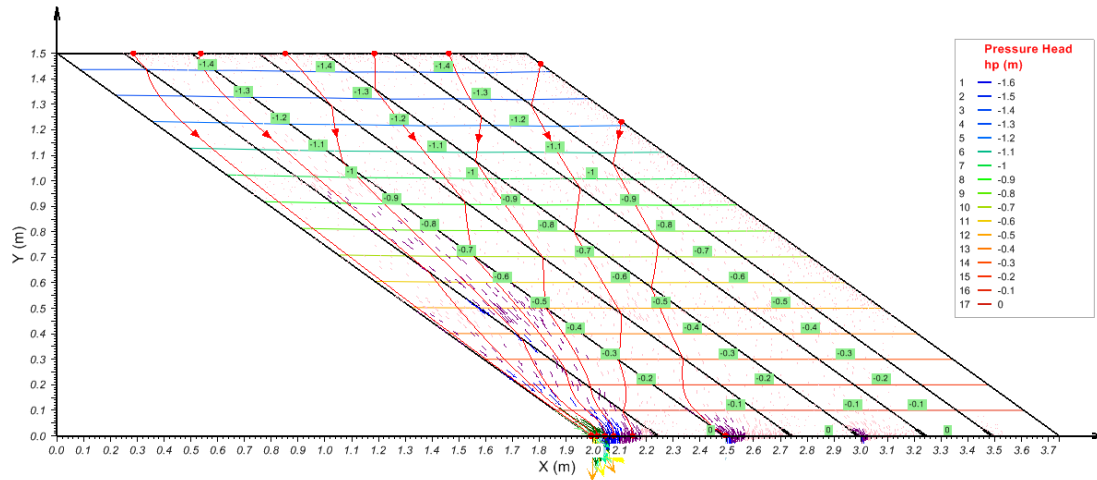


Figure L.1 Simulation of Panel-1 Under A Base Suction of 0.0 kPa and a Precipitation of 10 mm/Day

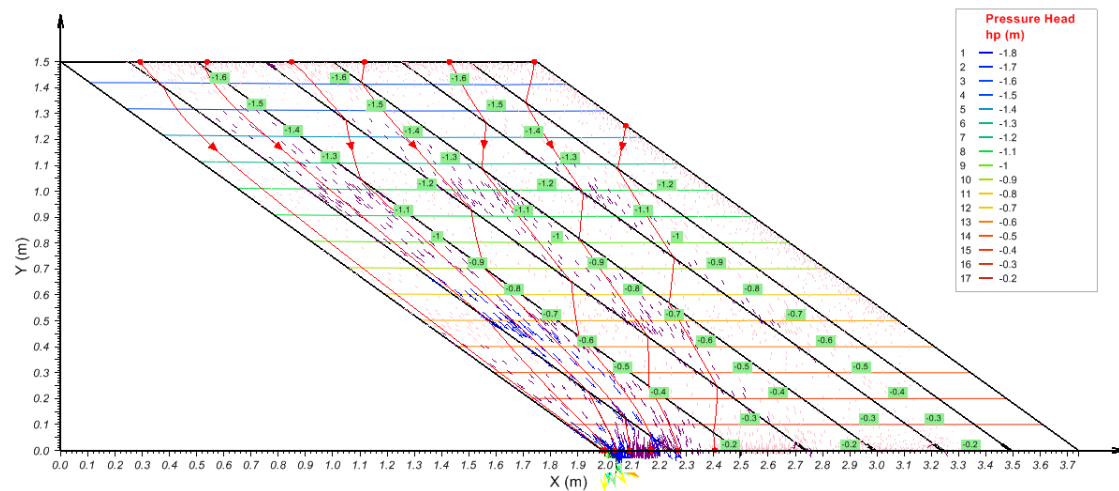


Figure L.2 Simulation of Panel-1 under a Base Suction of 2.0 kPa and a Precipitation of 2 mm/Day

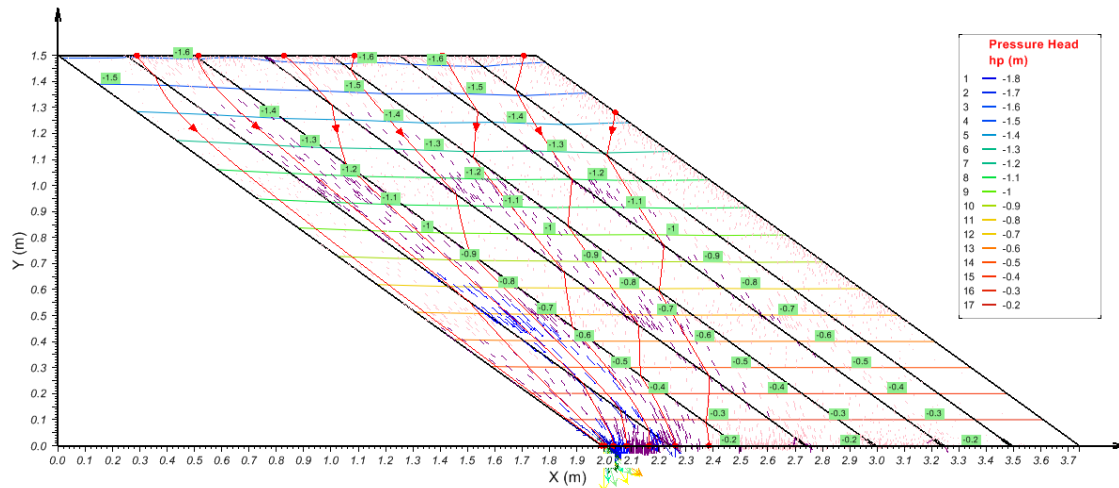


Figure L.3 Simulation of Panel-1 under a Base Suction of 2.0 kPa and a Precipitation of 10 mm/Day

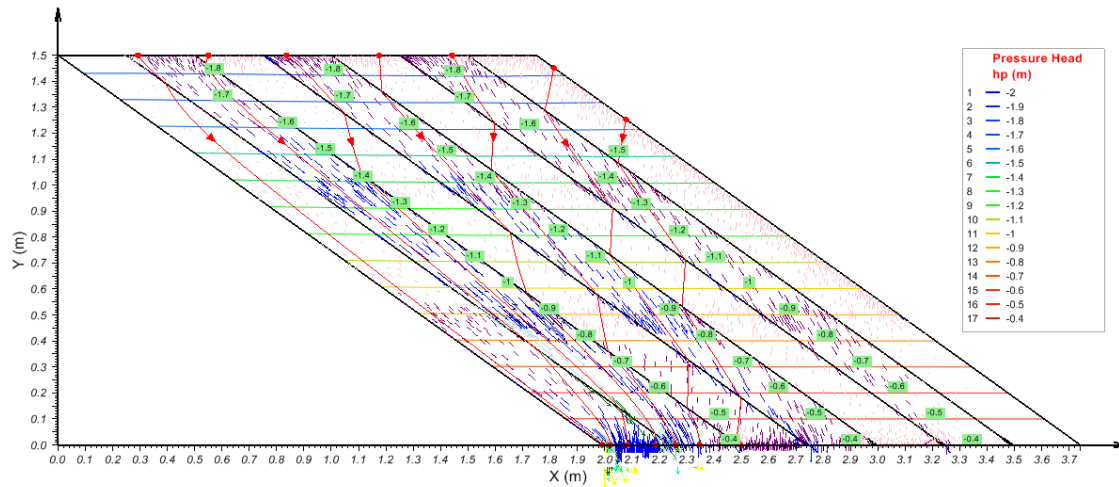


Figure L.4 Simulation of Panel-1 under a Base Suction of 4.0 kPa and a Precipitation of 2 mm/Day

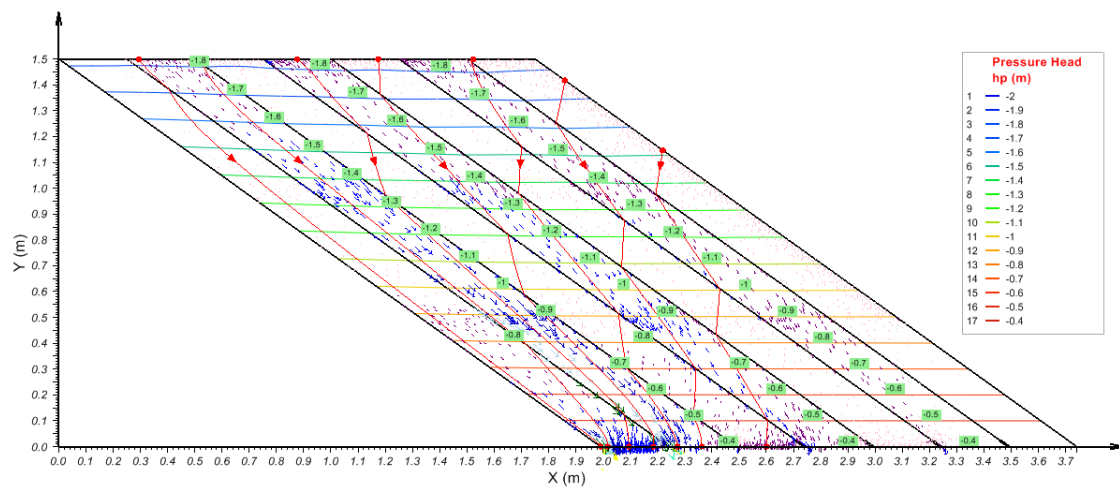


Figure L.5 Simulation of Panel-1 under a Base Suction of 4.0 kPa and a Precipitation of 5 mm/Day

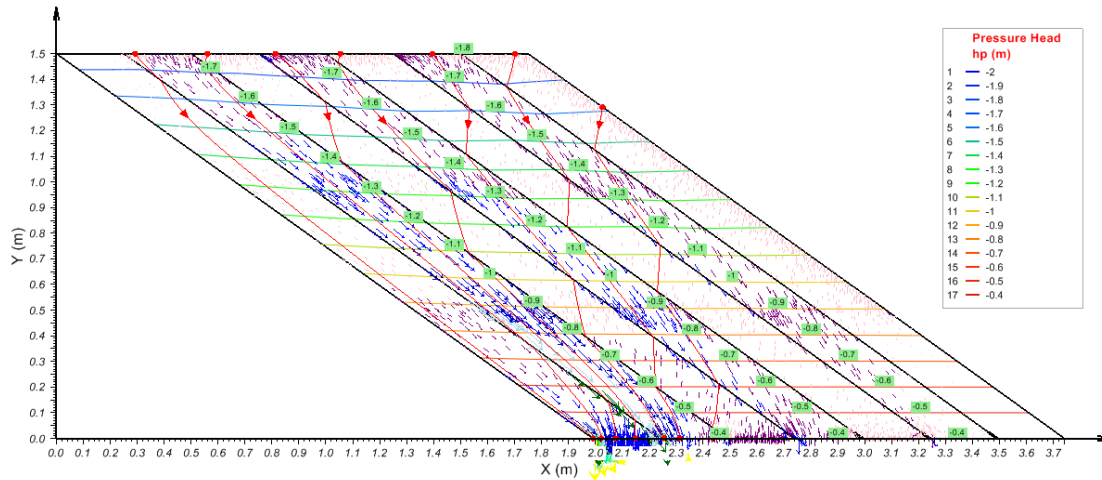


Figure L.6 Simulation of Panel-1 under a Base Suction of 4.0 kPa and a Precipitation of 10 mm/Day

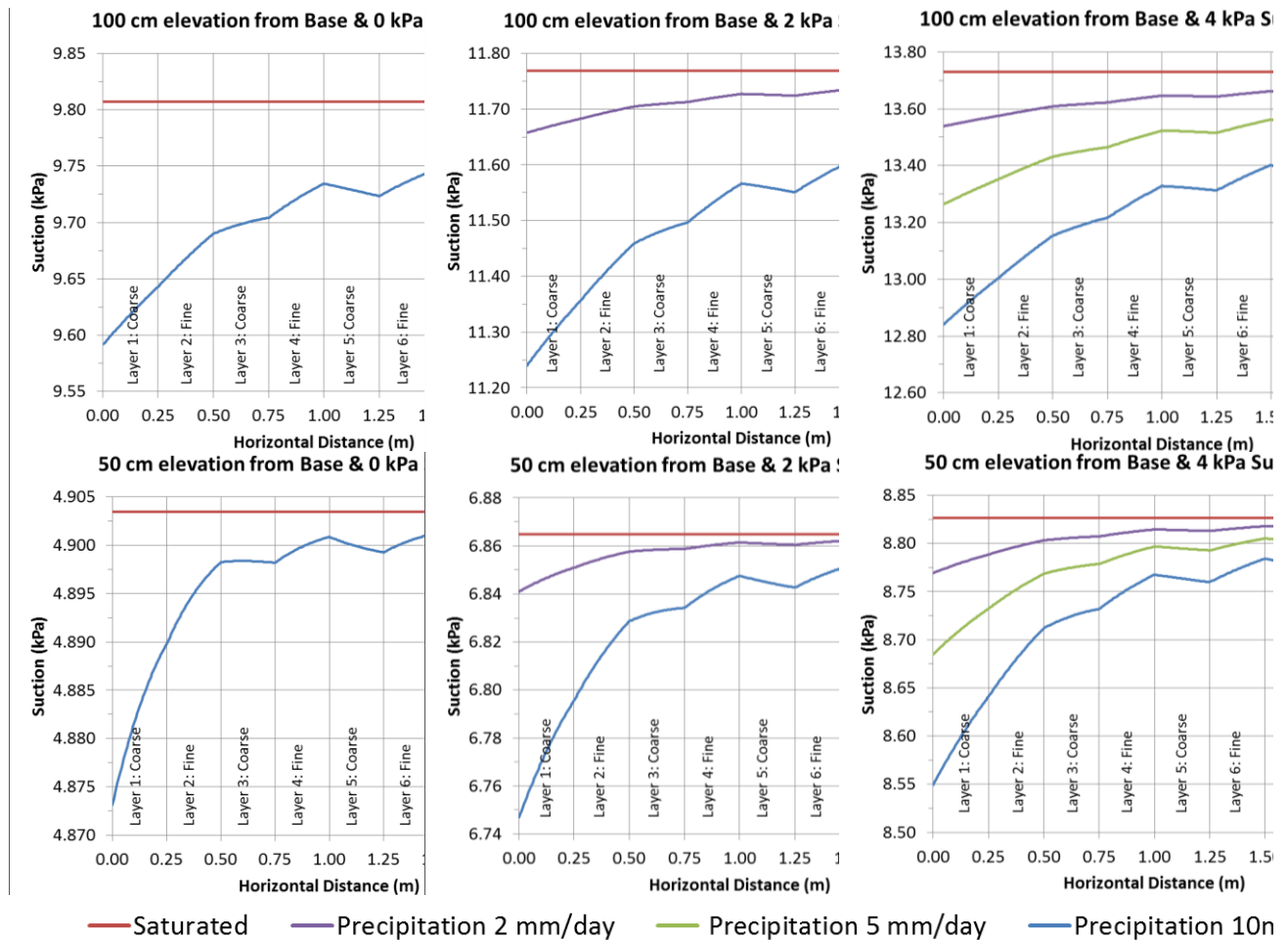


Figure L.7 Change in Matrix Suction at 0.5 m and 1.0 m Elevations

M. SIMULATION PROFILES IN PANEL-2

The following figures show profile of h_p , flow vectors, and stream traces from the simulations in Panel-2 (case 3). The model configuration uses the calibrated properties for the acid rock in Panel-1. In addition, the top layer of C-L matches the calibrated properties of the C-AR.

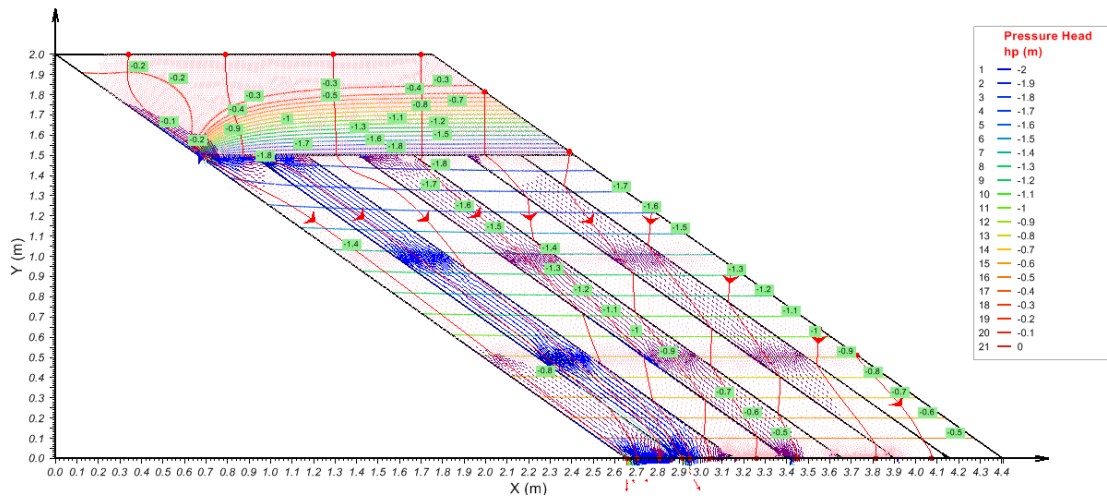


Figure M.1 Simulation of Panel-2 under a Base Suction of 4.0 kPa and a Precipitation of 2 mm/Day

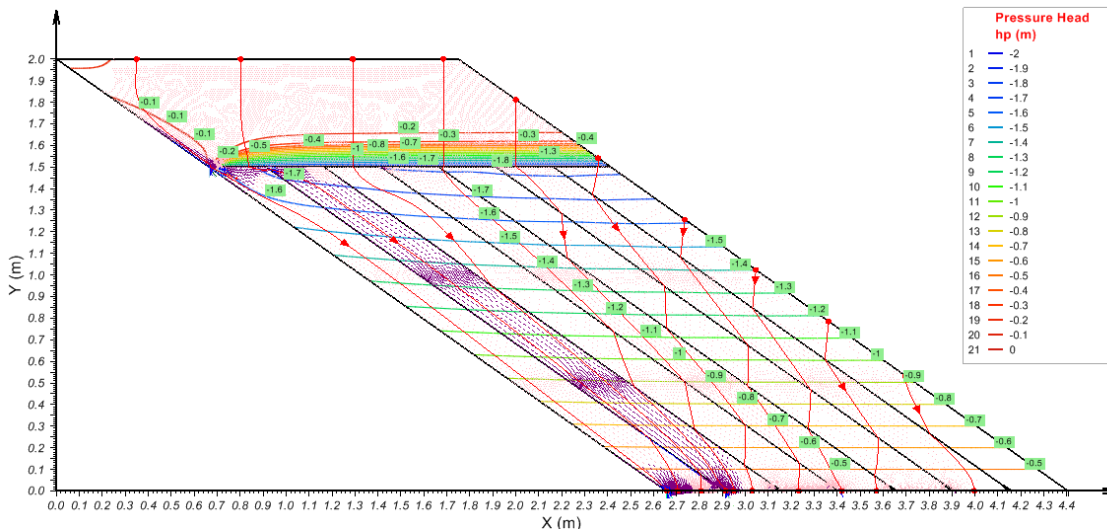


Figure M.2 Simulation of Panel-2 under a Base Suction of 4.0 kPa and a Precipitation of 5 mm/Day

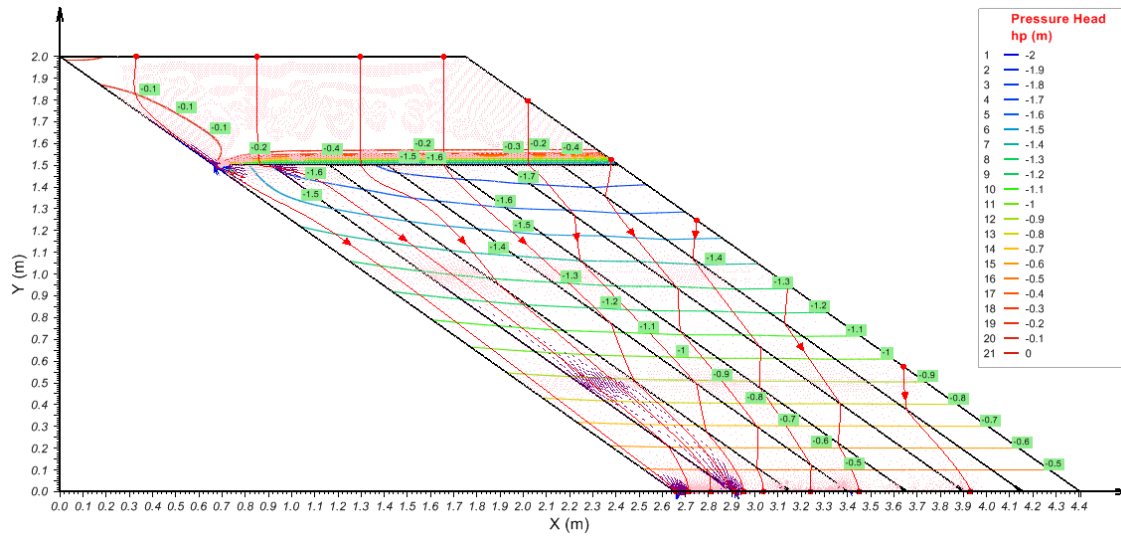


Figure M.3 Simulation of Panel-2 under a Base Suction of 4.0 kPa and a Precipitation of 10 mm/Day

The profiles from the simulations showed increase in suction with the elevation, at 50 cm suctions reaches around 9.0 kPa, at 100 cm suctions reaches around 14 kPa, and at 150 cm suctions reaches 18 kPa.

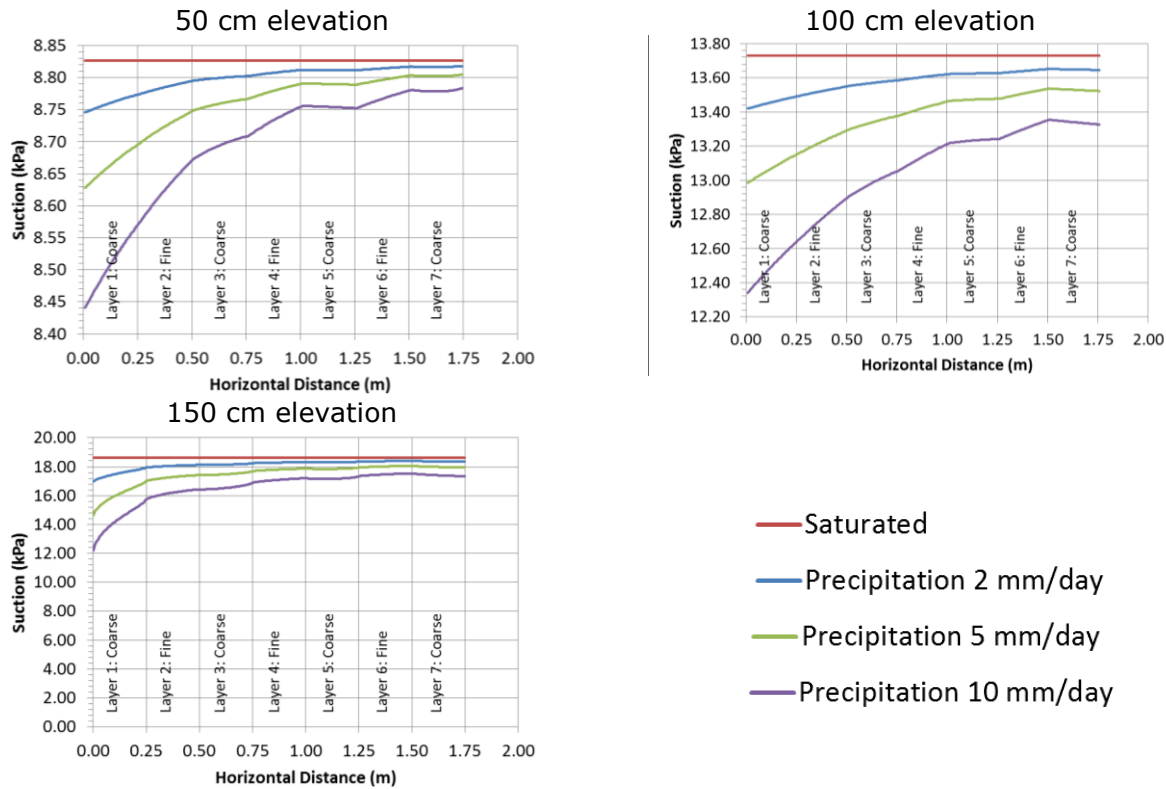


Figure M.4 Change in Matric Suction at 0.5 m, 1.0 m, and 1.5 m Elevations for a Base Suction of 4.0 kPa in Panel-2

N. SIMULATION PROFILES IN PANEL-3

The following figures show the profile of h_p , flow vectors and stream traces from the simulations in Panel-3. The model configuration uses the calibrated properties for the acid rock in Panel-1. In addition, the model uses the material properties from the laboratory experiment for the fine fraction of the limestone (F-L), while the coarse grain (C-L) matches the calibrated properties of the C-AR.

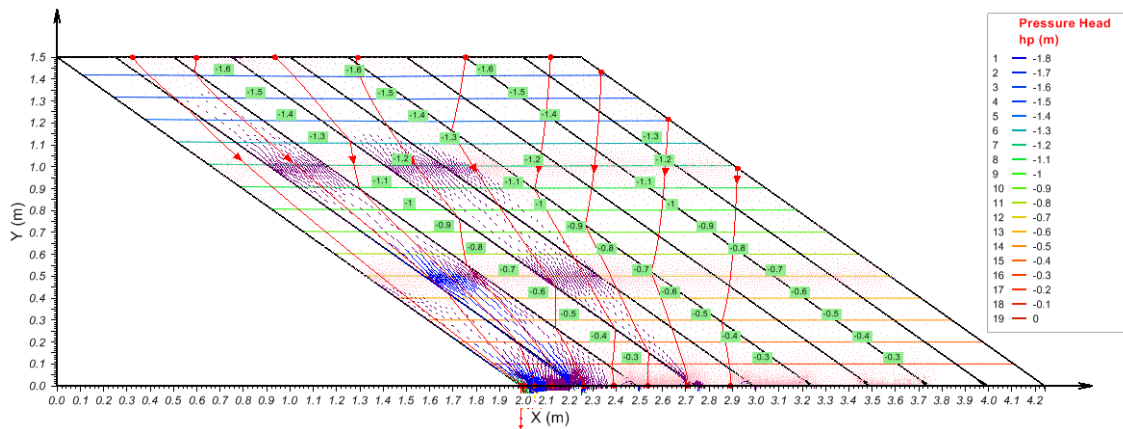


Figure N.1 Simulation of Panel-3 under a Base Suction of 2.0 kPa And a Precipitation of 2 mm/Day

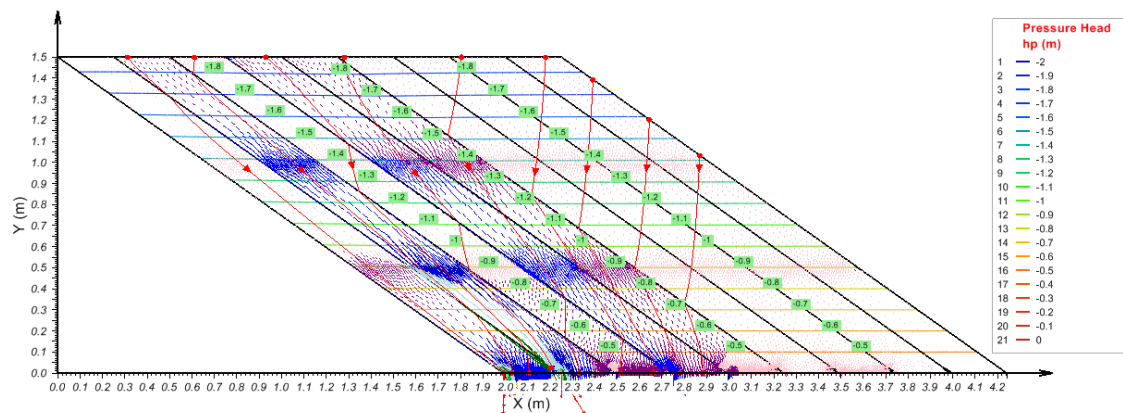


Figure N.2 Simulation of Panel-3 under a Base Suction of 4.0 kPa And a Precipitation of 2 mm/Day

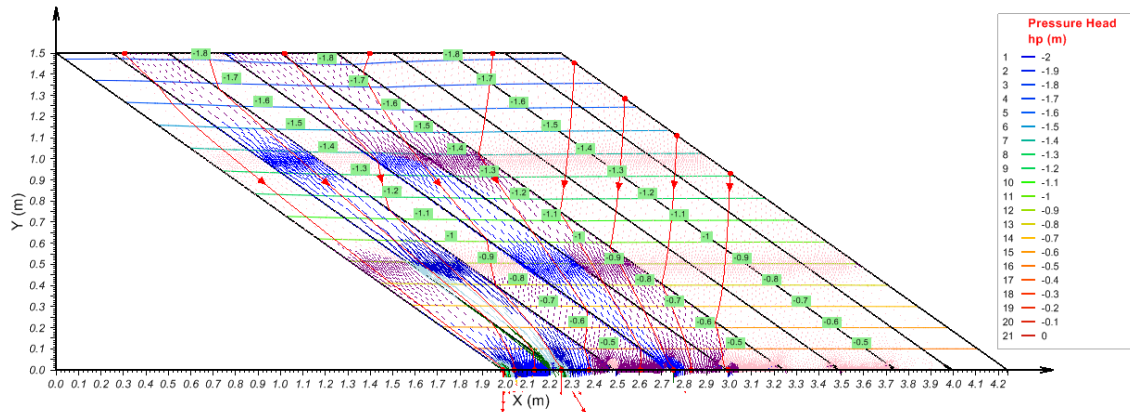


Figure N.3 Simulation of Panel-3 under a Base Suction of 4.0 kPa And a Precipitation of 5 mm/Day

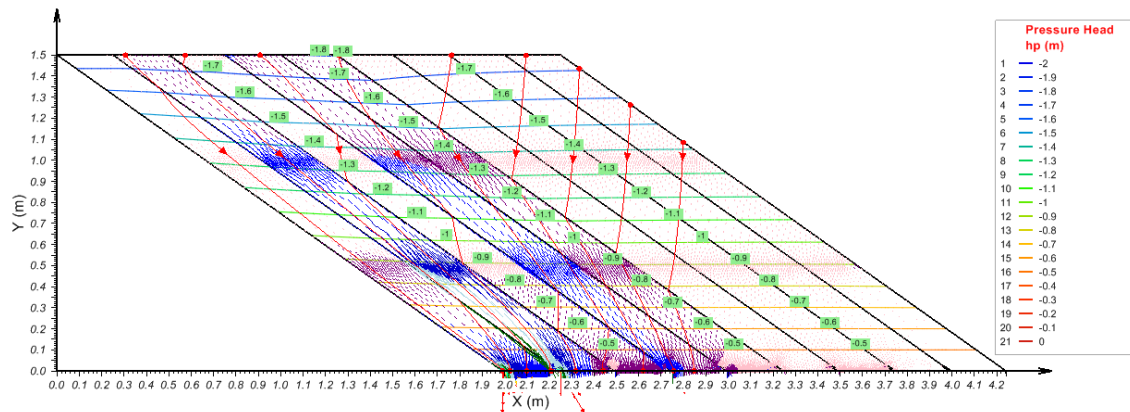


Figure N.4 Simulation of Panel-3 under a Base Suction of 4.0 kPa And a Precipitation of 10 mm/Day

The profiles from the simulations demonstrate that suction increases with the elevation and base suction, but is inversely proportional to the precipitation. At 50 cm elevation, the variation in suction is less than 0.3 kPa and reaches a maximum of 8.8 kPa. At 100 cm elevation, the variation increases, but it is less than 1.0 kPa suctions and reaches a maximum of 13.7 kPa.

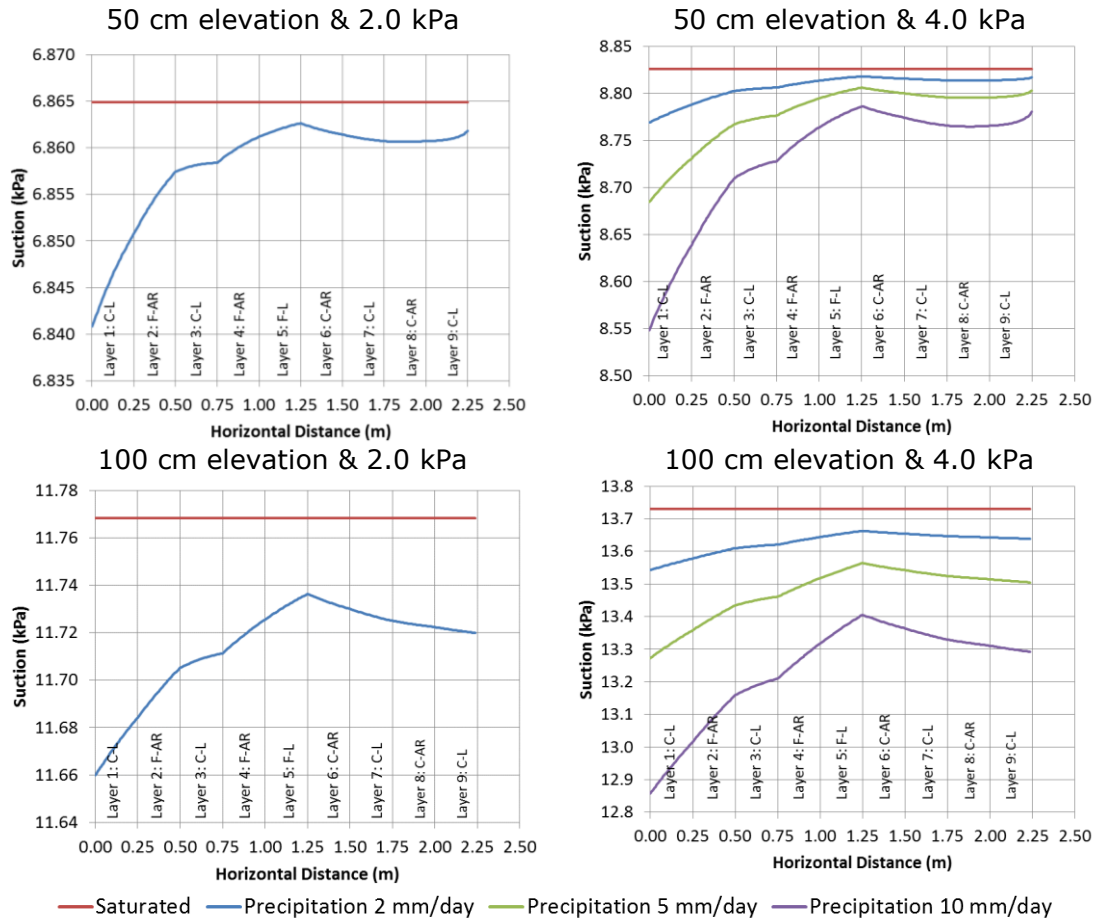


Figure N.5 Change In Matric Suction At 0.5 m, And 1.0 m Elevations For A Base Suction Of 2.0 kPa And 4.0 kPa In Panel-3

In all tests, the simulations demonstrate that the two fine layers in the system (L4 and L5) generate a pick of higher suction in the system. This increment tends to be higher as it gets closer to the precipitation boundaries. The increment in suction makes these layers decrease the permeability as the VWC also decreases.

O. SIMULATION OF PANEL-1 UNDER DIFFERENT MATERIAL PROPERTIES

The Meso-scale Panel-1 is simulated using three additional material properties for the model; four tests in Panel-1 allow the comparison of the changes in discharge and flow paths under different material conditions. The first test corresponds to the panel using the calibrated properties of the waste rock from Grasberg Mine presented in Chapter 5. The second test presented in this Appendix corresponds to a simulation applying the calibrated properties from sandy materials that Column-1 presented in Chapter 4. The third test corresponds to a simulation applying the calibrated properties of waste rock from Golden Sunlight Column-2 presented in Chapter 4. The four tests correspond to a simulation that applied material properties from a tailings beach sand (TBS) and Devon-Silt based on the material characterization by colleges at the University of Alberta (Abdulnabi, 2015; Kouakou, 2014; Torghabeh, 2013).

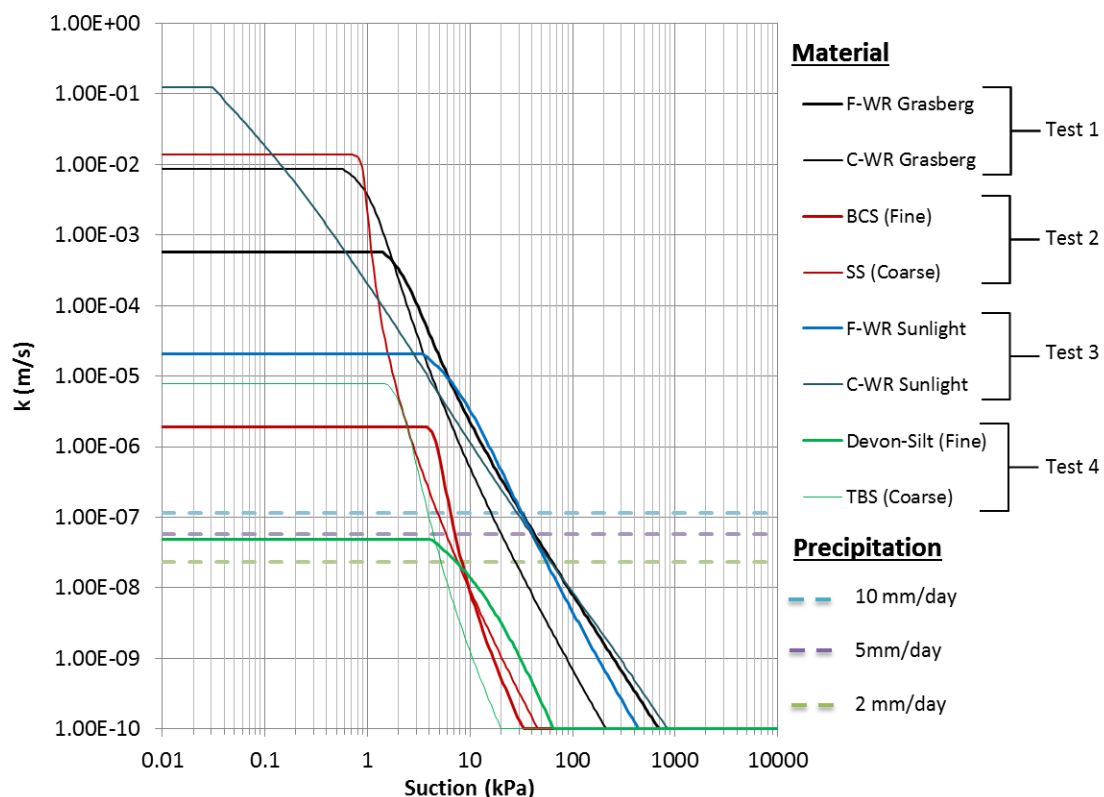


Figure O.1 HCCs from the Four Tests Applied To the Fine and Coarse Layers in Panel-1

The previous curves show that for Test 1, 2, and 3, the saturated hydraulic conductivity (k_{sat}) of the materials is greater than the three tested precipitation fluxes; however, each test has different proportions between the k_{sat} and precipitations, as well of the relationship of the curves at suction above the AEV of the fine material for the respective test. Test 4 has the k_{sat} of the fine material (Devon Silt) below a precipitation of 5 mm/day ($5.8 \times 10^{-8} m/s$). As mentioned earlier, for all the materials a k_{min} of $1.0 \times 10^{-10} m/s$ is assumed.

The following results show the model response of discharge from the materials as well the effect in changes in precipitation and suction for the internal response.

IV. SIMULATIONS OF PANEL-1 USING BEAVER CREEK SAND AND SILICA SAND (TEST-2)

The following results show the simulated response of Panel-1 using the calibrated properties from the simulation of Column-1 (See section 4.5.1.3).

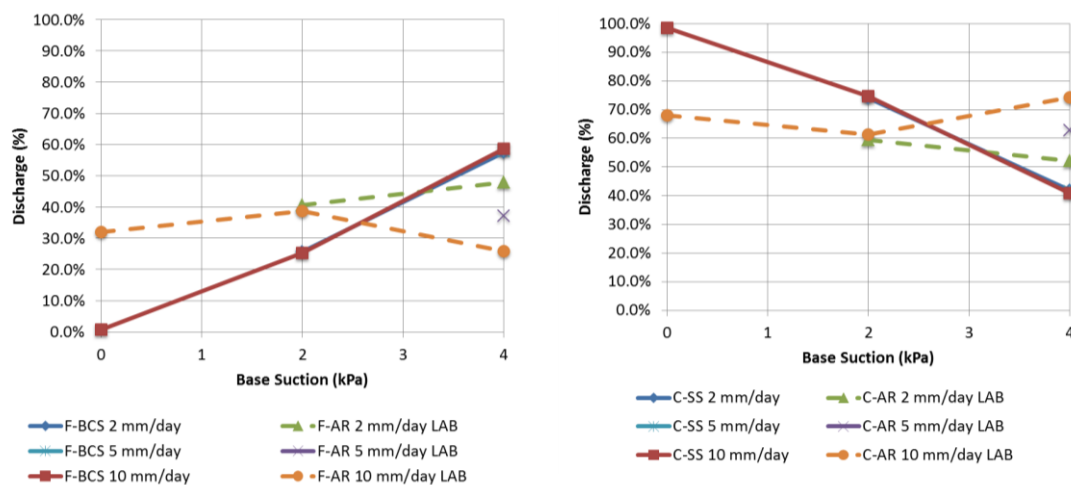


Figure 0.2 Simulation Discharge from the Coarse Material (Right) and Fine Material (Left) Using the Calibrated Properties of Sandy Soils from Column-1

The results display the same tendency as the model using waste rock from Grasberg Mine: an increase in the discharge from the Fine material (BCS) as suction increases. Suction has great impact on the discharge of the fine material increasing 50% total discharge from 0.0 to 4.0 kPa of suction.

Comparing BCS and F-AR, the results show that a coarser material has a higher discharge flow for bigger grain size. This might be considered as a contradiction of water flow in the unsaturated system; however, as this is a coupled system, the properties and

conditions of any adjacent material or layer affect the behavior and response of every material.

As mentioned previously, for an overall discharge there is no effect in changing the precipitation; internally, however, the panel profiles show high changes in the h_p , starting at an elevation of 0.5 m and up. Increasing the precipitation from 2 mm/day to 10 mm/day decreases the suction at the crest of the slope to approximately 3.0 kPa. Figure O.3 displays the changes in head pressure with elevation, flux vectors, and streamlines for different precipitation rates having a base suction in each layer of 2.0 kPa.

The simulations display more vertical flow than in Test 1. Only through the first two layers does water flow parallel to the the inclination. The main flow path is through the first two layers (L1 and L2) regardless of the precipitation. However, increasing precipitation drives water to flow more through the second layer of F-AR, but at the base the water moves to the C-AR in the first layer, keeping the preferential discharge.

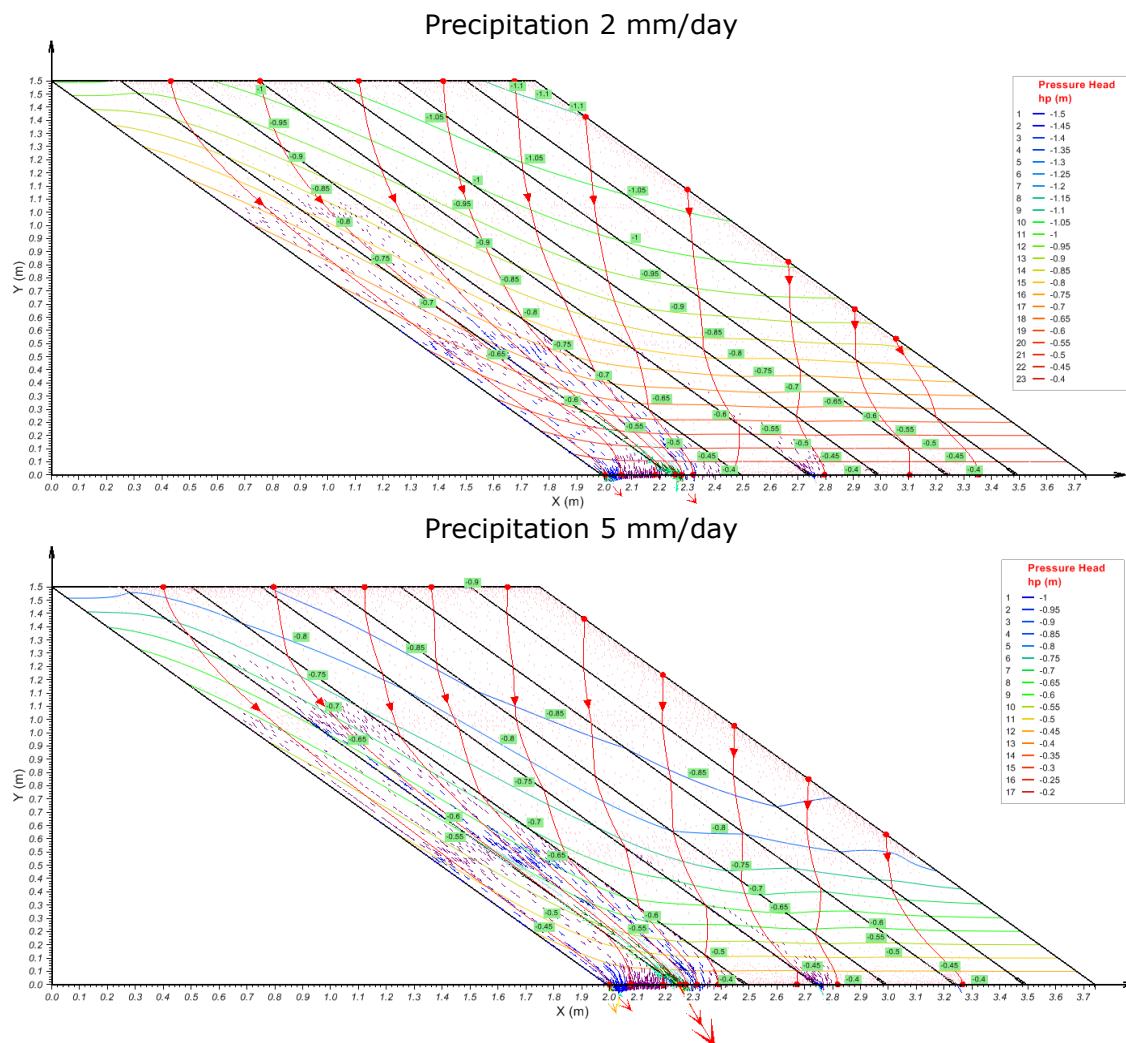


Figure O.3 Contrast Profile from Changes in Precipitation in Test 2
Applying a Base Suction of 4.0 kPa

The simulations do not expose a clear distribution on the discharge in the panel (Figure O.4); contrary to Test 1 where the water discharge decreases evenly towards the outer layer (L7). In Test 2, most of the flow is discharged from the fine layers and the first coarse layer.

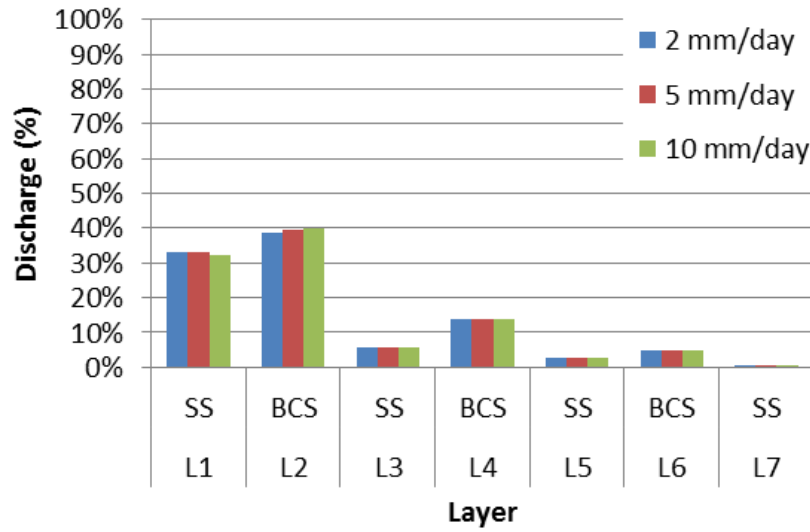


Figure O.4 Contrast Discharge at Three Precipitation Rates in Test 2
Applying a Base Suction of 4.0 kPa

In addition, the simulations showed that change in base suction generates significant changes to the h_p distribution, changing the preferential flow path in the model. Figure O.5 displays the change in head pressure with elevation, flux vectors, and streamlines for different base suction applying a precipitation of 10 mm/day.

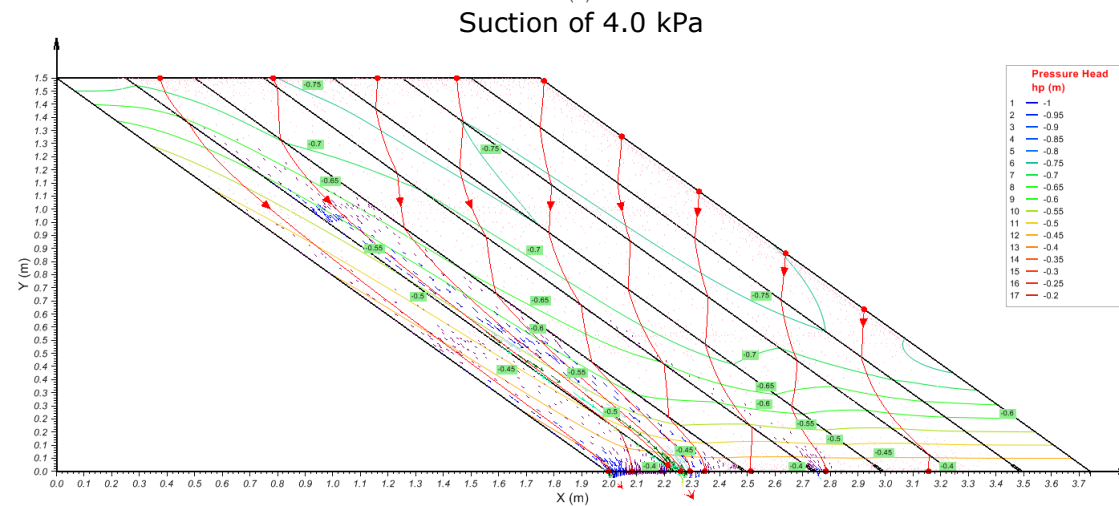
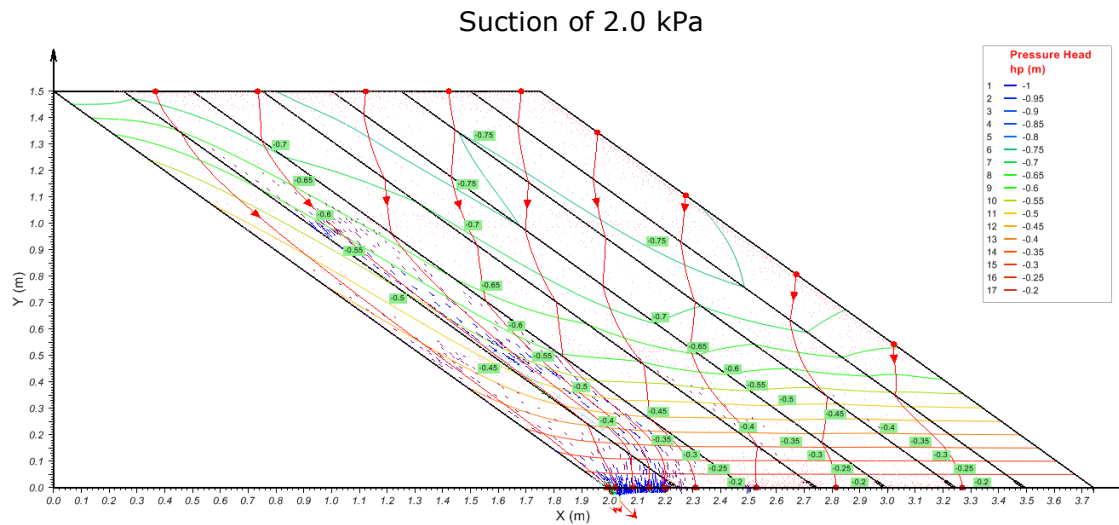
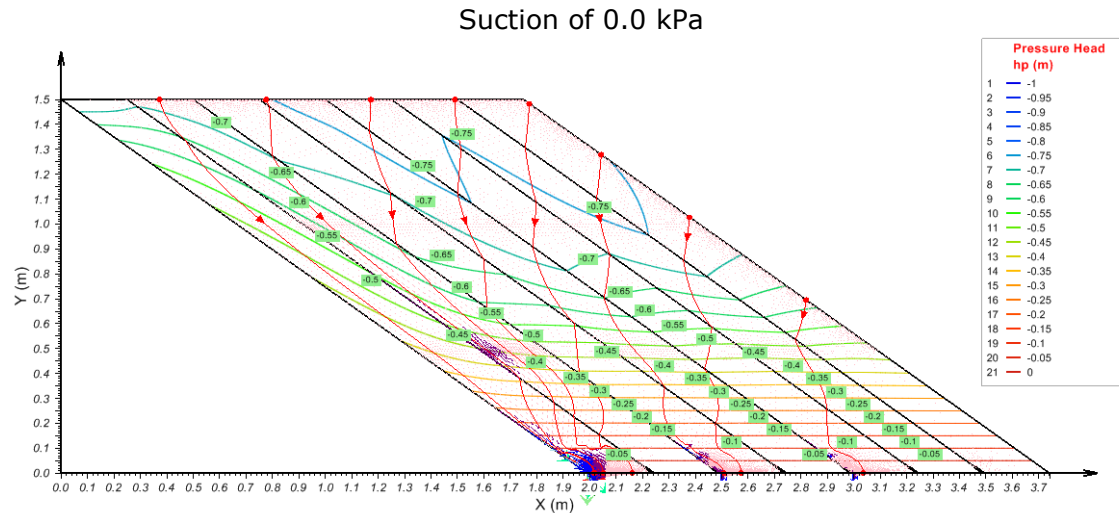


Figure 0.5 Contrast Profile from Changes in Base Suction in Test 2
at a Precipitation of 10 mm/Day

For a Panel 1.0 with sandy material, the effects of change in base suction are similar but at a lower scale. A change in suction has a medium impact on the water flow through the panel. As suction increases, more water flows through the fine layers, particularly L2 and L4. In sand, suction changes the preferential discharge material from coarse to fine; at 0 kPa to 4 kPa, discharge of the coarse decreases from 98% to 40%.

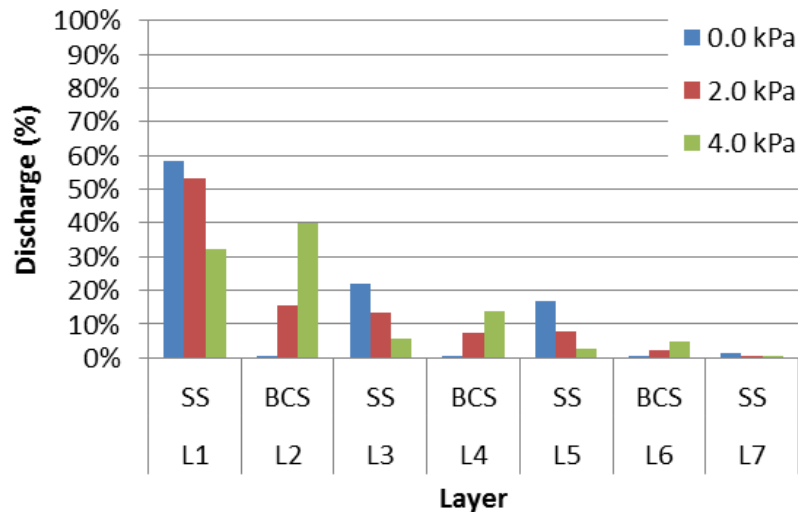


Figure O.6 Contrast Discharge from Changes in Base Suction in Test 2 at a Precipitation of 10 mm/Day

Increasing suction generates decrements in the SS and increments in the BCS. The changes decrease with an increase of suction and distance to L7. At Layer 2 and suction 4 kPa, the discharge contradicts this statement. The reason for this is that the suction at the base is close to the AEV of the BCS, meaning the material is almost kept at saturation.

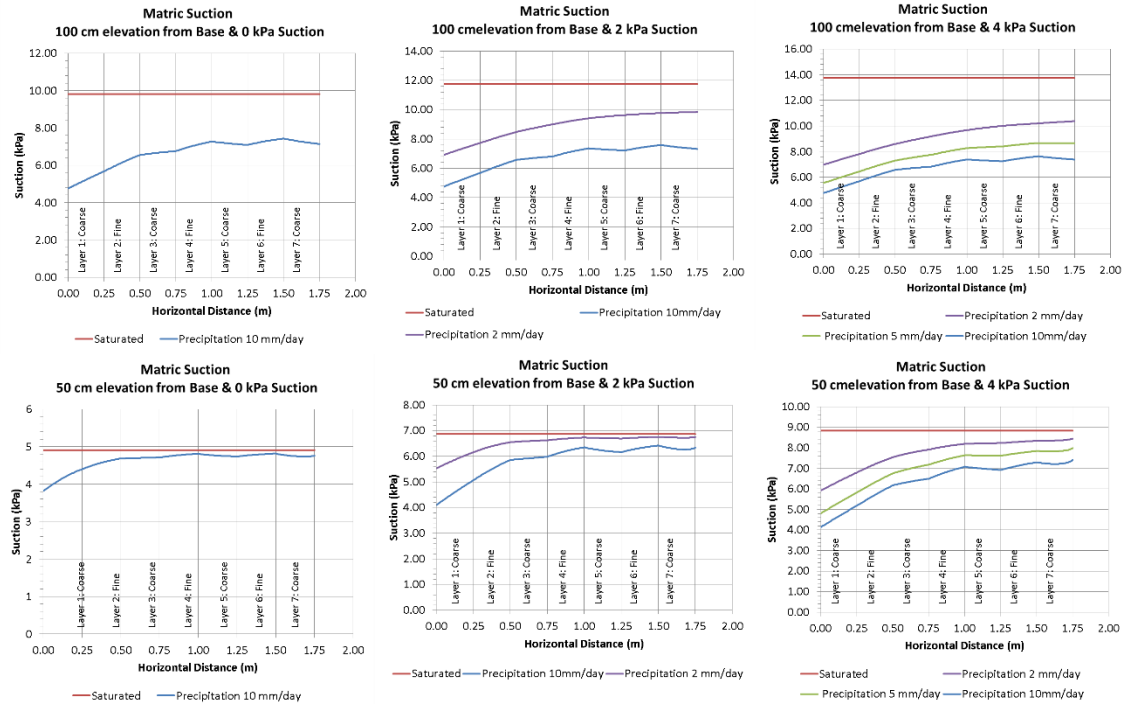


Figure 0.7 Change In Matric Suction in Test 2 at 0.5 m and 1.0 m Elevations

For sandy materials, the variance of h_p with the distance ranges from 4.8 kPa up to 10 kPa at 100 cm of elevation and from 3.8 kPa to 8.4 kPa at 50 cm of elevation. The graphs also show that changes in precipitation have minimal effect in suction from L1 to L7

For the highest precipitation rate, the profile shows a slight decrease in the increment of suction at the coarse layers. However, this reduction of increment suction decreases as precipitation decreases.

V. SIMULATION OF PANEL-1 USING WASTE ROCK FROM GOLDEN SUNLIGHT MINE (TEST 3)

The following results show the simulated response of Panel-1 using the calibrated properties from the simulation of Column-2 (See section 4.5.2.1).

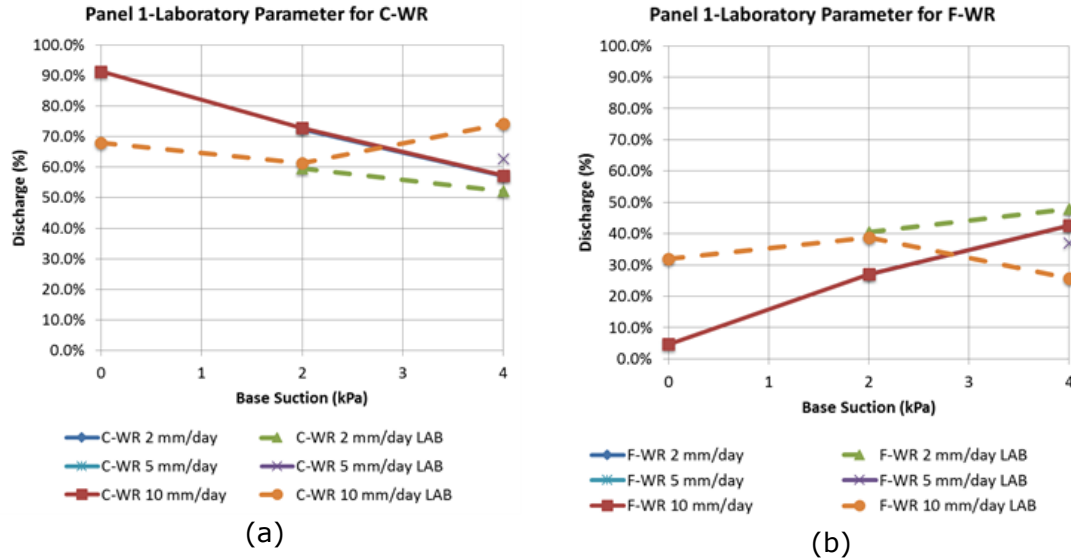


Figure O.8 Simulation Discharge from the Coarse Material (a) and Fine Material (b) Using the Calibrated Properties of Waste Rock From Column-2

The results display the same tendency of the model using waste rock from Grasberg Mine: an increase in the discharge from the Fine material (F-WR) as suction increases. Suction has great impact on the discharge of the fine material, increasing 35% total discharge from 0 to 4 kPa of suction. Nevertheless, the preferential flow path for the WR from Golden Sunlight was through the C-AR for any of the applied suction values. This preferential flow occurs due to the small difference of permeability between the materials after the suction at the intersection between both materials hydraulic conductivity curves.

As mentioned before, for an overall discharge there is no effect in changing the precipitation; internally the panel profiles show approximately equal h_p . There is a small increase of h_p towards the right side of the panel, however.

The simulations profile (Figure O.9) show that the main flow path is through the fine layers (L2, L4, and L6) regardless of the change in precipitation. Nevertheless, near the base of the panel, water breakthrough to the first layer of C-WR (L1) kept the coarse material as the main discharge material regardless of precipitation.

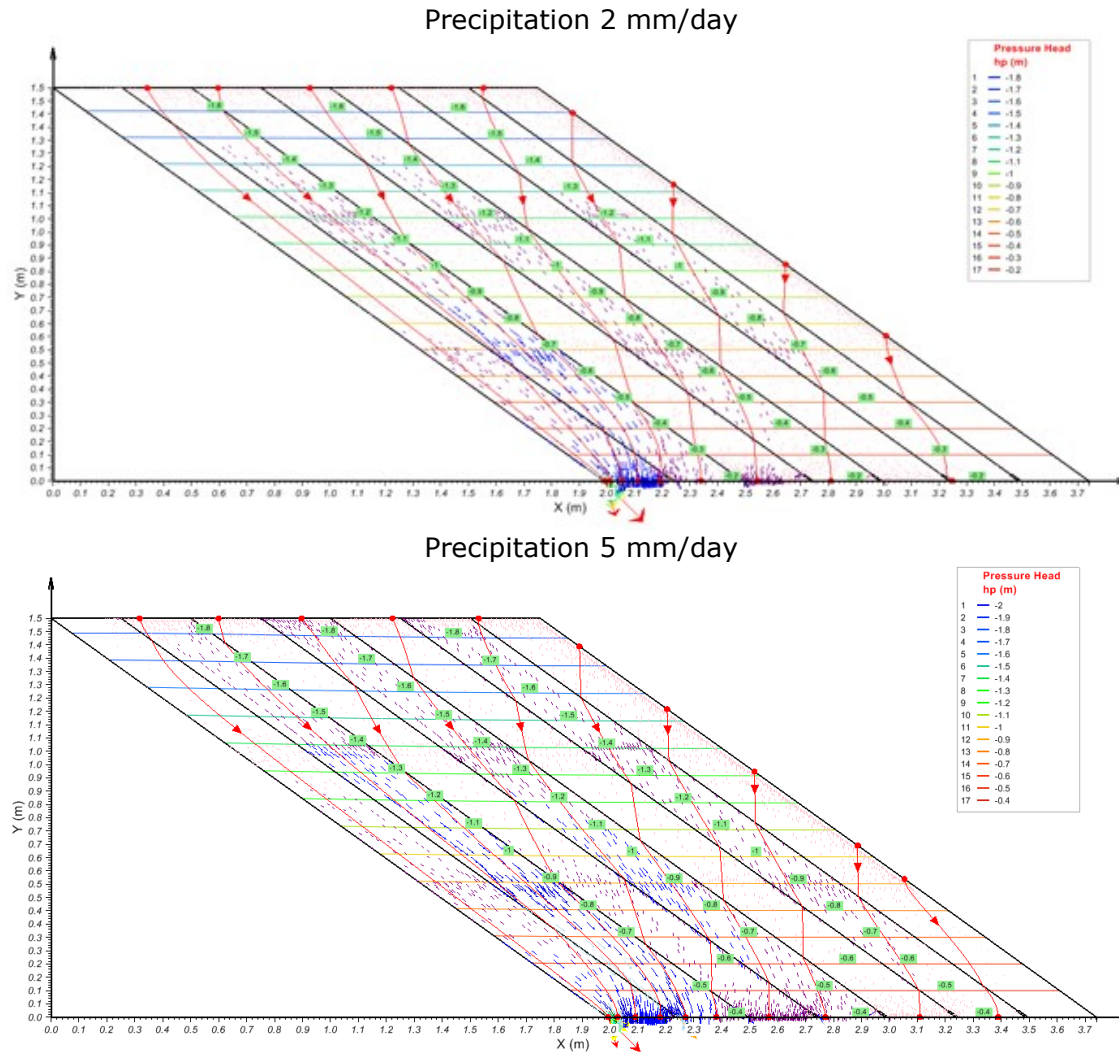


Figure O.9 Contrast Profile from Changes in Precipitation in Test 3
Applying a Base Suction of 4.0 kPa

The simulations expose a similar distribution as demonstrated in Test 1 on the discharge in the panel (see Figure O.4), water discharge decreases evenly towards the outer layer (L7) as shown in Figure O.10.

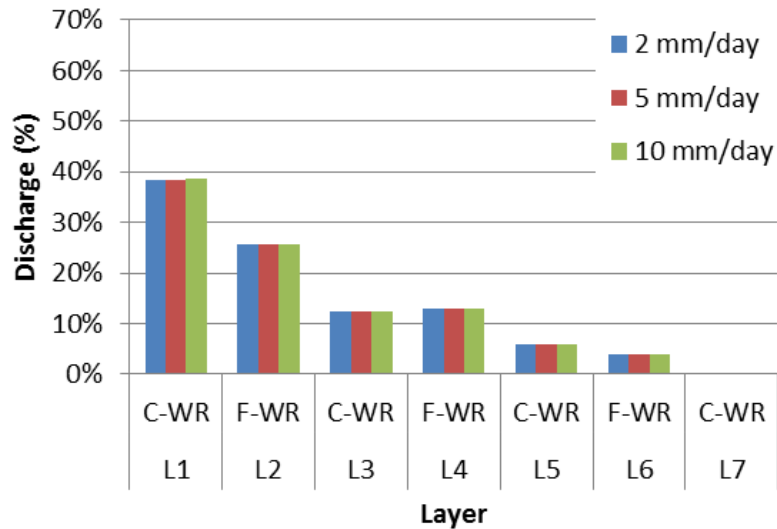


Figure O.10 Contrast Discharge at Three Precipitation Rates in Test 3
Applying a Base Suction of 4.0 kPa

The simulations showed that a change in the base suction generates significant changes to the h_p distribution, changing the preferential flow path in the model. Figure O.11 displays the change in head pressure with elevation, flux vectors, and streamlines for different base suctions applying a precipitation of 10 mm/day.

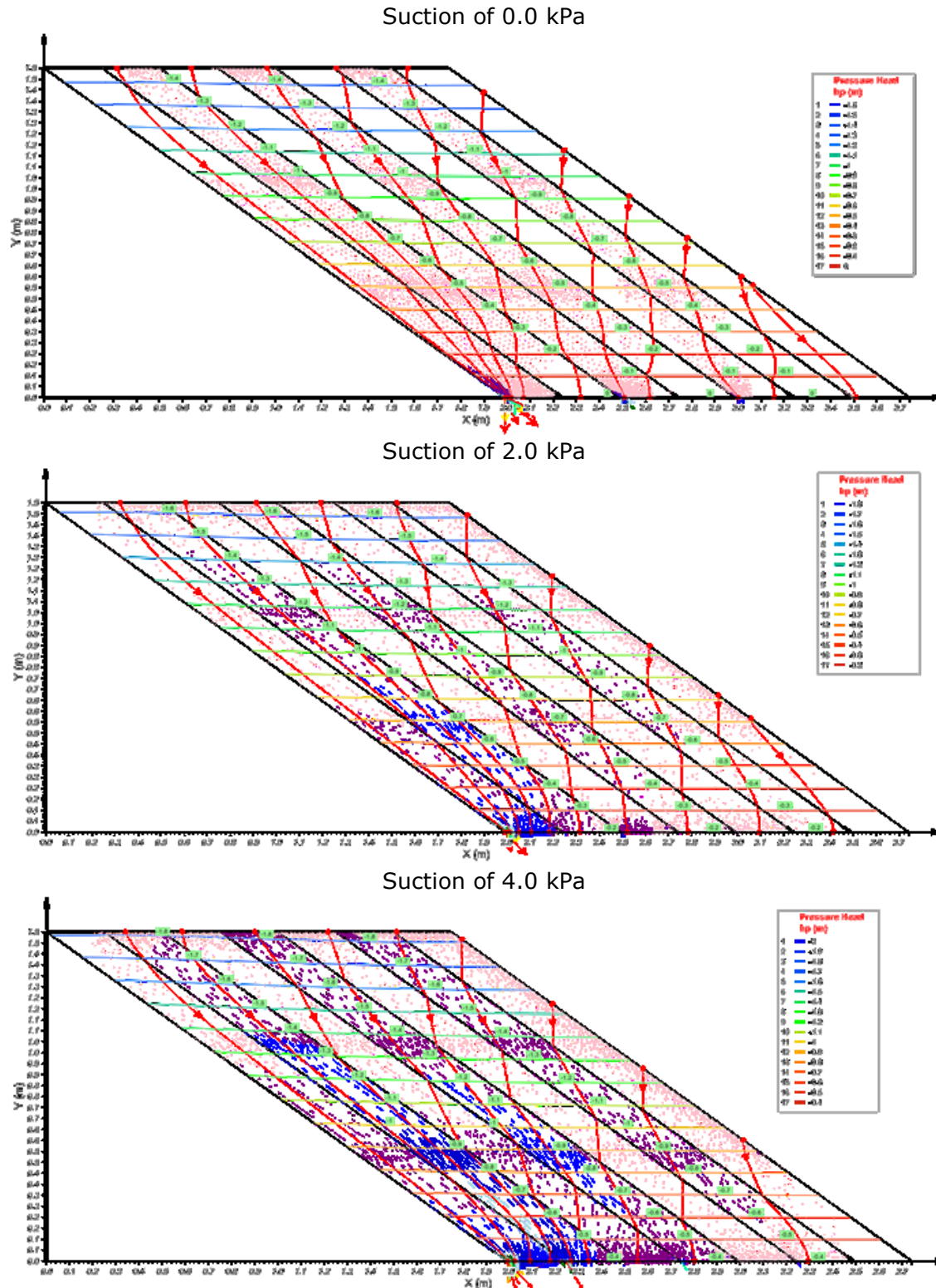


Figure 0.11 Contrast Profile from Changes in Base Suction in Test 3 at a Precipitation of 10 mm/Day

In Test 3 of Panel-1 at 0 kPa of suction, most water is diverted to the C-WR, principally L1 and L3. The change in suction has a large impact on the water flow through the panel. As suction increases, more water flows through the fine layers; however, at the same time, more water breaks through the coarse layers. The flow from L2 discharges through L1 and from L4 through L3.

For Waste Rock, suction does not change the Coarse materials as the preferential discharge; still it decreases the discharge in 35 % from at 0 kPa to 4 kPa. Increasing suction generates decrements in the C-WR and increments in the F-WR. The changes seem to be constant with the increase of suction; thus the internal h_p has changes equal to the change in suction at the base.

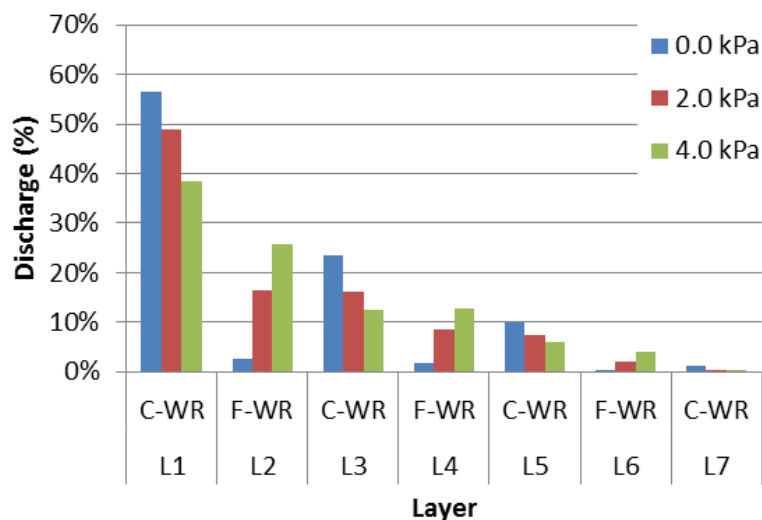


Figure O.12 Contrast Discharge from Changes in Base Suction in Test 3 at a Precipitation of 10 mm/Day

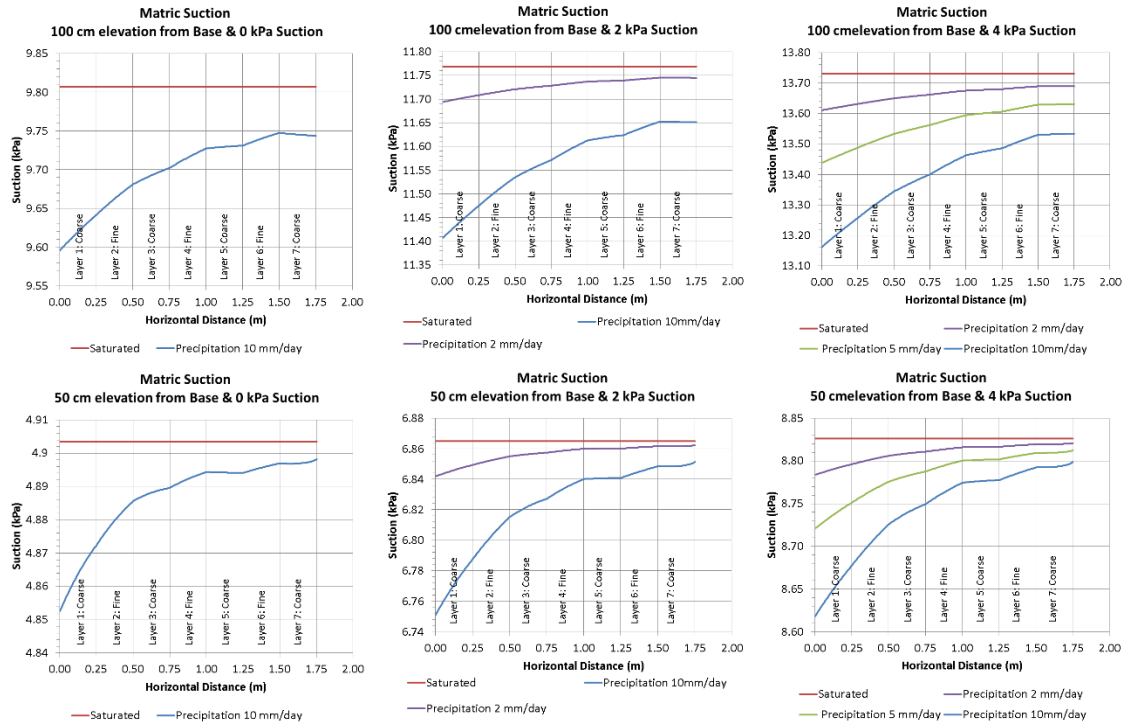


Figure O.13 Change in Matric Suction at 0.5 m and 1.0 m Elevations

For Waste Rock the minimum and maximum of h_p for all cases ranges from 9.6 kPa up to 13.7 kPa at 100 cm of elevation and from 4.85 kPa to 8.82 kPa at 50 cm of elevation, this being always the minimum value for the internal side of the panel (towards L1). The variance is minimal for most cases with changes of approximately less than 0.4 kPa. The suction profiles show that decreasing precipitation increases the matric suction, as well as generates a lower gradient between the inner and outer layers.

VI. SIMULATION OF PANEL-1 USING TAILINGS BEACH SAND AND DEVON SILT (TEST 4)

The following results show the simulated response of Panel-1 using material properties from a tailings beach sand (TBS) and Devon-Silt based on the material characterization by colleges at the University of Alberta (Abdulnabi, 2015; Kouakou, 2014; Torghabeh, 2013).

Table O.1 Material Characteristics for TBS and Devon Silt

Property\Material	Fine/ Devon Silt	Coarse/ Tailings Beach Sand
Particle size	94% Pass No 200	3% Pass No 200
AEV (kPa)	-	-
VWC	0.34	0.45
mv (1/kPa)	2.40E-03	2.70E-03
Dry Density (kN/m ³)	15.68	14.31
GS	2.67	2.65
K _{sat} (m/s)	1.00E-07	1.00E-05
k _{min} (m/s)	1.00E-14	1.00E-14

Similar to the other tests, the SWCC (Figure O.14) from the materials was measured using temple cell, and it allowed the estimation of the HCC used in the model applying Fredlund & Xing regression.

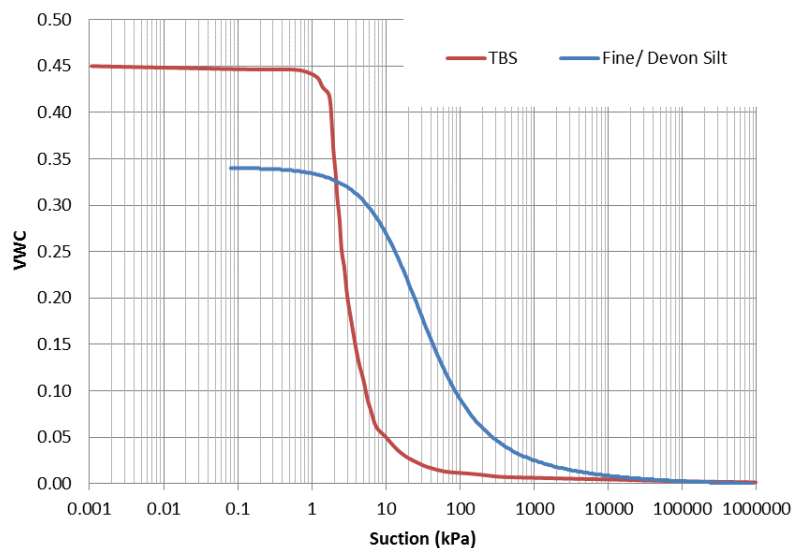


Figure O.14 SWCC for TBS and Devon Silt

The results show the same behavior as “Tests 1, 2 and 3”, an increase in the discharge from the Fine material (Devon Silt) as the suction increases. The increment in the discharge of the fine material is much less than in the other tests despite a higher differences in permeability after the intersection suction between HCCs of both materials. These results indicate that the internal suction developed within the panel was below the intersection suction, allowing the coarse material to carry a higher permeability than the fine material.

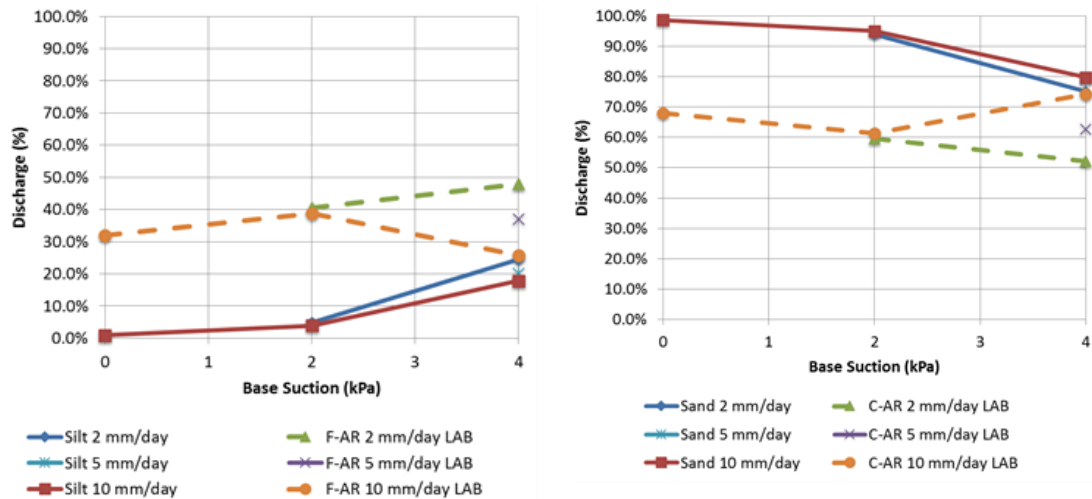


Figure 0.15 Simulation Discharge from the Coarse Material (Right) and Fine Material (Left) Using the Calibrated Properties of Waste Rock From Column-2

Suction has small impact on the discharge of the fine material, increasing up to 20% the total discharge from 0 to 4 kPa of suction. These materials modeled in Panel-1 show small variance in discharge due to changes in precipitation; at 4 kPa of suction, the results reveal a higher discharge from the fine material as precipitation increases. This higher discharge occurs to the relationship between the fine k_{sat} and the precipitation.

Contrary to the other test in Panel-1, Test 4 shows a higher effect in the discharge due to an increase in the precipitation rate. Compared to the other three tests, Test 4 has a lower difference between the permeability of both materials and the in flux. The increment in effect is related to the difference between the precipitation rates and the saturated hydraulic conductivity of the materials.

The results demonstrate for L2 to L7 that as precipitation increases, discharge decreases, regardless of the material. Nonetheless, in the first layer (L1) display, a contrary response occurs: the discharge increases in coarse material as the precipitation increases. This change occurs due to the relation between the k_{sat} of the Silt and the precipitation

values. At 2 mm/day, the precipitation is lower than the k_{sat} of the fine material, at 5 mm/day the precipitation is almost equal the k_{sat} , and at 10 mm/day the precipitation is higher.

Figure O.16 illustrates a much different profile than in the previous tests. The model shows that water describes a flow path driving most of the water applied at the top of the layers towards the discharge point in the first layer. The flow produced from the precipitation along the slope of the last layer (L7) is drawn vertically to the discharge points in the coarse layers.

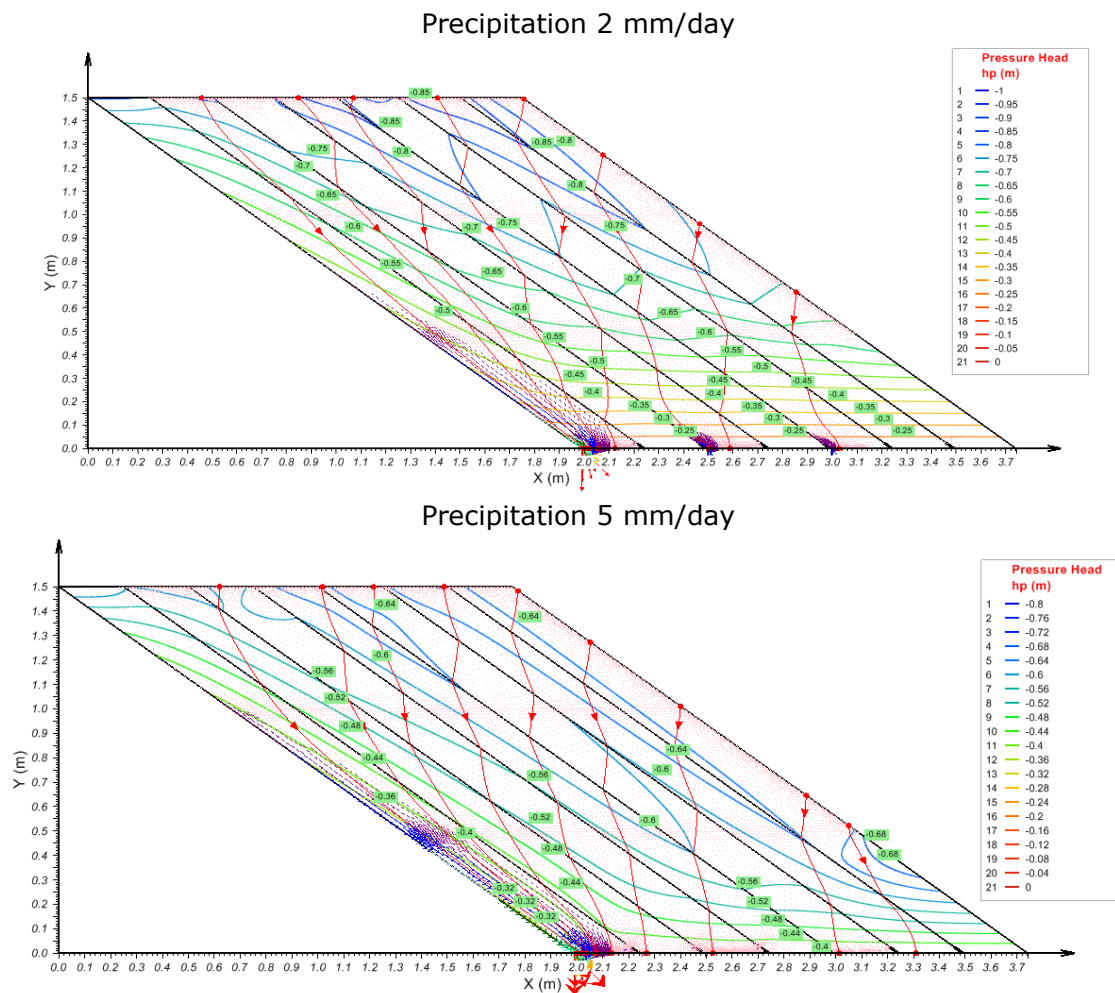


Figure O.16 Contrast Profile from Changes in Precipitation in Test 4 Applying a Base Section of 4.0 kPa

This tests shows a similar distribution in the discharge as Test 1 and Test 3. The discharge is decreased toward the outer layers. The profiles show that as precipitation

increases, the suction decreases in approximately 3 kPa and the elevation of constant h_p also decreases from 0.3 m to 0.15 m.

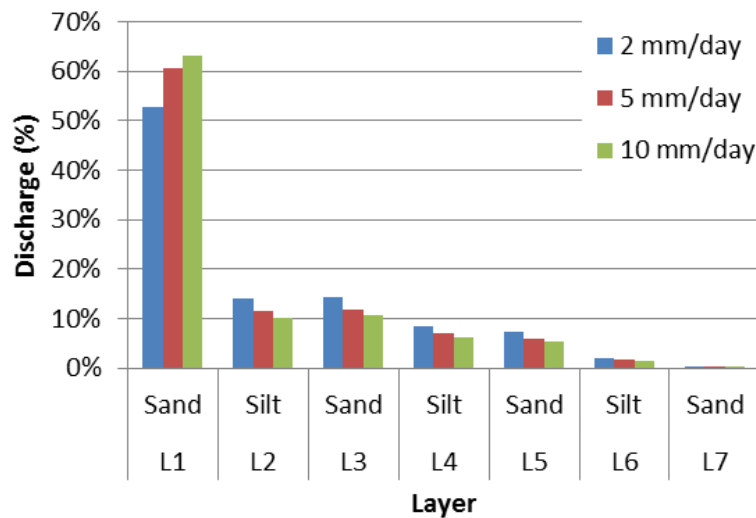


Figure O.17 Contrast Discharge at Three Precipitation Rates in Test 4
Applying a Base Suction of 4.0 kPa

The model is also affected by changes in the base suction. The increment of base suction increases the matric suction of the system but at a lower degree than in the other tests. Figure O.18 displays the change in head pressure with elevation, flux vectors, and streamlines for different base suction applying a precipitation of 10 mm/day.

At 0 kPa the results for L1 are contrary to the results of the other materials. The profiles show that as suction increases, the elevation at which the panel reaches constant head pressure decreases. Similarly, increasing suction decreases the discharge from the coarse materials. Additionally, the model shows the preferential flow path is equal to the preferential discharge materials, contrary to the other tests. This similarity occurs as water is flowing vertically down from the point of application, crossing coarse and fine layers up to an elevation where h_p is constant, and as suction increases, the verticality path is longer.

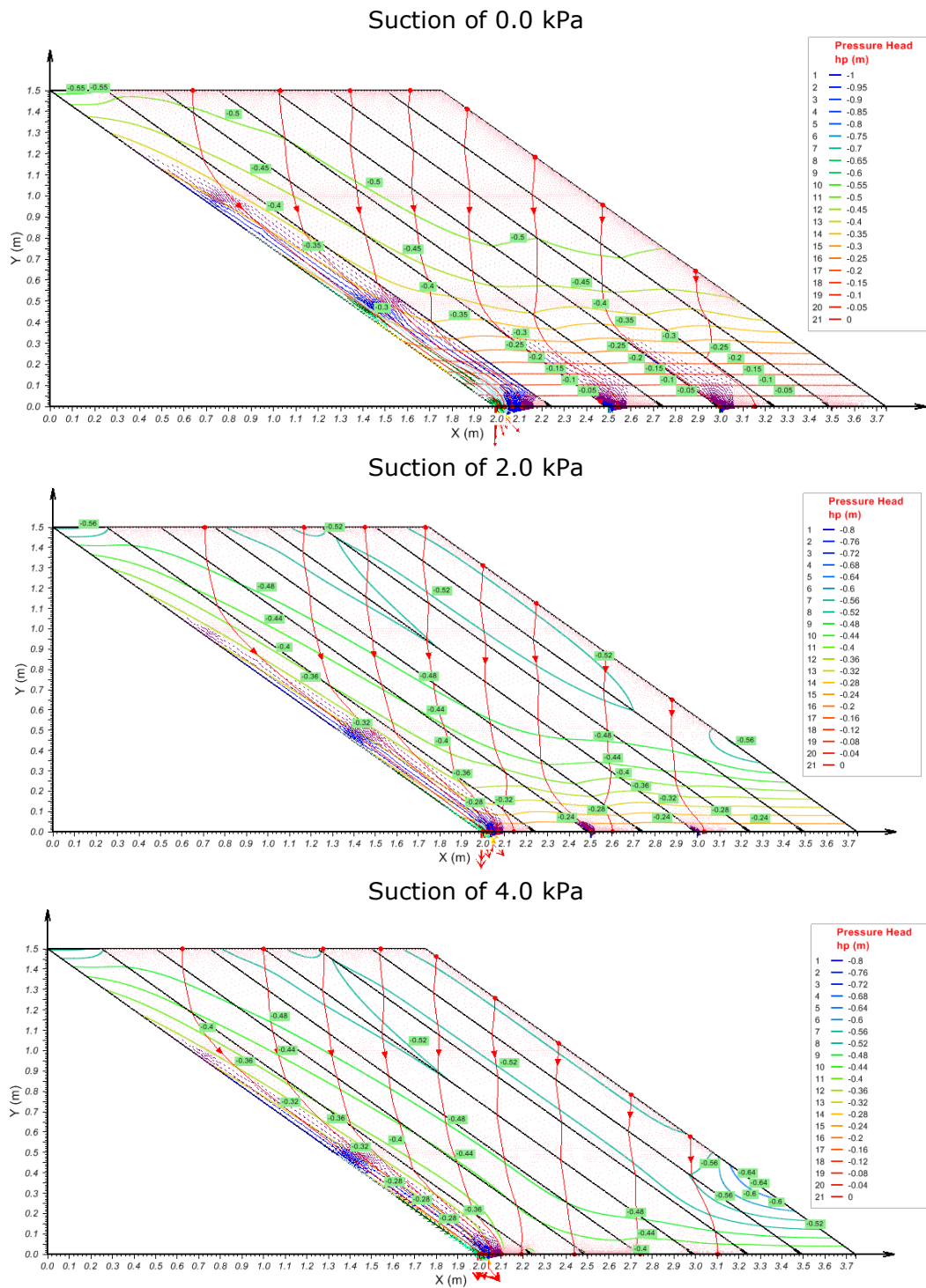


Figure 0.18 Contrast Profile from Changes in Base Suction in Test 4 at a Precipitation of 10 mm/Day

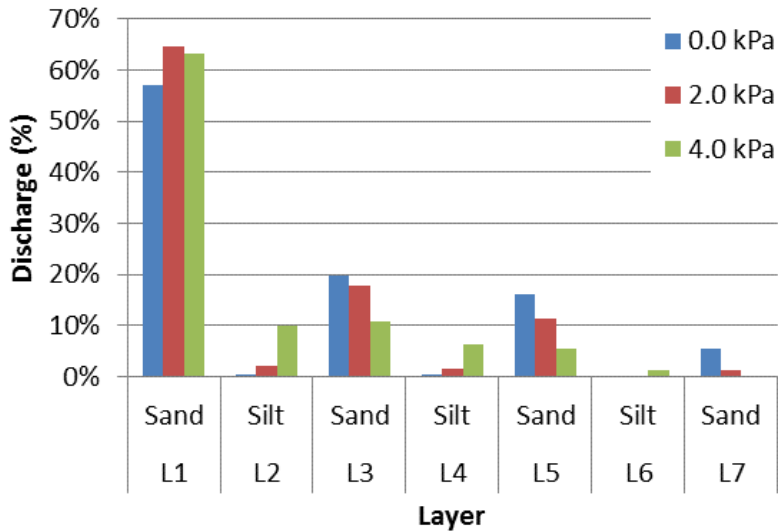


Figure 0.19 Contrast Discharge from Changes in Base Suction in Test 4 at A Precipitation of 10 mm/Day

For Silt and Sand, the minimum and maximum of h_p for all cases range from 3.2 kPa up to 8.0 kPa at 100 cm of elevation and from 2.8 kPa to 7.4 kPa at 50 cm of elevation, this being always the minimum value of the internal side of the panel (towards L1). The variance of suction with the horizontal distance for most cases is approximately 2.2 kPa; the variance increases with suction and decreases with elevation.

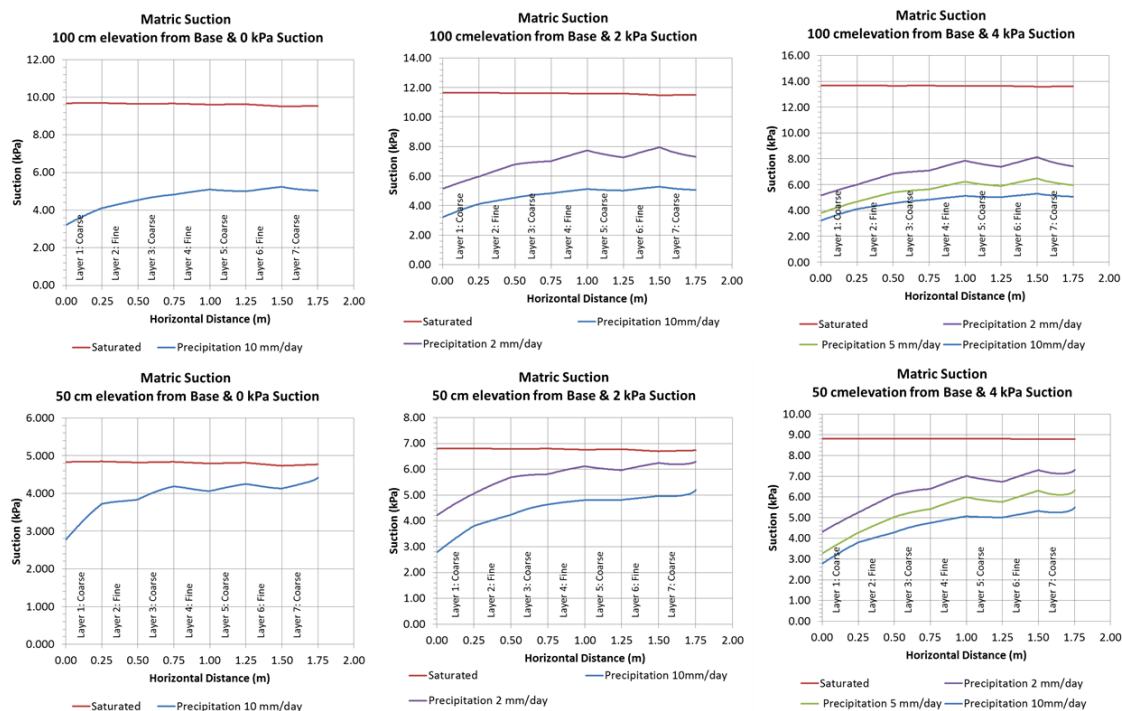


Figure 0.20 Change In Matric Suction at 0.5 M And 1.0 M Elevations

REFERENCES

- Andrina, J. (2009). Physical and geochemical behaviour of mine rock stockpiles in high rainfall environments. Ph.D. Thesis, University of British Columbia, Vancouver, Canada.
- Aubertin, M., Cifuentes, E., Apithy, S. A., Bussiere, B., Molson, J., & Chapuis, R. P. (2009). Analyses of water diversion along inclined covers with capillary barrier effects. *Canadian Geotechnical Journal*, 45, 1146-1164.
- Broda, S., Blessent, D., & Aubertin, M. (2013). A novel approach to analyze water flow in waste rock piles to assess slope stability and groundwater contamination. Paper presented at the
- Fala, O., Aubertin, M., Molson, J., Bussière, B., Wilson, G. W., Chapuis, R., et al. (2003). Numerical modelling of unsaturated flow in uniform and heterogeneous waste rock piles. 6th International Conference of Acid Rock Drainage, North Queensland, Australia. , 22. (2) pp. 895-902.
- Fine, P. E. (2006). Hydrologic characterization of two full-scale waste rock piles. M.Sc. Thesis, University of British Columbia, Vancouver, Canada.
- Fredlund D.G., Rahardjo H., Fredlund M.D. (2012). Unsaturated soil mechanics in engineering practice (2nd Edition ed.) John Wiley & Sons, Inc.
- Fredlund M.D. (2004). Finite element stochastic analysis. Paper presented at the 57th Canadian Geotechnical Conference and 5th Joint IAH-CGS Conference, Quebec City, Quebec.
- Fredlund, M. D., & Thode, R. (2013). Modeling of seepage through segregating waste rock: Part I. Tailings & Mine Waste Conference, Banff, Canada.
- Fredlund, M. D., & Thode, R. (2015). Modeling of seepage through segregating waste rock: Part 2. Tailings & Mine Waste Conference, Vancouver, Canada.
- Fredlund, D. G. (2006). Unsaturated soil mechanics in engineering practice. *Journal of Geotechnical and Geoenvironmental Engineering*, 132(3), 286-321.

- Fredlund, D. G., & Xing, A. (1994 A). Equations for the soil-water characteristic curve. *Canadian Geotechnical Journal*, 31, 521-532.
- Fredlund, D. G., Xing, A., & Huang, S. B. (1994 B). Predicting the permeability function for unsaturated soils using the soil-water characteristic curve. *Canadian Geotechnical Journal*, 31(533-546)
- Freeport-McMoran. Tailings and waste rock. Retrieved 10/01, 2015, from <http://www.fcx.com/sd/env/tailings.htm>
- Geo-Slope International Ltd. (1991). SEEP/W ver. 2.0 guide. Calgary, Canada:
- Gui, M., Wu, C., & Lu, C. (2011). Comparison of two water storage functions of soil on pore-water pressure of earth filled dam under changing environment. Paper presented at the 28th Isarc, pp. 538-543.
- Herasymuik, G. M. (1996). Hydrogeology of A sulphide waste rock dump. M.Sc. Thesis, University of Saskatchewan, Saskatoon, Canada.
- Horton, J. H., & Hawkins, R. H. (1965). Flow path of rain from the soil surface to the water table. *Soil Science*, 100(6), 377-383.
- INAP. (2009). Global acid rock drainage guide. Retrieved 11/06, 2014, from <http://www.gardguide.com/>
- Kouakou, W. A. (2014). Geotechnical characterisation of oil sand tailings beach deposits in flume tests. M.Sc. Thesis, University of Alberta, Edmonton, Canada.
- Lu, N., & Likos, W. J. (2004). *Unsaturated soil mechanics* (1st Edition ed.). New Jersey: John Wiley & Sons.
- Lv, M., Hao, Z., Liu, Z., & Yu, Z. (2013). Conditions for lateral downslope unsaturated flow and effects of slope angle on soil moisture movement. *Journal of Hydrology*, 486, 321-333.
- Nagy, L., Takács, A., Huszák, T., Mahler, A., & Varga, G. (2013). Comparison of permeability testing methods. *Proceedings of the 18th International Conference on Soil Mechanics and Geotechnical Engineering, Paris.* , 1. pp. 399-402.

- Newman, L. L. (1999). Preferential flow in vertically oriented, unsaturated soil layers. M.Sc. Thesis, University of Saskatchewan, Saskatoon, Canada.
- Richards, L. A. (1931). Capillary conduction of liquids through porous mediums. *Journal of Applied Physics*, 1(5), 318-333.
- Smith, L., Lopez, D. L., Beckie, R., Morin, K., Dawson, R., & Price, W. (1995). Hydrogeology of waste rock dumps No. 23440-4-1317/01-SQ). Vancouver; B.C.; Canada: Department of Natural Resources Canada.
- SoilVision Systems Ltd. (2012). SvFlux V.7 theory manual. Saskatoon, Canada:
- Tami, D., Rahardjo, H., Leong, E., & Fredlund, D. G. (2004). Design and laboratory verification of a physical model of sloping capillary barrier. *Canadian Geotechnical Journal*, 41, 814-830.
- Thieu, N. T. M., Fredlund, M. D., Fredlund, D. G., & Hung, V. Q. (2001). Seepage modeling in a Saturated/Unsaturated soil system. International Conference on Management of the Land and Water Resources,
- Torghabeh, E. A. (2013). Stabilization of oil sands tailings using vacuum consolidation. Ph.D. Thesis, University of Alberta, Edmonton, Canada.
- Wilson, J. A. (2003). Numerical modelling of unsaturated flow in vertical and inclined waste rock layers using the Seep/w model. M.Sc. Thesis, University of Saskatchewan, Saskatoon, Canada.
- Wilson, G. W., Fredlund, D. G., & Barbour, S. L. (1997). The effect of soil suction on evaporative fluxes from soil surfaces. *Canadian Geotechnical Journal*, 34(1), 145-155. doi:10.1139/t96-078
- Wilson, G. W. (1990). Soil evapotranspiration fluxes for geotechnical engineering problems. Ph.D. Thesis, University of Saskatchewan, Saskatoon, Canada.
- Wilson, G. W. (1995). Assessment of protective covers and dump behaviour. Paper presented at the Proceedings of Second Australian Acid Mine Drainage Workshop, pp. 147-164.
- Wilson, G. W. (2001). Hydrology and unsaturated flow in waste rock. In W. A. Hustrulid, M. K. McCarter & Van Zyl, Dirk J.A. (Eds.), *Slope stability in surface*

mining embankment (1st Edition ed., pp. 305-310). University of British Columbia, Vancouver: Society for Mining, Metallurgy, and Exploration.